1-1-2011

Delineating the Steps of BAX Pore Activation

Eric Christenson
Washington University in St. Louis

WASHINGTON UNIVERSITY IN ST. LOUIS

The Division of Biology and Biomedical Sciences

Program in Molecular Cell Biology

Dissertation Examination Committee:

Paul H. Schlesinger, Chair
John A. Cooper
William A. Frazier
Phyllis I. Hanson
Katherine A. Henzler-Wildman
Daniel S. Ory

DELINEATING THE STEPS OF BAX PORE ACTIVATION

MODULATION BY PROTEIN-PROTEIN INTERACTIONS AND THE BULK MEMBRANE ENVIRONMENT

by

Eric Thomas Christenson

A dissertation presented to the
Graduate School of Arts and Sciences
of Washington University in
partial fulfillment of the
requirements for the degree
of Doctor of Philosophy

August 2011

Saint Louis, Missouri

ABSTRACT OF THE DISSERTATION

Delineating the Steps of BAX Pore Activation

by

Eric Thomas Christenson

Doctor of Philosophy in Biology and Biomedical Sciences
(Molecular Cell Biology)

Washington University in St. Louis, 2011

Professor Paul H. Schlesinger, Chair

The BCL2 protein family is the primary gatekeeper of mitochondrial apoptosis and governs integrity of the organelles' outer membranes. Permeabilization of mitochondrial outer membranes permits egress of cytochrome *c* and other apoptogenic factors, resulting in apoptosome formation, caspase activation, and subsequent proteolytic demolition of cells. Proapoptotic BAX & BAK effect the release of cytochrome *c* while their antiapoptotic counterparts like BCL-2, BCL-X_L, & MCL-1 oppose this permeabilization. A third class of the BCL2 family, the prodeath BH3-only proteins, act as sentinels of cell stress and exert their influences by occupying antiapoptotic BCL2 members and/or activating BAX/BAK. Cell-free reconstitution assays have revealed that BAX/BAK undergo significant conformational changes to oligomerize and form pores in membranes.

Previously unresolved was the basis for the outer cell membranes' escape from BAX poration during apoptosis. Unlike outer cell membranes, which are roughly 40% cholesterol, mitochondrial outer membranes are only 5-10% cholesterol. Vesicle leakage assays demonstrated that BAX pore activation is severely inhibited by the sterol. Inclusion of the total enantiomer of cholesterol in our assays uncovered that this BAX functional suppression was

due to bilayer structure alteration rather than a stereospecific protein-cholesterol interaction. Real-time observation of BAX-vesicle binding showed that cholesterol curbs membrane integration by the protein, thus suppressing oligomerization and pore formation.

Oxysterols and bile acids are physiological derivatives of cholesterol. Further employment of our vesicle leakage regime revealed that 25-hydroxycholesterol at low micromolar concentrations accelerates BAX pore formation, suggesting a compensatory mechanism for BAX inhibition by cholesterol. Bile acids lithocholic and chenodeoxycholic acids are toxic and induce apoptosis at high concentrations, thus we reasoned that the physiological detergents may directly activate BAX. While truncated BAX (ΔC) was effectively activated by monomeric detergent, the full-length protein required micellar bile acids, implying that bile acids could play at most only an amplification role in BAX-mediated apoptosis.

In nonstressed cells, BAX exists as a soluble, cytosolic monomer or loosely affiliated with mitochondria while cellular recognition of death signals induces BAX transition to a membrane-integral state. The physical basis of this translocation and locale of BAX activation are poorly characterized. Assemblage of a cell-free scheme comprising full-length BAX, antiapoptotic BCL-X_L, and BH3-only activators cBID & BIM_S, and synthetic vesicles revealed that BIM_S more effectively activates BAX and is less suppressible by BCL-X_L. Each of these four proteins can independently adsorb to membranes and that BCL-X_L "outraces" BAX to their in-membrane functional sites. Membrane-bound cBID and BIM_S robustly accelerate the bilayer integrations of BAX & BCL-X_L; the two activators recruit equivalently at the membrane surface, however, suggesting that BIM_S, unlike cBID, can activate BAX prior to interaction on a bilayer scaffold.

ACKNOWLEDGMENTS

First and foremost, I wish to thank my thesis advisor, Dr. Paul Schlesinger, for affording me the opportunity to train in his laboratory and permitting me substantial freedom to pursue my curiosity. I am grateful for Paul's patience, investigative guidance, unvarnished ardor for inquiry, and challenges to my interpretations or presumptions.

I am deeply appreciative of my former lab mates, whose aid lessened experimental tedium and friendship brightened workdays. I would like to thank Olena Ivashyna for enlightening discussions, her inveterate affability, and many entertaining conversations across our cluttered bench. I want to thank Sean Merlin for his precision in lab work and especially for development of a technique on which much of my dissertation is based. I also want to thank Mitsu Saito for starting me on my first project in this lab and providing ideas usually orthogonal to my own. I am grateful to Francesca Mascarenhas for much-needed technical assistance.

I would like to thank my thesis committee—Drs. Nathan Baker, Emily Cheng, John Cooper, Bill Frazier, Phyllis Hanson, Katie Henzler-Wildman, and especially Dan Ory—for their tutelage and constructive criticisms. As my committee chair, Dan was an invaluable resource.

Many thanks to Hua Pan for her technical assistance and diverting conversations. Also, I'm very appreciative of Sam Wickline for permitting my use of an instrument that both made my life much easier and drove me bonkers.

I want to thank my collaborators at Wash U, Hyungjin Kim of Emily Cheng's lab and Bryson Katona of Doug Covey's lab. While our efforts did not succeed as splendidly as we'd hoped, they were rewarding nevertheless. Also, I wish to thank Doug Covey for providing me a number of valuable steroids whose synthesis is arduous.

I am grateful for my collaborators outside the Wash U sphere—Ana García-Saéz at the University of Heidelberg, Petra Schwille at BIOTEC der TU Dresden, Ghee Hwee Lai & Gerard Wong at UCLA, and Yen Sun & Huey Huang at Rice University. Their expertises are terrifically useful and our partnerships have proven highly insightful.

I'm profoundly thankful for my mother, Jane, who instilled in me the value of insatiable inquisitiveness. Also for my father, Herschel "Buzz", from whom I inherited my attentiveness to detail.

Finally, I am unfathomably appreciative of my wife, Pam, who is exceptionally tolerant of my demanding schedule and resultant negligence. And when I whine, groan, and complain about lab, she sympathizes in the best manner possible–with a proverbial swift kick in the pants.

To Frëd

TABLE OF CONTENTS

LIST OF FIGURES & TABLES

Chapter 1

Chapter 2

Chapter 3

Chapter 4

Appendix I

Appendix II

Appendix III

Appendix IV

Appendix V

CHAPTER 1

Introduction

1.1 | Distillation

BAX is a proapoptotic member of the BCL2 family and lies at the convergence of a multitude of cell death signaling pathways. This dissertation is primarily concerned with interrogating the sequence of events culminating in BAX pore formation which, inside mammalian cells, results in cytochrome *c* liberation from mitochondria and subsequent cellular demise. BAX is a soluble, cytosolic, and monomeric protein that transitions to a bilayer-integral, oligomeric assemblage that permeabilizes biological membranes. This process can be delineated into three basic steps: 1) translocation to a membrane, 2) integration, and 3) oligomerization from which membrane pores emanate (Fig. 1.1). This first chapter describes the tripartite regulatory scheme of the BCL2 protein family which governs BAX activation. The second chapter details our investigation of BAX-membrane integration and oligomerization kinetics and the inhibitory effect of cholesterol on the proceeding. Chapter Three extends our study of BAX pore activation as influenced by cholesterol derivatives. The fourth chapter examines BAX translocation, integration, and pore formation and their modulations by anti- and proapoptotic BCL2 kin. Chapter Five proposes further investigative efforts and Appendix I marshals biophysical and structural evidences to proffer a model of active, membrane-integral BAX. Appendices II-V comprise experimental inquiries, to which this dissertation's author contributed substantially, that address BAX in-membrane oligomerization and elucidate physical mechanisms by which BAX induces bilayer poration.

Fig. 1.1

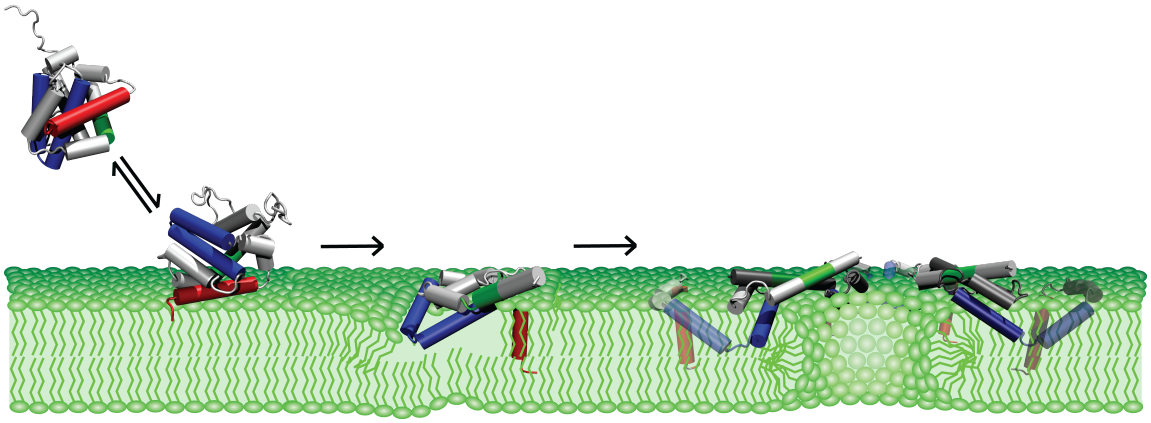

Fig. 1.1 | **Sequence of BAX pore formation.** Translocation to membranes, integration, and subsequent oligomerization.

1.2 | Vertebrate Apoptosis

Apoptosis is the most prevalent form of programmed cell death in animals and is a tightly-regulated process used to sculpt tissue during development and is critical for maintaining homeostasis (1). First defined morphologically, apoptosis was characterized by cell shrinkage, membrane blebbing, chromatin condensation, and DNA fragmentation (2). Dysregulation of this death program manifests as a multitude of pathologies – insufficient ablation of aberrant cells can lead to cancer or autoimmunity whereas excess educes the likes of type I diabetes and neurodegeneration (3).

The apoptotic process is a coordination of genetic and biochemical pathways, proximally effected by cysteine-aspartate proteases (i.e. caspases) which drive the demolition and packaging of dying cells for clearance (4). Caspases are produced as proenzymes and thus require activation to become catabolically competent. In vertebrates, caspase activation is elicited primarily by two pathways—the extrinsic and intrinsic (or mitochondrial) (Fig. 1.2). The extrinsic pathway promulgates death signals received via cell membrane death receptors like TNFR1 (tumor necrosis factor 1), Fas (APO1/CD95), and TRAILR1/2 (TNR-related apoptosis inducing ligand receptor 1/2) which are activated when engaged by their cognate death ligands outside the cell (1). Active receptors then assemble into a death-inducing signaling complex (DISC), resulting in activation of initiator caspases-8 and -10 which then cleave and activate effector caspases-3 and -7.

The intrinsic apoptotic pathway is a complementary death signaling cascade that responds to genotoxicity, ER and oxidative stresses, and cytokine or growth factor deprivation. These signals converge at mitochondria, resulting in their outer membrane permeabilization

(MOMP) and egress of apoptogenic factors into the cytosol. MOMP occurs at an indefinite time after reception of a death signal due to varying intracellular concentrations of signaling molecules; caspase activation and apoptosis, however, usually ensue permeabilization within minutes (5). Foremost of the mitochondrial proapoptotic factors is cytochrome *c*, whose liberation from the intermembrane space allows it to bind inactive adapter protein Apaf-1 (6). Cytochrome *c* binding initiates the adapter's conformational change and heptamerization into a complex termed the apoptosome which then recruits and activates caspase-9 for subsequent cleavage and activation of effector caspases-3 and -7 (7). MOMP also releases other proapoptotic factors such as Smac/DIABLO, AIF, HtrA2/Omi, and EndoG to further promulgate death signals (8,9). Notably, the extrinsic and intrinsic pathways operate largely in parallel but not without some intersection. Cells undergoing apoptosis induced by Fas are grouped into two categories: type I cells, such as lymphocytes, are effectively killed by the extrinsic pathways whereas type II cells, like pancreatic β–cells and hepatocytes, require amplification of the death signal via the intrinsic pathway (10).

Fig. 1.2

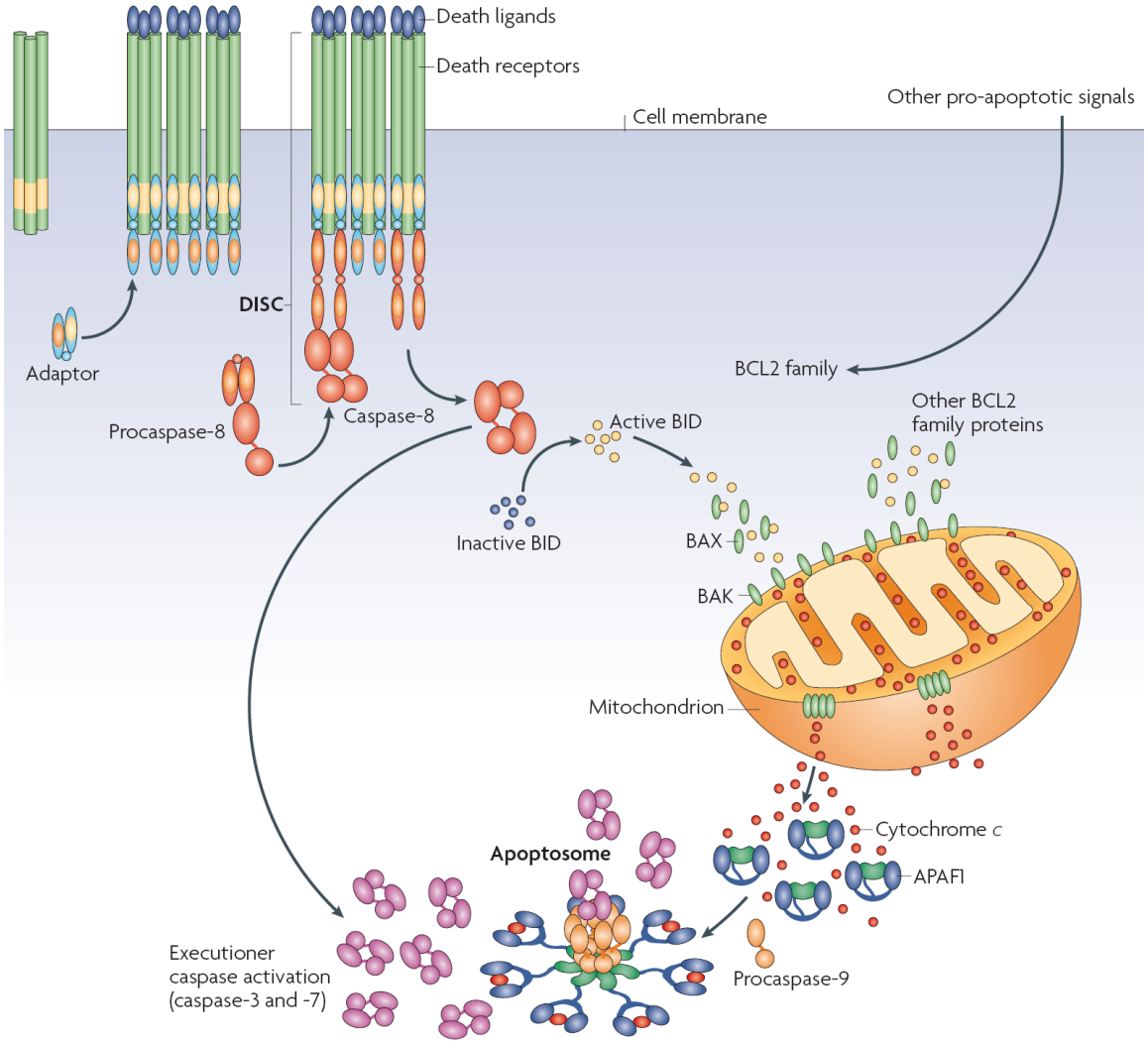

Fig. 1.2 | **Convergence of intrinsic & extrinsic apoptosis pathways.** Executioner caspases can be activated either directly by initiator caspases or through apoptosome assembly consequent of MOMP. The BCL2 family governs MOMP via complex balance of interactions between pro- and antideath members. Adapted from Y-L P. Ow *et al*. (2008) *Nat Rev Mol Cell Biol* **9**, 532-542.

1.3 | The BCL2 Family

The BCL2 protein family is the primary governor of mitochondrial outer membrane integrity; it comprises both anti- and proapoptotic members whose regulation and interactions dictates a cell's commitment to survival or suicide (11) (Table 1.1). Membership in this family is largely assigned by conservation in four sequence-defined BCL2 homology (BH1-4) domains that control binding between members. The antiapoptotic members encompass all four BH domains and are typically localized to their active sites—mitochondrial outer membranes—but also may be cytosolic or affiliated with ER and nuclear membranes (12) (Fig. 1.3 & Table 1.1). BCL-2, BCL-X_L, MCL-1, A1/BFL-1, & BCL-w constitute the predominant members of the class and antagonize MOMP via heterotypic binding of proapoptotic BCL2 proteins. The proapoptotic members are subdivided into multidomain effectors and BH3-only signaling proteins. BAX and BAK are the pore-forming effectors and include BH1-3 and a degenerate BH4 (13,14); counterintuitively, BAX/BAK share a similar tertiary fold with the antiapoptotic proteins despite their oppositional functions (15,16) (Fig. 1.4). While BAK constitutively affiliates with mitochondrial outer membranes, BAX resides largely in the cytosol or loosely associated with intracellular membranes (17-19). Following activation, BAX/BAK homodimerize and further assemble into multimeric complexes which elicit MOMP (20). As even healthy cells express both BAX and BAK abundantly, the two death proteins' are neutralized until damage is recognized (21-23).

Table 1.1 | **BCL2 family proteins** (non-exhaustive compilation)

Antiapoptotic *(multidomain; BH1-4)*	Proapoptotic *(multidomain; BH1-4)*	Proapoptotic *(BH3-only)*	*Direct Activator*	*Sensitizer*
BCL-2	BAX	BID	X	
BCL-X_L	BAK	BIM	X	
MCL-1		PUMA	X	
A1		BAD		X
BCL-w		NOXA		X
		BIK/BLK		X
		BMF		X
		HRK/DP5		X
		Beclin-1		X
		BNIP3/NIP3		X
		BNIP3L/NIX		X

Fig. 1.3

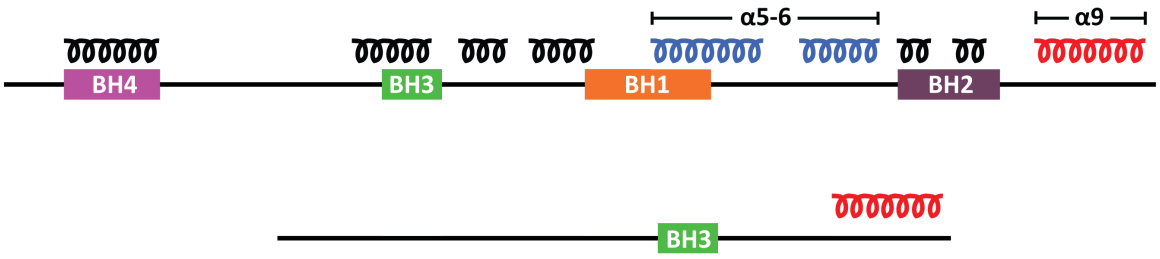

Fig. 1.3 | **Generalized schematic of BCL2 protein structure.** Depicted are representations of 1° and 2° structures of multidomain (anti- & proapoptotic) and BH3-only proteins (top & bottom panels respectively). α-helices in blue indicate central, mostly hydrophobic hairpin and α-helices in red signify membrane anchors.

Fig. 1.4

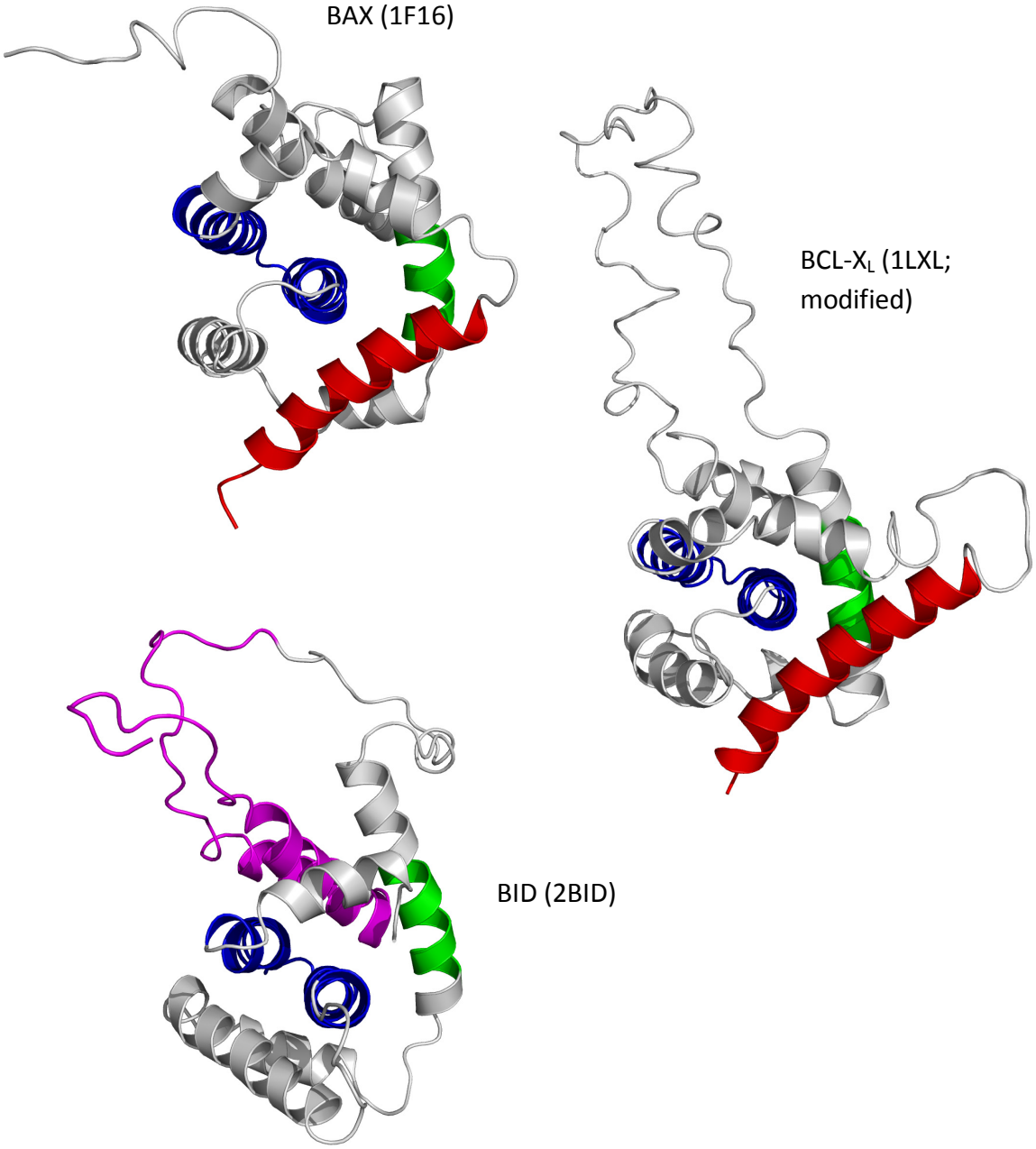

Fig. 1.4 | **Ribbon representations of BAX, BCL-X$_L$, & BID.** Illustrated are representatives of pro- and antiapoptotic multidomain BCL2 proteins. BID also depicted to demonstrate structural homology; it is the lone BH3-only protein known to adopt a defined tertiary fold. Colors of domains correlate with Fig. 1.3: central hairpin (blue), membrane anchor (red), and BH3 domain (green). For BID, the N-terminal, solubilizing fragment is colored magenta. For BCL-X$_L$, the C-terminus is homology-modeled based on BAX & BCL-w.

BH3-only proteins are the most diverse and least conserved of the BCL2 family, containing only the titular BH3 domain (24-26). These proteins integrate disparate cell stress pathways and are classified according to their multidomain BCL2 binding partners – sensitizer/derepressor BH3s antagonize only the antiapoptotic contingent while direct activator BH3s interact both with the antiapoptotics and trigger activation and multimerization of prodeath effectors BAX and BAK (27,28). The complex interaction network between the three classes of BCL2 proteins—antiapoptotic, BH3-only, and proapoptotic effectors—shifts the balance toward or away from MOMP and apoptosis.

Distinct BH3-only proteins initialize the cell death program in response to a host of cellular insults, thus their activities are stringently regulated by transcriptional and post-translational mechanisms. BH3s that are transcriptionally-upregulated include PUMA, BIK, & NOXA (by tumor suppressor p53) and BIM & BNIP3L (by FOXO3A) (29-33). Modifications like phosphorylation or proteolytic cleavage are also common—BID becomes active and translocates to mitochondria after cleavage by caspase-8, calpains, granzyme B, or cathepsin (34,35). BAD is activated by dephosphorylation in an Akt-dependent manner (36,37). BIM is further governed by multiple mechanisms: alternative splicing, phosphorylation, and sequestration away from mitochondria (38,39). RNA interference has recently emerged as a means for regulating BMF, PUMA, & BIM (40-42).

1.4 | Two Schemes of BAX/BAK Activation

The process by which BAX/BAK transition from inactive monomers to apoptotically-proficient oligomers has been scrutinized for nearly 18 years since discovery of the first proapoptotic BCL2 family member, BCL-2 associated X protein (i.e. BAX) (43); subsequently,

BAX comrade-in-arms BAK (BCL-2 homologous antagonist/killer) was uncovered as another prodeath BCL2 member (44-46). Genetic knockout mouse models of *bax*$^{-/-}$ and *bak*$^{-/-}$ have shown the two to be largely compensatory but, when both ablated, indispensable for eliciting MOMP (22,23,47,48). With the discovery of BAX, BCL2 family governance of apoptosis (and MOMP) was initially proposed to be a rheostat, a simple ratio between BCL-2 and BAX that tilted cells from living to dying (43). This model was soon obviated by discoveries of multiple antiapoptotic, BCL-2-like proteins and the BH3-only protein subclass; genetic and biochemical evidence was marshaled in support of two succeeding models – the displacement and the direct activation schemes (28,49). The displacement model posits that BAX/BAK are intrinsically active and the proteins' oligomerization must be continually repressed via sequestration by antiapoptotics to prevent MOMP. Upon death signaling, BH3-only proteins liberate BAX/BAK from inhibitory interactions thus allowing the prodeath effectors to homooligomerize and induce MOMP. Conversely, the direct activation model provides that BAX/BAK are intrinsically nonactive and require interaction with some activating molecule (typically a BH3-only protein) to trigger the prodeath effectors' oligomerization. Accordingly, antiapoptotics sequester BH3-only proteins to preclude BAX/BAK activation and also bind BAX/BAK to prevent homooligomerization. The direct activation regime has since been further refined by the hierarchical and embedded-together schemes – the former defines three BAX/BAK direct activator BH3s (BID, BIM, & PUMA) with other BH3s serving to occupy the antiapoptotics and the latter integrating the protein conformational changes induced by membrane localization (27,50).

The origin of this rift in models of BCL2 function derives from conflicting evidence from differing experimental systems. A few lines of evidence support the displacement model (51): when first identified, overexpression of BAX and BAK resulted in mammalian cell death (43-45). Ectopic BAX expression in yeast, which have no endogenous BCL2 homologs, induces a lethal phenotype by abrogating mitochondrial respiration, an effect suppressible by co-expression of BCL-2 or BCL-X_L (52,53). Direct interactions of BH3-only proteins with BAX/BAK are difficult to detect via immunoprecipitation from cellular extracts and *in vitro* measures of BAX/BAK binding to BH3-only proteins or BH3 peptides reveal very weak affinities (54-56). Double knockout *bid*$^{-/-}$ *bim*$^{-/-}$ mouse models have unimpaired apoptosis and complementary cultured tissue experiments found that mutating antiapoptotics to prevent BAX/BAK incarceration are driven to apoptosis without stimulus (57,58).

Despite these findings, the displacement model has been largely subverted by evidence from cell-free reconstitution and other biochemical/physical assays where components are tightly coordinated. BAX applied to synthetic vesicles requires an activator BH3 peptide or BH3-only protein to efficiently induce leakage (59-61). Employment of hydrocarbon-stapled BH3 peptides (to enforce α-helicity) allowed measurement of nanomolar BAX affinities for activator BH3s BID and BIM (56) and an engineered soluble BAK construct was found by NMR to weakly bind a BID BH3 peptide (15). Perhaps most convincingly conveying the direct activation model was discovery of FRET (Förster resonance energy transfer) between labeled BAX and tBID, but only when the two proteins were bound to vesicles (62). As *in vivo* validation of the direct activation paradigm, recent work demonstrated that a *bid*$^{-/-}$ *bim*$^{-/-}$ *puma*$^{-}$

$^{-/-}$ triple knockout mouse model evoked a similar phenotype as the *bax*$^{-/-}$ *bak*$^{-/-}$ double knockout (63). Notable, however, was a disparity in embryonic lethality, with the TKO surviving postnatally with much greater success than the *bax*$^{-/-}$ *bak*$^{-/-}$ DKO, suggesting that while BID, BIM, and PUMA may provide the dominant activating function, BAX/BAK can become apoptotically proficient by other means.

Indeed, the less severe lethality of *bid*$^{-/-}$ *bim*$^{-/-}$ *puma*$^{-/-}$ TKO is not unexpected as BAX/BAK activators beyond those three BH3-only proteins have been identified. Specifically, both changes in pH and mild heat can induce BAX/BAK activity (64-66). The tumor suppressor p53 can directly interact with and activate BAX & BAK (67,68) and prostaglandins were recently shown to activate BAX (69). Nonionic detergents drastically alter BCL2 protein structure and elicit a BAX conformation that porates vesicles and isolated mitochondria (70,71). A new report employing BH3 peptides found that while BID & BIM most potently activate BAX/BAK, BMF & NOXA could also mildly activate, while PUMA, BIK, & HRK weakly activated (and BAD was completely ineffective) (72). In fact, the binary delineation between intrinsically active (on) vs. intrinsically inactive (off) may be artificial, as *in vitro* experimental regimes have shown a small degree of BAX/BAK activity on synthetic LUVs (which lack antiapoptotic defense mechanisms of mitochondria) in the absence of activators (72-75).

1.5 | Structural Details of BCL2 Interactions

During the first eight years of BCL2 study, the biochemical bases of their oppositional anti- and proapoptotic functions remained elusive. Clearly demonstrated, however, was that

homo-* and heterodimerization were decisive in the mortality decision and that BCL2 proteins localized to intracellular membranes, especially the mitochondrial outer membrane (76). BCL2 governance of mitochondrial outer membrane integrity was significantly alluded to by a pair of 1996 discoveries: 1) that egress of cytochrome *c* from the intermembrane space could induce apoptosis and 2) the elucidation of BCL-X_L structure (77,78). BCL-X_L was found to comprise a tertiary fold remarkably similar to those of bacterial pore-forming colicins A & E1 and diphtheria toxins—a central, mostly hydrophobic α-hairpin (α5-6) shielded from solution by six amphipathic α-helices. Research then coalesced around the premise that BCL2 proteins formed ion channels (79-82); subsequently, the liberation of cytochrome *c* was found to be a function of BAX and BAK and their homooligomerizations (83-87).

* [An unfortunate early diversion in the BCL2 field was discovery of BCL-2 homodimers in cell extracts (43,88). It was not until five years later that non-ionic detergents were found to substantially alter the conformations of BCL2 proteins (71,89). Homodimerizations between full-length BCL-2 and BCL-X_L isoforms were actually artifacts of extraction by non-ionic detergents (90). These detergents, like Triton X-100 or n-octylglucoside, destabilize the BCL2 core and induce eversion of their BH3 helices to allow homodimerization. These findings, however, pointed to the relevance of shortened forms of BCL-2, BCL-X_L, and MCL-1, deleted of their stabilizing BH4 domains, that genuinely expose their BH3s to allow incarceration (91-94).]

In addition to BCL-X_L, the structures of antiapoptotic BCL-2, MCL-1, BCL-w, A1, & BCL-B, proapoptotic BAX & BAK, and BH3-only BID have been solved by x-ray crystallography and NMR (15,16,95-101). The multidomain proteins all share a conformation that is strikingly similar to that of BCL-X_L; even BH3-only BID adopts an α-helical fold

reminiscent of the multidomain proteins. BID, however, is an outlier of its subclass, as other BH3-only proteins are intrinsically disordered in solution (102); BID requires proteolytic cleavage for activation which generates a carboxy-terminal p15 fragment that is α-helical but dynamically disordered when separated from its amino-terminal p7 fragment (103).

For multidomain BCL2 proteins, the conserved BH domains 1-3 define a pocket on the protein surface that can accommodate an α-helix (Fig. 1.5). Solution structures of BAX and BCL-w (& BCL-X_L) reveal that these proteins occlude this pocket with a hydrophobic C-terminal α-helix that is common to all multidomain BCL2 members and can be utilized as a membrane anchor (16,104) (Yong Yao, personal communication). Whereas proapoptotic BAX is predominantly cytosolic, its co-executioner BAK obligately associates with mitochondrial outer membranes via its C-terminus where it is incarcerated by the mitochondrial porin VDAC2 (105). Localization to membranes via tail anchor is the typical means of targeting BH3-only proteins as well (106); BID again is an exception as it lacks a lengthy C-terminal helix but employs its hydrophobic central hairpin (α6-7) to target mitochondria (107).

The hydrophobic pocket bounded at one end by BH1-2 (&3) of BCL-2 was initially identified by mutational analyses as being required for homodimerization and heterodimerization with BAX (88). A year later, BAX/BAK BH3 domains were revealed to be necessities for their homodimerizations and sequestration by antiapoptotic proteins (108,109). Solution of the BCL-X_L structure led to speculation that the pocket formed by BH1-3 (and α3-4) could act as an acceptor surface for another BH3 domain (78). This hypothesis was confirmed biochemically by the discovery of BH3-only BID, whose incarceration by BCL-2 was uncovered to be dependent on BID BH3 and the BCL-2 BH1-3 pocket (26), and structurally

by NMR of BCL-X_L bound to an α-helical BAK BH3 peptide (110) (Fig. 1.6). To date, all the major antiapoptotic BCL2 proteins have been structurally resolved, as monomers or complexed with pocket-bound BH3 peptides.

A number of studies have undertaken quantification of antiapoptotic/BH3 peptide affinities and have established that antiapoptotic BCL2 proteins promiscuously bind BH3s but with varying proclivities (101,111,112). For example, BAD is sequestered by BCL-2, BCL-X_L, and BCL-w while NOXA is restrained only by MCL-1 and A1. Nevertheless, all antiapoptotics tightly incarcerate direct activator BH3s BID, BIM, & PUMA as well as BH3s from BAX & BAK (111).

Fig. 1.5

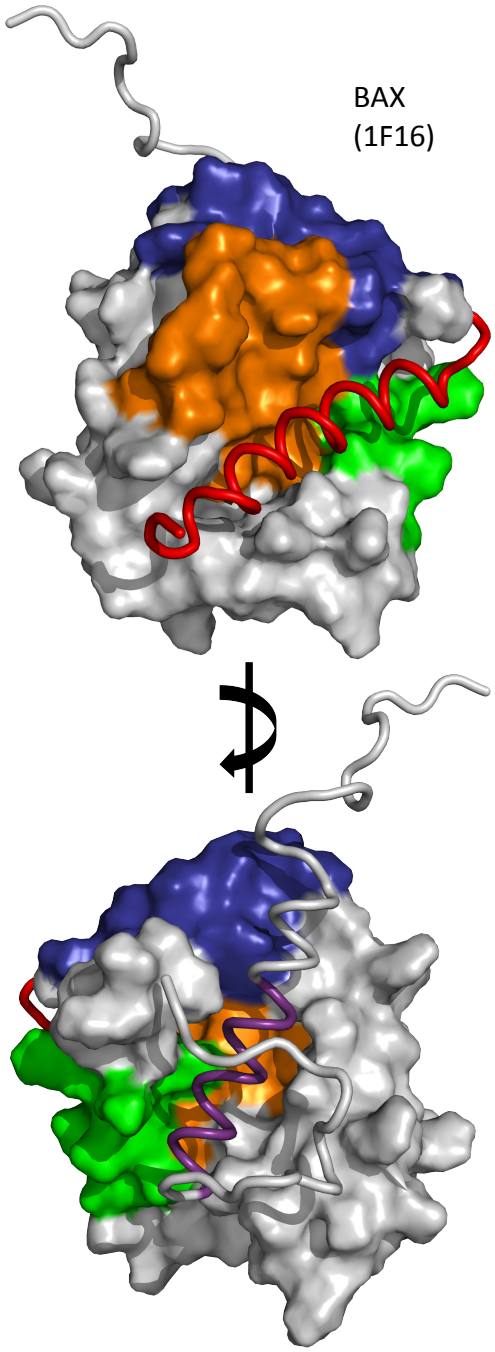

Fig. 1.5 | **BAX BH domains.** Connolly surface representations of BAX with BH domains colored as in Fig. 1.3: BH1 (orange), BH2 (blue), BH3 (green), BH4 (purple). Top panel shows BAX canonical BH3 binding groove, bounded partly by BH1-3 & occluded by its C-terminal (α9) membrane anchor. Bottom panel depicts fold-stabilizing (α1) BH4 helix.

Fig. 1.6

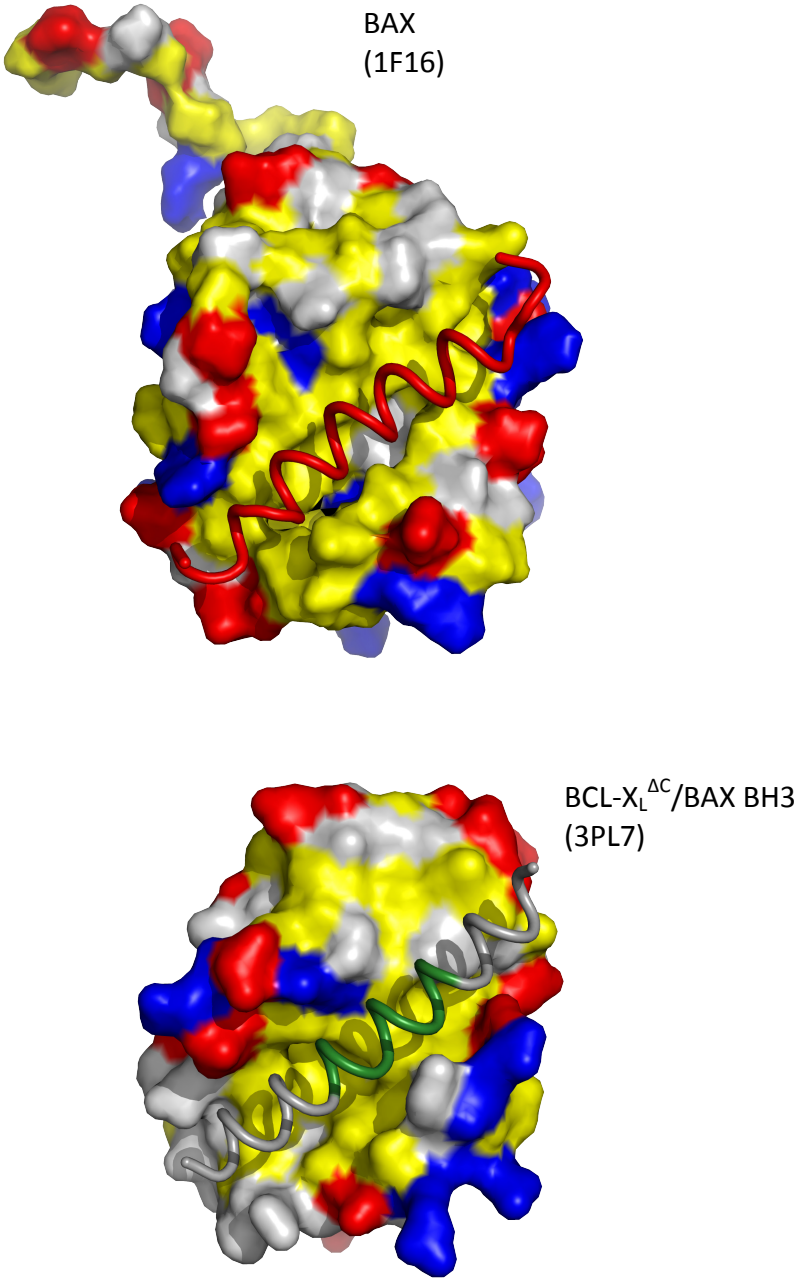

Fig. 1.6 | **Connolly surface representations of BAX & BCL-X$_L^{\Delta C}$/BAX BH3 complex.** BAX (top) in solution occludes its canonical BH3 binding pocket with a C-terminal membrane anchor (red). BCL-X$_L^{\Delta C}$ (bottom) sequestering a BAX BH3 peptide. Helices are colored similar to Fig. 1.3. Surface residues are pigmented: polar (grey), nonpolar (yellow), acidic (red), basic (blue).

The BH4 region, identified last and least conserved sequentially, embodies the first α-helix of the BCL2 core and is structurally distant from the hydrophobic pocket defined by BH1-3 (113,114) (Fig. 1.5). BH4, however, acts to stabilize the overall fold of the proteins (78,97,115). When the BH4 domain is proteolytically-cleaved from BCL-2, the protein reverses its anti-death role and becomes proapoptotic (116). Nuclear receptor Nur77 has been shown to bind BCL-2; this interaction triggers BH4 disengagement, BH3 eversion, and allows heterodimerization with BCL-X_L (93,94). BCL-X_S and MCL-1_S, uncommon splicing variants which delete BH1 & 2, heterodimerize with and antagonize full-length BCL-X_L and MCL-1 respectively (91,92). Proteolytic removal of BH4 from proapoptotic BAX has also been suggested to render the protein non-functional as a pore-former but retains antagonism of antiapoptotics (117). In neurons, BAK can be regulated by mRNA splicing, resulting in a protein that lacks BH1 & 2 and functions like a BH3-only signaler (118). These findings collectively uncover that multidomain BCL2 members can be transmuted into prodeath, BH3-only-like proteins by post-transcriptional and -translational mechanisms. Their relevance in cellular mortality decisions, however, is not well-plumbed.

What is clear is that BAX & BAK activation to pore competence encompasses multiple conformational intermediates (Fig. 1.1; detailed further in Appendix I). For instance, BAX targeting to membranes is consequential of exposure of the C-terminal α9 helix and this exposure correlates to eversion of the N-terminal α1 (119,120). The two pore-forming effectors evict their BH3 helices, normally packed against α5.6, for homodimerization or sequestration by antiapoptotic proteins (75,110,111,121) (Fig. 1.6). These rearrangements result in membrane insertion of the α5-6 hairpin to disrupt bilayer integrity (73,122,123).

1.6 | References

1. Danial, N. N., and Korsmeyer, S. J. (2004) *Cell* **116**, 205-219
2. Kerr, J. F., Wyllie, A. H., and Currie, A. R. (1972) *Br J Cancer* **26**, 239-257
3. Thompson, C. B. (1995) *Science* **267**, 1456-1462
4. Thornberry, N. A., and Lazebnik, Y. (1998) *Science* **281**, 1312-1316
5. Spencer, S. L., Gaudet, S., Albeck, J. G., Burke, J. M., and Sorger, P. K. (2009) *Nature* **459**, 428-432
6. Wang, X. (2001) *Genes Dev* **15**, 2922-2933
7. Shi, Y. (2006) *Curr Opin Cell Biol* **18**, 677-684
8. Ravagnan, L., Roumier, T., and Kroemer, G. (2002) *J Cell Physiol* **192**, 131-137
9. Verhagen, A. M., and Vaux, D. L. (2002) *Apoptosis* **7**, 163-166
10. Barnhart, B. C., Alappat, E. C., and Peter, M. E. (2003) *Seminars in Immunology* **15**, 185-193
11. Cory, S., Huang, D. C., and Adams, J. M. (2003) *Oncogene* **22**, 8590-8607
12. Petros, A. M., Olejniczak, E. T., and Fesik, S. W. (2004) *Biochim Biophys Acta* **1644**, 83-94
13. Kvansakul, M., Yang, H., Fairlie, W. D., Czabotar, P. E., Fischer, S. F., Perugini, M. A., Huang, D. C., and Colman, P. M. (2008) *Cell Death Differ* **15**, 1564-1571
14. Borner, C. (2003) *Mol Immunol* **39**, 615-647
15. Moldoveanu, T., Liu, Q., Tocilj, A., Watson, M., Shore, G., and Gehring, K. (2006) *Mol Cell* **24**, 677-688
16. Suzuki, M., Youle, R. J., and Tjandra, N. (2000) *Cell* **103**, 645-654
17. Griffiths, G. J., Dubrez, L., Morgan, C. P., Jones, N. A., Whitehouse, J., Corfe, B. M., Dive, C., and Hickman, J. A. (1999) *J Cell Biol* **144**, 903-914
18. Hsu, Y. T., Wolter, K. G., and Youle, R. J. (1997) *Proc Natl Acad Sci U S A* **94**, 3668-3672
19. Wolter, K. G., Hsu, Y. T., Smith, C. L., Nechushtan, A., Xi, X. G., and Youle, R. J. (1997) *J Cell Biol* **139**, 1281-1292
20. Korsmeyer, S. J., Wei, M. C., Saito, M., Weiler, S., Oh, K. J., and Schlesinger, P. H. (2000) *Cell Death Differ* **7**, 1166-1173
21. Cheng, E. H., Wei, M. C., Weiler, S., Flavell, R. A., Mak, T. W., Lindsten, T., and Korsmeyer, S. J. (2001) *Mol Cell* **8**, 705-711
22. Lindsten, T., Ross, A. J., King, A., Zong, W. X., Rathmell, J. C., Shiels, H. A., Ulrich, E., Waymire, K. G., Mahar, P., Frauwirth, K., Chen, Y., Wei, M., Eng, V. M., Adelman, D. M., Simon, M. C., Ma, A., Golden, J. A., Evan, G., Korsmeyer, S. J., MacGregor, G. R., and Thompson, C. B. (2000) *Mol Cell* **6**, 1389-1399
23. Wei, M. C., Zong, W. X., Cheng, E. H., Lindsten, T., Panoutsakopoulou, V., Ross, A. J., Roth, K. A., MacGregor, G. R., Thompson, C. B., and Korsmeyer, S. J. (2001) *Science* **292**, 727-730

24. Boyd, J. M., Gallo, G. J., Elangovan, B., Houghton, A. B., Malstrom, S., Avery, B. J., Ebb, R. G., Subramanian, T., Chittenden, T., Lutz, R. J., and et al. (1995) *Oncogene* **11**, 1921-1928
25. Kelekar, A., Chang, B. S., Harlan, J. E., Fesik, S. W., and Thompson, C. B. (1997) *Mol Cell Biol* **17**, 7040-7046
26. Wang, K., Yin, X. M., Chao, D. T., Milliman, C. L., and Korsmeyer, S. J. (1996) *Genes Dev* **10**, 2859-2869
27. Kim, H., Rafiuddin-Shah, M., Tu, H. C., Jeffers, J. R., Zambetti, G. P., Hsieh, J. J., and Cheng, E. H. (2006) *Nat Cell Biol* **8**, 1348-1358
28. Letai, A., Bassik, M. C., Walensky, L. D., Sorcinelli, M. D., Weiler, S., and Korsmeyer, S. J. (2002) *Cancer Cell* **2**, 183-192
29. Dijkers, P. F., Medema, R. H., Lammers, J. W., Koenderman, L., and Coffer, P. J. (2000) *Curr Biol* **10**, 1201-1204
30. Mathai, J. P., Germain, M., Marcellus, R. C., and Shore, G. C. (2002) *Oncogene* **21**, 2534-2544
31. Nakano, K., and Vousden, K. H. (2001) *Mol Cell* **7**, 683-694
32. Oda, E., Ohki, R., Murasawa, H., Nemoto, J., Shibue, T., Yamashita, T., Tokino, T., Taniguchi, T., and Tanaka, N. (2000) *Science* **288**, 1053-1058
33. Real, P. J., Benito, A., Cuevas, J., Berciano, M. T., de Juan, A., Coffer, P., Gomez-Roman, J., Lafarga, M., Lopez-Vega, J. M., and Fernandez-Luna, J. L. (2005) *Cancer Res* **65**, 8151-8157
34. Cullen, S. P., Adrain, C., Luthi, A. U., Duriez, P. J., and Martin, S. J. (2007) *J Cell Biol* **176**, 435-444
35. Li, H., Zhu, H., Xu, C. J., and Yuan, J. (1998) *Cell* **94**, 491-501
36. Datta, S. R., Dudek, H., Tao, X., Masters, S., Fu, H., Gotoh, Y., and Greenberg, M. E. (1997) *Cell* **91**, 231-241
37. Zha, J., Harada, H., Yang, E., Jockel, J., and Korsmeyer, S. J. (1996) *Cell* **87**, 619-628
38. O'Connor, L., Strasser, A., O'Reilly, L. A., Hausmann, G., Adams, J. M., Cory, S., and Huang, D. C. (1998) *Embo J* **17**, 384-395
39. Puthalakath, H., Huang, D. C., O'Reilly, L. A., King, S. M., and Strasser, A. (1999) *Mol Cell* **3**, 287-296
40. Gramantieri, L., Fornari, F., Ferracin, M., Veronese, A., Sabbioni, S., Calin, G. A., Grazi, G. L., Croce, C. M., Bolondi, L., and Negrini, M. (2009) *Clin Cancer Res* **15**, 5073-5081
41. Terasawa, K., Ichimura, A., Sato, F., Shimizu, K., and Tsujimoto, G. (2009) *Febs J* **276**, 3269-3276
42. Zhang, C. Z., Zhang, J. X., Zhang, A. L., Shi, Z. D., Han, L., Jia, Z. F., Yang, W. D., Wang, G. X., Jiang, T., You, Y. P., Pu, P. Y., Cheng, J. Q., and Kang, C. S. (2010) *Mol Cancer* **9**, 229
43. Oltvai, Z. N., Milliman, C. L., and Korsmeyer, S. J. (1993) *Cell* **74**, 609-619

44. Chittenden, T., Harrington, E. A., O'Connor, R., Flemington, C., Lutz, R. J., Evan, G. I., and Guild, B. C. (1995) *Nature* **374**, 733-736
45. Kiefer, M. C., Brauer, M. J., Powers, V. C., Wu, J. J., Umansky, S. R., Tomei, L. D., and Barr, P. J. (1995) *Nature* **374**, 736-739
46. Farrow, S. N., White, J. H., Martinou, I., Raven, T., Pun, K. T., Grinham, C. J., Martinou, J. C., and Brown, R. (1995) *Nature* **374**, 731-733
47. Knudson, C. M., Tung, K. S., Tourtellotte, W. G., Brown, G. A., and Korsmeyer, S. J. (1995) *Science* **270**, 96-99
48. Zong, W. X., Lindsten, T., Ross, A. J., MacGregor, G. R., and Thompson, C. B. (2001) *Genes Dev* **15**, 1481-1486
49. Willis, S. N., and Adams, J. M. (2005) *Curr Opin Cell Biol* **17**, 617-625
50. Leber, B., Lin, J., and Andrews, D. W. (2007) *Apoptosis* **12**, 897-911
51. Adams, J. M., and Cory, S. (2007) *Curr Opin Immunol* **19**, 488-496
52. Hanada, M., Aime-Sempe, C., Sato, T., and Reed, J. C. (1995) *J Biol Chem* **270**, 11962-11969
53. Greenhalf, W., Stephan, C., and Chaudhuri, B. (1996) *FEBS Lett* **380**, 169-175
54. Youle, R. J. (2007) *Science* **315**, 776-777
55. Kuwana, T., Bouchier-Hayes, L., Chipuk, J. E., Bonzon, C., Sullivan, B. A., Green, D. R., and Newmeyer, D. D. (2005) *Mol Cell* **17**, 525-535
56. Walensky, L. D., Pitter, K., Morash, J., Oh, K. J., Barbuto, S., Fisher, J., Smith, E., Verdine, G. L., and Korsmeyer, S. J. (2006) *Mol Cell* **24**, 199-210
57. Willis, S. N., Chen, L., Dewson, G., Wei, A., Naik, E., Fletcher, J. I., Adams, J. M., and Huang, D. C. (2005) *Genes Dev* **19**, 1294-1305
58. Willis, S. N., Fletcher, J. I., Kaufmann, T., van Delft, M. F., Chen, L., Czabotar, P. E., Ierino, H., Lee, E. F., Fairlie, W. D., Bouillet, P., Strasser, A., Kluck, R. M., Adams, J. M., and Huang, D. C. (2007) *Science* **315**, 856-859
59. Kuwana, T., Mackey, M. R., Perkins, G., Ellisman, M. H., Latterich, M., Schneiter, R., Green, D. R., and Newmeyer, D. D. (2002) *Cell* **111**, 331-342
60. Oh, K. J., Barbuto, S., Meyer, N., Kim, R. S., Collier, R. J., and Korsmeyer, S. J. (2005) *J Biol Chem* **280**, 753-767
61. Terrones, O., Antonsson, B., Yamaguchi, H., Wang, H. G., Liu, J., Lee, R. M., Herrmann, A., and Basanez, G. (2004) *J Biol Chem* **279**, 30081-30091
62. Lovell, J. F., Billen, L. P., Bindner, S., Shamas-Din, A., Fradin, C., Leber, B., and Andrews, D. W. (2008) *Cell* **135**, 1074-1084
63. Ren, D., Tu, H. C., Kim, H., Wang, G. X., Bean, G. R., Takeuchi, O., Jeffers, J. R., Zambetti, G. P., Hsieh, J. J., and Cheng, E. H. (2010) *Science* **330**, 1390-1393
64. Cartron, P. F., Oliver, L., Mayat, E., Meflah, K., and Vallette, F. M. (2004) *FEBS Lett* **578**, 41-46
65. Khaled, A. R., Kim, K., Hofmeister, R., Muegge, K., and Durum, S. K. (1999) *Proc Natl Acad Sci U S A* **96**, 14476-14481

66. Pagliari, L. J., Kuwana, T., Bonzon, C., Newmeyer, D. D., Tu, S., Beere, H. M., and Green, D. R. (2005) *Proc Natl Acad Sci U S A* **102**, 17975-17980
67. Chipuk, J. E., Kuwana, T., Bouchier-Hayes, L., Droin, N. M., Newmeyer, D. D., Schuler, M., and Green, D. R. (2004) *Science* **303**, 1010-1014
68. Leu, J. I., Dumont, P., Hafey, M., Murphy, M. E., and George, D. L. (2004) *Nat Cell Biol* **6**, 443-450
69. Lalier, L., Cartron, P. F., Olivier, C., Loge, C., Bougras, G., Robert, J. M., Oliver, L., and Vallette, F. M. (2010) *Cell Death Differ*
70. Antonsson, B., Montessuit, S., Lauper, S., Eskes, R., and Martinou, J. C. (2000) *Biochem J* **345 Pt 2**, 271-278
71. Hsu, Y. T., and Youle, R. J. (1997) *J Biol Chem* **272**, 13829-13834
72. Du, H., Wolf, J., Schafer, B., Moldoveanu, T., Chipuk, J. E., and Kuwana, T. (2011) *J Biol Chem* **286**, 491-501
73. Oh, K. J., Barbuto, S., Pitter, K., Morash, J., Walensky, L. D., and Korsmeyer, S. J. (2006) *J Biol Chem* **281**, 36999-37008
74. Oh, K. J., Singh, P., Lee, K., Foss, K., Lee, S., Park, M., Aluvila, S., Kim, R. S., Symersky, J., and Walters, D. E. (2010) *J Biol Chem* **285**, 28924-28937
75. Bleicken, S., Classen, M., Padmavathi, P. V., Ishikawa, T., Zeth, K., Steinhoff, H. J., and Bordignon, E. (2010) *J Biol Chem* **285**, 6636-6647
76. Yang, E., and Korsmeyer, S. J. (1996) *Blood* **88**, 386-401
77. Liu, X., Kim, C. N., Yang, J., Jemmerson, R., and Wang, X. (1996) *Cell* **86**, 147-157
78. Muchmore, S. W., Sattler, M., Liang, H., Meadows, R. P., Harlan, J. E., Yoon, H. S., Nettesheim, D., Chang, B. S., Thompson, C. B., Wong, S. L., Ng, S. L., and Fesik, S. W. (1996) *Nature* **381**, 335-341
79. Antonsson, B., Conti, F., Ciavatta, A., Montessuit, S., Lewis, S., Martinou, I., Bernasconi, L., Bernard, A., Mermod, J. J., Mazzei, G., Maundrell, K., Gambale, F., Sadoul, R., and Martinou, J. C. (1997) *Science* **277**, 370-372
80. Minn, A. J., Velez, P., Schendel, S. L., Liang, H., Muchmore, S. W., Fesik, S. W., Fill, M., and Thompson, C. B. (1997) *Nature* **385**, 353-357
81. Schendel, S. L., Xie, Z., Montal, M. O., Matsuyama, S., Montal, M., and Reed, J. C. (1997) *Proc Natl Acad Sci U S A* **94**, 5113-5118
82. Schlesinger, P. H., Gross, A., Yin, X. M., Yamamoto, K., Saito, M., Waksman, G., and Korsmeyer, S. J. (1997) *Proc Natl Acad Sci U S A* **94**, 11357-11362
83. Eskes, R., Antonsson, B., Osen-Sand, A., Montessuit, S., Richter, C., Sadoul, R., Mazzei, G., Nichols, A., and Martinou, J. C. (1998) *J Cell Biol* **143**, 217-224
84. Jurgensmeier, J. M., Xie, Z., Deveraux, Q., Ellerby, L., Bredesen, D., and Reed, J. C. (1998) *Proc Natl Acad Sci U S A* **95**, 4997-5002
85. Rosse, T., Olivier, R., Monney, L., Rager, M., Conus, S., Fellay, I., Jansen, B., and Borner, C. (1998) *Nature* **391**, 496-499

86. Wei, M. C., Lindsten, T., Mootha, V. K., Weiler, S., Gross, A., Ashiya, M., Thompson, C. B., and Korsmeyer, S. J. (2000) *Genes Dev* **14**, 2060-2071
87. Eskes, R., Desagher, S., Antonsson, B., and Martinou, J. C. (2000) *Mol Cell Biol* **20**, 929-935
88. Yin, X. M., Oltvai, Z. N., and Korsmeyer, S. J. (1994) *Nature* **369**, 321-323
89. Hsu, Y. T., and Youle, R. J. (1998) *J Biol Chem* **273**, 10777-10783
90. Conus, S., Kaufmann, T., Fellay, I., Otter, I., Rosse, T., and Borner, C. (2000) *Embo J* **19**, 1534-1544
91. Bae, J., Leo, C. P., Hsu, S. Y., and Hsueh, A. J. (2000) *J Biol Chem* **275**, 25255-25261
92. Chang, B. S., Kelekar, A., Harris, M. H., Harlan, J. E., Fesik, S. W., and Thompson, C. B. (1999) *Mol Cell Biol* **19**, 6673-6681
93. Kolluri, S. K., Zhu, X., Zhou, X., Lin, B., Chen, Y., Sun, K., Tian, X., Town, J., Cao, X., Lin, F., Zhai, D., Kitada, S., Luciano, F., O'Donnell, E., Cao, Y., He, F., Lin, J., Reed, J. C., Satterthwait, A. C., and Zhang, X. K. (2008) *Cancer Cell* **14**, 285-298
94. Lin, B., Kolluri, S. K., Lin, F., Liu, W., Han, Y. H., Cao, X., Dawson, M. I., Reed, J. C., and Zhang, X. K. (2004) *Cell* **116**, 527-540
95. Chou, J. J., Li, H., Salvesen, G. S., Yuan, J., and Wagner, G. (1999) *Cell* **96**, 615-624
96. McDonnell, J. M., Fushman, D., Milliman, C. L., Korsmeyer, S. J., and Cowburn, D. (1999) *Cell* **96**, 625-634
97. Petros, A. M., Medek, A., Nettesheim, D. G., Kim, D. H., Yoon, H. S., Swift, K., Matayoshi, E. D., Oltersdorf, T., and Fesik, S. W. (2001) *Proc Natl Acad Sci U S A* **98**, 3012-3017
98. Day, C. L., Chen, L., Richardson, S. J., Harrison, P. J., Huang, D. C., and Hinds, M. G. (2005) *J Biol Chem* **280**, 4738-4744
99. Hinds, M. G., Lackmann, M., Skea, G. L., Harrison, P. J., Huang, D. C., and Day, C. L. (2003) *Embo J* **22**, 1497-1507
100. Rautureau, G. J., Day, C. L., and Hinds, M. G. (2010) *Proteins* **78**, 2181-2186
101. Smits, C., Czabotar, P. E., Hinds, M. G., and Day, C. L. (2008) *Structure* **16**, 818-829
102. Hinds, M. G., Smits, C., Fredericks-Short, R., Risk, J. M., Bailey, M., Huang, D. C., and Day, C. L. (2006) *Cell Death Differ*
103. Yao, Y., Bobkov, A. A., Plesniak, L. A., and Marassi, F. M. (2009) *Biochemistry* **48**, 8704-8711
104. Denisov, A. Y., Madiraju, M. S., Chen, G., Khadir, A., Beauparlant, P., Attardo, G., Shore, G. C., and Gehring, K. (2003) *J Biol Chem* **278**, 21124-21128
105. Cheng, E. H., Sheiko, T. V., Fisher, J. K., Craigen, W. J., and Korsmeyer, S. J. (2003) *Science* **301**, 513-517
106. Shamas-Din, A., Brahmbhatt, H., Leber, B., and Andrews, D. W. *Biochimica et Biophysica Acta (BBA) - Molecular Cell Research* **In Press, Corrected Proof**
107. Hu, X., Han, Z., Wyche, J. H., and Hendrickson, E. A. (2003) *Apoptosis* **8**, 277-289

108. Chittenden, T., Flemington, C., Houghton, A. B., Ebb, R. G., Gallo, G. J., Elangovan, B., Chinnadurai, G., and Lutz, R. J. (1995) *Embo J* **14**, 5589-5596
109. Zha, H., Aime-Sempe, C., Sato, T., and Reed, J. C. (1996) *J Biol Chem* **271**, 7440-7444
110. Sattler, M., Liang, H., Nettesheim, D., Meadows, R. P., Harlan, J. E., Eberstadt, M., Yoon, H. S., Shuker, S. B., Chang, B. S., Minn, A. J., Thompson, C. B., and Fesik, S. W. (1997) *Science* **275**, 983-986
111. Ku, B., Liang, C., Jung, J. U., and Oh, B. H. (2010) *Cell Res*
112. Chen, L., Willis, S. N., Wei, A., Smith, B. J., Fletcher, J. I., Hinds, M. G., Colman, P. M., Day, C. L., Adams, J. M., and Huang, D. C. (2005) *Mol Cell* **17**, 393-403
113. Borner, C., Martinou, I., Mattmann, C., Irmler, M., Schaerer, E., Martinou, J. C., and Tschopp, J. (1994) *J Cell Biol* **126**, 1059-1068
114. Hunter, J. J., Bond, B. L., and Parslow, T. G. (1996) *Mol Cell Biol* **16**, 877-883
115. Hirotani, M., Zhang, Y., Fujita, N., Naito, M., and Tsuruo, T. (1999) *J Biol Chem* **274**, 20415-20420
116. Cheng, E. H., Kirsch, D. G., Clem, R. J., Ravi, R., Kastan, M. B., Bedi, A., Ueno, K., and Hardwick, J. M. (1997) *Science* **278**, 1966-1968
117. Cartron, P. F., Oliver, L., Juin, P., Meflah, K., and Vallette, F. M. (2004) *J Biol Chem* **279**, 11503-11512
118. Uo, T., Kinoshita, Y., and Morrison, R. S. (2005) *J Biol Chem* **280**, 9065-9073
119. Goping, I. S., Gross, A., Lavoie, J. N., Nguyen, M., Jemmerson, R., Roth, K., Korsmeyer, S. J., and Shore, G. C. (1998) *J Cell Biol* **143**, 207-215
120. Kim, H., Tu, H. C., Ren, D., Takeuchi, O., Jeffers, J. R., Zambetti, G. P., Hsieh, J. J., and Cheng, E. H. (2009) *Mol Cell* **36**, 487-499
121. Dewson, G., Kratina, T., Sim, H. W., Puthalakath, H., Adams, J. M., Colman, P. M., and Kluck, R. M. (2008) *Mol Cell* **30**, 369-380
122. Annis, M. G., Soucie, E. L., Dlugosz, P. J., Cruz-Aguado, J. A., Penn, L. Z., Leber, B., and Andrews, D. W. (2005) *Embo J* **24**, 2096-2103
123. Heimlich, G., McKinnon, A. D., Bernardo, K., Brdiczka, D., Reed, J. C., Kain, R., Kronke, M., and Jurgensmeier, J. M. (2004) *Biochem J* **378**, 247-255

CHAPTER 2

Cholesterol Effects on BAX Pore Activation

(The content of this chapter has been adapted from Christenson E., Merlin, S., Saito, M., Schlesinger, P. (2008) *J Mol Biol* 381, 1168-1183)

2.1 | Summary

The importance of BCL2 family proteins in the control of cell death has been clearly established. One of the key members of this family, BAX, has soluble, membrane-bound, and membrane-integrated forms that are central to the regulation of apoptosis. Using purified monomeric human BAX, defined liposomes, and isolated human mitochondria, we have characterized the soluble to membrane transition and pore formation by this protein. For the purified protein, activation, but not oligomerization, is required for membrane binding. The transition to the membrane environment includes a binding step that is reversible and distinct from the membrane integration step. Oligomerization and pore activation occur after the membrane integration. In cells, BAX targets several intracellular membranes but notably does not target the plasma membrane while initiating apoptosis. When cholesterol was added to either the liposome bilayer or mitochondrial membranes, we observed increased binding but markedly reduced integration of BAX into both membranes. This cholesterol inhibition of membrane integration accounts for the reduction of BAX pore activation in liposomes and mitochondrial membranes. Our results indicate that the presence of cholesterol in membranes inhibits the pore-forming activity of BAX by reducing the ability of BAX to transition from a membrane-associated protein to a membrane-integral protein.

2.2 | Introduction

Genetically programmed apoptotic cell death occurs in all multicellular organisms (1). Control of the death decision prominently involves a three-part regulatory ensemble of proteins, the BCL2 family (2). Twenty-five genes comprise this family and they generate three functional classes of proteins: proapoptotic and antiapoptotic actors with a supporting cast of BH3-only proteins that modulate their interaction (3,4). To function as the apoptotic decision agent, these proteins collaborate to form a gateway, "pore", in the outer mitochondrial membrane (OMM) (5-7). The formation of this pore requires the availability of active and uninhibited BAK or BAX in the OMM (8). BAX and many of the other proteins are soluble and move to the mitochondrial outer membrane in concert with the death signaling (9,10). Others have demonstrated the formation of BAX homo-oligomers in mitochondria and inferred a correlation with a mortality decision in the OMM (11-14). However, the nature of the BCL2 family protein interactions while in membranes is not clear. Furthermore, the molecular events and environmental conditions that trigger BAX transformation to an active state have remained elusive. Recent studies have indicated that suppression of BAX inhibition is critical in the mortality decision (15-17). While it is possible that negative regulation is a dominant theme in apoptosis, this gives no explanation of the mechanism by which BAX becomes situated in the OMMs and is availed of the negative regulation. Furthermore, if the regulation is entirely negative by antiapoptotic BCL2 family members in the OMM, then the escape of the remaining and vastly larger membrane surface of the cell from BAX predation is a mystery.

Both pore-forming and regulatory interactions of BCL2 family proteins occur at the mitochondrial outer membrane. Previously, we have shown that one proapoptotic protein, genetically engineered active BAX ($BAX^{\Delta C}$), can form large pores in planar lipid bilayers (18). Subsequently, we characterized these pores in defined liposomes as consisting of dimers and tetramers of $BAX^{\Delta C}$. The tetrameric pore was able to accommodate cytochrome *c* for release from the liposome (19). From the kinetics of pore activation upon addition of soluble monomeric $BAX^{\Delta C}$, we concluded that the oligomerization into pores occurred after membrane insertion and postulated that it would be dependent upon the membrane environment. Therefore, we have undertaken studies to explore the role of membrane lipids on BCL2 family protein pore activation.

In these studies, we have determined the $BAX^{\Delta C}$ pore activation in the presence of cholesterol and the enantiomer of cholesterol (20). Cholesterol is necessary for membrane function in eukaryotic cells, but the chemical and physical basis for the cholesterol requirement remains unclear (21). Cholesterol is synthesized in the endoplasmic reticulum and is internalized with the plasma membrane and by receptor-mediated endocytosis. From both the endoplasmic reticulum and the late endosomal pathway, cholesterol enters other compartments of the cell (22). In steroidogenic tissues, for example, adrenal and placenta, hormone production is initiated by side-chain cleavage in the mitochondrial matrix (23,24). In other cells, mitochondrial cholesterol oxidation occurs at lower rates but can become pathogenic when the cells are cholesterol overloaded (25). When cholesterol is taken up by mitochondria, it first resides in the OMM and is then transferred through the contact sites using the

peripheral benzodiazepine receptor to the matrix for oxidation (26,27). It has been suggested that movement of cholesterol from the OMM to the inner mitochondrial membrane, where oxidation occurs, is facilitated by a cholesterol recognition/ interaction amino acid consensus motif that is observed in the peripheral benzodiazepine receptor (28). In mammalian cells, the plasma membrane has the highest cholesterol content but significant cholesterol, oxysterols, and bile acids are found in the mitochondria because of the matrix oxidative production of these steroids (29,30). Cholesterol has been reported to be elevated in cultured tumor cells (31,32). Recently, bilayer cholesterol content has been shown to influence BAX oligomerization and trypsin resistance in liposomes and mitochondria (33). Others have reported complex relationships among lipids, cholesterol, BAX, and permeability transition pore activation (34). These observations have been used to explain the effects of cholesterol upon cellular apoptosis. We have studied the effect of cholesterol on BAX pore formation in liposomes and mitochondria and conclude that the cholesterol content of the plasma membrane protects it from the pore formation when BAX is activated. In particular, the addition of cholesterol to the outer membrane of mitochondria inhibits pore formation by BAX. We discuss the mechanism of cholesterol inhibition of BAX pore activation in terms of membrane binding and integration and speculate on how this might influence apoptosis in mammalian cells.

2.3 | Results

Although the BCL2 family proteins are clearly the arbiters of a mortality decision, the biochemical steps that conclude in the mitochondrial death decision are not yet clear. We have pursued a reconstitution methodology to study these phenomena in order to clearly define the biochemical and biophysical processes in the reaction steps leading to the initiation of apoptosis. Initially, these studies revealed that a carboxy-terminally truncated form of active BAX, $BAX^{\Delta C}$, could form a cytochrome *c* competent pore in liposomes (19). Hill analysis revealed that in liposomes, active $BAX^{\Delta C}$ inserted into the membrane as a monomer, formed a functioning pore as a dimer, and displayed a concentration-dependent progression to a tetramer complex that transferred cytochrome *c* out of the liposomes. We are revisiting this method of analysis in order to study the effects of lipid environment on BAX membrane integration and pore formation.

Human BAX expression, purification, and studies of pore activation

Native BAX in mammalian cells is a soluble protein that must be activated to induce apoptosis (3,35). This protein can be activated *in vitro* in several ways. In this study, we have used a genetically-engineered form of active human BAX, $BAX^{\Delta C}$, which has a portion of the α-helix 9 removed. In 0.1% n-octylglucoside, this form of human $BAX^{\Delta C}$ is monomeric with a molecular weight of 19,000 ± 1200 Da as determined by dynamic light scattering and SDS-PAGE (Fig. 2.1A). In these studies, we used the human $BAX^{\Delta C}$ because we would employ human mitochondria to study pore formation in these organelles. The pore activation and stoichiometry of human $BAX^{\Delta C}$ have not been previously reported. The human and mouse

BAX proteins are very similar in sequence but arginine 64 in the critical BH3 region is replaced with a lysine. In addition, there is a rearrangement of the prolines adjacent to the first α-helix (residues 46–53). Proteolytic cleavage and phosphorylation in this region of BAX influence the mitochondrial translocation and pore formation (36,37).

We concluded that confirmation of a similar mechanism of pore formation by the human protein was warranted. Using liposomes loaded with carboxyfluorescein (CF) at quenching concentrations, we studied the activation of pores by human $BAX^{\Delta C}$ (Fig. 2.1B). The time-series data normalized to the total dequenching for each preparation of liposomes are an exponential release. This is consistent with a single pore producing full dequenching from a liposome and the exponential time course representing pore activation in the liposomes. The measured time constants were used in a Hill analysis of the human $BAX^{\Delta C}$ pore activation (Fig. 2.1C). The concentration dependence of human $BAX^{\Delta C}$ activation in liposomes indicates a pore activation stoichiometry of 2 and 4, similar to the previously published model for the murine protein (19).

Fig. 2.1

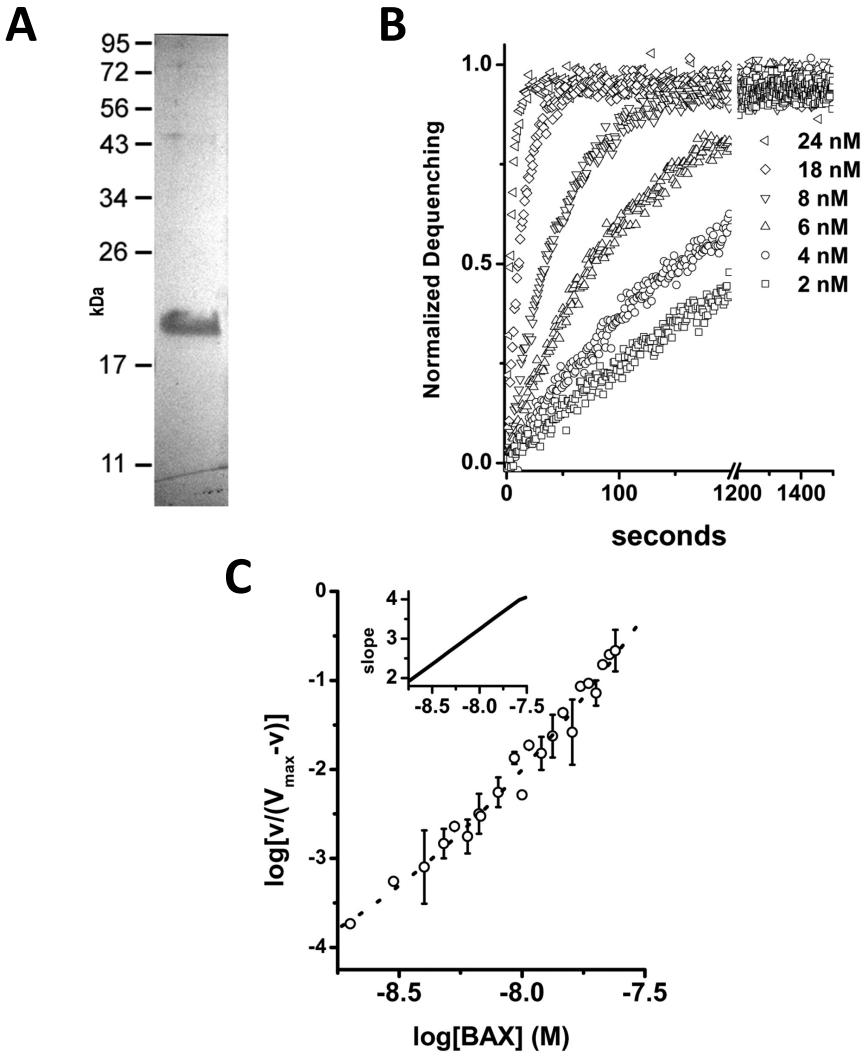

Fig. 2.1 | **Human BAX$^{\Delta C}$ pore-forming activity in liposomes.** Using human BAX$^{\Delta C}$, we studied the kinetics of pore activation in liposomes by the purified protein. The liposome assay was done as previously described (19). *A*, Preparation of human BAX$^{\Delta C}$ expressed and purified as described in Materials and Methods and run on SDS-PAGE gel to demonstrate size and purity. *B*, Time-series examples of human BAX$^{\Delta C}$ pore activation as added protein concentration is increased. Using the time-series data curve fitting to an exponential function, we determined the time constant and the extent of release. *C*, The time constants determined from the time series and concentration dependence of pore activation were subjected to Hill analysis. Each plotted point represents the average of two to three determinations with standard deviations shown when they were bigger than the symbol. The data were fitted to a polynomial using the Levenberg–Marquardt algorithm. The slope of the fitted line was determined at each point and is plotted in the inset graph.

Mitochondrial preparation for the study of OMM permeability

The permeability of the OMM is a key factor in the apoptosis death decision (38). These studies have used HeLa cell mitochondria and human BAX protein. We have adapted the fusion of liposomes with purified mitochondria to create a preparation for the study of OMM permeability (39,40). The unfused liposomes were removed by low-speed pelleting of the resulting mitochondria. The fused mitochondria (fM) have a normal double-membrane morphology (Fig. 2.2A). The captured CF produced photoconversion of diaminobenzidine and electron-dense deposition in the intermembrane space (Fig. 2.2A, photoconverted). CF-containing mitochondria and liposomes were identified by this method, but the insoluble photoconversion product obscures the membranes (41,42).

Cytochrome *c*-dependent oxygen consumption can be used to evaluate the continuity of the OMM (43). When our preparation was studied using a Clark electrode to determine site IV-dependent oxygen consumption in the presence of saturating substrate and oxygen, they consumed 43.1 ± 0.4 nAtom mg^{-1} min^{-1}, which is similar to that of rat liver mitochondria (48.5 ± 0.4 nAtom mg^{-1} min^{-1}) but less than that of skeletal muscle or kidney mitochondria (44). This rate of oxygen uptake suggests that in the preparation, the OMM is intact and cytochrome *c* is retained within the intermembrane space. Using the membrane-active peptide melittin, we interrupted the uptake of oxygen by the mitochondria as shown in Fig. 2.2B. This reduction is reversed by the addition of 100 μM horse cytochrome *c* to the electrode chamber. The oxygen consumption in these preparations is dependent upon ADP and phosphate and is

sensitive to azide. We conclude that our isolated mitochondria have an intact OMM and that cytochrome *c* is retained during the isolation procedure.

Ca^{2+} dependence of fM permeability

The fM preparation was performed in media containing ethylene glycol bis(β-aminoethyl ether)N,N′-tetraacetic acid (EGTA) so that Ca^{2+} concentration is less than 10 nM. At this low calcium concentration, the CF is retained within the OMM barrier. Increasing the media calcium to 100 or 200 μM initiated rapid dequenching of the CF from the intermembrane space (Fig. 2.2C). Dequenching is normalized to the maximum dequenching produced by 1% Triton X-100. The dequenching is rapid and dependent upon calcium concentration and is consistent with activation of the voltage-dependent anion-selective channel (VDAC) of the OMM (45).

Fig. 2.2

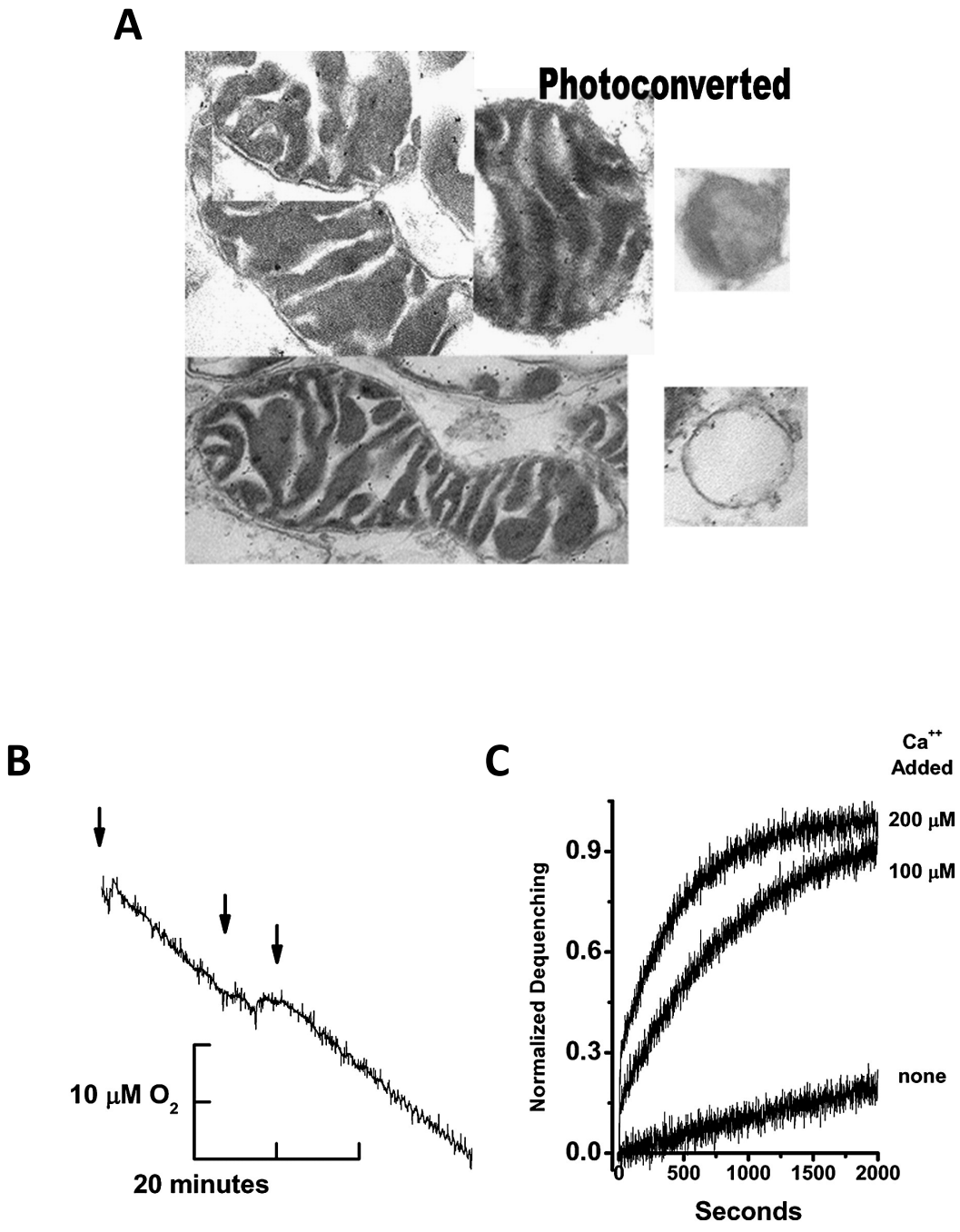
A
Photoconverted
B
10 μM O2
20 minutes
C
Ca++
Added
200 μM
100 μM
none
Normalized Dequenching
0.0
0.3
0.6
0.9
0
500
1000
1500
2000
Seconds

Fig. 2.2 | **Studies on isolated mitochondria after fusion with CF liposomes.** *A*, Mitochondria were prepared and fused with 200 nm liposomes containing 20 mM CF as described in Materials and Methods. These mitochondria were then pelleted, fixed, and embedded for sectioning and electron microscopy. In all cases, the mitochondria have a traditional two-membrane morphology after fusion with liposomes. Exposure of the isolated mitochondria to UV light photoconverted the CF and photooxidized diaminobenzidine, producing the electron-dense depositions in the intermembrane space. Two large unilamellar liposomes that were used in the fusion loading of the mitochondria are seen on the right. The upper liposome was photoconverted and the lower one was not exposed to UV light (see Materials and Methods). *B*, After isolation and fusion with liposomes containing CF, the mitochondrial suspension was diluted to 1 mg/mL protein and O_2 consumption was measured. At the first arrow, 10 mM ascorbate and TMPD were added, initiating rapid O_2 uptake that was dependent upon cytochrome *c* and cytochrome oxidase; at the second arrow, 200 nM melittin was added; at the third arrow, 100 µM horse cytochrome *c* was added. *C*, Mitochondria were isolated and fused with liposomes as described in Materials and Methods in the presence of 1 mM EGTA. Subsequently, the washed mitochondrial suspension was diluted 1:100 into the assay buffer or buffer added with 100 or 200 µM $CaCl_2$ (from bottom to top), and fluorescence dequenching followed for the indicated times. All dequenching values were normalized to the 1% Triton X-100-initiated dequenching.

Presence of porin-like channel activity in the mitochondrial preparation

The release of anionic CF by Ca^{2+} elevation suggests that VDAC is present but in a low conductance state in our fM preparation (45). We have directly assessed the channel activity of the fM in planar lipid bilayers. Using our preparation of mitochondria that was post-liposome fusion, we allowed these to interact with a planar lipid bilayer. After addition of the fM to the *cis* bilayer chamber, fusion transients were observed within 5 min. of continuous stirring. After fusions had occurred, the resulting bilayer currents were studied using a ± 60-mV voltage ramp or by voltage steps under voltage clamp (Fig. 2.3A and 2.3B). The ramp current pattern was typical of many studies of VDAC currents in mitochondrial membrane preparations or reconstituted VDAC protein (46,47). The conductance of these currents was decreased when the Ca^{2+} was reduced with EGTA, consistent with the reported calcium-dependent shift of VDAC to a low conductance channel (45,48) (Fig. 2.3C). The fM currents also displayed voltage-dependent inactivation as described for the VDACs (49).

Fig 2.3

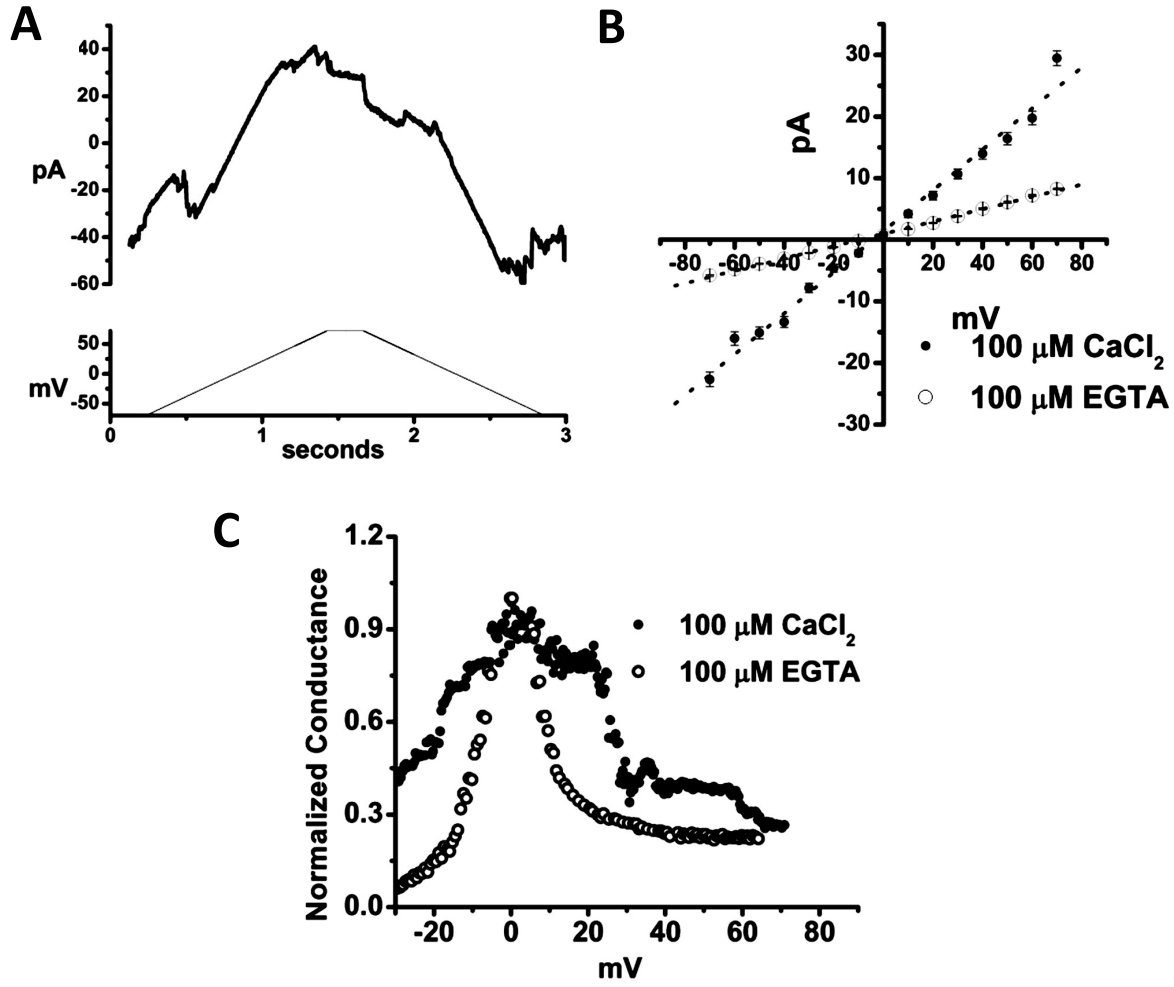

Fig. 2.3 | **Channel activity in membranes of liposome–fused mitchondria.** *A*, Isolated, liposome–fM from cultured HeLa cells were studied in planar lipid bilayers as described in Materials and Methods. Mitochondria were added to the *cis* chamber of a planar lipid bilayer cuvette with a 450- to 150-mM KCl from the *cis* to *trans* chambers. After 3–7 min., current levels stabilized and the *cis* solution was perfused to 150 mM KCl. Using voltage clamp configuration, command ramps (lower panel) were applied to the bilayer after fusion events were observed. *B*, Using buffer containing 100 μM $CaCl_2$ ± 100 μM EGTA, we studied the stable voltage dependence of fM. Data were obtained by holding the indicated membrane potential for 10 s and using the average current of the final 2 s. EGTA (100 μM) was added to the *cis* chamber, and after 5 min., the voltage dependence was determined again. The high-calcium perfusion, voltage dependence, EGTA addition, and voltage dependence redetermination were repeated until the bilayer membrane collapsed (three cycles). These were averaged for this panel, and the standard deviation at each point is shown in the figure. *C*, Bilayer conductance was calculated from voltage ramps (± 60 mV) collected at 1.67 kHz with a 1.2 s duration for each ramp. The bilayers were formed and Ca^{2+} concentration was adjusted as described in (A). The currents were normalized to a peak conductance of 1 for comparison.

$BAX^{\Delta C}$ pore activation in the OMM

Isolated mitochondria used in these studies were loaded with CF by pH-dependent fusion of liposomes with the OMM as described in Experimental Procedures. This fusion-mediated transfer effectively loads the mitochondria intermembrane space with CF but at reduced concentration from that present in the liposomes. Therefore, the dequenching response of the mitochondria per mole of lipid is less than that of the primary liposomes. Consequently, in the assay of BAX pore activation using the fM, we have increased the concentration of mitochondria lipid to 4.3 μM, which compensated for the reduced dequenching from the fM preparation. The application of $BAX^{\Delta C}$ to this mitochondrial preparation produces a rapid time course of CF dequenching. As shown in Fig. 2.4A, the kinetics and concentration dependence of $BAX^{\Delta C}$-initiated dequenching from mitochondria are qualitatively consistent with that observed in defined liposomes. There is a distinct difference between specific activity of $BAX^{\Delta C}$ pore formation in mitochondria and liposomes. The higher activity of BAX in liposomes can be compensated by correcting for the difference in lipid content in the assay (Fig. 2.4B). After this adjustment of the rate of pore activation for the increased lipid in the mitochondrial assay, the Hill analysis for pore formation in mitochondria closely resembles what we have observed in liposomes (Fig. 2.4C). Because of the additional lipid in the mitochondrial assay, the lowest $BAX^{\Delta C}$ concentrations (≈ 1 nM) do not generate sufficient activity for accurate analysis.

Fig. 2.4

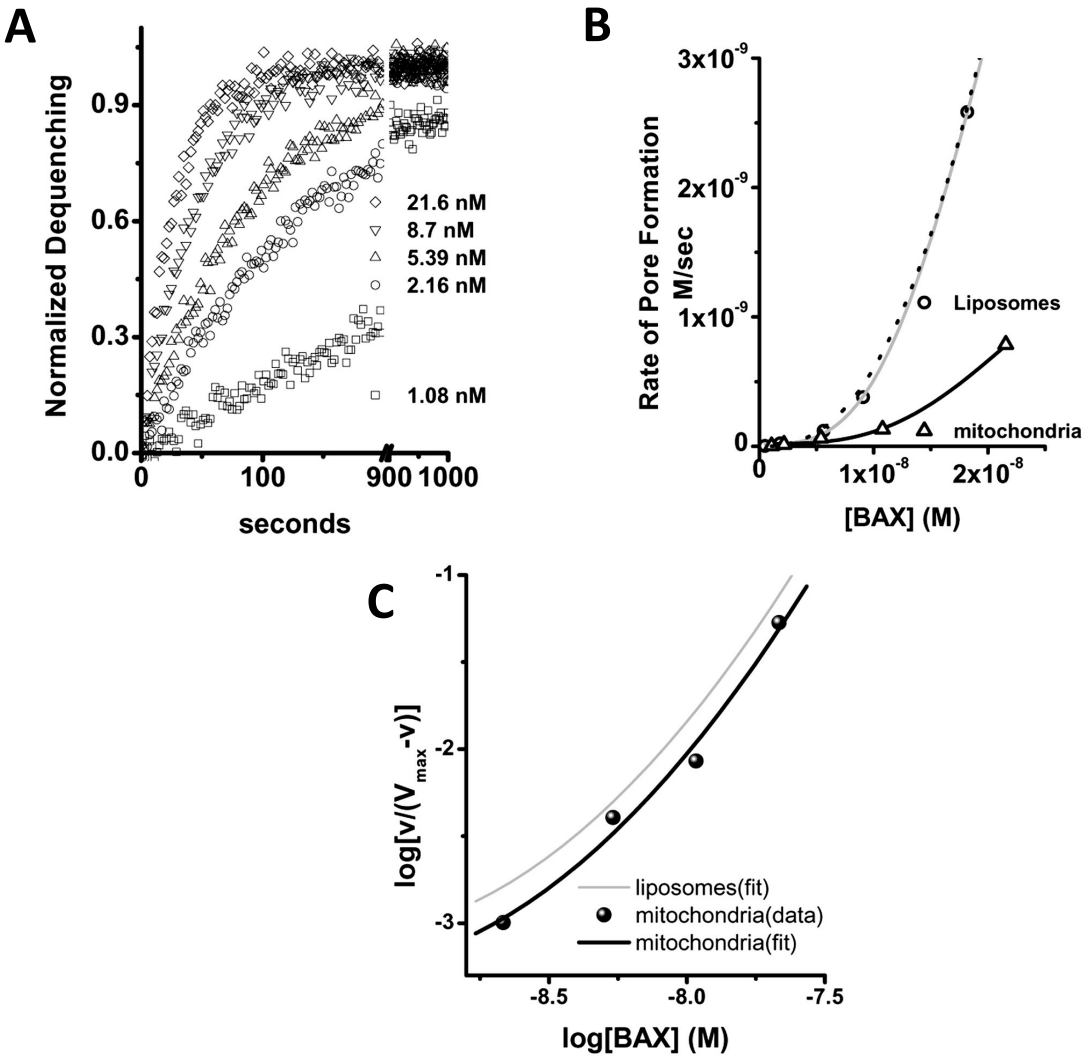

Fig. 2.4 | **BAX$^{\Delta C}$ pore activation in isolated mitochondria.** Mitochondria were isolated from cultured HeLa cells and fused with liposomes using a modification of a previously described technique as described in Materials and Methods. *A*, Mitochondria were diluted into a 500 µL assay volume to give a protein concentration of 0.3 mg/mL and a phospholipid concentration of 4.3 µM. The fractional dequenching was fitted to an exponential model in order to determine the time constant (τ) for analysis of the kinetics of BAX pore activation. *B*, Comparison of the rate of BAX$^{\Delta C}$ pore activation in mitochondria (up triangle, open) and liposomes (circle, open). Both sets of data are fitted by Hill functions (black and gray lines, respectively). The rate of pore activation in mitochondria was then normalized for the increased lipid in this assay and then was fitted by the dotted black line. The normalized pore activation data points are not shown in this panel. *C*, The pore activation time constants that have been normalized for lipid concentration are plotted in the standard logarithmic form for Hill analysis. The data were fitted as in Fig. 2.1, and the fitted curve was plotted in black. The liposome fitted line is shown in gray for comparison.

Effect of cholesterol on BAX pore activation in defined liposomes

BAX is found in the cytosol of most eukaryotic cells, but when activated in response to proapoptotic stimuli, it becomes integrated into the mitochondrial outer membrane and the endoplasmic reticulum (50). Because the membranes in which BAX integrates *in vivo* have less cholesterol than the plasma membrane, we have studied the effect of this sterol on interaction of BAX with membranes.

Cholesterol-containing liposomes were prepared and characterized as described in Experimental Procedures. The final cholesterol concentration in the liposomes was 20 mol%, and the size of the liposomes was verified by dynamic light scattering. The effect of the cholesterol was to dramatically decrease the $BAX^{\Delta C}$ pore activation (Fig. 2.5A and B). As a consequence, τ values (time constants) were large as was the error in their determination. From these data, we could analyze the Hill plot but not the pore size. Here, we have succeeded in extending the Hill analysis to low enough BAX concentrations that we can discern the curvature in spite of the greater error in the measurements of the time constant. When we plot the time constants, the effect of cholesterol is dramatic and increases at lower BAX concentrations (Fig. 2.5C).

The sterol-mediated inhibition of $BAX^{\Delta C}$ pore formation could be due to a direct and stereospecific interaction between steroids and the BAX protein. To test this, we prepared liposomes using the enantiomer of cholesterol. This analog of cholesterol has the configuration inverted at each asymmetric site in the cholesterol molecule (20). This compound was a generous gift from Dr. D. Covey of the Department of Developmental Biology, Washington

University School of Medicine. The comparison of pore activation in liposomes containing *nat*-cholesterol (natural enantiomer of cholesterol) or *ent*-cholesterol (full enantiomer of cholesterol) indicates that the enantiomer is as effective as the natural compound at the inhibition of BAX pore activation (Fig. 2.5D). This suggested that the effect resulted primarily from cholesterol condensing and other effects upon the lipid membrane environment and not from a stereospecific interaction with BAX (51-53).

Fig. 2.5

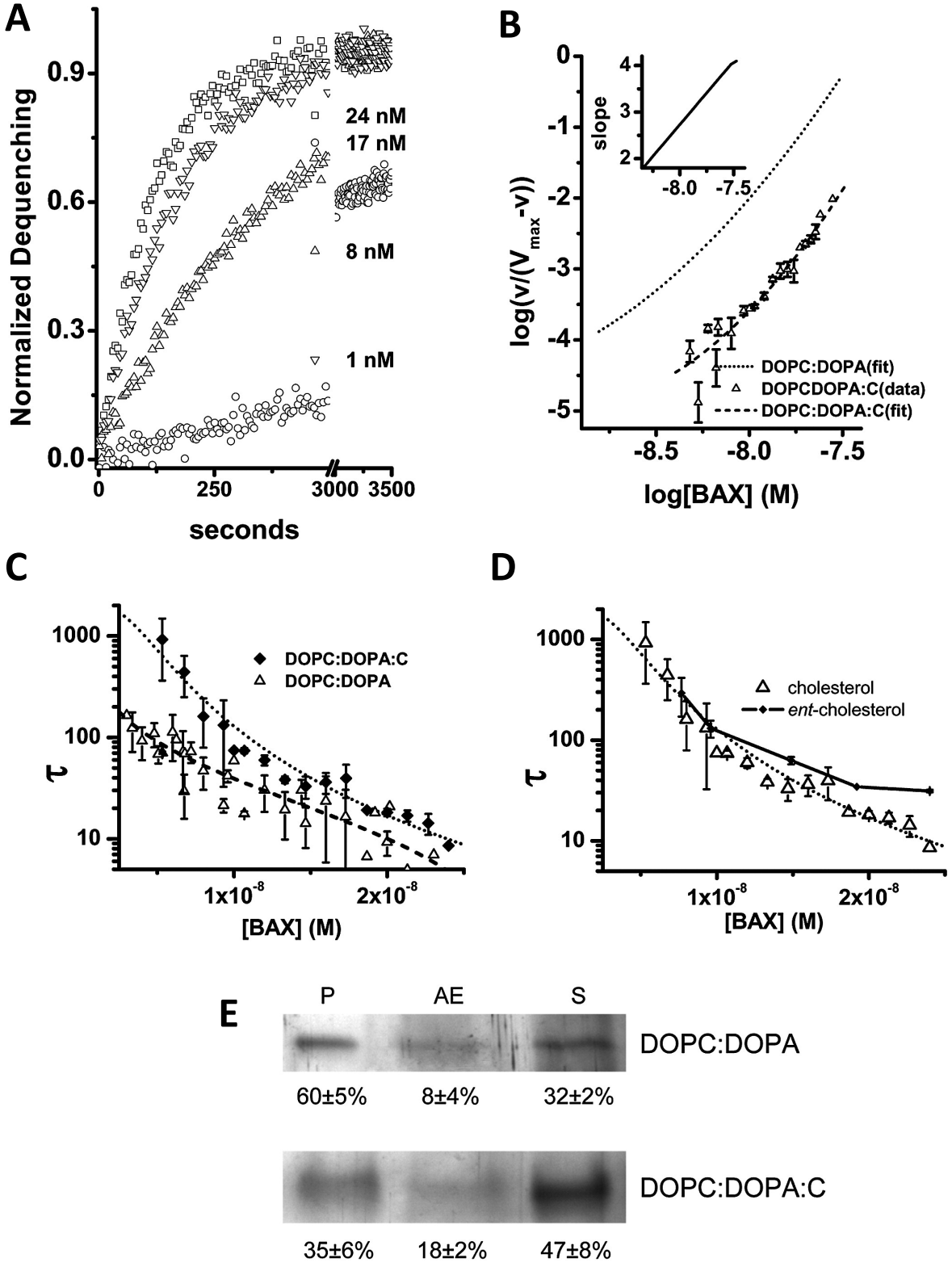
A
Normalized Dequenching
0.0
0.3
0.6
0.9
24 nM
17 nM
8 nM
1 nM
0
250
3000
3500
seconds
B
log(v/(V_max-v))
0
-1
-2
-3
-4
-5
slope
4
3
2
-8.0
-7.5
DOPC:DOPA(fit)
DOPCDOPA:C(data)
DOPC:DOPA:C(fit)
-8.5
-8.0
-7.5
log[BAX] (M)
C
τ
1000
100
10
DOPC:DOPA:C
DOPC:DOPA
1x10-8
2x10-8
[BAX] (M)
D
τ
1000
100
10
cholesterol
ent-cholesterol
1x10-8
2x10-8
[BAX] (M)
E
P
AE
S
DOPC:DOPA
60±5%
8±4%
32±2%
DOPC:DOPA:C
35±6%
18±2%
47±8%

Fig. 2.5 | **BAX pore activation and binding in liposomes ± cholesterol.** Liposomes containing cholesterol were prepared as described in Materials and Methods. *A*, Selected examples of time-series dequenching by human $BAX^{\Delta C}$ in DOPC:DOPA:C (mole fraction, 0.59:0.21:0.20) liposomes. Fractional dequenching was computed by comparison with Triton X-100 dequenching. *B*, Hill analysis of the human $BAX^{\Delta C}$ pore activation in DOPC:DOPA:C liposomes. Each determination of the time constant is shown with the standard deviation error bars (n ≥ 3). The series of time constants was fitted to a polynomial, and the slope of the fitted line is determined and presented in the inset plot. Also shown is the fitting from Fig. 2.1C in DOPC:DOPA liposomes, indicated by the dotted line. *C*, Comparison of the concentration dependence of the time constant for pore activation in DOPC:DOPA (up triangle, open) and DOPC:DOPA:C (diamond, filled) liposomes. Each of the determinations is shown with standard deviation (n ≥ 3). Dotted lines are the nonlinear least-squares fitting of the time constants to the Hill equation. *D*, Comparison of BAX pore activation in liposomes composed of DOPC:DOPA:C (up triangle, open) and DOPC:DOPA:*ent*-C (mole fraction, 0.59:0.21:0.20) (circle, open). Each of the determinations is shown with standard deviation (n ≥ 3). Dotted lines are the nonlinear least-squares fitting of the time constants to the Hill equation. *E*, Defined liposomes were suspended in 200 nM $BAX^{\Delta C}$ and incubated for 10 min. at room temperature. As indicated in the figure, the liposomes were ± cholesterol. The liposomes were sedimented at 150,000 × *g* as described in Materials and Methods to give the pellet (P) and alkaline extraction (AE) or supernatant (S). Each sample was separated by SDS-PAGE with silver staining. The region at 19–20 kDa of the gel was analyzed for density, and the percent distribution of the protein in each fraction was calculated for the figure.

Effect of cholesterol on BAX pore activation in mitochondria

The inhibition of $BAX^{\Delta C}$ pore activation by the inclusion of cholesterol in the liposome membrane composition is dramatic. The simple composition of our liposomes might contribute to this inhibition and generate an artificially large inhibition that will not be seen in a more complicated membrane. We wanted to test the effect of cholesterol in a physiologic membrane in which we could alter the composition in a known fashion. Our fM fulfilled these requirements. The native mitochondria supported $BAX^{\Delta C}$ pore formation well, and by fusing them with dioleoylphosphatidylcholine (DOPC)/dioleoylphosphatidic acid (DOPA)/C liposomes, we could increase the cholesterol content of the OMM to at least 16 mol% during the fusion step. It has previously been shown that the cholesterol of the OMM is slowly metabolized in isolated mitochondria, indicating that the elevated cholesterol was maintained during our experiments (23). The addition of cholesterol to OMM produced a substantial inhibition of the pore activation (Fig. 2.6). However, this reduced the $BAX^{\Delta C}$ activity to such an extent that it was not possible for us to characterize the effects on oligomerization and pore size.

Fig. 2.6

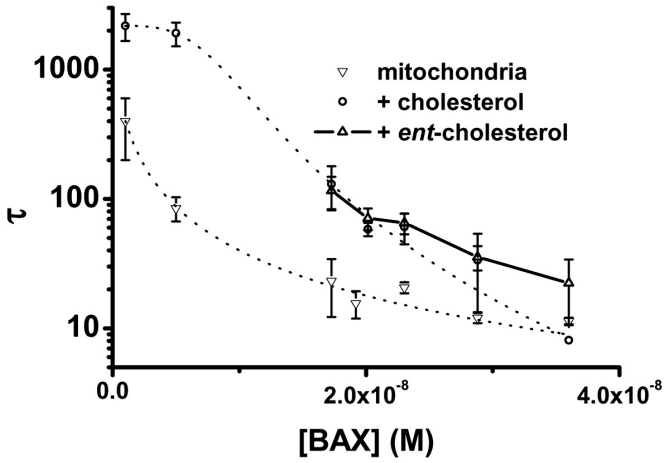

Fig. 2.6 | **Inhibition of BAX$^{\Delta c}$ pore activation by sterols in mitochondria.** The effect of cholesterol on BAX pore activation in isolated mitochondria fused with liposomes containing 20 mol% cholesterol. Pore activation in these mitochondria (circles, open) was greatly reduced compared to mitochondria fused with DOPC:DOPA liposomes (down triangle, open). Mitochondria were also fused with liposomes prepared using the enantiomer of cholesterol (up triangle, open). The dotted lines are the results of nonlinear least-squares fitting of the time constants for pore activation in mitochondria fused to liposomes and cholesterol liposomes. Time constants of pore activation in mitochondria fused with liposomes prepared with the enantiomer of cholesterol are not fitted.

BAX interaction with liposome membranes

BAX pore formation requires the translocation of the soluble BAX protein to a bilayer membrane. This step is critical in vivo and is thought to be a consequence of BAX activation in cells (37,54,55). The mechanism of the membrane translocation of BAX must progress along a binding followed by an integration model (56). The progress of translocation will be influenced by contributions from both the protein structure and the membrane environment. The interaction of BAX with membranes can be clearly shown in a defined liposome experimental system (Fig. 2.5E). Furthermore, the effect of cholesterol appears to be a reduction of membrane-incorporated BAX protein. We have extended the use of defined liposomes to the study of BAX membrane translocation by employing surface plasmon resonance. In this approach, defined liposomes were supported at the sensor surface using the hydrophobic chips (L1) from the Biacore Corporation (57). With the use of these immobilized liposomes, it was possible to study the interaction of $BAX^{\Delta C}$ with the liposome bilayer membrane in concentration- and time-dependent experiments.

For three preparations of activated $BAX^{\Delta C}$, the concentration dependence and time course of binding and membrane integration were determined and averaged (Fig. 2.7A). The membrane-associated BAX populations were characterized by total binding to supported liposome membranes at the end of the injection period (60 s) and the mean stable bound protein after an extended wash period (300–350 s). These populations were determined and are plotted in Fig. 2.7B as the average of the individual trials along with the fitted lines. The total BAX membrane binding at 60 s was tested against one- and two-state interaction models.

A χ^2 analysis indicated a two-state model to be preferable with residuals that were reduced 10-fold. The resulting high- and low-affinity estimates for membrane binding are listed in Table 2.1. The concentration dependence of BAX integration into the liposome membrane was clearly dominated by a single interaction, and the results of that analysis are also presented in Table 2.1. From this analysis of the binding and integration curves, the size of the membrane populations of BAX was estimated and is presented as mole fractions to correct for small changes in liposome immobilization on the Biacore chip. Inspection of these fitted results for membrane association reveals three populations of membrane-associated BAX: high- and low-affinity populations that rapidly dissociate and the membrane-integrated fraction that slowly dissociates. The ratio of total membrane-bound to membrane-integrated BAX increases at low BAX concentrations and then begins to fall as membrane capacity becomes saturated (Fig. 2.7C).

Fig. 2.7

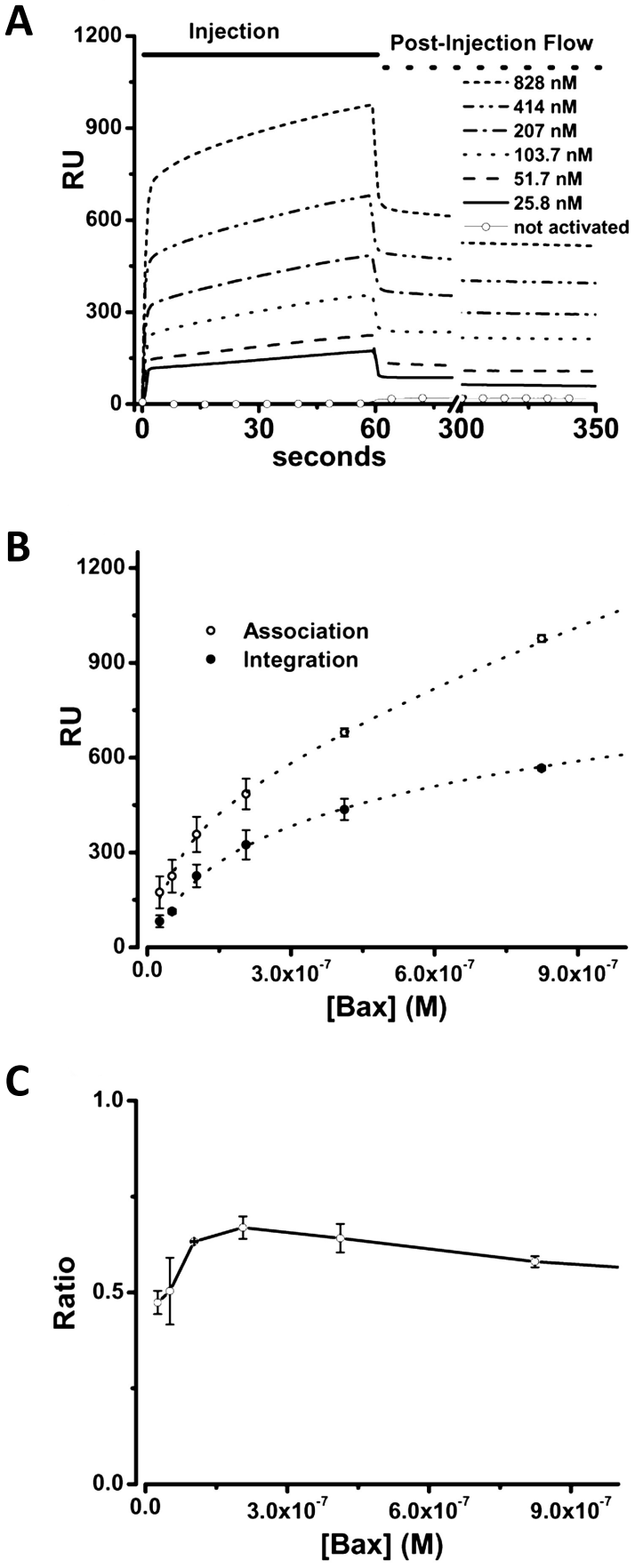
A
Injection
Post-Injection Flow
828 nM
414 nM
207 nM
103.7 nM
51.7 nM
25.8 nM
not activated
RU
1200
900
600
300
0
0
30
60
300
350
seconds
B
Association
Integration
RU
1200
900
600
300
0
0.0
3.0x10-7
6.0x10-7
9.0x10-7
[Bax] (M)
C
Ratio
1.0
0.5
0.0
0.0
3.0x10-7
6.0x10-7
9.0x10-7
[Bax] (M)

Fig. 2.7 | **BAX$^{\Delta C}$ binding to supported DOPC/DOPA liposomes.** The binding and membrane integration of BAX$^{\Delta C}$ were studied by surface plasmon resonance using supported liposomes. *A*, BAX$^{\Delta C}$ was injected over an L1 chip covered with immobilized DOPC/DOPA (74:26 mol%) liposomes as described in Materials and Methods. This protein was prepared as described above without the use of detergent. Prior to exposure of the BAX$^{\Delta C}$ to detergent, the protein did not bind to the liposomes as shown by the open circles (○ ○ ○) at the bottom of the graph that indicate the averaged RU response for the 25–3000 nM BAX$^{\Delta C}$ concentration range. After treatment with detergent, the RU response for the following concentrations is shown: 25.8 nM (solid), 51.7 nM (dash), 103.7 nM (dot), 207 nM (dash–dot), 414 nM (dash–dot–dot), 828 nM (short dash). The injection phase is indicated by the solid line and the wash phase is denoted by the dashed line at the top of the graph. *B*, Comparison of membrane-associated (□) and membrane-integrated (○) protein using the criteria described in the text and calculating the average values and standard deviation as described in Materials and Methods. The dotted lines represent the best fit to an interaction model as described in the text. *C*, The ratio of binding and integration fraction of protein plotted as the added concentration of BAX$^{\Delta C}$ is increased. Means and standard deviations are computed as described in Materials and Methods.

Table 2.1 | **Analysis of BAX$^{\Delta C}$ membrane interaction**

Type of membrane interaction[a]	K_1 (M)	BAX (mole fraction)[b]	K_2 (M)	BAX (mole fraction)[b]
DOPC:DOPA				
Membrane binding	$2.2 \pm 0.4 \times 10^{-6}$	$5.9 \pm 0.7 \times 10^{-3}$	$1.37 \pm 0.45 \times 10^{-8}$	$0.78 \pm 0.31 \times 10^{-3}$
Membrane integration			$2.5 \pm 0.27 \times 10^{-7}$	$1.8 \pm 0.07 \times 10^{-3}$
DOPC:DOPA:C				
Membrane binding	$1.6 \pm 1.2 \times 10^{-6}$	$8.6 \pm 4.2 \times 10^{-3}$	$1.4 \pm 0.46 \times 10^{-8}$	$1.2 \pm 0.2 \times 10^{-3}$
Membrane integration			$1.06 \pm 0.22 \times 10^{-8}$	$0.86 \pm 0.3 \times 10^{-3}$

[a] As described in the text, the BAX membrane populations were identified by binding and integration with the membrane.

[b] We have used mole fraction to represent membrane-associated BAX populations to allow a direct comparison between experiments as a membrane concentration (58).

BAX interaction with liposome membranes containing cholesterol

In cells, BAX pores are described in the OMM but pores in other membranes have not been noted. Specifically, pores in the plasma membrane produce osmotic lysis and necrosis (59,60). The osmotic lysis of cells would be inconsistent with the apoptotic program of cells, and the molecular basis for this membrane selectivity is important to explaining the physiology of cell death. One of the distinctions between intracellular membranes and the plasma membrane is the high cholesterol composition of the plasma membrane in most cells. Using cholesterol-containing liposomes and mitochondria, we and others observed reduced BAX pore activation (33). In the preceding section, we have shown that $BAX^{\Delta C}$ interaction with membranes involves a rapid but reversible binding to the membrane followed by integration into the membrane, resulting in a very slow dissociation of the integrated protein population from the bilayer. Using surface plasmon resonance, we investigated the effect of cholesterol on the liposome binding and integration of BAX.

The cholesterol-containing liposomes loaded onto the L1 chip similarly to the DOPC:DOPA liposomes and blocked albumin access to the chip surface (see Experimental Procedures). The interaction of human $BAX^{\Delta C}$ with liposome membranes containing cholesterol is shown in Fig. 2.8. As with the DOPC:DOPA liposomes, detergent activation of human $BAX^{\Delta C}$ was required for significant interaction with the cholesterol-containing membranes. For three preparations of activated $BAX^{\Delta C}$, the concentration dependence of binding and membrane integration were determined and averaged (Fig. 2.8A). Visual inspection of $BAX^{\Delta C}$ interaction with DOPC:DOPA:C liposomes indicated that it was

distinct from the $BAX^{\Delta C}$ interaction with DOPC:DOPA liposomes. The initial membrane association was still rapid and larger for the cholesterol-containing membranes. Paradoxically, from this larger pool of membrane-associated BAX, the membrane integration was reduced (Fig. 2.8B). Analysis of the concentration-dependent membrane association once again demonstrated both low- and high-affinity binding populations as shown in Table 1. The binding pools were approximately 60% larger than those in the DOPC:DOPA liposomes. In spite of this, the integrated fraction was significantly reduced and reached a maximum value that was 58% of that seen in the liposomes without cholesterol. In addition, the ratio of membrane-integrated to membrane-associated BAX demonstrated a very distinct concentration dependence in that there was no increase of the integrated fraction at low concentrations of added BAX (Fig. 2.8C).

Fig. 2.8

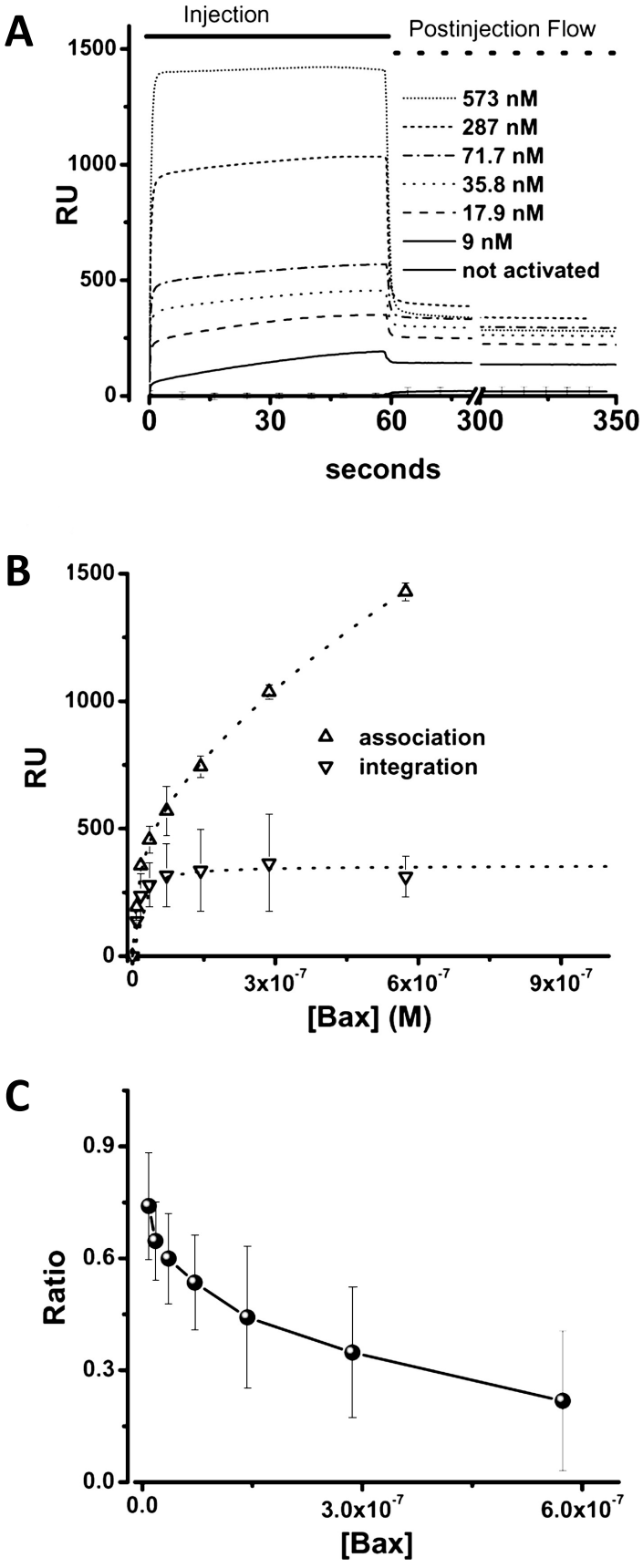
A
Injection
Postinjection Flow
1500
1000
500
0
RU
573 nM
287 nM
71.7 nM
35.8 nM
17.9 nM
9 nM
not activated
0
30
60
300
350
seconds
B
1500
1000
500
0
RU
association
integration
0
3x10-7
6x10-7
9x10-7
[Bax] (M)
C
0.9
0.6
0.3
0.0
Ratio
0.0
3.0x10-7
6.0x10-7
[Bax]

Fig. 2.8 | **BAX$^{\Delta C}$ binding to supported DOPC/DOPA/cholesterol-containing liposomes.** The binding and membrane integration of BAX$^{\Delta C}$ were studied by surface plasmon resonance using supported liposomes containing cholesterol. *A*, BAX$^{\Delta C}$ was injected over an L1 chip covered with DOPC:DOPA:C (59:21:20 mol%) liposomes. This protein was prepared as described in Materials and Methods without the use of detergent. Prior to exposure of the BAX$^{\Delta C}$ to detergent, the protein did not bind to the liposomes as shown by the open circles (○ ○ ○) at the bottom of the graph that indicate the averaged RU response for the 25–3000 nM BAX$^{\Delta C}$ concentration range of unactivated protein. After treatment with detergent, the RU response for the following concentrations is shown: 9 nM (solid), 17.9 nM (dash), 35.8 nM (dot), 71.7 nM (dash–dot), 287 nM (dash–dot–dot), 573 nM (short dash). The injection phase is indicated by the solid line and the wash phase is denoted by the dashed line at the top of the graph. *B*, Comparison of membrane-associated (up triangle, open) and membrane-integrated (down triangle, open) protein using the criteria described in the text and calculating the average values and standard deviation as described in Materials and Methods. The dotted lines represent the best fit to an interaction model as described in the text. *C*, The ratio of binding and integration of protein plotted as the fraction integrated as concentration of BAX$^{\Delta C}$ is increased. Means and standard deviations are computed as described in Materials and Methods.

2.4 | Discussion

Because BCL2 family proteins are central arbiters of the mitochondrial mortality decision, (3) we have undertaken a detailed analysis of their biochemical activities. Although 25 genes comprise this family and they generate both pro- and antiapoptotic proteins, (8) apoptosis regulation centers on the activation of a "pore" in the mitochondrial outer membrane by BAX and BAK (61). We have taken the view that by studying this pore activation in detail, it will become possible to clarify the influences of the regulatory BCL2 family members. Therefore, we have compared BAX pore activation in liposomes with that activity in mitochondria. Our reconstitution approach permitted a detailed study of the stages of BAX membrane translocation using surface plasmon resonance. This analysis was applied to the mechanism of cholesterol inhibition of BAX pore activation.

Mitochondrial preparation for the study of $BAX^{\Delta C}$ pore activation

The *in vivo* death decision polling occurs in the OMM, which has a complex composition of protein and lipid. We have developed a mitochondrial preparation in which to study the translocation and pore-forming activity of BAX protein. Photoconversion of the CF produced deposition of an electron-dense polymeric product in the intermembrane space representing the localization of the CF between the inner mitochondrial membrane and OMM (62). We conclude that the fM preparation is an intact double-membrane mitochondrion having an OMM that provides a diffusion barrier similar to that described for native mitochondria (39,63,64).

$BAX^{\Delta C}$ pore activation in the OMM

Our mitochondrial preparation, fM, satisfied morphologic, metabolic, and OMM functional criteria to be a useful preparation for the study of BAX pore-forming activity. By using the fM preparation, we are able to study the activation of human $BAX^{\Delta C}$ in some detail. The pore activation rate and kinetics in mitochondrial and liposome $BAX^{\Delta C}$ activity are comparable, as shown in Fig. 4C. The activation of this pore is proposed to be a critical decision point in cell death, with the OMM forming the environment for the BCL2 family proteins to negotiate this decision (3,8,65). By using fM, a strong correlation with the pores that we have characterized in defined liposomes is apparent. The specific activity of the purified pore-forming protein is very similar once the necessary correction of the lipid concentration in our assays is considered. Our Hill analysis suggests that the added BAX undergoes a two-stage oligomerization in the membrane that is consistent with our studies in defined liposomes. This comparison suggests that the BAX forms a dimer and tetramer pore in the OMM, a model that is consistent with chemical cross-linking of BAX in the OMM (13,66).

Effect of cholesterol on BAX pore activation in defined liposomes and mitochondria

Cholesterol is an important component of eukaryotic membranes, having many effects upon membrane characteristics and the activity of membrane components. In beginning these studies, we were attracted by the possibility that the difference in cholesterol content between the plasma membrane and the OMM was an important factor in directing the formation of $BAX^{\Delta C}$ pores. Our data and the data of others support this conclusion (33). Adding cholesterol (≈ 20 mol%) to liposomes and the OMM significantly inhibits $BAX^{\Delta C}$ pore formation. This

has more cholesterol than the concentrations reported to be present in the OMM and is less than the cholesterol content of the plasma membranes (23,32,67,68). Therefore, we conclude that the sterol concentrations of defined liposome membranes can play a role in regulating the pore formation by BAX. To verify that cholesterol was effective in a complex lipid environment, we used liposomes to adjust the cholesterol content of the mitochondrial outer membrane. Direct analysis of the cholesterol content of the fM indicates that the incorporation was successful and produced a cholesterol concentration of≈20 mol%. Although cholesterol side-chain oxidation can be brisk in isolated mitochondria, this occurs in the inner membrane, whereas outer-membrane cholesterol is quite stable and not oxidized in the isolated organelle (23). Therefore, our experiments show that the incorporation of exogenous cholesterol into the OMM reduced $BAX^{\Delta C}$ pore formation substantially compared with mitochondria fused with liposomes containing only phospholipids. The observation that the cholesterol effect was similar in the simple liposome and the complex mitochondrial membrane environment seems to favor a direct interaction between the sterol and the BAX protein. Direct interactions are also suggested by the putative cholesterol recognition/interaction motif in α-helix 5 (at positions 113–120) (28,69). However, in both liposomes and mitochondria, the *ent*-cholesterol was as effective as the natural compound in reducing BAX pore formation, strongly indicating that cholesterol exerts its effect by influencing the lipid environment and having secondary effects upon BAX pore formation (20,70). In addition, the reduced pore activation by *ent*-cholesterol at high BAX concentrations in both liposomes and mitochondria may reflect chiral

sterol–phospholipid interactions that are reported for the *ent*-cholesterol in phospholipid monolayers (71).

We conclude that cholesterol could have a significant effect on the mortality decision in cells that are overloaded with this steroid. Mitochondrial cholesterol overload has rarely been studied but has been observed in tumor cell lines (31,72,73) and in cultured cells where mitochondrial cholesterol has been increased pharmacologically (33). Likewise, cholesterol depletion is reported to enhance apoptosis in statin treatment (74). However, the mitochondrial membrane environment is complex and steroid oxidation is an active process in these organelles (23,24). Therefore, when multiple membrane parameters are changed, decreased permeability transition pore activation has also been reported (34). Our studies have focused on cholesterol in a controlled experimental situation to understand the mechanism by which cholesterol inhibits BAX pore activation.

The interaction of BAX$^{\Delta C}$ with liposomes studied by surface plasmon resonance

In order to address the mechanism of cholesterol inhibition of BAX pore activation, we have used surface plasmon resonance to compare the interaction of BAX$^{\Delta C}$ with immobilized liposomes (± cholesterol). Surface plasmon resonance has been applied to the study of membrane binding and integration of a number of pore-forming proteins and peptides (75-79). We have used the attached liposome configuration to quantitatively study the rapid binding of soluble BAX$^{\Delta C}$ and concentration-dependent membrane integration of the membrane-bound protein. The data in Fig. 7 clearly demonstrate that the membrane binding of BAX$^{\Delta C}$ is completely dependent upon detergent activation of the purified protein. The maximum

response to nonactivated $BAX^{\Delta C}$ was ≈5 RU, which is consistent with the predicted response from the mass of nonassociated protein [3.3 μM $BAX^{\Delta C}$] injected over the supported liposomes. Therefore, essentially no membrane association occurs by the nonactivated BAX protein. In cells, BAX also does not associate with the mitochondrial membrane until it is activated (54,61).

These surface plasmon resonance studies confirm that the interaction of activated BAX with liposome membranes clearly displays the two observed stages of binding and integration (54). The binding stage is rapid and displays high- and low-affinity components. Membrane integration of BAX is slower but dissociates very slowly, if at all. Analysis of the concentration dependence of binding indicates a high- and a low-affinity population of membrane-associated BAX. The concentration dependence of BAX membrane integration suggests a single population. We plotted the ratio of membrane-integrated to total membrane-associated BAX to study the relationship between these two. In the DOPC/DOPA liposomes, the ratio has an increasing phase, suggesting that binding of BAX to the liposomes enhances the integration step. Membrane binding and integration of BAX saturate even though no protein or typical molecular receptor is present in the membrane. This saturation occurs as the maximum mole fraction (solubility) of the BAX protein associated with the membrane surface or integrated into the membrane is reached. This saturation produces the falling ratio of membrane-integrated to total membrane-associated BAX as higher concentrations of added BAX engage nonproductive modes of membrane association. Interestingly, in the DOPC/DOPA/C membranes, the increasing ratio at low BAX concentration is eliminated. However, since both binding populations are increased in the DOPC/DOPA/C membranes, the integration

promoting step and its cholesterol inhibition must occur after the binding steps that we have observed.

Analysis of the cholesterol inhibition of BAX$^{\Delta C}$ pore activation

The results of our analysis of BAX association with membranes are presented in Table 1. In this table, the effect of cholesterol on BAX integration into bilayer membranes is apparent. BAX binds to a greater extent (both high- and low-affinity pools are increased by 60%) to membranes that contain cholesterol, but membrane integration is dramatically inhibited (42% reduction). These changes produce the inhibition of BAX pore formation that we observe in liposomes and mitochondria. The effect upon BAX pore activation is consistent with our proposed mechanism of pore activation that includes the in-membrane dimer and tetramer oligomerization of BAX protein. In this model of in-membrane oligomerization, a reduction of membrane integration by cholesterol will suppress pore activation. Cholesterol is known to have a condensing effect upon membranes by reducing the phospholipid area that is especially prominent for the liquid-disordered phase that we have in our DOPC/DOPA liposomes (52,80). This condensation can be observed as a lateral phase separation in membranes of appropriate composition (81). Membrane condensation itself could reduce BAX integration without a direct cholesterol–BAX interaction. The equivalence of cholesterol and *ent*-cholesterol inhibition at low BAX integration levels favors membrane condensation over direct sterol–protein interaction. The increased inhibition by *ent*-cholesterol as BAX integration approaches membrane-saturating levels might reflect stereospecific cholesterol interactions with BAX or with membrane phospholipids (71). If we extrapolate the effect of

cholesterol upon the concentration dependence of membrane integration, it appears to explain the inhibition of pore activation. Thus, we have no evidence to suggest stereospecific interaction with the BAX and inhibition of the in-membrane oligomerization steps. However, this does not necessarily contrast with the prior report on effects of cholesterol on BAX (33). That work compared the BAX integrated to the total membrane-associated protein using trypsin sensitivity. This measure is very similar to the ratio that we calculate, and although we observe that the ratio in DOPC/DOPA/C membranes has a distinct BAX concentration dependence, there is a range where it is similar to that in DOPC/DOPA membranes. Our data only support a cholesterol effect on the membrane integration of BAX that is mediated by altering the membrane environment.

There have now been three investigations showing that the pore-forming activity of BAX is inhibited by cholesterol in liposome membranes. All have increased the cholesterol of the OMM to produce BAX inhibition in that membrane also. By comparison with our results, the cholesterol levels of cell surface membranes will certainly reduce BAX pore formation. It remains to be demonstrated how the cholesterol levels of intracellular membranes change and influence cell death. Resistance of tumor cells to therapy, the persistence and growth of atheromatous lesions and their final rupture, the extent of reperfusion cell death in infarct and stroke regions, and skeletal muscle apoptosis may all be affected by cholesterol levels and the inhibition of BAX activity.

2.5 | Conclusion

The 25 BCL2 family proteins are central regulators of apoptosis. As one of these, BAX is a critical instigator of apoptosis by transitioning from a soluble protein to a membrane-integrated pore. We have characterized this transition in liposomes and human mitochondria. Activation of the soluble protein is required for membrane binding, membrane integration, and in-membrane oligomerization to form pores. Cholesterol is a major inhibitor of BAX pore activation in mitochondria and liposomes. This inhibition does not require direct interaction with the BAX protein but appears to function on the membrane environment to inhibit BAX integration into the membrane bilayer.

2.6 | Experimental Procedures

Preparation of BAX$^{\Delta C}$

Two methods for producing recombinant BAX$^{\Delta C}$ were employed. For dequenching experiments, the cDNA for human BAX, with the putative transmembrane carboxy-terminal □-helix truncated, was subcloned into pGEX-KG vector, expressed in BL21(DE3) *Escherichia coli*, and purified as a glutathione S-transferase fusion protein. After harvesting by centrifugation, cells were resuspended in lysis buffer [phosphate-buffered saline, pH 7.4, 1% Triton X-100, 1 mM DTT, and Complete Protease Inhibitor Cocktail (Roche, Indianapolis, IN)] and sonicated, and the clarified lysate was applied to glutathione–agarose. Resin was subjected to high salt wash (including 0.1% Triton X-100) and flushed with cleavage buffer [50 mM Tris, pH 7.5, 150 mM NaCl, 0.1% n-octyl-β-D-glucopyranoside (OG), 2.5 mM $CaCl_2$, and 1 mM DTT], and BAX$^{\Delta C}$ was cleaved from glutathione S-transferase tag using thrombin (Novagen, Madison, WI).

For surface plasmon resonance experiments, human BAX$^{\Delta C}$ cDNA was subcloned into pTYB1 vector (NEB, Ipswich, MA), expressed in BL21(DE3) *E. coli*, and purified as an intein/chitin-binding domain fusion protein. After harvesting by centrifugation, cells were resuspended in lysis buffer [phosphate-buffered saline, pH 7.4, and Complete Protease Inhibitor Cocktail (Roche)] and sonicated, and clarified lysate was applied to a chitin affinity column. Resin was subjected to high salt wash followed by flushing with cleavage buffer (20 mM Tris, pH 8.0, 500 mM NaCl, 1 mM ethylenediaminetetraacetic acid (EDTA), and 50 mM DTT) and incubated at 4 °C for 48 h to allow intein self-cleavage and release of recombinant

$BAX^{\Delta C}$. Eluted proteins were estimated to be > 95% pure by Coomassie staining SDS-PAGE gels and stored at 4°C. $BAX^{\Delta C}$ was activated by addition of 2% OG for 1 h at 4°C and then dialyzed overnight against EB (10 mM HEPES, pH 7.0, 100 mM KCl, and 0.01% NaN_3). $BAX^{\Delta C}$ retained pore-forming capacity for > 72 h after dialysis with no diminution of activity.

Liposome preparation by reverse-phase method

Liposomes were prepared using the reverse-phase procedure of Szoka and Papahadjopoulos (82). Lipids were obtained as solutions in chloroform from Avanti Polar Lipids, Inc. (Alabaster, AL). Mixtures of DOPC and DOPA (monosodium salt) and 5-cholestene-3β-ol [cholesterol (C); Sigma-Aldrich, St. Louis, MO] were prepared at a mole fraction ratio of DOPC:DOPA=0.74:0.26 or DOPC:DOPA:C=0.59:0.21:0.20 in chloroform. Chloroform was first evaporated under a stream of N_2 gas and then further removed by vacuum (10− 5 Torr) for 2 h. Dried lipids were stored in N_2 gas at −20°C. CF (molecular weight = 376 Da) (Molecular Probes, Eugene, OR) was prepared at 20 mM in EB, adjusted to pH 7.2, and stored at 4°C. Dried lipids were reconstituted by addition of 1 mL ethyl ether and 0.5 mL CF solution. The suspension was sonicated at 1200 W for 20 s, producing a stable suspension, and ether was evaporated on a rotary evaporator at 40 rpm under reduced pressure (water aspiration) for 13 min. at room temperature. The 0.5 mL suspension was supplemented with an additional 0.5 mL of the 20 mM CF solution. This mixture was passed through a 22-gauge needle affixed to a mini-extruder (Avanti) containing a 200-nm membrane (Nuclepore, Pleasanton, CA) for three complete cycles. The extravesicular CF was removed by passing the liposome–dye mixture over a 1 × 20 cm Sephadex G-25-80 (Sigma, St. Louis, MO) column in

EB. A liposome peak was collected and analyzed by dynamic light scattering (N5 Submicron Particle Size Analyzer, Beckman Coulter, Fullerton, CA), with a diameter of 207 ± 12.5 nm. Phospholipid concentration in this fraction was determined to be 3.3 mg/mL (83).

Dequenching analysis of BAX pore activation

We have used the analysis of dequenching to study the activation of pores in bilayer membranes (19,84-86). Using monodisperse unilamellar vesicles, we studied the activation of membrane pores by measurement of the increased fluorescence as CF exits from the membrane compartment and is diluted into the assay volume. All assays were done at a total lipid concentration of 0.4 ± 0.05 μM. The time dependence of the dequenching from our liposome and mitochondria preparations is well described in Eq. (1), without additional exponential terms.

$$F_{520} = F_0 A_1 (1 - e^{(\text{time}/\tau)}) + m \times \text{time} \quad (1)$$

The formation of a 10- to 30-Å pore in a 200-nm vesicle (or mitochondrion, see Fig. 2) will permit the equilibration of CF with the media within 30–100 ms (87,88). In the timescale of our assay, a single pore opening will not be resolved and the exponential dequenching we observe represents the kinetics of pore activation. A linear component in the time series was frequently not observed but represents pores that are unstable and which close before single vesicle dequenching is complete with subsequent pore activation being required to complete dequenching (89). For a time-series experiment, the fractional dequenching at each time point was determined by normalizing the fluorescence (Fl) with the Triton X-100-generated total dequenching for each assay [Eq. (2)].

$$F_{520} = (Fl_{time} - Fl_{baseline}) / (Fl_{Triton\ X100} - Fl_{baseline}) \quad (2)$$

The analysis of BAX pore activation was undertaken by determining the time constant, τ, and the total exponential fluorescence change, A_1, for each time-series dequenching. The kinetic constants were determined by nonlinear least-squares analysis using the Levenberg–Marquardt algorithm, which yielded χ^2 values of < 0.001 for each time series.

Assessment of BAX$^{\Delta C}$ –liposome interaction by centrifugation and silver staining

OG-activated BAX$^{\Delta C}$ was dialyzed overnight against EB. BAX was applied to liposomes ± cholesterol (1.1 μM total lipid concentration), incubated for 10 min. at room temperature, and ultracentrifuged at 150,000 × *g* for 20 min. at 4°C. The supernatant was collected and the proteoliposome pellet was subjected to alkaline extraction by resuspension in 100 mM sodium carbonate for 30 min. on ice. Samples were again ultracentrifuged and supernatant and pellet fractions were collected. After SDS-PAGE and silver staining, relative intensities of BAX bands were quantified using QuantityOne software (Bio-Rad, Hercules, CA).

Preparation of mitochondria

Mitochondria were prepared from cultured cells following published procedures (90,91). The mitochondria were isolated from HeLa cells maintained in culture where the unstimulated rate of apoptosis is < 5%. We used 250 mM sucrose for osmotic stabilization (pH 7.0, 10 mM HEPES) and added 1 mM EGTA to maintain low Ca^{2+}. All procedures were performed at 4°C on ice baths except as noted. Cell cultures were washed with ice-cold sucrose solution to remove media and serum, and the cells were mechanically scraped from the dishes. After homogenization (40 strokes with a loose Dounce), the nuclei and undisrupted cells were

removed by centrifugation at 500 × *g*. Mitochondria were then collected by centrifugation at 9000 × *g*. The mitochondrial pellet was resuspended, and protein concentration was determined using the Micro BCA Protein Assay Kit (Pierce Chemical Co., Rockford, IL). The mitochondria were suspended at 1 mg/mL protein in the unilamellar liposome preparation for fusion as described previously (39,40). The CF-loaded liposomes were 1 mM in lipid and contained 2×10^{12} liposomes/mL. The mitochondria and liposomes were incubated together at 15°C for 60 min. and then the pH dropped to 6.5 by addition of 60 μL of 100 mM PIPES (pH 6) for 5 min. The fM were pelleted at 9000 × *g* and washed two further times in 250 mM sucrose buffer to remove unfused liposomes. Lipid analysis by Dr. Richard Gross of the Department of Medicine at Washington University allowed us to adjust the fusion protocol in order to incorporate the desired amount of cholesterol into the mitochondria. This analysis showed that the liposome fusion increased DOPA to three times the DOPA in the isolated mitochondria before fusion (92). We used this ratio to calculate the OMM cholesterol concentration, which increased to 16 ± 0.4 mol%, when we were using liposomes containing 20 mol% cholesterol. Cholesterol in liposome and mitochondria preparations was converted to trimethylsilyl ethers and determined using gas chromatography–mass spectrometry by Dr. Dan Ory of the Department of Medicine, Washington University School of Medicine (93). Mitochondria fused to these levels were used in all of the experiments to test the effect of cholesterol on BAX activity in mitochondria.

Electron microscopy and photoconversion of the mitochondrial preparations

Mitochondria were purified as above and fixed with 2.5% glutaraldehyde in 0.1 M sodium cacodylate for 30 min. on ice, after which they were spun at top speed in a tabletop microcentrifuge to form a tight pellet. After rinsing, the pellet was sequentially stained with osmium tetroxide and uranyl acetate and then dehydrated and embedded in Polybed 812. Tissue was thin sectioned on a Reichert–Jung Ultracut, viewed on a Zeiss 902 electron microscope, and recorded with Kodak E.M. film. For photoconversion, the mitochondria were washed after fixation and treated with 6 mM potassium cyanide and then suspended in cacodylate buffer with 2.8 mM 3,3′-diaminobenzidine tetrahydrochloride for exposure to a 75-W xenon lamp. After 6 min., the mitochondria are washed by centrifugation and processed for electron microscopy as above.

Measurement of mitochondrial oxygen consumption

Mitochondria were prepared as described above. Mitochondria at a protein concentration of ≈ 1 mg/mL were placed into the Instech dissolved oxygen measuring system (Warner Instruments, Hamden, CT) in 150 mM KCl (pH 7.0), 1 mM EGTA, and 5 mM DTT at 20°C. The buffer was equilibrated with 95% O_2 and stored in an airtight syringe prior to use. The concentration of dissolved O_2 was corrected for atmospheric pressure. During the assay, the mitochondria were sequentially treated with 5 mM malate, 5 mM ADP, 2 μM rotenone, 5 mM succinate, 10 mM ascorbate, and N,N,N,N-tetramethyl-p-phenylenediamine (TMPD) and a baseline obtained in 10 mM azide. After the addition of ascorbate–TMPD, the rate of oxygen consumption was dependent upon site IV, which employs cytochrome *c* and

cytochrome oxidase in the transfer of electrons to molecular oxygen (94). The rates of oxygen consumption were normalized for protein concentration.

Planar lipid bilayer studies on isolated fM

Planar lipid bilayers were prepared from the phospholipids DOPC:DOPA (74:26 mol%). Phospholipids were obtained from Avanti Polar lipids in chloroform solution and were mixed to the correct ratio, and the chloroform was removed under nitrogen. The lipids were then stored under nitrogen at−20 °C until dissolved in decane at 20 mg/mL. Briefly, 2 μL of lipid solution was applied to 0.25 mm orifice of a polystyrene cuvette (Warner Instruments), and the solvent was allowed to evaporate. The cuvette was then placed into a bilayer chamber and connected to a bilayer clamp (BC525-c; Warner Instruments) by Ag/AgCl electrodes via agar bridges. Data were collected using CLAMPEX 9.0 (Axon Instruments, Foster City, CA), archived on videotape using a Neurocorder DR-484 (Neuro Data Instruments, Delaware Water Gap, PA), and analyzed using Origin (OriginLab Corporation, Northampton, MA) and CLAMPFIT (Axon Instruments). Bilayers were formed by spreading with a polished glass rod and allowed to thin to a capacitance of 0.4 $\mu F/cm^2$, at which point the noise was typically 0.2 pA and the leak conductance was 2 pS. The salt concentrations are described in the appropriate figure legends. Outward (positive) currents were defined as K^+ moving *cis* to *trans*. All solutions were buffered to pH 7.0 with 10 mM K-HEPES. Mitochondria (10 μg of protein) were added to the *cis* chamber with mixing. To vary calcium concentration, we added EGTA and $CaCl_2$ as indicated. The milliQ water employed for buffers in these studies averaged 30 μM Ca^{2+}, and

mitochondrial isolation buffer contained 1 mM EGTA to reduce free Ca^{2+} to < 1 μM. Calcium was varied by adding 100 μM $CaCl_2$ or 100 μM EGTA to the bilayer chamber.

Surface plasmon resonance studies of BAX–liposome interaction

These studies were done using Biacore X instrumentation and software (Biacore Division of GE Healthcare, Uppsala, Sweden) at an ambient temperature of 20°C. Buffers were filtered through 0.22 μm filter prior to use. Liposomes were prepared as described above. The buffer was EB unless noted. The sensor surface of an L1 chip (Biacore) was equilibrated in EB. Liposomes were injected at a phospholipid concentration of 0.6 mg/mL across the sensor surface at a flow rate of 3 μL/min. for 12 min. Loosely associated liposomes were washed from the surface by increasing the flow rate of running buffer to 500 μL/min. for 30 s. Bovine serum albumin (1 mg/mL) was injected at 15 μL/min. for 2 min. to ascertain the extent of liposome coverage of the surface and to block remaining nonspecific binding sites (58). The DOPC:DOPA liposomes loaded to 13 ± 0.9 ng lipid/μm^2 and the DOPC:DOPA:C liposomes loaded to 12.3 ± 1.2 ng lipid/μm^2. Variation in loading was primarily due to variation in the liposome size distribution. $BAX^{\Delta C}$ protein was injected over supported liposomes at 30 μL/min., and the dissociation was observed for 5 min. at the same flow rate at which the protein was injected. The response was corrected for injection artifacts. Data were analyzed and displayed using BIAevaluation (Biacore) and Origin 7.5 (OriginLab Corporation) software. At each concentration of BAX protein, the line presented results from the averaging of two to four independent binding studies. The standard deviation from this averaging is shown in the binding plots when its value is larger than the symbols or line that is being displayed.

2.7 | References

1. Steller, H. (1995) *Science* **267**, 1445-1449
2. Adams, J. M., and Cory, S. (2007) *Curr Opin Immunol* **19**, 488-496
3. Danial, N. N., and Korsmeyer, S. J. (2004) *Cell* **116**, 205-219
4. Korsmeyer, S. J., Wei, M. C., Saito, M., Weiler, S., Oh, K. J., and Schlesinger, P. H. (2000) *Cell Death Differ* **7**, 1166-1173
5. Dejean, L. M., Martinez-Caballero, S., and Kinnally, K. W. (2006) *Cell Death Differ* **13**, 1387-1395
6. Green, D. R., and Kroemer, G. (2004) *Science* **305**, 626-629
7. Jiang, X., and Wang, X. (2004) *Annu Rev Biochem* **73**, 87-106
8. Reed, J. C. (2006) *Cell Death Differ* **13**, 1378-1386
9. Youle, R. J. (2007) *Science* **315**, 776-777
10. Leber, B., Lin, J., and Andrews, D. W. (2007) *Apoptosis* **12**, 897-911
11. Annis, M. G., Soucie, E. L., Dlugosz, P. J., Cruz-Aguado, J. A., Penn, L. Z., Leber, B., and Andrews, D. W. (2005) *Embo J* **24**, 2096-2103
12. Gross, A., Jockel, J., Wei, M. C., and Korsmeyer, S. J. (1998) *Embo J* **17**, 3878-3885
13. Mikhailov, V., Mikhailova, M., Degenhardt, K., Venkatachalam, M. A., White, E., and Saikumar, P. (2003) *J Biol Chem* **278**, 5367-5376
14. Mikhailov, V., Mikhailova, M., Pulkrabek, D. J., Dong, Z., Venkatachalam, M. A., and Saikumar, P. (2001) *J Biol Chem* **276**, 18361-18374
15. Kim, H., Rafiuddin-Shah, M., Tu, H. C., Jeffers, J. R., Zambetti, G. P., Hsieh, J. J., and Cheng, E. H. (2006) *Nat Cell Biol* **8**, 1348-1358
16. Uren, R. T., Dewson, G., Chen, L., Coyne, S. C., Huang, D. C., Adams, J. M., and Kluck, R. M. (2007) *J Cell Biol* **177**, 277-287
17. Willis, S. N., Fletcher, J. I., Kaufmann, T., van Delft, M. F., Chen, L., Czabotar, P. E., Ierino, H., Lee, E. F., Fairlie, W. D., Bouillet, P., Strasser, A., Kluck, R. M., Adams, J. M., and Huang, D. C. (2007) *Science* **315**, 856-859
18. Schlesinger, P. H., Gross, A., Yin, X. M., Yamamoto, K., Saito, M., Waksman, G., and Korsmeyer, S. J. (1997) *Proc Natl Acad Sci U S A* **94**, 11357-11362
19. Saito, M., Korsmeyer, S. J., and Schlesinger, P. H. (2000) *Nat Cell Biol* **2**, 553-555
20. Westover, E. J., and Covey, D. F. (2004) *J Membr Biol* **202**, 61-72
21. Mouritsen, O. G., and Zuckermann, M. J. (2004) *Lipids* **39**, 1101-1113
22. Soccio, R. E., and Breslow, J. L. (2004) *Arterioscler Thromb Vasc Biol* **24**, 1150-1160
23. Cheng, B., Hsu, D. K., and Kimura, T. (1985) *Mol Cell Endocrinol* **40**, 233-243
24. Tuckey, R. C., Headlam, M. J., Bose, H. S., and Miller, W. L. (2002) *J Biol Chem* **277**, 47123-47128
25. Leonarduzzi, G., Biasi, F., Chiarpotto, E., and Poli, G. (2004) *Mol Aspects Med* **25**, 155-167
26. Casellas, P., Galiegue, S., and Basile, A. S. (2002) *Neurochem Int* **40**, 475-486

27. Lacapere, J. J., and Papadopoulos, V. (2003) *Steroids* **68**, 569-585
28. Jamin, N., Neumann, J. M., Ostuni, M. A., Vu, T. K., Yao, Z. X., Murail, S., Robert, J. C., Giatzakis, C., Papadopoulos, V., and Lacapere, J. J. (2005) *Mol Endocrinol* **19**, 588-594
29. Omura, T. (2006) *Chem Biol Interact* **163**, 86-93
30. Russell, D. W. (2000) *Biochim Biophys Acta* **1529**, 126-135
31. Campbell, A. M., and Chan, S. H. (2007) *Arch Biochem Biophys* **466**, 203-210
32. Feo, F., Canuto, R. A., Bertone, G., Garcea, R., and Pani, P. (1973) *FEBS Lett* **33**, 229-232
33. Lucken-Ardjomande, S., Montessuit, S., and Martinou, J. C. (2008) *Cell Death Differ* **15**, 484-493
34. Martinez-Abundis, E., Garcia, N., Correa, F., Franco, M., and Zazueta, C. (2007) *Febs J* **274**, 6500-6510
35. Chen, C., Cui, J., Lu, H., Wang, R., Zhang, S., and Shen, P. (2007) *Biophys J* **92**, 4304-4315
36. Cartron, P. F., Arokium, H., Oliver, L., Meflah, K., Manon, S., and Vallette, F. M. (2005) *J Biol Chem* **280**, 10587-10598
37. Er, E., Oliver, L., Cartron, P. F., Juin, P., Manon, S., and Vallette, F. M. (2006) *Biochim Biophys Acta* **1757**, 1301-1311
38. Kroemer, G., Galluzzi, L., and Brenner, C. (2007) *Physiol Rev* **87**, 99-163
39. Cortese, J. D., Voglino, A. L., and Hackenbrock, C. R. (1991) *J Cell Biol* **113**, 1331-1340
40. Gupte, S. S., and Hackenbrock, C. R. (1988) *J Biol Chem* **263**, 5248-5253
41. Deerinck, T. J., Martone, M. E., Lev-Ram, V., Green, D. P., Tsien, R. Y., Spector, D. L., Huang, S., and Ellisman, M. H. (1994) *J Cell Biol* **126**, 901-910
42. Schikorski, T., and Stevens, C. F. (2001) *Nat Neurosci* **4**, 391-395
43. Komarov, A. G., Deng, D., Craigen, W. J., and Colombini, M. (2005) *Biophys J* **89**, 3950-3959
44. Hulbert, A. J., Turner, N., Hinde, J., Else, P., and Guderley, H. (2006) *J Comp Physiol B* **176**, 93-105
45. Bathori, G., Csordas, G., Garcia-Perez, C., Davies, E., and Hajnoczky, G. (2006) *J Biol Chem* **281**, 17347-17358
46. Pavlov, E., Grigoriev, S. M., Dejean, L. M., Zweihorn, C. L., Mannella, C. A., and Kinnally, K. W. (2005) *Biochim Biophys Acta* **1710**, 96-102
47. Rostovtseva, T., and Colombini, M. (1997) *Biophys J* **72**, 1954-1962
48. Rostovtseva, T. K., Tan, W., and Colombini, M. (2005) *J Bioenerg Biomembr* **37**, 129-142
49. Schein, S. J., Colombini, M., and Finkelstein, A. (1976) *J Membr Biol* **30**, 99-120
50. Scorrano, L., Oakes, S. A., Opferman, J. T., Cheng, E. H., Sorcinelli, M. D., Pozzan, T., and Korsmeyer, S. J. (2003) *Science* **300**, 135-139

51. Feigenson, G. W. (2007) *Annu Rev Biophys Biomol Struct* **36**, 63-77
52. Hung, W. C., Lee, M. T., Chen, F. Y., and Huang, H. W. (2007) *Biophys J* **92**, 3960-3967
53. Smaby, J. M., Momsen, M. M., Brockman, H. L., and Brown, R. E. (1997) *Biophys J* **73**, 1492-1505
54. Goping, I. S., Gross, A., Lavoie, J. N., Nguyen, M., Jemmerson, R., Roth, K., Korsmeyer, S. J., and Shore, G. C. (1998) *J Cell Biol* **143**, 207-215
55. Wolter, K. G., Hsu, Y. T., Smith, C. L., Nechushtan, A., Xi, X. G., and Youle, R. J. (1997) *J Cell Biol* **139**, 1281-1292
56. Cho, W., and Stahelin, R. V. (2005) *Annu Rev Biophys Biomol Struct* **34**, 119-151
57. Erb, E. M., Chen, X., Allen, S., Roberts, C. J., Tendler, S. J., Davies, M. C., and Forsen, S. (2000) *Anal Biochem* **280**, 29-35
58. Anderluh, G., Besenicar, M., Kladnik, A., Lakey, J. H., and Macek, P. (2005) *Anal Biochem* **344**, 43-52
59. Ownby, C. L., Powell, J. R., Jiang, M. S., and Fletcher, J. E. (1997) *Toxicon* **35**, 67-80
60. Shaposhnikova, V. V., Egorova, M. V., Kudryavtsev, A. A., Levitman, M., and Korystov Yu, N. (1997) *FEBS Lett* **410**, 285-288
61. Youle, R. J., and Strasser, A. (2008) *Nat Rev Mol Cell Biol* **9**, 47-59
62. Harata, N., Ryan, T. A., Smith, S. J., Buchanan, J., and Tsien, R. W. (2001) *Proc Natl Acad Sci U S A* **98**, 12748-12753
63. Cortese, J. D., and Hackenbrock, C. R. (1993) *Biochim Biophys Acta* **1142**, 194-202
64. Rostovtseva, T. K., Kazemi, N., Weinrich, M., and Bezrukov, S. M. (2006) *J Biol Chem* **281**, 37496-37506
65. Willis, S. N., and Adams, J. M. (2005) *Curr Opin Cell Biol* **17**, 617-625
66. Cheng, E. H., Sheiko, T. V., Fisher, J. K., Craigen, W. J., and Korsmeyer, S. J. (2003) *Science* **301**, 513-517
67. Hauser, H., and Poupart, G. (2005) *The Structure of Biological Membranes*, 2nd ed., CRC Press, Boca Raton, FL
68. Rouslin, W., MacGee, J., Gupte, S., Wesselman, A., and Epps, D. E. (1982) *Am J Physiol* **242**, H254-259
69. Epand, R. M. (2006) *Prog Lipid Res* **45**, 279-294
70. Crowder, C. M., Westover, E. J., Kumar, A. S., Ostlund, R. E., Jr., and Covey, D. F. (2001) *J Biol Chem* **276**, 44369-44372
71. Alakoskela, J. M., Sabatini, K., Jiang, X., Laitala, V., Covey, D. F., and Kinnunen, P. K. (2008) *Langmuir* **24**, 830-836
72. Crain, R. C., Clark, R. W., and Harvey, B. E. (1983) *Cancer Res* **43**, 3197-3202
73. Graham, J. M., and Green, C. (1970) *Eur J Biochem* **12**, 58-66
74. Werner, M., Sacher, J., and Hohenegger, M. (2004) *Br J Pharmacol* **143**, 715-724
75. Anderluh, G., Macek, P., and Lakey, J. H. (2003) *Toxicon* **42**, 225-228

76. Bastos, M., Bai, G., Gomes, P., Andreu, D., Goormaghtigh, E., and Prieto, M. (2008) *Biophys J* **94**, 2128-2141
77. Bavdek, A., Gekara, N. O., Priselac, D., Gutierrez Aguirre, I., Darji, A., Chakraborty, T., Macek, P., Lakey, J. H., Weiss, S., and Anderluh, G. (2007) *Biochemistry* **46**, 4425-4437
78. Besenicar, M., Macek, P., Lakey, J. H., and Anderluh, G. (2006) *Chem Phys Lipids* **141**, 169-178
79. Papo, N., and Shai, Y. (2003) *Biochemistry* **42**, 458-466
80. Ali, S., Smaby, J. M., Brockman, H. L., and Brown, R. E. (1994) *Biochemistry* **33**, 2900-2906
81. McConnell, H. M., and Vrljic, M. (2003) *Annu Rev Biophys Biomol Struct* **32**, 469-492
82. Szoka, F., Jr., and Papahadjopoulos, D. (1978) *Proc Natl Acad Sci U S A* **75**, 4194-4198
83. Stewart, J. C. (1980) *Anal Biochem* **104**, 10-14
84. Djedovic, N., Ferdani, R., Harder, E., Pajewska, J., Pajewski, R., Weber, M. E., Schlesinger, P. H., and Gokel, G. W. (2005) *New J Chem* **29**, 291-305
85. Gokel, G. W., Schlesinger, P. H., Djedovic, N. K., Ferdani, R., Harder, E. C., Hu, J., Leevy, W. M., Pajewska, J., Pajewski, R., and Weber, M. E. (2004) *Bioorg Med Chem* **12**, 1291-1304
86. Schlesinger, P. H., and Saito, M. (2006) *Cell Death Differ* **13**, 1403-1408
87. Hille, B. (2001) *Ionic Channels of Excitable Membranes, Chapter 11*, 3rd ed., Sinuaer Associates, Inc., Sunderland, MA
88. Miller, C. (1984) *Annu Rev Physiol* **46**, 549-558
89. Rex, S., and Schwarz, G. (1998) *Biochemistry* **37**, 2336-2345
90. Frezza, C., Cipolat, S., and Scorrano, L. (2007) *Nat Protoc* **2**, 287-295
91. Pallotti, F., and Lenaz, G. (2001) *Methods Cell Biol* **65**, 1-35
92. Mancuso, D. J., Sims, H. F., Han, X., Jenkins, C. M., Guan, S. P., Yang, K., Moon, S. H., Pietka, T., Abumrad, N. A., Schlesinger, P. H., and Gross, R. W. (2007) *J Biol Chem* **282**, 34611-34622
93. Frolov, A., Zielinski, S. E., Crowley, J. R., Dudley-Rucker, N., Schaffer, J. E., and Ory, D. S. (2003) *J Biol Chem* **278**, 25517-25525
94. Nicholls, D. G., and Ferguson, S. J. (2001) *Bioenergetics 3, Chap. 5: Respiratory Chains*, Academic Press, London, UK

CHAPTER 3

Steroid Effects on BAX Pore Activation

3.1 | Summary

The cell suicide program of apoptosis is regulated not only by protein constituents but also lipids and steroids. The BCL2 protein family provides a conduit through which lipid/steroid imbalance effects cell death. As we've demonstrated, membrane cholesterol inhibits the pore-forming ability of BAX by interfering with its bilayer integration. The functional locales of BAX, mitochondria, perform many enzymatic modifications of cholesterol to generate oxysterols and bile acids. These molecules are known to induce apoptosis in a variety of cell types but the molecular mechanisms are poorly characterized. In this chapter, we extend our BAX-vesicle leakage assay to investigate the effects of steroids 25-hydroxycholesterol (25-HC) and lithocholic acid (LCA) on the efficiency of BAX pore activation. At low micromolar concentrations, 25-HC accelerates formation of BAX pores. This promotion by 25-HC lies in contrast to inhibition by cholesterol; we attribute this functional disparity to the two sterols' oppositional effects on membrane fluidity, with cholesterol condensing the bilayer and 25-HC spreading it. The bile acid lithocholic acid was found to activate $BAX^{\Delta C}$ at sub-critical micelle concentrations whereas activation of full-length BAX required micellar LCA. From these data, we conclude that instigation of cellular apoptosis by 25-HC and LCA is likely a product of cell stress recognition, not direct allosteric perturbation of inactive BAX, but the two steroids may intensify BAX's membrane attack by modulation of bilayer physical properties.

3.2 | Introduction

Lipids compose the local environment in which the BCL2 family functions. While the proteinaceous machinery of mitochondrial apoptosis has been subjected to intense scrutiny, complementary research into lipidic components has lagged (1). During apoptosis, the lipid composition of MOM is altered substantially, especially by oxidative stress (2). Most of the phospholipid changes, however, appear to occur subsequent to mitochondrial outer membrane permeabilization (MOMP) with the exception of lysolipid (including monolysocardiolipin) accumulation (1) and likely play at most an amplificatory role in forwarding the death signal.

Mitochondria are cholesterol-poor organelles (3) but, as we and others have demonstrated, the presence of cholesterol in vesicle and mitochondrial outer membranes (MOM) inhibits the efficiency of BAX pore activation (4-6). Enhancement of the mitochondrial cholesterol store has been implicated in the pathogeneses of steatohepatitis, (hepato)carcinomas, and Alzheimer's disease (7). Mitochondrial cholesterol pools are dynamic as the organelles perform cholesterol modifications necessary for steroid, bile acid, and oxysterol syntheses. Besides acting in cellular signaling, conversion of cholesterol into an oxysterol significantly improves solubility and facilitates clearance from the system during states of cholesterol excess (8).

The relationship between elevated levels of oxysterols and atherosclerosis has been widely-investigated using both *in vivo* and *in vitro* models; evidence is mounting that oxysterols also play a role in the pathogenesis of degenerative diseases like Alzheimer's and Parkinson's diseases, multiple sclerosis, and age-related macular degeneration (9-12). Oxysterols are known

to be inducers of apoptosis in a variety of cell types (13) and the apoptotic signal is propagated by both death receptor and mitochondrial pathways (but the latter appears to be dominant) (14). Of vascular wall constituent cell types, 25-hydroxycholesterol (25-HC) can instigate apoptosis in monocyte/macrophage, aortic endothelial, and smooth muscle cells (15-17). Lymphoid cell lines have also been observed to undergo apoptosis after exposure to 25-HC (18). A number of reports have demonstrated that oxysterols induce cytochrome *c* release in a variety of cell types (14). In vascular SMCs, oxysterol-induced apoptosis appeared to be dependent on BAX translocation to mitochondria (19,20). In macrophage-like cell lines, siRNA knockdown of BAX completely ablated apoptosis induced by 25-HC (21) while overexpression of BCL-2 could partially suppress cell death (22).

Besides oxysterols, other physiologically-significant cholesterol derivatives are bile acids. These molecules act essentially as biological detergents, secreted into the intestinal lumen to solubilize ingested lipids. High concentrations of bile acids, however, are toxic and can induce apoptotic and necrotic cell death. Multiple studies have demonstrated that bile acids induce apoptosis in a variety of cell types, including colon cancer cells and hepatocytes (23-31). Though the direct mechanism is not well-characterized, cell death by bile acids appears to be a function of both intrinsic and extrinsic apoptotic pathways. Several studies have found that bile acids can induce mitochondrial dysfunction (32-37); unclear is the molecular specificity of this relationship, be it a detergent-like disruption of mitochondrial membranes or protein interaction.

Our collaborators Drs. Bryson Katona & Doug Covey discovered that the prominent intestinal bile acid lithocholic acid (LCA) could induce apoptosis in cultured colon adenocarcinoma cells and that BAX translocation to mitochondria occurred rapidly in response to application of the bile acid. This finding piqued our curiosity, as BAX activation has been (until recently) largely nebulous and revelation of a non-proteinaceous, but physiologically-tolerable, activator could prove pharmacologically useful.

3.3 | Results

For this chapter, two forms of BAX were employed—C-terminally truncated BAX ($BAX^{\Delta C}$) and full-length BAX. While $BAX^{\Delta C}$ was useful as a probe of the final step of BAX activity, i.e. the kinetics of pore formation (Chap. 2), we sought to more closely mimic the physiological molecule and its regulation, thus experimental adoption of full-length BAX. Also adopted into our regime was BH3-only protein BID which is the prototypical BAX-activating protein; activation of BID into apoptotically-proficient cBID was performed by cutting the protein with recombinant caspase-8. Hence, for this chapter, we use two BAX forms ($BAX^{\Delta C}$ & FL BAX) and two activation methods (incubation with detergent & cBID) (38,39). Also, LUV compositions differ depending on which BAX is under study. Vesicles encapsulate either 5(6)-carboxyfluorescein (0.38 kDa) for $BAX^{\Delta C}$ or 10 kDa FITC-dextran for BAX. The two formulations were necessary because while native $BAX^{\Delta C}$ interacts very weakly with membranes (and fails to induce leakage), full-length BAX binds more avidly and can generate small disruptions sufficient for small dye leakage (see Chap. 4).

25-hydroxycholesterol enhances $BAX^{\Delta C}$ pore activation

Since we found that cholesterol inhibited $BAX^{\Delta C}$-mediated vesicle leakage and that oxysterols have been shown to induce apoptosis, we were curious as to whether the cholesterol derivative 25-hydroxycholesterol (25-HC) could promote BAX activity in our reconstituted leakage assays. Incorporation of 25-HC to the vesicles was accomplished simply by diluting the oxysterol into assay cuvets—25-HC is more hydrophilic than cholesterol but readily partitions from an aqueous environment into bilayers (40). As depicted in Fig. 3.1, 25-HC does indeed

have an effect contrary to that of cholesterol—the oxysterol accelerates pore formation by detergent-activated $BAX^{\Delta C}$. Promotion of leakage by 25-HC is dramatic as shown by the representative traces in Fig. 3.1A. Visual examination of the data suggested that the leakage-enhancing effect of 25-HC saturates at high concentrations of the oxysterol. To quantify the degree of this acceleration of pore formation, we applied the method from Chap. 2 and fit the leakage traces to a single exponential to extract time constants, τ (4,41). From this kinetic analysis, we observed the leakage enhancing effect of 25-HC is most pronounced below 10 μM with the time constants dropping from $\approx$110 to under 50. Effectively, the oxysterol can double the leakage rate elicited by $BAX^{\Delta C}$ (Fig. 3.1B).

Fig. 3.1

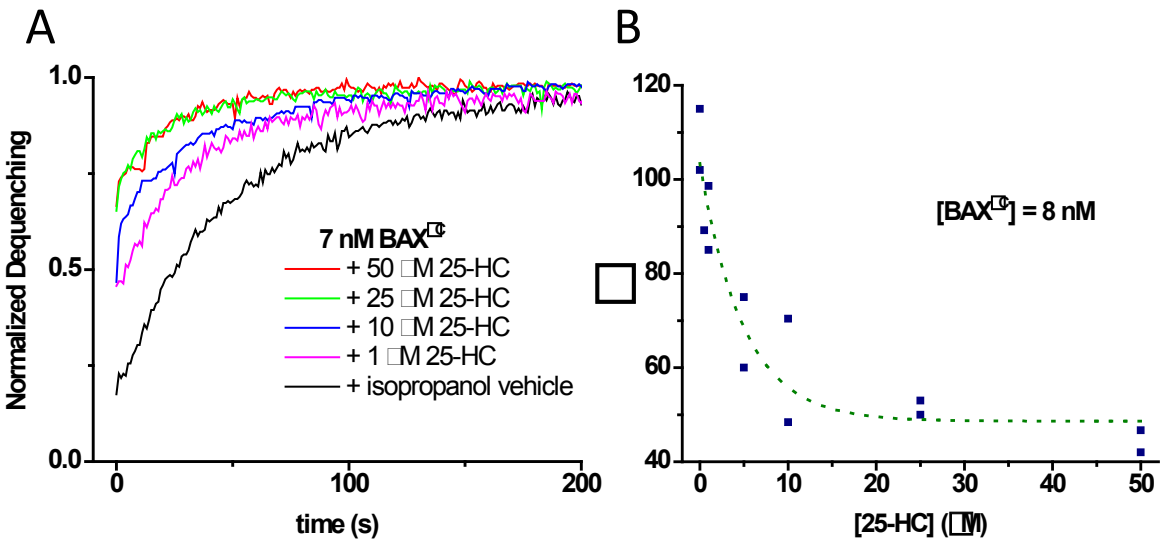

Fig. 3.1 | **25-hydroxycholesterol accelerates BAX$^{\Delta C}$ pore formation**. *A*, CF LUVs (70:30 DOPC:DOPA), 5 μM total lipid, were equilibrated (1 hr) with indicated solution concentrations of 25-HC. Detergent-activated BAX$^{\Delta C}$ (see Chap. 2) was then added to induce CF leakage at 22°C. *B*, BAX$^{\Delta C}$ pore acceleration saturates above 10 μM 25-HC. CF-leakage traces (not shown) were fit to a single exponential [Chap. 2, Eq. 1: $F_{520} = F_0 A_1 (1 - e^{(\text{time}/\tau)}) + m \times \text{time}$] to extract τ values. τ values at constant [BAX$^{\Delta C}$] were then plotted as a function of 25-HC concentration.

cBID activates BAX and is potentiated by cardiolipin

The membrane targeting specificity of the BCL2 family is partly dependent on a unique lipid—cardiolipin (CL). This anionic lipid comprises four acyl chains and is synthesized in mitochondria. Previous studies have indicated that cardiolipin acts in a receptor-like fashion for BH3-only protein BID, which is typically localized to the cytosol (42-44). As we were interested in investigating the regulatory sequence of BAX activation leading to pore formation, not only that final step, it was necessary to assess the fidelity of our reconstituted vesicle leakage system.

We first employed LUVs comprising the small dye 5(6)-carboxyfluorescein (0.38 kDa). This formulation, however, proved to be ill-suited as BAX and cBID separately induced substantial leakage (see Chap. 4). We then adapted a method devised by Kuwana *et al*. whereby a large dye, 10 kDa dextran conjugated to FITC (FD10), was incorporated into LUVs (45). Illustrated in Fig. 3.2, these FD10 vesicles provided a useful means of observing cBID-BAX pore activation. Notably, and in accordance with prior findings, replacement of 10 mol% DOPA with 10 mol% CL in our vesicles drastically accelerated leakage (Fig. 3.2, black vs. magenta traces). Inclusion of CL more than 5-fold enhanced the efficacy of cBID-BAX activation (red vs. magenta traces). BAX by itself caused only trivial leakage, also in agreement with its default intracellular inactivity (green trace). These results revealed that our experimental model broadly recapitulates the physiological process and would likely be extensible for addition of modulating factors (e.g. oxysterols).

Fig. 3.2

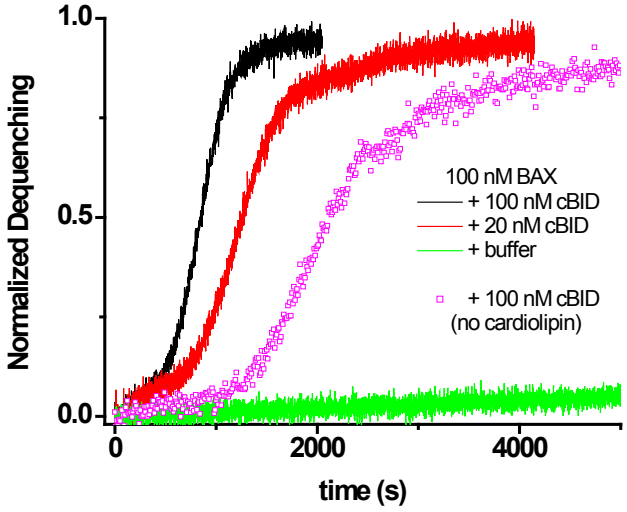

Fig. 3.2 | **Cardiolipin dependence of cBID activation of BAX**. The presence of mitochondrial lipid cardiolipin substantially enhances BAX pore formation. LUVs encapsulating FD10 were synthesized with a composition of 70:20:10 DOPC:DOPA:CL or 70:30 DOPC:DOPA (mol%) and diluted into cuvets for a final concentration of 10 µM total lipid. BAX ± cBID was then added to LUVs and leakage monitored at 22°C.

25-hydroxycholesterol enhances cBID-BAX pore activation

Having established the viability of our cell-free system including full-length BAX and activator cBID, we then revisited incorporating 25-HC. Since the oxysterol proved effective in promoting LUV poration by a detergent-treated, truncated BAX, we hypothesized that 25-HC would similarly affect poration by native BAX + cBID. Of concern to us was the inclusion of another protein (cBID) and the unusual diphospholipid CL and their potential confounding effects. These concerns turned out to apparently unwarranted as 25-HC enhanced vesicle leakage by BAX as it did in Fig. 3.1.

Time courses in Fig. 3.3A & B show dose-dependent 25-HC promotion of BAX pore formation as elicited by 10 nM and 20 nM cBID respectively. To better illustrate this acceleration, the inverse times to half-maximal dequenching ($1/t_{1/2}$) were plotted in Fig. 3.3C. (Unlike τ [in Fig. 3.1B] which *decreases* as $BAX^{\Delta C}$ pore formation becomes more rapid, $1/t_{1/2}$ *increases* as full-length BAX pore formation accelerates. The second metric was devised since cBID-BAX pore activation shows an initial lag phase and cannot be fit by a single exponential like $BAX^{\Delta C}$ pore activation.) Congruous with the enhancement of $BAX^{\Delta C}$ pore formation, promotion of cBID-BAX pore formation levels off above 10 μM 25-HC (Fig. 3.3C). Interestingly, the oxysterol enhances activation by 10 nM cBID proportionately greater than by 20 nM cBID; the rate of leakage induced by 10 nM cBID-BAX increases 62% (2.1×10^{-4} s^{-1} → 3.4×10^{-4} s^{-1}) while the rate of 20 nM cBID-BAX increases only 41% (2.7×10^{-4} s^{-1} → 3.8×10^{-4} s^{-1}).

Visual comparison of the leakage kinetics between Fig. 3.2 and 3.3 reveals a large disparity—the leakage in Fig. 3.2 is very rapid relative to that in Fig. 3.3. The source of this discrepancy is the age and aggregation state of the BAX protein preparations. Frustratingly, BAX aggregates over time and loses as much as ½ of its activity in one week (46,47) (data not shown). For Fig. 3.2, the BAX was freshly purified but for Fig. 3.3 the protein had been in storage at 4°C for a couple weeks. These experiments were performed prior to our discovery of this complication. While the two datasets in Fig. 3.2 and 3.3 cannot be directly compared, meaningful comparisons of the data in 3.3 can be made since all were collected on the same day.

Fig. 3.3

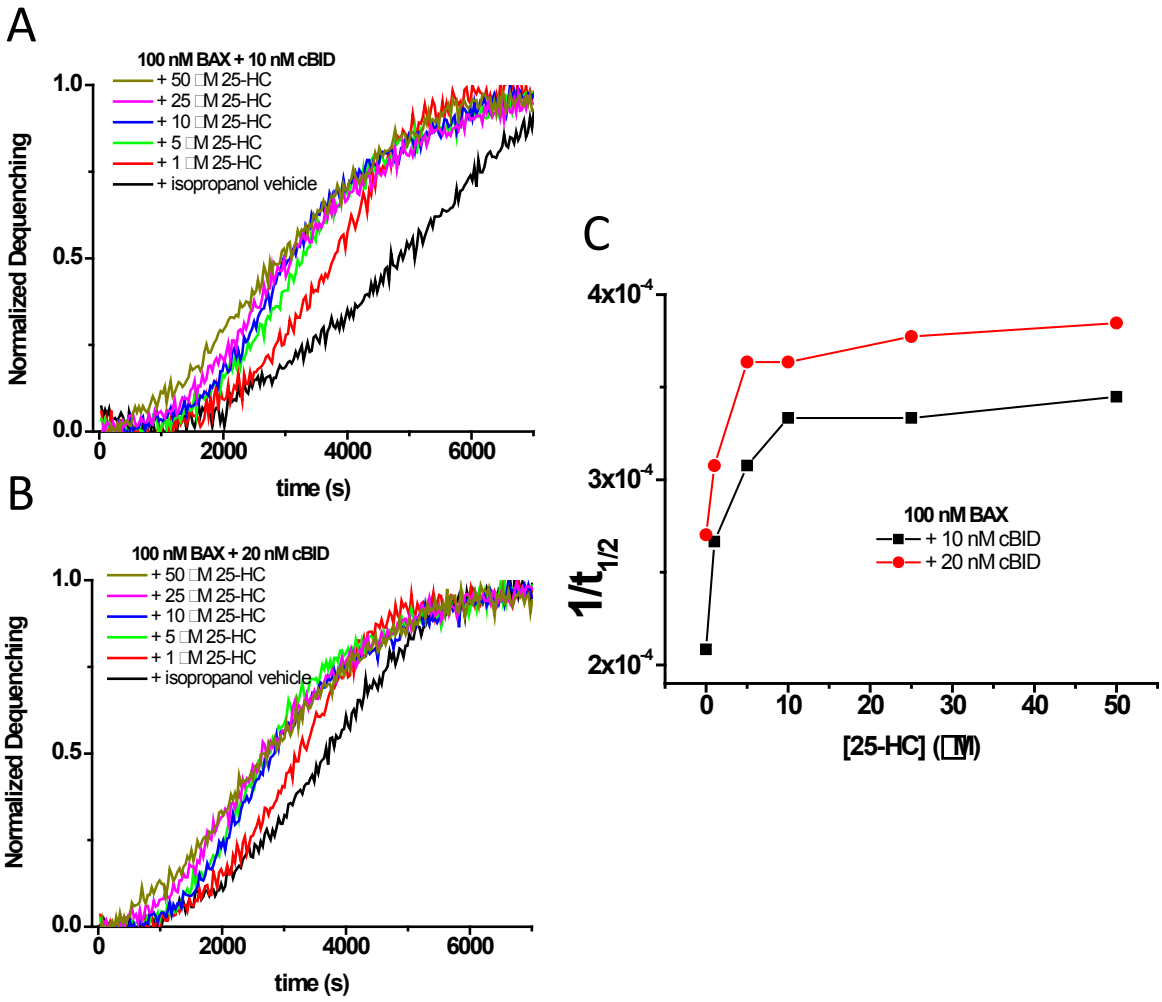

Fig. 3.3 | **25-hydroxycholesterol accelerates full-length BAX pore formation**. *A & B*, LUVs (10 μM lipid) encapsulating FD10 were equilibrated with indicated solution concentrations of 25-HC for an hour; vesicle composition was 70:20:10 DOPC:DOPA:CL (mol%). 100 nM BAX and 10 nM cBID (*A*) or 20 nM cBID (*B*) were then added to induce FD10 leakage. Assays were performed at 22°C. *C*, Saturation of 25-HC enhancement of BAX pore formation. $1/t_{1/2}$ values were derived from curves in *A* & *B* and defined as the inverse of the time to half-maximal leakage. $1/t_{1/2}$ values were then plotted as a function of 25-HC concentration at constant [BAX] (100 nM) and two concentrations of activator cBID (10 & 20 nM).

Bile acids can activate BAX

Biochemical studies have indicated that synthetic, non-ionic detergents alter the conformation and activate the pore-forming capacity of BAX (38,48-50); conversely, the zwitterionic detergent CHAPS elicited no such changes. Notably, these detergent-evoked BAX alterations required the presence of detergent micelles. Given that bile acids act as physiological non-ionic detergents and have been demonstrated to induce apoptosis, we adduced a reductionist mechanism whereby bile acids could directly activate BAX to drive cells to their deaths. Graciously provided by Drs. Katona & Covey, we incorporated lithocholic acid (LCA), a known apoptosis promoter, to our BAX-LUV leakage system. Initial experiments were promising—non-active $BAX^{\Delta C}$ could be effectively activated by micromolar concentrations of LCA (Fig. 3.4A). Importantly, the tested concentrations—1-100 μM—are well-below the critical micelle concentration of LCA (≈275 μM). LCA's activating effect on $BAX^{\Delta C}$ also displayed intriguing concentration dependence. A second bile acid, chenodeoxycholic acid (CDCA), was also tested; this bile acid was previously shown to elicit mitochondrial cytochrome *c* release (32,33,36). CDCA also provoked $BAX^{\Delta C}$ pore activation, albeit less efficiently (data not shown).

Having success in purification of full-length BAX, we chose to revisit our bile acid activation findings. Using the same activation protocol, we found that full-length BAX was resistant to the detergent and required LCA micelles to produce an active protein, similar to BAX activation by synthetic, non-ionic detergents (Fig. 3.4B). Only with LCA concentrations

of 400-800 μM was even mild activation demonstrated. Parallel assays with CDCA (CMC ≈10 mM) revealed no BAX activation (data not shown).

Fig. 3.4

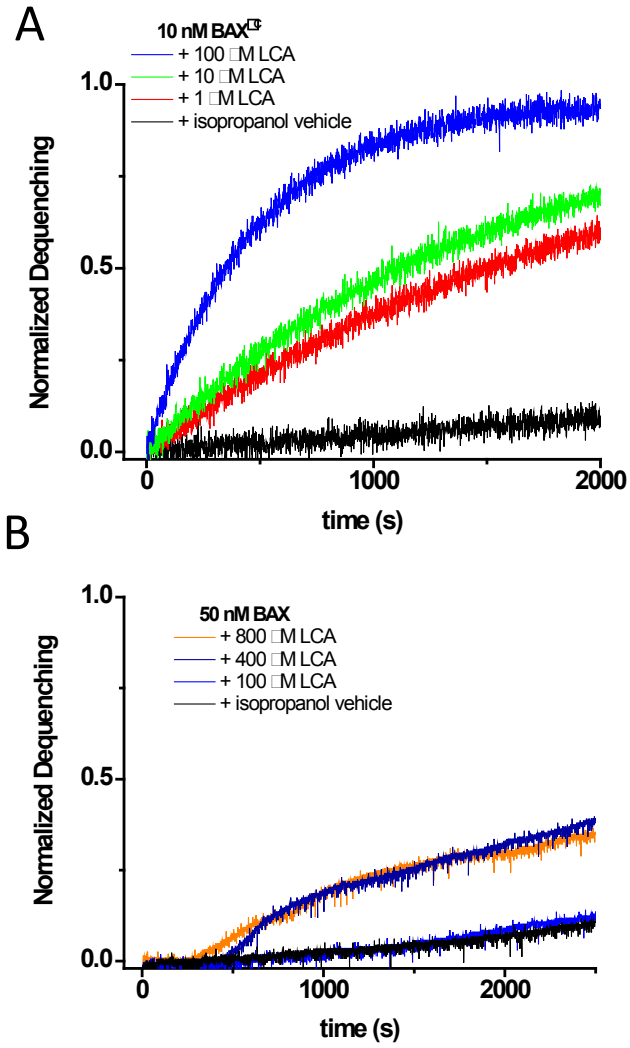

Fig. 3.4 | **Lithocholic acid activations of BAX$^{\Delta C}$ and full-length BAX**. *A*, Non-micellar lithocholic acid (LCA; critical micelle concentration ≈275 μM) activates BAX$^{\Delta C}$. Non-active, detergent-free BAX$^{\Delta C}$ was incubated overnight with indicated concentrations of LCA and applied to CF LUVs (5 μM lipid) at 22°C; vesicle composition was DOPC:DOPA 70:30 (mol%). *B*, Full-length BAX activated by LCA micelles. BAX was incubated overnight with indicated concentrations of LCA and applied to FD10 LUVs (5 μM lipid) at 22°C; vesicle composition was DOPC:DOPA 70:30 (mol%). LCA solution concentration in the assay cuvets was <4 μM which failed to cause dye leakage (data not shown).

3.4 | Discussion

25-HC promotion of BAX pore formation

The mechanisms of cholesterol homeostasis and related pathogeneses have been under investigation for some time. Well-established is the notion that cellular proteins directly bind to cholesterol and other steroids to mobilize the sterols and effect changes in various signaling and synthesis pathways. Becoming recognized is that sensing of bulk membrane environment modulation also contributes to cellular recognition of sterol content, as well as to the apoptotic and pathological effects of sterol imbalance (40,51).

Having two hydroxyl groups (one on each end) affords 25-hydroxycholesterol much greater solubility in aqueous solution than cholesterol. Whereas cholesterol orients perpendicular to the membrane surface to maximize hydrogen bonding for its 3-OH, 25-HC can adopt a variety of orientations, including parallel to the plane of the bilayer where both hydroxyls are solvent-exposed (13,40,52). Thus cholesterol condenses and thickens the bilayer by decreasing the mobility of phospholipid acyl tails while 25-HC can induce an opposite bilayer effect.

We attribute the acceleration of BAX pore formation by 25-HC to the sterol's capacity to increase the mean area per lipid, i.e. spread apart the lipids, to facilitate BAX membrane integration. This effect is the converse of our finding that cholesterol inhibits poration by suppressing BAX membrane integration (4-6). Enhancement of pore activation by 25-HC was demonstrated regardless of how a membrane-competent BAX form was generated, by both detergent and BH3-only activator cBID. Significantly, enhancement was noted at ≤1 μM 25-

HC, suggesting that even mild intracellular accumulation of the oxysterol could render mitochondrial membranes more susceptible to BAX predation and tilt the life/death balance toward apoptosis.

Bile acid activation of BAX

Elucidation of BAX (& BAK) activation and identification of BAX/BAK regulators are the subjects of continuing research. Preliminary work on the naturally-occurring bile acid lithocholic acid hinted that it may be one of these strongly sought after BAX activators. Unfortunately, *in vitro* interrogation of this hypothesis provided mixed results at best. Deletion of the C-terminal α-helix of BAX allowed activation by monomeric, non-micellar LCA. Conversely, full-length BAX required LCA micelles to elicit a pore-competent conformation, a finding reminiscent of previous reports employing non-physiological detergents (38,48,50). This ninth α-helix (truncated from $BAX^{\Delta C}$) serves to address BAX to mitochondrial membranes yet also stabilizes its globular, cytosolically-localized conformation (53-55). Given that it is unlikely for bile acids to sufficiently accumulate inside cells to generate micelles—such aggregates would disrupt membranes and instigate necrosis—physiological detergents like LCA probably induce apoptosis by typical cell stress recognition pathways. Indeed, after failure to produce active BAX *in vitro* by low concentrations of LCA, Dr. Katona uncovered that LCA exerts an apoptotic influence via increased oxidative stress, which leads to caspase-8 activation, BID cleavage, and subsequently BAX/BAK activation (56).

Though LCA seems to compel apoptosis via stress pathways rather than direct remodeling of inactive BAX, the hydrophilic bile acid tauroursodeoxycholic acid (TUDCA)

has been shown to protect isolated mitochondria against BAX membrane integration and cytochrome *c* liberation (57). TUDCA was chosen as protective agent since it is used as a therapy against chronic cholestatic liver diseases and can inhibit apoptosis in hepatocytes and non-liver cells alike (58). Protection by TUDCA appears to be conferred at least partly by stabilization of organelle membranes (59).

In conclusion, we have employed a simplified reconstitution scheme to illuminate that steroids can enhance the activity of proapoptotic BAX. A direct alteration of BAX structure by low micromolar 24-HC and LCA are not supported but instead their modulation of membrane properties facilitates BAX perforation. In cells, where the balance between life and death is finely calibrated, even small perturbations can have dire consequences.

3.5 | Experimental Procedures

Protein expression and purification

$BAX^{\Delta C}$ was produced as described in Chap. 2. For oxysterol experiments, $BAX^{\Delta C}$ was purified in the presence of detergent to activate the protein. For bile acid experiments, $BAX^{\Delta C}$ was prepared detergent-free so as to leave the protein inactive unless activated by incubation with bile acids. Purifications of BAX and BID are fully described in Chapter 4. Briefly, full-length BAX and BID were expressed as chitin-binding domain/intein fusion proteins and purified without detergent. After affinity column binding and on-column cleavage, proteins were further polished by anion exchange FPLC. BID was then cut by addition of caspase-8 to generate the active form, cBID.

For activation of $BAX^{\Delta C}$ and BAX by bile acids, the steroids were first dissolved in isopropanol to generate 35 mM stock solutions. From these stocks, the bile acids were diluted at least 44-fold into 10 μM $BAX^{\Delta C}$/BAX solutions to produce figure-indicated solution concentrations of bile acid. Protein/bile acid mixtures were then incubated overnight at 4°C for use in dequenching assays. Protein/bile acid mixtures were diluted at least 200-fold into assay cuvets, producing a final bile acid solution concentration of <4 μM, a quantity that resulted in no dye leakage.

Large unilamellar vesicle preparation

LUVs were prepared by two methods. Carboxyfluorescein-containing liposomes of indicated lipid compositions were produced by the ether/buffer emulsification & evaporation ("reverse phase") method detailed in Chap. 2. For LUVs containing 10 kDa FITC-dextran

(FD10), 200 nm vesicles were prepared by freeze-thawing and extrusion. Ten mg total lipid (dissolved in chloroform) were mixed to yield indicated compositions; chloroform was evaporated by nitrogen then lipids further dried under vacuum for two hours. Equilibration buffer (EB; 10 mM HEPES-KOH, pH 7.0, 100 mM KCl, 0.5 mM DTT) was supplemented with 50 mg/mL FD10 and added to dried lipid films and lipids rehydrated by a 30 s immersion in a bath sonicator. The mixture was then subjected to ten freeze/thaw cycles in liquid nitrogen and extruded 15 times through a membrane with 0.2 μm pores. Extravesicular FD10 was removed by Sephadex G-200 gel filtration respectively.

For oxysterol experiments, stocks of 35 mM 25-HC in isopropanol were generated. These stocks were diluted >700-fold into assay cuvets to yield figure-indicated solution concentrations, followed by addition of LUVs. LUV/oxysterol mixtures were then incubated 1 hr at room temp to allow equilibration of the oxysterol between aqueous buffer and liposome bilayers.

3.6 | References

1. Crimi, M., and Esposti, M. D. (2010) *Biochim Biophys Acta*
2. Tyurin, V. A., Tyurina, Y. Y., Kochanek, P. M., Hamilton, R., DeKosky, S. T., Greenberger, J. S., Bayir, H., and Kagan, V. E. (2008) *Methods Enzymol* **442**, 375-393
3. van Meer, G., Voelker, D. R., and Feigenson, G. W. (2008) *Nat Rev Mol Cell Biol* **9**, 112-124
4. Christenson, E., Merlin, S., Saito, M., and Schlesinger, P. (2008) *J Mol Biol* **381**, 1168-1183
5. Lucken-Ardjomande, S., Montessuit, S., and Martinou, J. C. (2008) *Cell Death Differ* **15**, 484-493
6. Montero, J., Morales, A., Llacuna, L., Lluis, J. M., Terrones, O., Basanez, G., Antonsson, B., Prieto, J., Garcia-Ruiz, C., Colell, A., and Fernandez-Checa, J. C. (2008) *Cancer Res* **68**, 5246-5256
7. Garcia-Ruiz, C., Mari, M., Colell, A., Morales, A., Caballero, F., Montero, J., Terrones, O., Basanez, G., and Fernandez-Checa, J. C. (2009) *Histol Histopathol* **24**, 117-132
8. Morrissey, P. M., and Kiely, M. (2006) Oxysterols: formation and biological function. in *Advanced Dairy Chemistry* (Fox, P. F., and McSweeney, P. L. H. eds.), 3rd Ed., Springer, New York. pp 641–674
9. Joffre, C., Leclere, L., Buteau, B., Martine, L., Cabaret, S., Malvitte, L., Acar, N., Lizard, G., Bron, A., Creuzot-Garcher, C., and Bretillon, L. (2007) *Curr Eye Res* **32**, 271-280
10. Vaya, J., and Schipper, H. M. (2007) *J Neurochem* **102**, 1727-1737
11. Bosco, D. A., Fowler, D. M., Zhang, Q., Nieva, J., Powers, E. T., Wentworth, P., Jr., Lerner, R. A., and Kelly, J. W. (2006) *Nat Chem Biol* **2**, 249-253
12. Diestel, A., Aktas, O., Hackel, D., Hake, I., Meier, S., Raine, C. S., Nitsch, R., Zipp, F., and Ullrich, O. (2003) *J Exp Med* **198**, 1729-1740
13. Massey, J. B., and Pownall, H. J. (2006) *Biochemistry* **45**, 10747-10758
14. Lordan, S., Mackrill, J. J., and O'Brien, N. M. (2009) *The Journal of Nutritional Biochemistry* **20**, 321-336
15. O'Callaghan, Y. C., Woods, J. A., and O'Brien, N. M. (2001) *Cell Biol Toxicol* **17**, 127-137
16. Pedruzzi, E., Guichard, C., Ollivier, V., Driss, F., Fay, M., Prunet, C., Marie, J. C., Pouzet, C., Samadi, M., Elbim, C., O'Dowd, Y., Bens, M., Vandewalle, A., Gougerot-Pocidalo, M. A., Lizard, G., and Ogier-Denis, E. (2004) *Mol Cell Biol* **24**, 10703-10717
17. Panini, S. R., Yang, L., Rusinol, A. E., Sinensky, M. S., Bonventre, J. V., and Leslie, C. C. (2001) *J Lipid Res* **42**, 1678-1686
18. Christ, M., Luu, B., Mejia, J. E., Moosbrugger, I., and Bischoff, P. (1993) *Immunology* **78**, 455-460
19. Rho, M. C., Kim, Y. K., Chang, J. S., Lee, H. S., Baek, J. A., Chung, M. Y., Lee, H. C., Lee, H. W., Rhim, B. Y., Reidy, M. A., and Kim, K. (2005) *J Mol Cell Cardiol* **39**, 823-832

20. Seye, C. I., Knaapen, M. W., Daret, D., Desgranges, C., Herman, A. G., Kockx, M. M., and Bult, H. (2004) *Cardiovasc Res* **64**, 144-153
21. Rusinol, A. E., Thewke, D., Liu, J., Freeman, N., Panini, S. R., and Sinensky, M. S. (2004) *J Biol Chem* **279**, 1392-1399
22. Harada, K., Ishibashi, S., Miyashita, T., Osuga, J.-i., Yagyu, H., Ohashi, K., Yazaki, Y., and Yamada, N. (1997) *FEBS Letters* **411**, 63-66
23. Guicciardi, M. E., and Gores, G. J. (2002) *Dig Liver Dis* **34**, 387-392
24. Hague, A., Elder, D. J., Hicks, D. J., and Paraskeva, C. (1995) *Int J Cancer* **60**, 400-406
25. Haza, A. I., Glinghammar, B., Grandien, A., and Rafter, J. (2000) *Nutr Cancer* **36**, 79-89
26. Higuchi, H., and Gores, G. J. (2003) *Am J Physiol Gastrointest Liver Physiol* **284**, G734-738
27. Milovic, V., Teller, I. C., Faust, D., Caspary, W. F., and Stein, J. (2002) *Eur J Clin Invest* **32**, 29-34
28. Park, S. E., Choi, H. J., Yee, S. B., Chung, H. Y., Suh, H., Choi, Y. H., Yoo, Y. H., and Kim, N. D. (2004) *Int J Oncol* **25**, 231-236
29. Powell, A. A., LaRue, J. M., Batta, A. K., and Martinez, J. D. (2001) *Biochem J* **356**, 481-486
30. Schlottman, K., Wachs, F. P., Krieg, R. C., Kullmann, F., Scholmerich, J., and Rogler, G. (2000) *Cancer Res* **60**, 4270-4276
31. Yui, S., Saeki, T., Kanamoto, R., and Iwami, K. (2005) *J Biochem* **138**, 151-157
32. Palmeira, C. M., and Rolo, A. P. (2004) *Toxicology* **203**, 1-15
33. Rolo, A. P., Oliveira, P. J., Moreno, A. J., and Palmeira, C. M. (2003) *Mitochondrion* **2**, 305-311
34. Rolo, A. P., Palmeira, C. M., Holy, J. M., and Wallace, K. B. (2004) *Toxicol Sci* **79**, 196-204
35. Sola, S., Brito, M. A., Brites, D., Moura, J. J., and Rodrigues, C. M. (2002) *Clin Sci (Lond)* **103**, 475-485
36. Wachs, F. P., Krieg, R. C., Rodrigues, C. M., Messmann, H., Kullmann, F., Knuchel-Clarke, R., Scholmerich, J., Rogler, G., and Schlottmann, K. (2005) *Int J Colorectal Dis* **20**, 103-113
37. Payne, C. M., Crowley-Weber, C. L., Dvorak, K., Bernstein, C., Bernstein, H., Holubec, H., Crowley, C., and Garewal, H. (2005) *Cell Biol Toxicol* **21**, 215-231
38. Hsu, Y. T., and Youle, R. J. (1998) *J Biol Chem* **273**, 10777-10783
39. Wei, M. C., Lindsten, T., Mootha, V. K., Weiler, S., Gross, A., Ashiya, M., Thompson, C. B., and Korsmeyer, S. J. (2000) *Genes Dev* **14**, 2060-2071
40. Gale, S. E., Westover, E. J., Dudley, N., Krishnan, K., Merlin, S., Scherrer, D. E., Han, X., Zhai, X., Brockman, H. L., Brown, R. E., Covey, D. F., Schaffer, J. E., Schlesinger, P., and Ory, D. S. (2009) *J Biol Chem* **284**, 1755-1764
41. Saito, M., Korsmeyer, S. J., and Schlesinger, P. H. (2000) *Nat Cell Biol* **2**, 553-555

42. Esposti, M. D., Cristea, I. M., Gaskell, S. J., Nakao, Y., and Dive, C. (2003) *Cell Death Differ* **10**, 1300-1309
43. Lutter, M., Fang, M., Luo, X., Nishijima, M., Xie, X., and Wang, X. (2000) *Nat Cell Biol* **2**, 754-761
44. Gonzalvez, F., Pariselli, F., Dupaigne, P., Budihardjo, I., Lutter, M., Antonsson, B., Diolez, P., Manon, S., Martinou, J. C., Goubern, M., Wang, X., Bernard, S., and Petit, P. X. (2005) *Cell Death Differ* **12**, 614-626
45. Kuwana, T., Mackey, M. R., Perkins, G., Ellisman, M. H., Latterich, M., Schneiter, R., Green, D. R., and Newmeyer, D. D. (2002) *Cell* **111**, 331-342
46. Bleicken, S., Classen, M., Padmavathi, P. V., Ishikawa, T., Zeth, K., Steinhoff, H. J., and Bordignon, E. (2010) *J Biol Chem* **285**, 6636-6647
47. Pitter, K., Bernal, F., Labelle, J., and Walensky, L. D. (2008) *Methods Enzymol* **446**, 387-408
48. Hsu, Y. T., and Youle, R. J. (1997) *J Biol Chem* **272**, 13829-13834
49. Lewis, S., Bethell, S. S., Patel, S., Martinou, J. C., and Antonsson, B. (1998) *Protein Expr Purif* **13**, 120-126
50. Montessuit, S., Mazzei, G., Magnenat, E., and Antonsson, B. (1999) *Protein Expr Purif* **15**, 202-206
51. Massey, J. B. (2006) *Curr Opin Lipidol* **17**, 296-301
52. Olsen, B. N., Schlesinger, P. H., and Baker, N. A. (2009) *J Am Chem Soc* **131**, 4854-4865
53. Gavathiotis, E., Reyna, D. E., Davis, M. L., Bird, G. H., and Walensky, L. D. (2010) *Mol Cell* **40**, 481-492
54. Nechushtan, A., Smith, C. L., Hsu, Y. T., and Youle, R. J. (1999) *Embo J* **18**, 2330-2341
55. Suzuki, M., Youle, R. J., and Tjandra, N. (2000) *Cell* **103**, 645-654
56. Katona, B. W., Anant, S., Covey, D. F., and Stenson, W. F. (2009) *J Biol Chem* **284**, 3354-3364
57. Rodrigues, C. M., Sola, S., Sharpe, J. C., Moura, J. J., and Steer, C. J. (2003) *Biochemistry* **42**, 3070-3080
58. Rodrigues, C. M., Fan, G., Ma, X., Kren, B. T., and Steer, C. J. (1998) *J Clin Invest* **101**, 2790-2799
59. Lazaridis, K. N., Gores, G. J., and Lindor, K. D. (2001) *J Hepatol* **35**, 134-146

CHAPTER 4

BAX & BCL-X_L Independently Insert Into Membranes, a Process Accelerated by Membrane-Bound Activators tBID & BIM_S

(The content of this chapter has been adapted from Christenson, E. T., Schlesinger, P. H. (2011) (*in preparation*))

4.1 | Summary

The BCL2 protein family is a primary regulator of apoptosis and its interaction network converges at the proapoptotic BAX/BAK nexus. BAX has soluble, membrane-bound, and membrane-integrated forms that are central to the management of mitochondrial permeabilization. These states—which lead to BAX oligomerization, pore formation, and cytochrome *c* egress—are modulated by antiapoptotic multidomain and proapoptotic BH3-only proteins. Using purified recombinant BCL2 proteins and defined liposomes, the soluble→membrane transitions and pore activity modulations have been characterized. Direct activators cBID and BIM_S instigate BAX pore formation, a process inhibitable by BCL-X_L, and these oppositional functions are dosage-dependent. Compared to cBID, BIM_S is more efficient an activator and less suppressible by BCL-X_L. Real-time kinetic measurements of protein-membrane binding reveal that BAX, cBID, BIM_S, and BCL-X_L are each capable of adsorbing to membranes and these adsorptions include a rapid binding step that is reversible and distinct from a subsequent membrane integration step. The integrated forms of each protein have comparable affinities for membranes indicating that the peripheral binding step is most determinative for their in-membrane concentrations. Of the four studied BCL2 proteins, BIM_S apparent affinity for membranes is strongest with 1.7×, 2×, & 13× the strengths of BCL-X_L, cBID, & BAX respectively. The membrane-integral forms of cBID and BIM_S are capable of driving BAX and BCL-X_L to tight membrane affinity conformations but the two BH3s' recruiting efficiencies are equivalent, suggesting a complementary activation mechanism besides

strictly utilizing a membrane interaction scaffold. Overall, these data reveal receptor-like roles for cBID & BIM_S for soluble BCL2 proteins during the initiation of apoptosis.

4.2 | Introduction

BCL2 family proteins are central regulators of apoptosis and comprise anti- and proapoptotic effectors partially defined by sequence conservation in four BCL2 homology (BH) domains (1,2). The family is further subclassified according to the number of BH domains each member contains. Antiapoptotic proteins (e.g. BCL-2, BCL-X_L) are multidomain—encompassing three or four BH domains—and share a core tertiary fold consisting of a central, mostly hydrophobic α-helical hairpin surrounded by six amphipathic helices (3). Multidomain proapoptotic members (i.e. BAX, BAK—the apoptosis "executioners") contain BH1-3 and counterintuitively display tertiary structures nearly identical to their antagonists (4,5). BH3-only proteins compose the third subclass and are stationed about the cell, serving to integrate disparate cell stress signaling pathways. In general, BH3-only proteins are predicted to be intrinsically-disordered, except BID whose α-helical arrangement mimics the multidomain proteins (6-9).

Solution interactions between antiapoptotic and BH3-only proteins and peptides have been fairly well characterized and quantified via *in vitro* reconstitution regimes and detergent extractions from organelles and whole cells; a recent and thorough examination by B.H. Oh and coworkers comprised an array of antiapoptotics and their binding affinities to BH3 peptides from BAX/BAK and numerous BH3-only proteins (10). Conversely, solution interactions between BAX/BAK and BH3-only proteins/peptides have historically proven

difficult to detect, leading to two competing models of activation—derepression of intrinsically active BAX/BAK vs. direct activation of inert BAX/BAK through a transient, hit-and-run interaction (11-13). The direct activation model was further refined by Kim *et al*. and Leber *et al*. in their hierarchical and embedded-together schemes (14,15).

A significant aspect that has been largely overlooked in biochemical elucidation of BCL2 protein function is the soluble→membrane transition. Many studies on membrane targeting have relied on cellular expression of truncated BCL2 family protein constructs and most often implicate the proteins' carboxy-termini as membrane addressing sequences. The death effector BAX is considered dormant when cytosolically dispersed but can nevertheless receive an activating signal inducing redistribution of the protein to cellular membranes. Due to the aforementioned inconsistency in detecting BAX-BH3-only protein interactions in solution, the mechanism, especially localizations, of BAX activation are speculative.

BCL-X_L is known to reside both on intracellular membranes and in the bulk cytosol whereas BAX and BID are largely cytosolic, though BAX can be "loosely associated" with mitochondria (16-18). Previous *in vitro* assays on BAX, however, showed it could transiently interact with liposome membranes and expose its amino-terminus for antibody binding and, more recently, electron paramagnetic resonance spectroscopy of spin-labeled BAX demonstrated the protein's intrinsic membrane binding functionality (19,20). BAX activator cBID (caspase-8 cut BID) has also been shown to disrupt membranes—rendering LUVs CF-permeant—while BIM_S, the most potent apoptosis-inducing BIM isoform, constitutively localizes to mitochondrial membranes (21,22). Targeting of BID & BIM BH3 peptides to

membranes strongly amplifies their capacity to induce mitochondrial cytochrome *c* egress and vesicular BAX pore formation (23-25).

Thus we sought to further illuminate the process by which BAX adsorbs to membranes, a necessary precursor to its in-membrane oligomerization and pore formation (26). By adopting the now standard vesicle leakage assay (24,27,28), we demonstrate the physiological relevance of our reconstituted system; kinetic analysis of LUV permeabilization reveals that BIM_S more efficiently than cBID provokes BAX pore activation and is less suppressible by BCL-X_L. Surface plasmon resonance spectroscopy allows real-time measurement of membrane interaction by soluble BCL2 proteins and these data are well-fit by a two-step binding mechanism as described previously (29). Further application of this technique demonstrates that membrane-bound BH3-only activators are sufficient and functionally comparable for recruiting BAX and BCL-X_L.

4.3 | Results

Vesicle membrane poration by BCL2 proteins

BAX, BCL-X_L, cBID & BIM_S differentially permeabilize LUVs

To confirm that these proteins can independently interact with membranes, LUVs encapsulating 20 mM carboxyfluorescein (MW: 0.38 kDa) were synthesized with a lipid composition modeling the mitochondrial outer membrane. As shown in Fig. 4.1A, 50 nM monomeric BAX, monomeric BCL-X_L, cBID (native p7/p15 complex (8)), & BIM_S are each capable of interacting with vesicles as revealed by CF dequenching. BIM_S is by far the most effective in permeabilizing vesicles, which corresponds to the protein's poor solubility and requirement of detergent to alleviate aggregation during purification. CF-leakage rate of BAX, BCL-X_L, and cBID are similar and substantially slower than that of BIM_S.

Conversely, similar concentrations of BCL-X_L, cBID, and BIM_S individually induce trivial LUV leakage of 10 kDa FITC-dextran (FD10) (Fig. 4.1B), revealing that these proteins' membrane interactions slightly disrupt bilayer integrity, rendering it permeant to small molecules but not to macromolecules. BAX, however, at 50 nM displays a low-level capacity to release FD10 from liposomes (Fig. 4.1B); this intrinsic activity is suppressible by addition of 10 nM BCL-X_L (data not shown) lending evidence that monomeric BAX (and BAK) can stochastically autoactivate (30-34).

Fig. 4.1

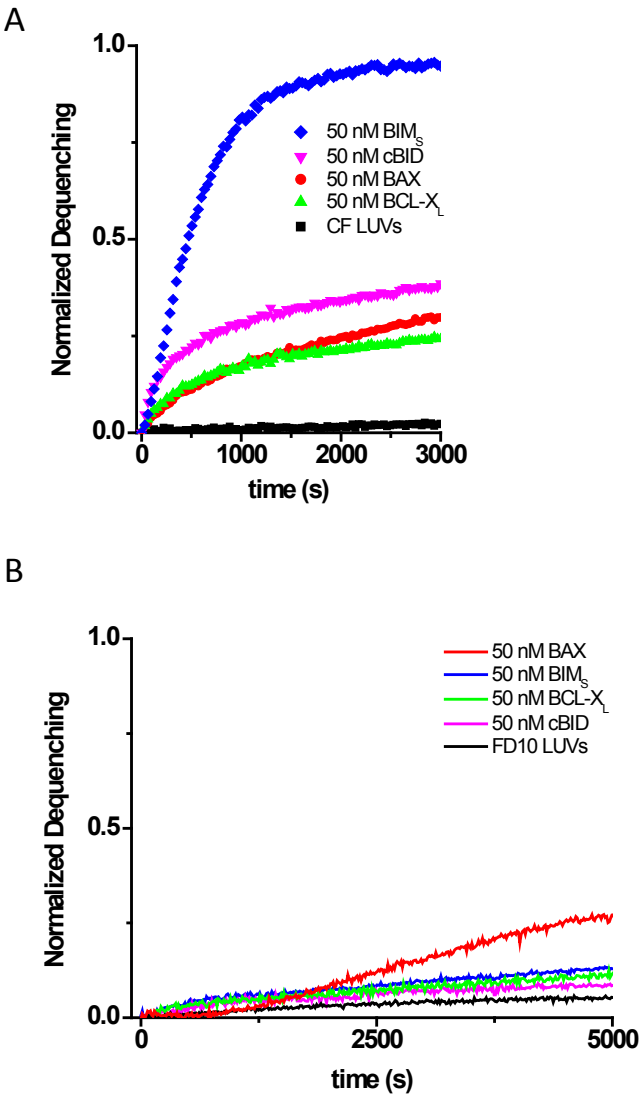

Fig. 4.1 | **Vesicle interaction and differential permeabilization by recombinant BCL2 proteins.** In all cases, LUVs were diluted into 1 cm assay cuvets to a lipid concentration of 10 µM (1 mL total volume) and brought to 37°C. BAX, BCL-X_L, cBID, & BIM_S were then diluted 100-fold from 5 µM stocks, resulting in 50 nM solution concentrations and 1:200 protein:lipid molar ratios. *A*, LUVs comprising the small dye (0.38 kDa) 5(6)-carboxyfluorescein were incubated with indicated BCL2 proteins. *B*, LUVs encapsulating 10 kDa FITC-dextran (FD10) were incubated with indicated BCL2 proteins.

BAX is more efficiently activated by BIM_S than cBID

To further validate our reconstituted *in vitro* experimental system, BAX pore activation by BH3-only direct activators cBID and BIM_S was assessed. Cut or truncated BID is a commonly used activator but very little biochemical characterization of BIM has been performed, thus we sought to make direct comparisons on the efficacies of the two BH3-only proteins. On a dose-dependent basis, cBID and BIM_S are both effective accelerators of BAX pore formation (Fig. 4.2). However, per nM of BH3-only protein, BIM_S (Fig. 4.2B) is a more effective BAX activator than cBID (Fig. 4.2A); the inverse times for half-maximal LUV dequenching are plotted to demonstrate this activation disparity (Fig. 4.4A). Interestingly, at 50 nM BAX, cBID-BAX activation saturates at roughly 50 nM activator and the cBID EC_{50} is 12 nM. Conversely, BIM_S-BAX activation saturates well above 100 nM activator and the BIM_S EC_{50} is 40 nM.

Fig. 4.2

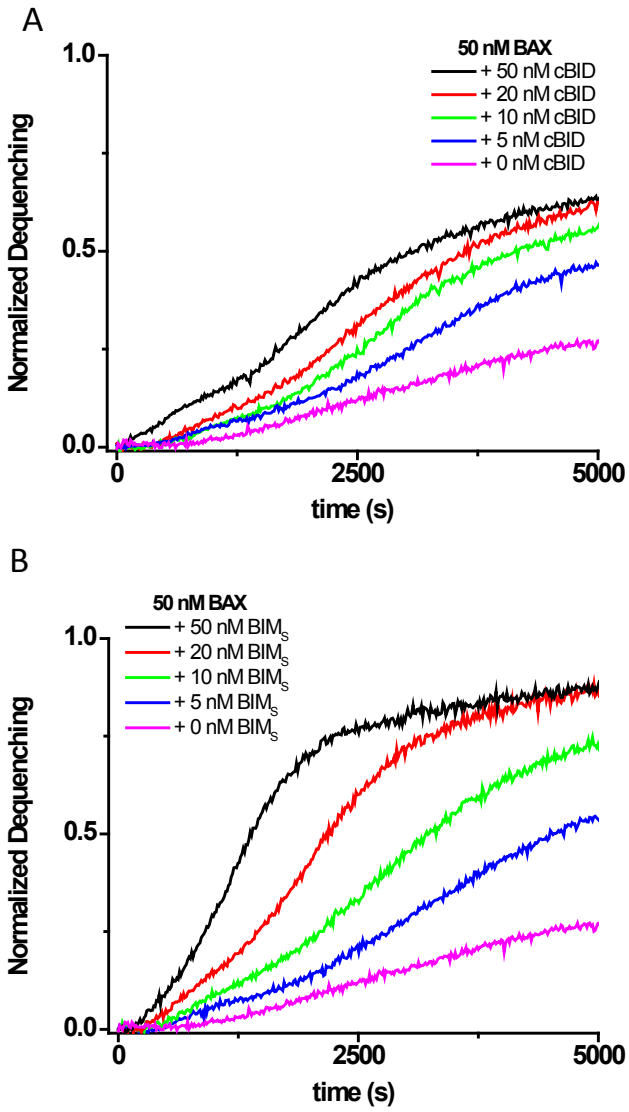

Fig. 4.2 | **BAX pore activation by cBID & BIM_S.** Leakage experiments were similar to Fig. 4.1 but proteins were diluted into 37°C assay cuvets sequentially—BAX, cBID/BIM_S—to preclude spurious solution interactions at superphysiological concentrations, followed by addition of FD10 LUVs within 30 seconds. In all traces, [BAX] is 50 nM. *A & B*, FD10 LUVs were incubated with BAX and concentrations of cBID/BIM_S are noted accordingly.

Having examined the differential activation efficacy of BIM_S and cBID, the extent of BCL-X_L suppression of BAX pore formation was then investigated; depicted in Fig. 4.3A & B are leakage traces of 50 nM BAX + 20 nM activator subjected to escalating concentrations of inhibitory BCL-X_L. These traces demonstrate that not only is cBID a less effective BAX activator, it is also more susceptible than BIM_S to inhibition by BCL-X_L. Stoichiometric addition of BH3-only activator and BCL-X_L most strikingly make apparent their BAX activation inequivalencies as 50 nM inhibitor completely ablates leakage induced by 50 nM cBID + BAX but merely delays pore formation elicited by 50 nM BIM_S + BAX (Fig. 4.3C & D). Per nM of BCL-X_L, cBID-BAX pore activation is proportionately suppressed to a greater extent than BIM_S-BAX pore activation (Fig. 4.4B). Were inhibition by BCL-X_L equivalent at similar concentrations of BH3-only activator, the fitted lines would intersect the X-axis at the same point. Points on the x-axis of Fig. 4.4B represent the theoretical quantities of BCL-X_L required for insurmountable suppression of BAX pore activation; 20 & 50 nM cBID can be fully inhibited by 27 & 33 nM BCL-X_L while 20 & 50 nM BIM_S require drastically greater [BCL-X_L] (45 & 83 nM respectively).

Fig. 4.3

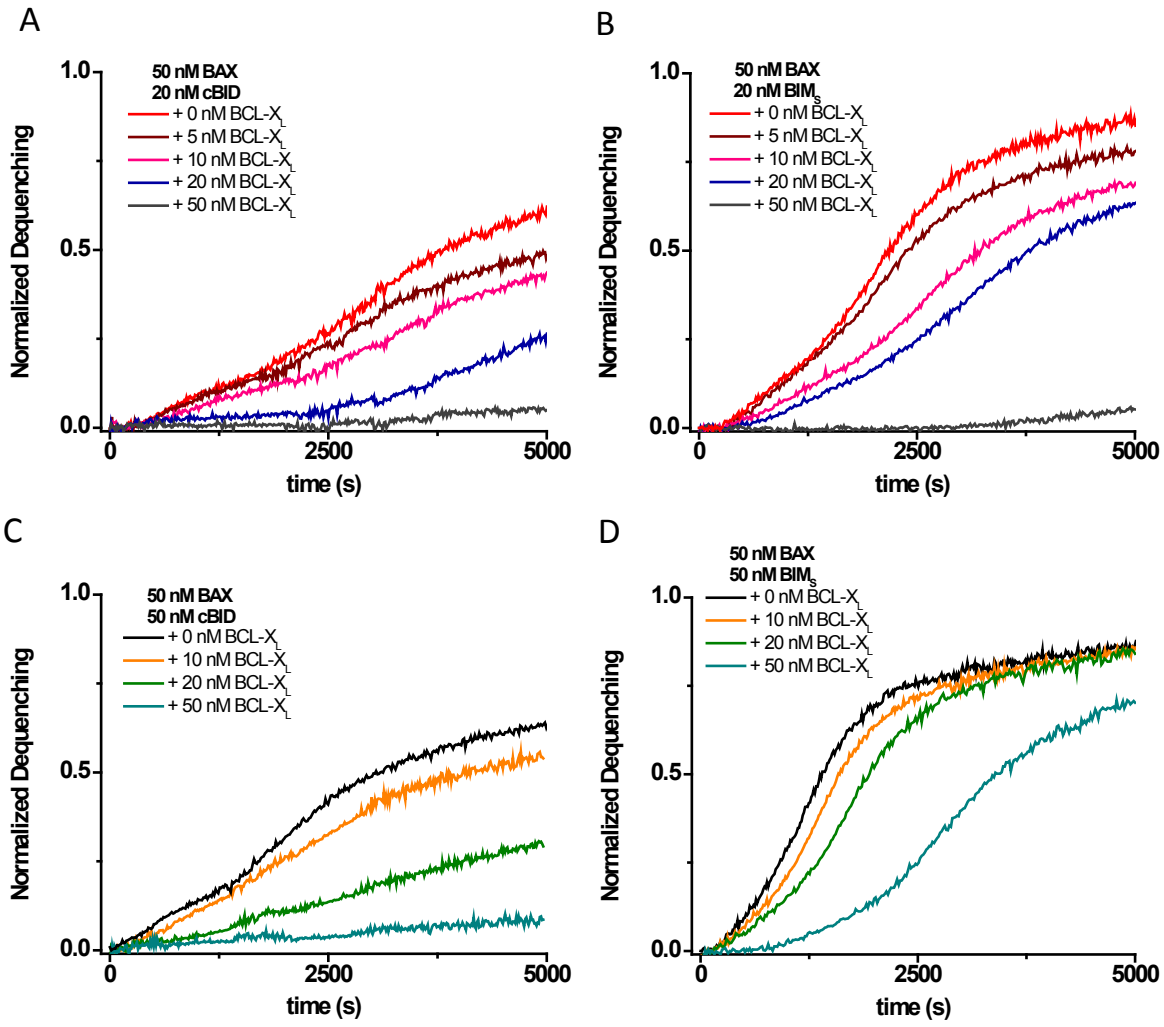

Fig. 4.3 | **BAX pore suppression by BCL-X$_L$.** Leakage experiments were conducted as in Fig. 4.2 and BCL2 proteins were added sequentially—BAX, BCL-X$_L$, cBID/BIM$_S$—and immediately followed by FD10 LUVs. In all traces, [BAX] is 50 nM and [BCL-X$_L$] varies from 0 to 50 nM as indicated. *A & B*, BCL-X$_L$ dose-dependent suppression of 20 nM cBID (*A*) & BIM$_S$ (*B*) activation of BAX. *C & D*, BCL-X$_L$ dose-dependent suppression of 50 nM cBID (*C*) & BIM$_S$ (*D*) activation of BAX.

Fig. 4.4

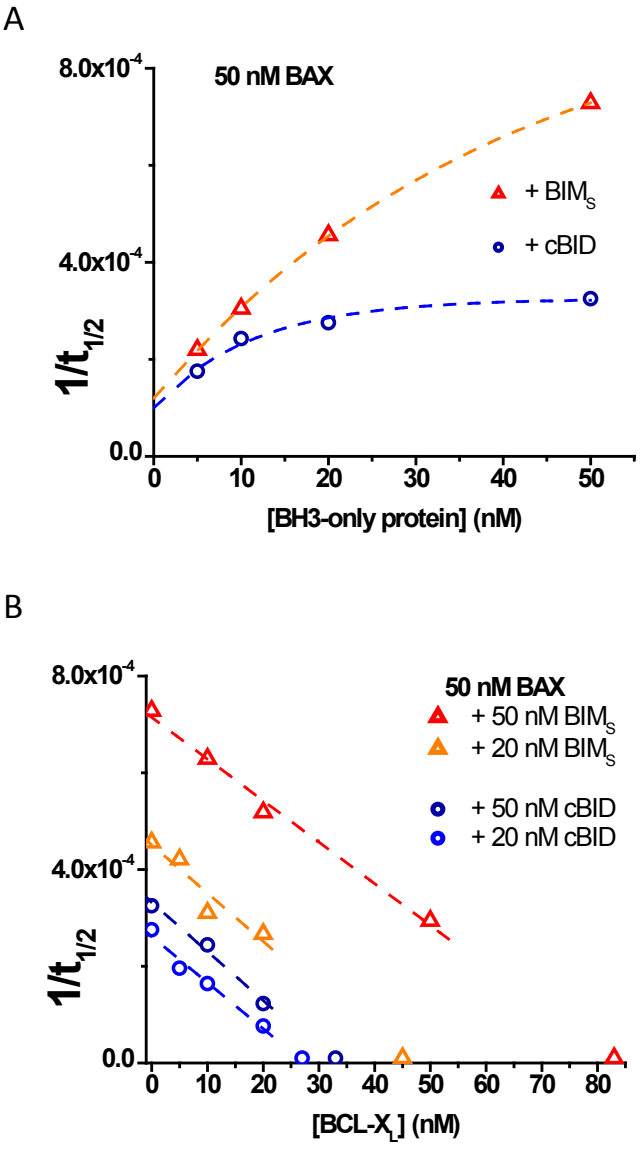

Fig. 4.4 | **Kinetic analyses of BAX pore activation by cBID/BIM$_S$ and suppression by BCL-X$_L$.** Plotted are inverse values of the time for half-maximal leakage of FD10 from LUVs taken from traces in Fig. 4.2 & Fig. 4.3; $1/t_{1/2}$ values plotted on the y-axis decrease as rate of FD10 leakage slows. Dashed lines are exponential (*A*) and linear (*B*) fits. *A*, Differential BAX pore activation by cBID & BIM$_S$. *B*, Differential suppressions by BCL-X$_L$ of cBID- & BIM$_S$-BAX pore activation. Points on the x-axis indicate intercepts of linear fits.

Vesicle membrane binding by BCL2 proteins

BAX, BCL-X_L, cBID, & BIM_S independently bind vesicle bilayers

To glean insight into these proteins' adsorption to membranes, surface plasmon resonance spectroscopy was exploited. SPR is advantageous in that it requires no potentially interfering modifications (such as fluorophore conjugation) of the components and the system can be monitored in real-time by direct measurement of mass accumulation near the sensorchip surface (demarcated in resonance units, RU). Two hundred nm LUVs—which retain their vesicular structure—can be immobilized on a sensor chip's hydrogel matrix to provide bilayers for protein binding (35). Given the dimensions of the L1 sensorchip flowcell (2.4 × 0.5 × 0.05 mm) and our LUVs, we estimate the experimental lipid concentration to be 250-300 μM. L1 sensorchip surfaces saturate at ≈7000 RU vesicles; from bound vesicle/protein values and molecular weights, relative concentrations can be readily calculated. For simplicity, membrane binding parameters (Table 4.1) are reported with respect to moles of binding sites rather than moles of lipid.

As shown in Fig. 4.5, each soluble BCL2 protein is independently capable of peripheral membrane interaction and assuming an integrated form. Kinetic parameters of protein-membrane binding are presented in Table 4.1. The membrane binding traces of BAX, cBID, and BIM_S are well-fit by a two-step sequential mechanism— $P + M \rightleftharpoons PM \rightleftharpoons PM^*$ —comprising a rapid peripheral binding step that is reversible and distinct from a subsequent and long-lived conformational change(s) and/or reorganization of the lipids. The rate equation was modified for cBID to account for dissociation of the N-terminal p7 fragment upon membrane

binding, rendering a membrane-integral p15 tBID (36). BCL-X_L also displays a rapid peripheral binding step but the successive steps are more complicated. The drop in RU over the last 20-30 s of protein injection is not artifactual as similar data were gathered using multiple protein and LUV preparations and sensorchips. Details on correcting the BCL-X_L traces to account for signal loss, which we attribute to immobilized vesicle swelling on the sensorchip surface, are included in the Supplement.

For the four proteins studied, their membrane affinities (K_d) vary over a 13-fold range with BIM_S binding membranes most tightly and BAX most weakly (Table 4.1). The apparent K_d values, however, mask important details of the membrane interaction progression. Correlating with its poor solubility, BIM_S peripherally binds most avidly (BIM_S k_{a1} ≈ 4.3× BCL-X_L k_{a1}, 6× cBID k_{a1}, & 35× BAX k_{a1}); while their k_{a1} rates vary widely, the four proteins' k_{d1} rates are fairly similar and very rapid, resulting in membrane peripheral affinities (K_{d1}) ranging from 5.5 μM (BIM_S) to 145 μM (BAX).

Unlike the peripheral binding steps which display widely varying kinetics, the integration steps for BIM_S, BCL-X_L, cBID, and BAX are somewhat comparable and parameters (k_{a2}) lie within a 4-fold range. Despite having the weakest membrane peripheral affinity, BAX integrates most rapidly but this integral form also dissociates from the membrane (k_{d2}) more readily compared to membrane-integral BCL-X_L, BIM_S, and tBID. The integrated proteins' membrane affinities (K_{d2}) vary over a 3-fold range and have half-lives greater than 3 hours. Overall, BIM_S apparent affinity (K_d) for membranes is 1.7×, 2×, and 13× that of BCL-X_L, cBID, and BAX respectively.

To clearly illustrate their accumulations on vesicles at equimolar concentrations, simulations of BCL2 protein-membrane interactions were compiled (Fig. 4.5E). The protein concentration input was 1250 nM (vs. 250 μM lipid) which approximates the highest (5:1000) protein:lipid ratio used in the LUV leakage experiments (Figures. 4.1-4.3). Simulated traces were also corrected to molar fractions to properly contextualize the protein adsorptions to bilayers. Correlating kinetics between the vesicle leakage and biosensor systems should be approached cautiously, however, because for SPR assays the solution protein concentrations are constant and the comparatively high concentration of vesicles are immobilized on a hydrogel matrix rather than diffusing freely in solution.

Fig. 4.5

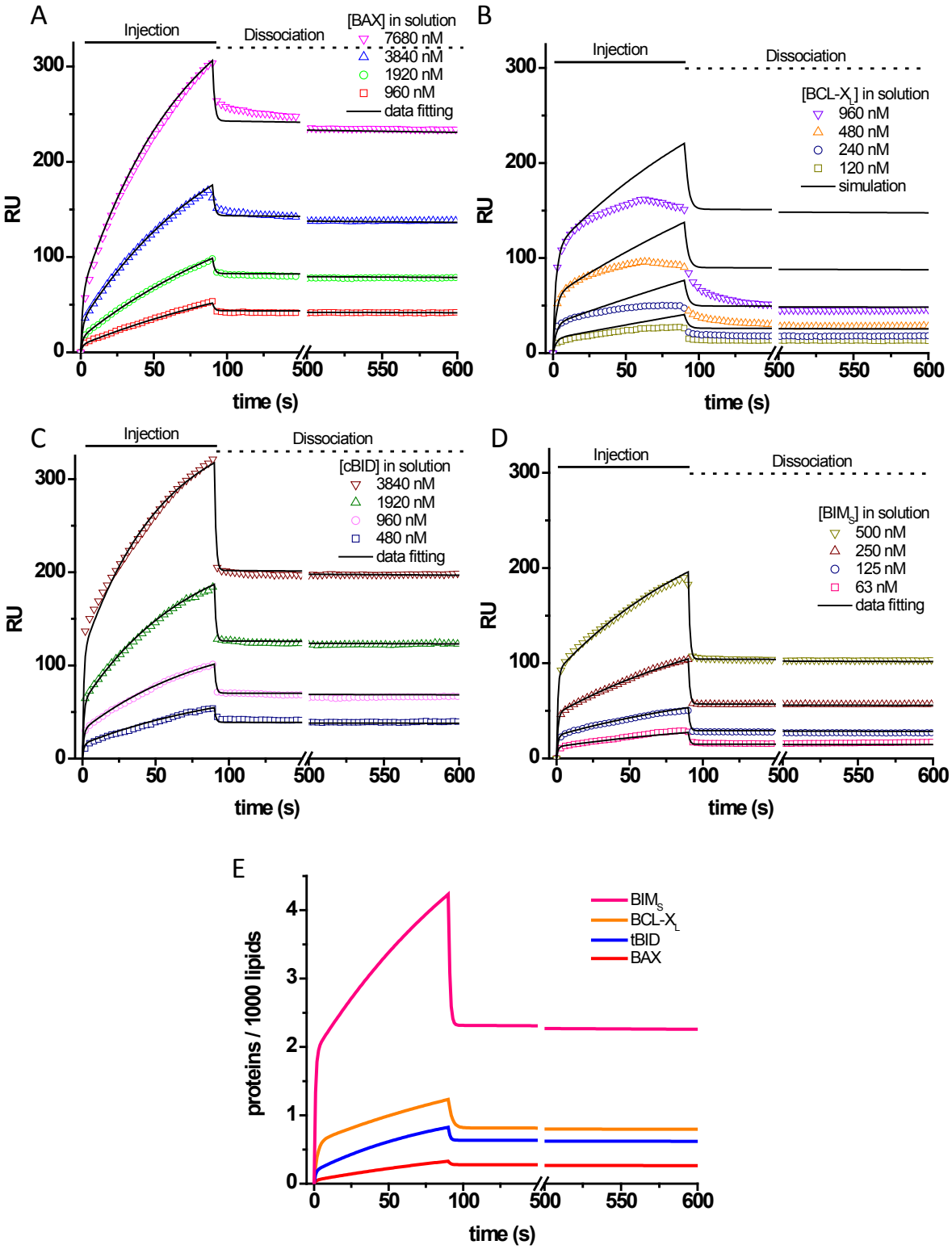
A
Injection
Dissociation
[BAX] in solution
7680 nM
3840 nM
1920 nM
960 nM
data fitting
RU
time (s)
B
Injection
Dissociation
[BCL-X$_L$] in solution
960 nM
480 nM
240 nM
120 nM
simulation
RU
time (s)
C
Injection
Dissociation
[cBID] in solution
3840 nM
1920 nM
960 nM
480 nM
data fitting
RU
time (s)
D
Injection
Dissociation
[BIM$_S$] in solution
500 nM
250 nM
125 nM
63 nM
data fitting
RU
time (s)
E
BIM$_S$
BCL-X$_L$
tBID
BAX
proteins / 1000 lipids
time (s)

Fig. 4.5 | **Real-time measurement of BCL2 protein-membrane binding by surface plasmon resonance spectroscopy.** *A-D*, Displayed are sensorgram traces and data fittings of protein-membrane adsorption. Soluble BCL2 proteins were injected at indicated concentrations for 90 s (30 µL/min.) over immobilized LUVs then dissociation monitored for 10 min.; note the breaks from 150-500 s in plots. The experimental data were globally fitted to their corresponding two-step kinetic models described in Materials & Methods. Correction for RU signal loss during BCL-X_L injections is described in the Supplement. *E*, Simulated traces of protein-membrane binding. Traces were corrected for protein molecular weights and presented as membrane mole fraction rather than mass bound (RU). Soluble protein concentration input to simulation was 1250 nM, approximating 5 soluble molecules per 1000 vesicular lipids as applied to LUVs for leakage experiments in Fig. 4.1 (i.e. 50 nM protein + 10 µM vesicular lipid).

Table 4.1 | **Kinetic parameters of BCL2 protein-membrane binding.**

	k_{a1}	k_{d1}	k_{a2}	k_{d2}	K_{d1}	K_{d2}	K_d
	$M^{-1} s^{-1} \times 10^{4}$	s^{-1}	$s^{-1} \times 10^{-2}$	$s^{-1} \times 10^{-4}$	$M \times 10^{-6}$	$\times 10^{-3}$	$M \times 10^{-9}$
BAX	0.55	0.8	7.3	1.0	145	1.37	199
BCL-X_L	4.44	0.44	1.9	0.5	9.91	2.63	26
cBID	3.21	1.04	5.7	0.5	32.4	0.88	28
BIM_S	19.0	1.04	1.8	0.5	5.47	2.78	15

Membrane-bound tBID & BIM_S robustly recruit BAX & BCL-X_L

Having examined the kinetics of membrane binding by each BCL2 protein, we then hypothesized that membrane-bound BH3-only proteins are sufficient to recruit the multidomain proteins to membrane-integral states. Previously, Oh *et al*. demonstrated that BID BH3 peptides tethered to vesicle surfaces potentiated BAX pore activity (24). We sought to expand on this finding by using full-length BH3-only proteins in our experimental regime which precludes the presence of non-membrane bound activators and allows delineation and temporally-resolved comparison of protein recruitment at the membrane. Kinetic assays of BAX/BCL-X_L membrane binding were performed as before except tBID & BIM_S were applied to LUVs prior to sensorchip immobilization.

As anticipated, membrane-bound tBID and BIM_S substantially enhance the membrane association of both BAX and BCL-X_L (Fig. 4.6). Presence of the BH3-only proteins (one protein per 6000 lipids) in the membrane increases the integrated quantities (●) of BAX & BCL-X_L and commensurately enhances the bound (peripherally associated + integrated) protein pool (★). Unexpectedly, membrane-bound tBID and BIM_S display similar efficiencies in recruiting the multidomain proteins (4.6A vs. 4.6C, 4.6B vs. 4.6D); this finding was surprising given the faster BAX pore activation elicited by BIM_S than by cBID. During the 90 s injections, tBID & BIM_S increase the BAX membrane integration rate ≈75%, from 0.073 s^{-1} to 0.128 s^{-1} at all measured soluble concentrations. Conversely, tBID/BIM_S enhance the membrane integration of BCL-X_L (k_{a2} = 0.019 s^{-1}) by progressively lower rates with increasing soluble protein concentration (120 nM - 0.031 s^{-1}; 240 nM - 0.029 s^{-1}; 480 nM - 0.028 s^{-1}; 960

nM - 0.025 s^{-1}; 1920 nM - 0.023 s^{-1}) (Fig. 4.6E). Both BH3s recruit superstoichiometric quantities of BAX & BCL-X_L; however, BCL-X_L recruitment levels off at ≈1.7 × [BH3] while BAX recruitment continues to rise with increasing [soluble BAX] (≈4.5 × [BH3] at 3.8 μM BAX). These findings comport with an interaction model in which BAX transiently binds BID/BIM whereas BCL-X_L sequesters BID/BIM strongly to prevent further propagation of death signals.

To provide a negative control, BID BH3 mutant L90A,D95A ($cBID^{mut}$) was purified; in studies using BH3 peptides, this mutant was ineffective in eliciting cytochrome *c* release from isolated mitochondria and activating BAX *in vitro* (23,37). Interestingly, 50 nM $cBID^{mut}$ weakly activated 50 nM BAX in FD10 leakage assays (Fig. 4.S2A), though at lower efficiency than 5 nM wild-type cBID. When applied to vesicles to assess recruiting efficiency of BAX and BCL-X_L, $cBID^{mut}$ (1 protein : 6000 lipids) also weakly recruited BAX (Fig. 4.S2B), accelerating the membrane integration (k_{a2}) ≈10% from 0.073 s^{-1} to 0.08 s^{-1}. Conversely, $cBID^{mut}$ had no discernable recruitment of BCL-X_L (data not shown).

Fig. 4.6

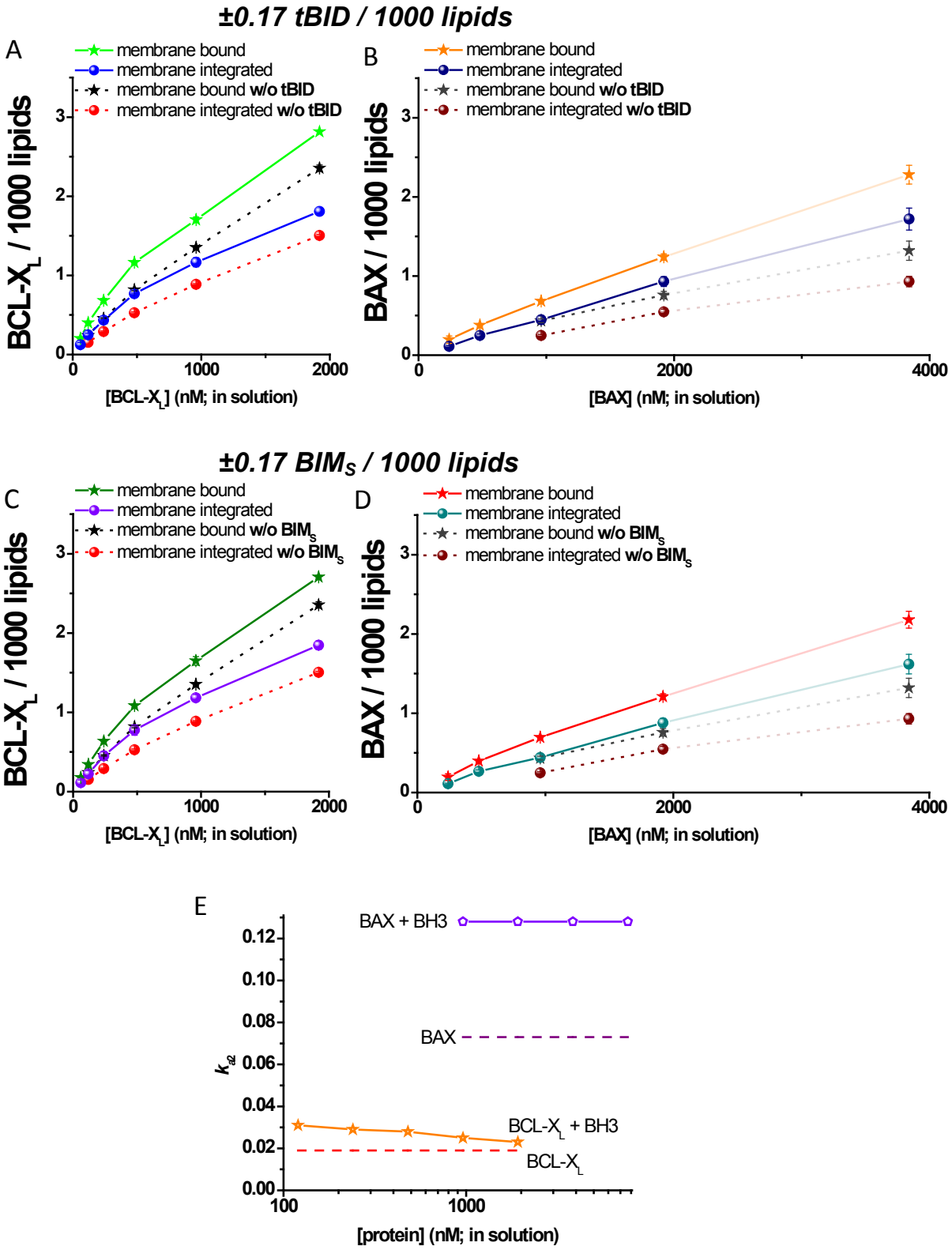
±0.17 tBID / 1000 lipids
A
membrane bound
membrane integrated
membrane bound w/o tBID
membrane integrated w/o tBID
BCL-X_L / 1000 lipids
[BCL-X_L] (nM; in solution)
B
BAX / 1000 lipids
[BAX] (nM; in solution)
±0.17 BIM_S / 1000 lipids
C
membrane bound w/o BIM_S
membrane integrated w/o BIM_S
D
E
BAX + BH3
BAX
BCL-X_L + BH3
BCL-X_L
k_a2
[protein] (nM; in solution)

Fig. 4.6 | **Membrane-bound tBID & BIM_S robustly recruit BAX and BCL-X_L.** LUVs (1 mM lipid) were preincubated with 170 nM cBID or BIM_S in EB for three hours at room temperature prior to loading onto the Biacore sensorchip, resulting in a 1:6000 BH3-only protein:lipid ratio. BAX and BCL-X_L injections commenced as in Fig. 4.5. Membrane-bound values (★) were taken from the end of soluble protein injection and membrane-integrated values (●) after 5 min. of dissociation; these values were converted into protein/1000 lipids from experimental RU values to facilitate analysis. Solid lines represent BAX/BCL-X_L injections over tBID/BIM_S-charged vesicles and dashed lines represent BAX/BCL-X_L injections over bare vesicles. *A*, BCL-X_L binding to vesicles ± tBID. *B*, BAX binding to vesicles ± tBID. *C*, BCL-X_L binding to vesicles ± BIM_S. *D*, BAX binding to vesicles ± BIM_S. *E*, BAX & BCL-X_L k_{a2} (integration) rates accelerated by membrane-bound BH3-only activators. BAX k_{a2} is accelerated by ≈75% regardless of membrane-bound BAX concentration whereas BCL-X_L k_{a2} acceleration diminishes (65%→20%) with increasing membrane-bound BCL-X_L. Dashed lines represent BAX & BCL-X_L k_{a2} in the absence of BH3-only activators and symbols+lines indicate k_{a2} accelerations in the presence of BH3-only activators.

4.4 | Discussion

Despite nearly two decades of work on the BCL2 protein family, the molecular mechanisms of their disparate functions are only recently becoming deciphered. Much of the difficulty in their study derives from the proteins' conformational promiscuity and amphitropicity, properties that are modulated by their bulk environments and a variety of discrete regulatory molecules both proteinacious and lipidic. Another hindrance is that traditional methods of isolating membrane proteins (i.e. detergent extraction) radically alter BCL2 protein conformation and the proteins themselves can affect micellar aggregation (38-42). Thus generating a consistent pool of recombinant protein for mechanistic *in vitro* studies has proven troublesome and, due to this constraint, the field has relied largely on biochemical assays that provide only functional snapshots and qualitative interpretations.

Lipid bilayer interaction and disruption has long been established as a function of the BCL2 family with the latter evinced by BCL-X_L structural homology to bacterial toxins (43). As an initial test for protein-membrane interaction, LUVs containing a small fluorescent dye (carboxyfluorescein) were subjected to leakage assays. The four proteins studied—BAX, cut BID, BIM_S, and BCL-X_L—represent the three main classes of the BCL2 family and all elicited leakage of CF at nanomolar concentrations and physiological pH. Early work on the channel-forming capacities of multidomain BCL2 proteins typically employed C-terminally truncated and detergent-treated forms of the proteins (44,45). Vesicle permeabilization to small dyes by detergent-free BCL-$X_L^{\Delta C}$ can be induced by acidic pH or tethering the protein to membranes via His-tag chelation of DOGS-NTA-Ni^{2+} lipids (46,47). BCL-$2^{\Delta C}$ tethered to membranes also

can generate small pores, though the addition of tBID was required for this activity (48). The disparity in BCL-$X_L^{\Delta C}$ and BCL-$2^{\Delta C}$ poration may be attributable to vesicle composition, with the former using a simple 99:1 PC:DOGS-NTA-Ni^{2+} mixture and the latter a complex mixture comprising PC, PI, PE, PS, CL, & DOGS-NTA-Ni^{2+} to mimic the mitochondrial outer membrane. Among BH3-only proteins, native cBID and detergent-separated tBID have also been shown to porate vesicles (47,49). Recent electrophysiological work on BAD has indicated that it can form membrane channels and this activity is largely a consequence of its C-terminus (50,51). Peptides encompassing BAX α5 and BID α6 induce leakage of calcein from vesicles and the C-terminal ≈20 residues of BAX, BAK, and BCL-2 also have the capacity to release CF from liposomes (52,53). Taken together, it is apparent that BCL2 protein-membrane interaction slightly disrupts bilayer integrity from both the α5-6 hairpins and C-terminal domains.

Much *in vitro* experimental work has been performed reconstituting vesicle leakage systems to model mitrochondrial permeabilization; however, BID has been nearly the exclusive BH3-only protein used for BAX or BAK activation. Inclusion of BH3 peptides in LUV leakage assays and *in vitro* translated proteins for mitochondrial cytochrome *c* releases have also revealed that BIM and PUMA can also directly activate BAX/BAK (14,54-57). Therefore we chose to compare the efficacies of recombinant, full-length (cut) BID and BIM_S in activating BAX; BID was cut by caspase-8 but left unseparated to more accurately mimic the native environment (8). As we surmised, the kinetics of FD10 leakage from LUVs elicited by cBID and BIM_S were substantially different, with BIM_S being the more effective trigger of BAX poration. Kinetic

analysis of LUV leakage elicited by escalating concentrations of the two activators exposes that their capacities to activate BAX saturate at dramatically different concentrations.

The strong efficacy of BIM_S for activating BAX lies in contrast to a report by Terrones *et al*. in which $BIM_L^{\Delta C}$ and $BIM_{EL}^{\Delta C}$ only weakly induced BAX pore activity even when tethered to vesicles (25); however, their data also showed that a myristoylated BIM BH3 peptide was more potent in activating BAX than a myr-BID BH3 peptide. When applied to isolated mitochondria, recombinant BIM_L was ineffective in promoting cytochrome *c* release and BAX membrane integration (58). It seems likely that the isoforms' functional disparities are a consequence of the relative accessibility of their BH3 domains as BAX coimmunoprecipitates with BIM_S but not BIM_L or BIM_{EL} (59,60).

Having investigated the LUV leakage kinetics induced by BAX + BH3-only activator, we further interrogated the process by including antiapoptotic BCL-X_L. In accordance with prior work, inclusion of BCL-X_L inhibited LUV permeabilization by BAX in a dosage-dependent manner (61). Surprising, however, was our finding that not only was BIM_S more effective in driving BAX pore formation, it was less suppressible by BCL-X_L than cBID-BAX activation (Fig. 4.4). Peptide binding studies of BCL-X_L have consistently shown that the antiapoptotic protein sequesters BIM BH3 more tightly than BID BH3 (10,37,62). The greater proportional suppression by BCL-X_L of cBID over BIM_S suggests that binding affinity is not the sole determinant of inhibition.

Our attention then turned to applying a real-time, quantitative method to BCL2 protein-membrane binding. One point of contention in deciphering the mechanisms of the

BCL2 family is the relevance of solution interactions, especially by those of BAX. Yethon *et al*. demonstrated that BAX independently associates with LUVs and studies using BH3 peptides tethered to vesicles strongly hinted that BAX can bind membranes prior to becoming activated (19,24,25). As our SPR data reveals, BAX can bind membranes independently of extrinsic factors, as can its cousins BCL-X_L, cBID, and BIM_S. This adsorption is well-described by a two-step mechanism whereby the soluble proteins assume a long-lived, membrane-integral form and the key disparity in their interaction progression lies in the initial, peripheral association. Relative to cBID and BAX, BCL-X_L and BIM_S have very rapid on-rates and their apparent affinities for membranes are also tighter. These data quantify the intrinsic membrane binding capacity of four representative members of the BCL2 family and clarify the mechanism proposed by Billen *et al*. in which BCL-X_L outcompetes BAX for tBID in membrane binding and permeabilization (61) (Fig. 4.5E).

Remaining unresolved was the origin of the disparity between BIM_S- and cBID-BAX activation. We speculated that membrane-bound BIM_S would more robustly recruit BAX than membrane-bound tBID in our real-time binding assays; this supposition proved to be incorrect as the two BH3-only activators were equivalent in escalating BAX integration. Membrane-bound tBID and BIM_S showed essentially identical recruitment of BCL-X_L as well. Notably, tBID/BIM_S recruitment of BCL-X_L was saturable, unlike recruitment of BAX which was enhanced similarly regardless of soluble concentration. This result comports with the findings that BCL-X_L sequesters tBID very strongly on membranes while tBID-BAX interaction is transient and exchangeable (36,47). The BH3-only protein BAD, when bound to vesicles, has

also shown a capacity to enhance BCL-X_L-membrane binding, demonstrating that multidomain protein recruitment at the membrane surface is a function of the sensitizer subclass, not only of direct activator BH3s (63).

This recruitment equivalency at the membrane surface suggests that the more rapid accumulation of BIM_S on bilayers is the origin of its greater BAX pore activation rate. However, BAX membrane binding is weakest and thus the limiting step; the maximal rate of pore activation by BIM_S and cBID would converge to similar values if membrane concentration of BH3s were the dominant parameter (Fig. 4.4A). Direct BAX-BIM_S binding in solution would provide a plausible explanation for BIM_S superiority over cBID in triggering BAX activation. Frustratingly, unlike those with antiapoptotic BCL2 proteins, BH3 domain interactions with BAX have proven resistant to investigation. By chemically enforcing α-helicity of BH3 peptides, Walensky *et al*. demonstrated direct binding by BID and BIM BH3s to BAX in solution (37); intriguingly, BIM SAHB bound BAX >30× tighter than BID SAHB. Conversely, FRET assays of BAX and full-length tBID indicated no interaction in the bulk solvent while the addition of vesicles facilitated association (36). Antiapoptotic MCL-$1^{\Delta C}$ incubated with cBID interact in solution via canonical BH3 domain-pocket binding; this association is very slow to due to the dissolution kinetics of the two cBID fragments and subsequent exposition of the BID BH3 domain (64). Solution interactions between BCL-$X_L^{\Delta C}$ & tBID also have been detected and quantified via fluorescence cross-correlation spectroscopy, NMR, and isothermal titration calorimetry (47,65). Given the observations of greatly stronger affinity of BAX for BIM SAHB vs. BID SAHB, inaccessibility of the BH3 domain in cBID, and tBID-BAX binding solely on

membranes, it seems likely that BAX can become activated via BH3 interaction both prior and subsequent to membrane interaction. Strongly supporting this hypothesis is a recent report in which BIM (and also BAX) SAHBs were employed to evoke conformational intermediates of the BAX activation pathway (30).

Solution interaction and activation of BAX by BIM_S, but not cBID, also reconciles the differential suppression by BCL-X_L of vesicle leakage. Whereas cBID could activate BAX only subsequent to their localizations at the membrane, BIM_S would lack this kinetic barrier. BCL-X_L has a stronger affinity for bilayers than cBID, thus the antiapoptotic protein has the advantage in "outracing" cBID, and especially BAX, to their in-membrane functional sites (Fig. 4.5E). BIM_S, on the other hand, could bypass this constraint via activating BAX prior to membrane binding. In the bulk solution, BCL-X_L and BAX would compete for BIM_S binding, but this impediment to BAX activation is comparatively surmountable due to BAX having nearly as strong an affinity as BCL-X_L (24 nM vs. 16 nM respectively) for BIM SAHB (37).

The weak activation and membrane recruitment of BAX by cBID BH3 mutant L90A,D95A was unexpected as the corresponding peptide was ineffective in promoting cytochrome *c* release from mitochondria and the corresponding tBID mutant also ineffective in promoting LUV leakage (23,24). Previously reported, however, was a BH3-independent enhancement of BAX pore formation by BH3 mutant tBID G94A that was attributed to the protein's alteration of bilayer architecture (25). Our vesicle leakage and membrane binding kinetic data is consistent with tBID promoting BAX poration via modulation of the bilayer structure; this BH3-independent effect is quite small as $cBID^{mut}$ was less than 10% as efficient in

driving BAX pore formation and accelerated BAX membrane integration only 15% as well as wild-type tBID.

In summary, we've demonstrated that BCL2 family proteins—anti- and proapoptotic multidomain and BH3-only—have intrinsic membrane binding capacity and quantified a two-step mechanism of their membrane interactions. BH3-only activators bound to bilayers robustly recruit BAX and BCL-X_L by enhancing their membrane integration rates. Kinetic analysis of vesicle leakage elicited by BAX reveals disparities in the activation efficacies of BIM_S and cBID and lends support to a model whereby BAX can be activated by BH3 interaction both in the cytosol and on the mitochondrial outer membrane.

4.5 | Supplement

Membrane poration by the BCL2 family has been proposed to be a function of the proteins' modulation of bilayer curvature (28,49,53,66); by small-angle x-ray scattering, we have observed that BAX and BCL-X_L promote oppositional negative and positive curvatures (Appendix V). We attribute SPR signal loss during BCL-X_L injections to LUV swelling. The evanescent field and thus SPR signal decays as a function of distance from the basal metal surface and becomes essentially undetectable at 300 nm (67). Therefore, vesicle swelling induced by positive membrane curvature displaces vesicle (and bound protein) mass outside the detection volume. We presume that BCL-X_L binds to membranes in a two-step fashion similar to BAX & BIM_S. BCL-X_L dissociation curves were fit to a three-component exponential decay to determine off-rates k_{d1} & k_{d2} and the rate of RU signal loss; global fitting established k_{d1} = 0.44 s^{-1} & $k_{d2} = 0.5 \times 10^{-4}$ s^{-1}. Fitting of the first 30-45 s of 120 nM & 240 nM BCL-X_L injections then produced lower boundary k_a parameters for simulating curves for higher concentrations of BCL-X_L (Fig. 4.5B). Simulated curves were subtracted from the raw data traces to yield the degree of signal loss (Fig. 4.S1A) and the first derivatives of the signal loss residuals (Fig. 4.S1B) were then obtained to assess consistency between the rates of signal loss at the end of injection (association period) and beginning of wash (dissociation period).

To verify that BCL-X_L can induce LUV swelling in solution, vesicles (10 μM total lipid) were diluted into EB (10 mM HEPES-KOH, pH 7.0, 100 mM KCl, 0.5 mM DTT) and incubated with indicated ratios of protein for 2 hr. at room temperature; each ratio was performed in triplicate. Vesicles were then sized by dynamic light scattering in an N5

Submicron Particle Size Analyzer (Beckman Coulter) and values obtained from the unimodal distribution analysis peaks (Fig. 4.S1C). BAX, cBID, & BIM_S (5 proteins / 1000 lipids) were also assessed for vesicle swelling activity but none produced statistically significant values different from the buffer control (data not shown).

Fig. 4.S1

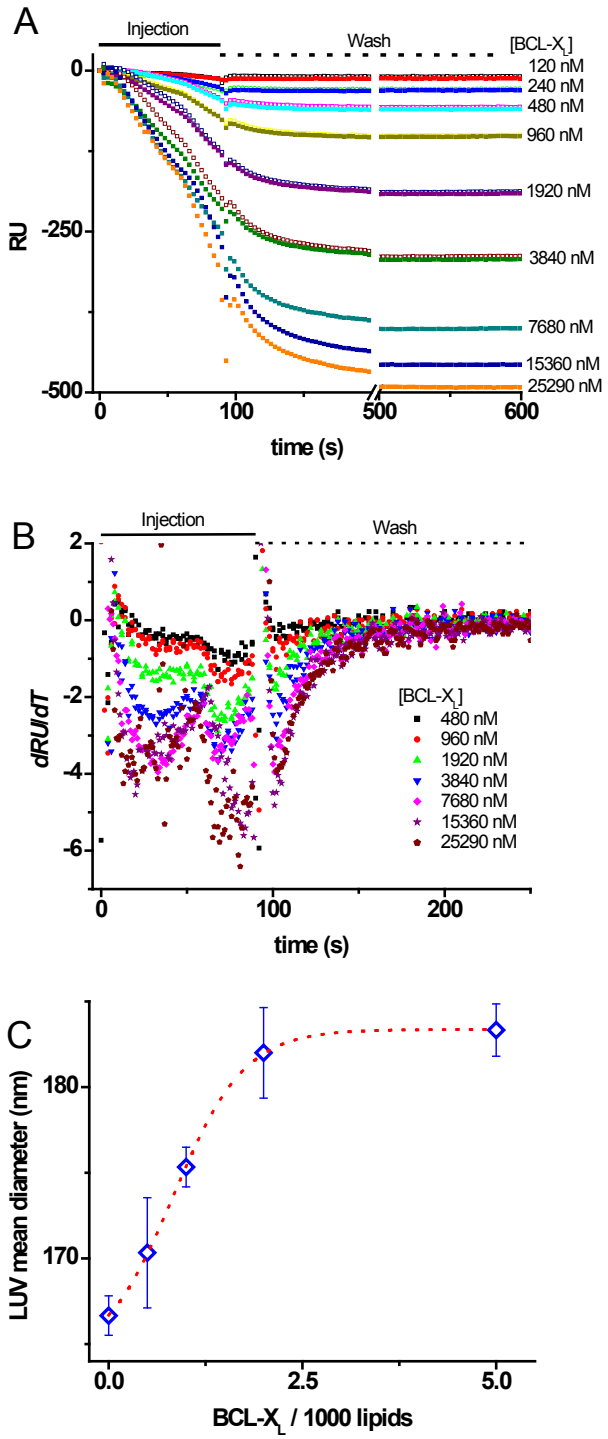

Fig. 4.S1 | **SPR trace correction of BCL-X$_L$-membrane binding.** *A*, Residuals from subtraction of simulated two-step binding curves from raw data traces at indicated concentrations of BCL-X$_L$. *B*, Slope of the residuals traces from Fig. 4.S1A, to assess consistency between signal loss during and after injection. *C*, BCL-X$_L$-induced LUV swelling in solution as determined by dynamic light scattering.

Fig . 4.S2

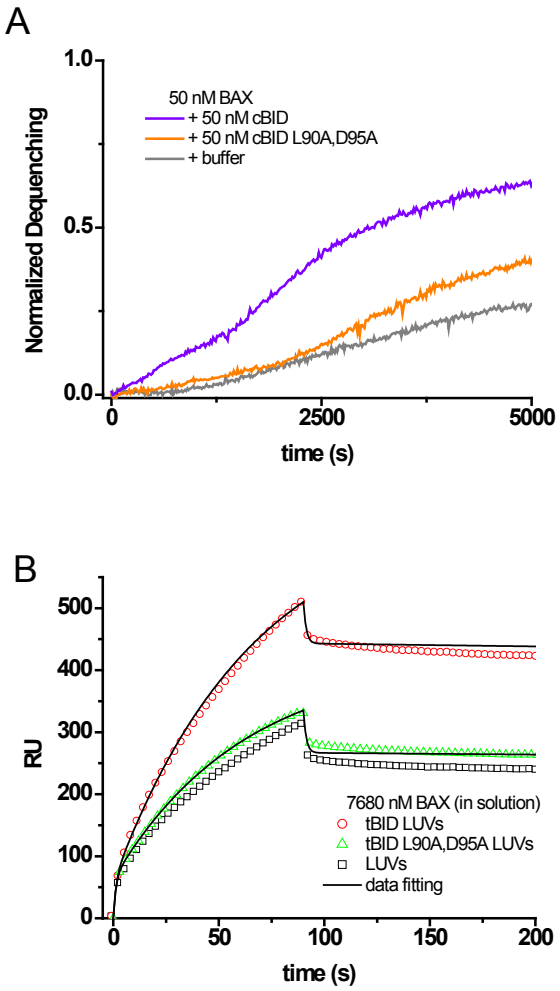

Fig. 4.S2 | **tBID^{mut} weakly recruits BAX at the membrane surface.** *A*, Dequenching assays were performed as in Fig. 4.2 and protein concentrations are noted in graphs. cBID^{mut} weakly activates BAX. For comparison, the blue trace is BAX + wt cBID as in Fig. 4.2. *B*, SPR data traces and fittings of 7680 nM BAX injected over bare vesicles, vesicles charged with tBID, or vesicles charged with tBID^{mut}. Assays were performed as in Fig. 4.5 w/ BAX injected for 90 s and dissociation monitored for 10 min. Data traces are averages of 2-3 independent experiments. tBID^{mut} accelerates BAX k_{a2} only 15% (0.073 s^{-1} → 0.08 s^{-1}) as efficiently as wt tBID (0.073 s^{-1} → 0.128 s^{-1}).

4.6 | Experimental Procedures

Protein purification

Full-length cDNAs for human BAX, BCL-X_L, and BID were subcloned into pTYB1 vector (NEB; Ipswich, MA) and constructs verified by DNA sequencing; a C-terminal glycine was introduced into BID to alleviate *in vivo* intein tag autocleavage. BCL-X_L, BID, and human BAX-PTYB1 expression constructs were transformed into BL21(DE3) *E. coli* and bacterial cultures grown in Terrific broth at 37°C until induction by 0.1 mM IPTG. Induced cultures were shaken for 16 hours at 23°C, bacteria were harvested by centrifugation, and pellets resuspended in lysis buffer (50 mM Tris, pH 8.0, 500 mM NaCl, 1 mM EDTA) + Complete protease inhibitor (Roche; Indianapolis, IN). Bacteria were lysed via three Microfluidizer passages at 1000 bar and lysate clarified by centrifugation. Clarified lysate was applied to chitin affinity resin followed by a high salt wash then equilibrated with cleavage buffer (lysis buffer + 30 mM DTT) and incubated overnight at 4°C to allow cleavage from intein tag. Recombinant proteins were eluted, dialyzed against 20 mM Tris, pH 8.0, and polished by MonoQ anion exchange chromatography. BAX and BCL-X_L were also gel filtered on a Superdex 200 column to remove non-monomeric species. BAX was initially monomeric but aggregated with time (20); BCL-X_L was largely aggregated (≈90%), both after initial elution from affinity resin and anion exchange and SEC-purified monomeric BCL-X_L also aggregated over time. Inclusion of 1% CHAPS in BCL-X_L purification mitigated aggregation only slightly.

For BIM_S, the full-length cDNA was subcloned into pTYB11 (NEB) and purified similarly to BAX, BCL-X_L, and BID except 1% CHAPS was added to lysis, column wash, and

cleavage buffers, and no FPLC was performed. Purifications of BCL-X_L and BID typically yielded 15-20 mg/L culture, BIM_S 2.0 mg/L, and BAX 0.75 mg/L. Concentrations were quantified by micro BCA assay (Pierce) or spectrophotometrically at 280 nm and proteins stored in 20 mM Tris, pH 8.0, 250 mM NaCl, 5 mM DTT, 1 mM EDTA, 0.01% NaN_3 (BIM_S also contained 1% CHAPS) at 4°C.

To generate cut BID (cBID), caspase-8 was added to BID (6 mg/mL) and incubated with 10 mM DTT overnight at room temperature. Mutants were generated via site-directed PCR mutagenesis.

Large unilamellar vesicle preparation

LUVs of 200 nm diameter modeling the mitochondrial outer membranes were prepared by freeze-thawing and extrusion. Ten mg total lipid (dissolved in chloroform) were mixed to yield a composition of DOPC:DOPE:DOPA:CL:cholesterol 49:28:10:5:8 (mol/mol); chloroform was evaporated by nitrogen then lipids further dried under vacuum for two hours. Equilibration buffer (EB; 10 mM HEPES-KOH, pH 7.0, 100 mM KCl, 0.5 mM DTT) was added to dried lipid films and lipids rehydrated by a 30 s immersion in a bath sonicator; EB was supplemented with 20 mM 5(6)-carboxyfluorescein (CF) or 50 mg/mL 10 kDa FITC-dextran (FD10) to yield liposomes for leakage assays. The mixture was then subjected to ten freeze/thaw cycles in liquid nitrogen and extruded 15 times through a membrane with 0.2μm pores. Extravesicular CF or FD10 was removed by Sephadex G -25 or G-200 gel filtration respectively.

LUV leakage assays

Dequenching of LUV-entrapped CF & FD10 were monitored by a Cary Eclipse fluorescence spectrophotometer (Varian; Palo Alto, CA) using a 1-cm path length thermostatted cuvette at 37°C. The fractional dequenching at each time point was quantified according to the equation $(F_t - F_0)/(F_1 - F_0)$ where F_t is the measured fluorescence of protein-treated LUVs at time t, F_0 is the initial fluorescence of the LUVs before protein addition, and F_1 is the fluorescence after complete LUV dissolution by addition of Triton X-100 to 0.2%. Lipid concentration of leakage assays was 10 μM after dilution into EB.

Surface plasmon resonance assays of protein-membrane binding

Experiments were performed using Biacore X100 instrumentation and software (Biacore division of GE Healthcare; Uppsala, Sweden) at an ambient temperature of 37°C. Biacore running buffer (EB) was filtered through a 0.22μm filter and degassed prior to use and LUVs were prepared as described above; recombinant proteins were exchanged into EB by dialysis or gel filtration. The sensor surface of an L1 sensorchip was equilibrated with EB and LUVs were deposited by injecting 1 mM lipid for 10 minutes at a flow rate of 1 μL/min. BSA (1 mg/mL) was then injected for two min. at 15μL/min. to assess extent of vesicle cove rage of the surface and block remaining nonspecific binding sites (29,35). Proteins were injected over the supported LUVs for 90 s at a rate of 30 μL/min. to circumvent mass transport effects and dissociation monitored for >10 minutes. Response traces were corrected for baseline & injection artifacts and data were analyzed and displayed using Berkeley Madonna 8.3.8

(University of California, Berkeley, CA) and Origin 7.5 (OriginLab). Data were globally fit to binding models derived from schemes:

I. $P + M \underset{k_{d1}}{\overset{k_{a1}}{\rightleftharpoons}} PM \underset{k_{d2}}{\overset{k_{a2}}{\rightleftharpoons}} PM^*$ BAX, BCL-X_L, BIM_S

II. $NC + M \underset{k_{d1}}{\overset{k_{a1}}{\rightleftharpoons}} NCM \underset{k_{d2}}{\overset{k_{a2}}{\rightleftharpoons}} CM$ cBID

where P/NC corresponds to soluble protein, M to the membrane, PM/NCM to the membrane-associated protein, and PM^*/CM to membrane-integrated protein conformations. Membrane affinity constants are calculated: $k_{d1}/k_{a1} = K_{d1}$; $k_{d2}/k_{a2} = K_{d2}$; $K_{d1} \times K_{d2} = K_d$.

For kinetic experiments of BAX & BCL-X_L membrane recruitment by BH3-only activators, assays were performed as above except LUVs (1 mM lipid) were preincubated with 170 nM cBID/BIM_S for three hours at room temperature to decorate the vesicles with BH3-only protein (1 protein per 6000 lipids).

4.7 | References

1. Danial, N. N., and Korsmeyer, S. J. (2004) *Cell* **116**, 205-219
2. Cory, S., Huang, D. C., and Adams, J. M. (2003) *Oncogene* **22**, 8590-8607
3. Petros, A. M., Olejniczak, E. T., and Fesik, S. W. (2004) *Biochim Biophys Acta* **1644**, 83-94
4. Suzuki, M., Youle, R. J., and Tjandra, N. (2000) *Cell* **103**, 645-654
5. Moldoveanu, T., Liu, Q., Tocilj, A., Watson, M., Shore, G., and Gehring, K. (2006) *Mol Cell* **24**, 677-688
6. Hinds, M. G., Smits, C., Fredericks-Short, R., Risk, J. M., Bailey, M., Huang, D. C., and Day, C. L. (2006) *Cell Death Differ*
7. Billen, L. P., Shamas-Din, A., and Andrews, D. W. (2008) *Oncogene* **27 Suppl 1**, S93-104
8. Chou, J. J., Li, H., Salvesen, G. S., Yuan, J., and Wagner, G. (1999) *Cell* **96**, 615-624
9. McDonnell, J. M., Fushman, D., Milliman, C. L., Korsmeyer, S. J., and Cowburn, D. (1999) *Cell* **96**, 625-634
10. Ku, B., Liang, C., Jung, J. U., and Oh, B. H. (2010) *Cell Res*
11. Uren, R. T., Dewson, G., Chen, L., Coyne, S. C., Huang, D. C., Adams, J. M., and Kluck, R. M. (2007) *J Cell Biol* **177**, 277-287
12. Wei, M. C., Lindsten, T., Mootha, V. K., Weiler, S., Gross, A., Ashiya, M., Thompson, C. B., and Korsmeyer, S. J. (2000) *Genes Dev* **14**, 2060-2071
13. Willis, S. N., Fletcher, J. I., Kaufmann, T., van Delft, M. F., Chen, L., Czabotar, P. E., Ierino, H., Lee, E. F., Fairlie, W. D., Bouillet, P., Strasser, A., Kluck, R. M., Adams, J. M., and Huang, D. C. (2007) *Science* **315**, 856-859
14. Kim, H., Rafiuddin-Shah, M., Tu, H. C., Jeffers, J. R., Zambetti, G. P., Hsieh, J. J., and Cheng, E. H. (2006) *Nat Cell Biol* **8**, 1348-1358
15. Leber, B., Lin, J., and Andrews, D. W. (2007) *Apoptosis* **12**, 897-911
16. Hsu, Y. T., Wolter, K. G., and Youle, R. J. (1997) *Proc Natl Acad Sci U S A* **94**, 3668-3672
17. Wolter, K. G., Hsu, Y. T., Smith, C. L., Nechushtan, A., Xi, X. G., and Youle, R. J. (1997) *J Cell Biol* **139**, 1281-1292
18. Wang, K., Yin, X. M., Chao, D. T., Milliman, C. L., and Korsmeyer, S. J. (1996) *Genes Dev* **10**, 2859-2869
19. Yethon, J. A., Epand, R. F., Leber, B., Epand, R. M., and Andrews, D. W. (2003) *J Biol Chem* **278**, 48935-48941
20. Bleicken, S., Classen, M., Padmavathi, P. V., Ishikawa, T., Zeth, K., Steinhoff, H. J., and Bordignon, E. (2010) *J Biol Chem* **285**, 6636-6647
21. Weber, A., Paschen, S. A., Heger, K., Wilfling, F., Frankenberg, T., Bauerschmitt, H., Seiffert, B. M., Kirschnek, S., Wagner, H., and Hacker, G. (2007) *J Cell Biol* **177**, 625-636

22. Kudla, G., Montessuit, S., Eskes, R., Berrier, C., Martinou, J. C., Ghazi, A., and Antonsson, B. (2000) *J Biol Chem* **275**, 22713-22718
23. Letai, A., Bassik, M. C., Walensky, L. D., Sorcinelli, M. D., Weiler, S., and Korsmeyer, S. J. (2002) *Cancer Cell* **2**, 183-192
24. Oh, K. J., Barbuto, S., Pitter, K., Morash, J., Walensky, L. D., and Korsmeyer, S. J. (2006) *J Biol Chem* **281**, 36999-37008
25. Terrones, O., Etxebarria, A., Landajuela, A., Landeta, O., Antonsson, B., and Basanez, G. (2008) *J Biol Chem* **283**, 7790-7803
26. Kim, H., Tu, H. C., Ren, D., Takeuchi, O., Jeffers, J. R., Zambetti, G. P., Hsieh, J. J., and Cheng, E. H. (2009) *Mol Cell* **36**, 487-499
27. Kuwana, T., Mackey, M. R., Perkins, G., Ellisman, M. H., Latterich, M., Schneiter, R., Green, D. R., and Newmeyer, D. D. (2002) *Cell* **111**, 331-342
28. Terrones, O., Antonsson, B., Yamaguchi, H., Wang, H. G., Liu, J., Lee, R. M., Herrmann, A., and Basanez, G. (2004) *J Biol Chem* **279**, 30081-30091
29. Christenson, E., Merlin, S., Saito, M., and Schlesinger, P. (2008) *J Mol Biol* **381**, 1168-1183
30. Gavathiotis, E., Reyna, D. E., Davis, M. L., Bird, G. H., and Walensky, L. D. (2010) *Mol Cell* **40**, 481-492
31. Ruffolo, S. C., and Shore, G. C. (2003) *J Biol Chem* **278**, 25039-25045
32. Tan, C., Dlugosz, P. J., Peng, J., Zhang, Z., Lapolla, S. M., Plafker, S. M., Andrews, D. W., and Lin, J. (2006) *J Biol Chem* **281**, 14764-14775
33. Cartron, P. F., Bellot, G., Oliver, L., Grandier-Vazeille, X., Manon, S., and Vallette, F. M. (2008) *FEBS Lett* **582**, 3045-3051
34. Oh, K. J., Singh, P., Lee, K., Foss, K., Lee, S., Park, M., Aluvila, S., Kim, R. S., Symersky, J., and Walters, D. E. (2010) *J Biol Chem* **285**, 28924-28937
35. Anderluh, G., Besenicar, M., Kladnik, A., Lakey, J. H., and Macek, P. (2005) *Anal Biochem* **344**, 43-52
36. Lovell, J. F., Billen, L. P., Bindner, S., Shamas-Din, A., Fradin, C., Leber, B., and Andrews, D. W. (2008) *Cell* **135**, 1074-1084
37. Walensky, L. D., Pitter, K., Morash, J., Oh, K. J., Barbuto, S., Fisher, J., Smith, E., Verdine, G. L., and Korsmeyer, S. J. (2006) *Mol Cell* **24**, 199-210
38. Ivashyna, O., Garcia-Saez, A. J., Ries, J., Christenson, E. T., Schwille, P., and Schlesinger, P. H. (2009) *J Biol Chem* **284**, 23935-23946
39. Zhang, Z., Lapolla, S. M., Annis, M. G., Truscott, M., Roberts, G. J., Miao, Y., Shao, Y., Tan, C., Peng, J., Johnson, A. E., Zhang, X. C., Andrews, D. W., and Lin, J. (2004) *J Biol Chem* **279**, 43920-43928
40. Denisov, A. Y., Chen, G., Sprules, T., Moldoveanu, T., Beauparlant, P., and Gehring, K. (2006) *Biochemistry* **45**, 2250-2256
41. Hsu, Y. T., and Youle, R. J. (1997) *J Biol Chem* **272**, 13829-13834

42. Losonczi, J. A., Olejniczak, E. T., Betz, S. F., Harlan, J. E., Mack, J., and Fesik, S. W. (2000) *Biochemistry* **39**, 11024-11033
43. Muchmore, S. W., Sattler, M., Liang, H., Meadows, R. P., Harlan, J. E., Yoon, H. S., Nettesheim, D., Chang, B. S., Thompson, C. B., Wong, S. L., Ng, S. L., and Fesik, S. W. (1996) *Nature* **381**, 335-341
44. Schlesinger, P. H., Gross, A., Yin, X. M., Yamamoto, K., Saito, M., Waksman, G., and Korsmeyer, S. J. (1997) *Proc Natl Acad Sci U S A* **94**, 11357-11362
45. Schendel, S. L., Montal, M., and Reed, J. C. (1998) *Cell Death Differ* **5**, 372-380
46. Thuduppathy, G. R., Terrones, O., Craig, J. W., Basanez, G., and Hill, R. B. (2006) *Biochemistry* **45**, 14533-14542
47. Garcia-Saez, A. J., Ries, J., Orzaez, M., Perez-Paya, E., and Schwille, P. (2009) *Nat Struct Mol Biol* **16**, 1178-1185
48. Peng, J., Tan, C., Roberts, G. J., Nikolaeva, O., Zhang, Z., Lapolla, S. M., Primorac, S., Andrews, D. W., and Lin, J. (2006) *J Biol Chem* **281**, 35802-35811
49. Epand, R. F., Martinou, J. C., Fornallaz-Mulhauser, M., Hughes, D. W., and Epand, R. M. (2002) *J Biol Chem* **277**, 32632-32639
50. Polzien, L., Baljuls, A., Rennefahrt, U. E., Fischer, A., Schmitz, W., Zahedi, R. P., Sickmann, A., Metz, R., Albert, S., Benz, R., Hekman, M., and Rapp, U. R. (2009) *J Biol Chem* **284**, 28004-28020
51. Polzien, L., Baljuls, A., Roth, H. M., Kuper, J., Benz, R., Schweimer, K., Hekman, M., and Rapp, U. R. (2010) *Biochim Biophys Acta*
52. Torrecillas, A., Martinez-Senac, M. M., Ausili, A., Corbalan-Garcia, S., and Gomez-Fernandez, J. C. (2007) *Biochim Biophys Acta* **1768**, 2931-2939
53. Garcia-Saez, A. J., Coraiola, M., Dalla Serra, M., Mingarro, I., Menestrina, G., and Salgado, J. (2005) *Biophys J* **88**, 3976-3990
54. Gavathiotis, E., Suzuki, M., Davis, M. L., Pitter, K., Bird, G. H., Katz, S. G., Tu, H. C., Kim, H., Cheng, E. H., Tjandra, N., and Walensky, L. D. (2008) *Nature* **455**, 1076-1081
55. Kuwana, T., Bouchier-Hayes, L., Chipuk, J. E., Bonzon, C., Sullivan, B. A., Green, D. R., and Newmeyer, D. D. (2005) *Mol Cell* **17**, 525-535
56. Du, H., Wolf, J., Schafer, B., Moldoveanu, T., Chipuk, J. E., and Kuwana, T. (2010) *J Biol Chem*
57. Cartron, P. F., Gallenne, T., Bougras, G., Gautier, F., Manero, F., Vusio, P., Meflah, K., Vallette, F. M., and Juin, P. (2004) *Mol Cell* **16**, 807-818
58. Terradillos, O., Montessuit, S., Huang, D. C., and Martinou, J. C. (2002) *FEBS Lett* **522**, 29-34
59. Marani, M., Tenev, T., Hancock, D., Downward, J., and Lemoine, N. R. (2002) *Mol Cell Biol* **22**, 3577-3589

60. Merino, D., Giam, M., Hughes, P. D., Siggs, O. M., Heger, K., O'Reilly, L. A., Adams, J. M., Strasser, A., Lee, E. F., Fairlie, W. D., and Bouillet, P. (2009) *J Cell Biol* **186**, 355-362
61. Billen, L. P., Kokoski, C. L., Lovell, J. F., Leber, B., and Andrews, D. W. (2008) *PLoS Biol* **6**, e147
62. Chen, L., Willis, S. N., Wei, A., Smith, B. J., Fletcher, J. I., Hinds, M. G., Colman, P. M., Day, C. L., Adams, J. M., and Huang, D. C. (2005) *Mol Cell* **17**, 393-403
63. Hekman, M., Albert, S., Galmiche, A., Rennefahrt, U. E., Fueller, J., Fischer, A., Puehringer, D., Wiese, S., and Rapp, U. R. (2006) *J Biol Chem* **281**, 17321-17336
64. Liu, Q., Moldoveanu, T., Sprules, T., Matta-Camacho, E., Mansur-Azzam, N., and Gehring, K. (2010) *J Biol Chem*
65. Yao, Y., Bobkov, A. A., Plesniak, L. A., and Marassi, F. M. (2009) *Biochemistry* **48**, 8704-8711
66. Basanez, G., Sharpe, J. C., Galanis, J., Brandt, T. B., Hardwick, J. M., and Zimmerberg, J. (2002) *J Biol Chem* **277**, 49360-49365
67. de Mol, N. J., and Fischer, M. J. (2010) *Methods Mol Biol* **627**, 1-14

CHAPTER 5

Conclusions & Future Directions

5.1 | Conclusions

The process by which BAX effects cell death comprises three basic steps: mitochondrial translocation, membrane integration, and oligomerization culminating in bilayer permeabilization. The components of this dissertation describe our interrogations of these steps, largely employing biophysical measurements of cell-free, reconstituted experimental regimes.

In Chapter 2, we established that cholesterol impedes BAX pore activation, which provides a rationale for the escape of cell outer membranes from BAX predation during apoptosis. Mitochondrial accumulation of cholesterol also provides a means for alleviating the pro-death function of BAX during cell stress. Using detergent-treated BAX—to bypass complicating activation factors—and dye-filled synthetic vesicles, we demonstrated that cholesterol severely impedes leakage induced by BAX while Hill analyses revealed that BAX retained oligomerization capacity. Development of a vesicle-mitochondria fusion technique allowed filling of the organelles with dye for leakage assays, providing a complex membrane that retains mitochondrial defense mechanisms against poration. These fused mitochondria recapitulated our finding that cholesterol inhibits BAX activity. Inclusion of the total enantiomer of cholesterol in leakage assays showed that BAX pore inhibition by cholesterol is due to the sterol's influence on bilayer architecture rather than a stereospecific interaction with the protein. Real-time SPR spectroscopic measurements uncovered that bilayer cholesterol exerts its influence on BAX function by mitigating the protein's integration into membranes and thus permits fewer in-membrane BAX monomers for assembly into pore structures.

Chapter 3 detailed our investigation into the effects of cholesterol derivatives—oxysterols and bile acids—on BAX activity. As with cholesterol, oxysterols and bile acids are associated with a number of pathological conditions and while mitochondria are typically cholesterol-poor organelles they perform many chemical modifications of the sterol. Whereas cholesterol inhibited BAX membrane permeabilization, 25-hydroxycholesterol accelerated it; importantly, the oxysterol promoted leakage by BAX when activated either by non-physiological detergent or BH3-only protein cBID. Most of this poration enhancement arose at physiologically-plausible solution concentrations up to 5 μM 25-HC. Bile acids are natural detergents used to solubilize dietary fats but are toxic at high concentrations. With the finding that lithocholic and chenodeoxycholic acids induce apoptosis in colon cancer cells, we reasoned that BAX may be activated by the bile acids. Intriguingly, both LCA and CDCA activated C-terminally truncated BAX at low μM (sub-CMC) quantities. Unfortunately, activation of full-length BAX, which includes the auto-inhibitory C-terminal helix, requires micellar bile acids. Thus we conclude that while bile acids promote destabilizing the soluble fold of BAX, in isolation they are most likely insufficient to elicit a death-effecting conformation.

The mechanism by which BCL2 proteins mitochondrially translocate was clarified by the investigations composing Chapter 4. Direct interactions between BAX and BH3-only proteins have been inconsistent and difficult to detect, fostering confusion over the process and localization of BAX activation. For the first time, two BH3-only direct activators were compared in their efficacies for triggering BAX poration. We demonstrated that BIM_S, relative to cBID, more strongly potentiates BAX activity and is less suppressible by antiapoptotic $BCL\text{-}X_L$. We established that soluble BCL2 proteins have intrinsic membrane-binding capacity and

quantified their affinities for bilayers; BCL-X_L binds membranes much more avidly than BAX, effectively "outracing" the proapoptotic protein to its membranous active sites. Vesicle-bound activators tBID & BIM_S were then shown to be equivalent in recruiting BAX & BCL-X_L, suggesting that BIM_S more efficiently than cBID activates BAX by a means other than strictly employing bilayers as interaction scaffolds.

Appendix I integrates a comprehensive array of data pertaining to BAX/BAK conformational alterations and mechanistic details of bilayer disruption to synthesize a new structural model of BAX/BAK pore activation. This model uncovers stages of BAX/BAK oligomer assembly that remain largely obscure and provides a framework for continued investigation of this deadly complex.

Chronicled in Appendices II-V are complementary interrogations of BAX, BCL-X_L, and cBID interactions. The contents of Appendix II reveal that BAX activation and oligomerization are separable events and demonstrate the feasibility of fluorescence correlation spectroscopy in study of the BCL2 family. Appendix III provides confocal microscopic visualizations of BAX-membrane distortions and for the first time directly demonstrates that BAX accumulates at pore edges. Also characterized are what we dubbed BAX mega-pores—micron-diameter membrane inclusions with half-lives on the minute to hour time scale. Integrating these discoveries with prior work uncovering a proteolipidic (toroidal) nature of BAX pores, we also extend membrane line tension theory to postulate a mechanism of BAX pore nucleation, persistence, and closure. Appendix IV comprises our investigation via fluorescence correlation spectroscopy of BAX auto-assembly and modulation by cBID & BCL-X_L. Correlating with our findings in Chapter IV, BAX demonstrates by FCS intrinsic

peripheral and integral membrane binding capability and that activator cBID accelerates this process. Inclusion of antiapoptotic BCL-X_L abrogates BAX oligomerization at multiple discrete steps: *simultaneous* BAX & BCL-X_L addition to vesicles prevents BAX oligomerization but not membrane integration while preincubation of vesicles with BCL-X_L, *prior to* BAX addition, prevented BAX membrane integration (and subsequent oligomerization). Excess addition of cBID rescues higher-order BAX assembly from repression by BCL-X_L. Finally, the oligomeric dynamism of BAX assembly was directly measured and these complexes increase in size in a time dependent manner, further supporting the hypothesis that BAX permeabilizes membranes by nucleating toroidal disruptions. Appendix V encompasses investigation by small-angle x-ray scattering of BAX pore structures. We and our collaborators uncovered that BAX and BCL-X_L generate opposing Gaussian membrane curvatures (negative & positive respectively) to regulate bilayer integrity. Toroidal, proteolipidic pores are consequent of negative curvature generation and our study provides the first structural evidence of the BAX lipidic pore. BCL-X_L was found to suppress negative curvature induced even by non-BCL2 molecules, providing a physical rationale for previous observations that BCL-X_L inhibits cell death even in the absence of BAX binding.

In aggregate, the contents of this dissertation quantify and temporally resolve unplumbed steps of BAX pore activation and deepen our understanding of the protein's physical deformation of membranes.

5.2 | Future Directions

Youle and Strasser previously deemed the biochemical mechanism of BAX/BAK activation to be the "holy grail of apoptosis research" (1). We've established that BAX and its brethren independently adsorb to biological membranes and that membrane-bound activators are sufficient to recruit BAX (& BCL-X_L) to membrane-integral states. The readily apparent next question to be resolved is the existence and relevance of BAX interactions with BH3-only activators in solution. Cell-free FRET assays have indicated that BAX and activator tBID do not bind in solution (2). Deletion of the C-terminal membrane anchor of PUMA mitigates mitochondrial targeting but nevertheless induces apoptosis and BAX N-terminus exposure (3). Conversely, deletion of the membrane anchor of BIM_S has been shown to abolish its prodeath activity, suggesting that mitochondrial targeting is a necessary prerequisite for BAX activation (4). To rectify this conundrum, direct BAX interactions by BIM/PUMA in solution could be probed by FRET or FCS using physiological, nanomolar protein concentrations. This experimental regime is easily extensible to include antiapoptotic proteins like BCL-X_L.

BAX has been shown to comprise two binding sites for activation by BH3 peptides—the canonical BH3 groove and a shallow activation groove on the opposite side of the protein. Employment of engineered, intramolecular disulfide tethers and deletions of α1 or α9 could allow entrapment of BAX conformations and facilitate investigation of the details of BH3 domain interactions (5-7). Engineered BAX conformational restraints would also be useful for interrogations of BAX unfolding mediated by membrane adsorption.

The structure of membrane-integral, active BAX has been sought for nearly 15 years. This investigation has proven technically challenging as the protein seemingly resists

crystallization, which is not surprising given its propensity to aggregate, while detergent-micellar BAX forms large complexes whose hydrodynamic volume is not amenable to solution NMR (8). Potential remedies for these experimental obstacles include generating BAX mutants that fail to oligomerize—G108E and G67R BAX mutants are oligomerization-defective, likely due to disruption of reciprocal BH3 helix:BH3 groove binding (9). Employment of cholic acid as membrane mimetic may mitigate large complex formation as this detergent activates BAX but generates macromolecular assemblies smaller than 50 kDa (Appendix II). Reconstitution of BAX into lipid bicelles for solution NMR is an attractive possibility but may be unfeasible due to the protein's distortion of bilayer architecture (Appendices III & V).

Deeper understanding the process of BAX activation and its structural details will facilitate rational therapeutic drug design. The anticancer compound ABT-737 mimics the BH3 domain of BAD and was developed via an NMR-based screen of small molecules which antagonize prosurvival BCL2 proteins (10). Similarly, compounds mimicking BH3 domains of activator proteins could be devised to more effectively oppose antiapoptotic BCL2 proteins (11) and simultaneously trigger activations of BAX/BAK. The opposite strategy could also prove fruitful, specifically in development of drugs that occlude the binding interfaces of BAX/BAK to prevent their activations or oligomerizations and subsequent cell death.

Tantalizing are the prospects of discovering compounds that modulate BCL2 protein function and devising carriers for compound delivery to specific tissues. We've previous demonstrated that molecularly-targeted nanoparticles can efficiently distribute the cytolytic peptide melittin to mouse tumors to reduce their growth (12). Application of this method, in

concert with BCL2-modulating drug design, may permit delivery of small molecules or peptides to relevant tissues for promotion or suppression of cell death (13,14).

Another promising research avenue encompasses the lipid dependence of BAX/BAK function. Mitochondrial lipid cardiolipin provides targeting specificity for BH3-only activator tBID but whether BIM, PUMA, BAD, etc. migrate preferentially to certain intracellular membranes is unknown. Though we and others found that cholesterol dampens BAX poration, not uncovered was whether the sterol suppresses steps of the permeabilization pathway prior to BAX membrane integration e.g. recruitment of BH3-only activators or oppositional antiapoptotic BCL2 proteins. BAK is constitutively mitochondrially-bound and may countervail cholesterol inhibition of BAX; this potential compensatory mechanism thus warrants further scrutiny.

Complementary to our studies, BAX pore suppression by cholesterol has also been demonstrated using cellular models (15,16). These reports employed drug-treated HeLa cells and hepatocarcinoma cells to generate cholesterol-amplified mitochondria. Cancers very often aberrantly overexpress or inactivate BCL2 family members and drug-treatment may introduce spurious and unnoticed metabolic defects thus further validation of cholesterol's repression of apoptosis should be characterized in a bona fide model of pathogenic cholesterol accumulation, for instance using *npc1*$^{-/-}$ mice. Anomalous cellular restriction of apoptosis can generate necrotic death or autophagy and discernment of BCL2 family dysregulation by cholesterol could provide another means for elucidating the crosstalk between various cell death pathways.

5.3 | References

1. Youle, R. J., and Strasser, A. (2008) *Nat Rev Mol Cell Biol* **9**, 47-59
2. Lovell, J. F., Billen, L. P., Bindner, S., Shamas-Din, A., Fradin, C., Leber, B., and Andrews, D. W. (2008) *Cell* **135**, 1074-1084
3. Yee, K. S., and Vousden, K. H. (2008) *Apoptosis* **13**, 87-95
4. Weber, A., Paschen, S. A., Heger, K., Wilfling, F., Frankenberg, T., Bauerschmitt, H., Seiffert, B. M., Kirschnek, S., Wagner, H., and Hacker, G. (2007) *J Cell Biol* **177**, 625-636
5. Dewson, G., Kratina, T., Sim, H. W., Puthalakath, H., Adams, J. M., Colman, P. M., and Kluck, R. M. (2008) *Mol Cell* **30**, 369-380
6. Edlich, F., Banerjee, S., Suzuki, M., Cleland, Megan M., Arnoult, D., Wang, C., Neutzner, A., Tjandra, N., and Youle, Richard J. (2011) *Cell* **145**, 104-116
7. Gavathiotis, E., Reyna, D. E., Davis, M. L., Bird, G. H., and Walensky, L. D. (2010) *Mol Cell* **40**, 481-492
8. Suzuki, M., Youle, R. J., and Tjandra, N. (2000) *Cell* **103**, 645-654
9. Kim, H., Tu, H. C., Ren, D., Takeuchi, O., Jeffers, J. R., Zambetti, G. P., Hsieh, J. J., and Cheng, E. H. (2009) *Mol Cell* **36**, 487-499
10. Oltersdorf, T., Elmore, S. W., Shoemaker, A. R., Armstrong, R. C., Augeri, D. J., Belli, B. A., Bruncko, M., Deckwerth, T. L., Dinges, J., Hajduk, P. J., Joseph, M. K., Kitada, S., Korsmeyer, S. J., Kunzer, A. R., Letai, A., Li, C., Mitten, M. J., Nettesheim, D. G., Ng, S., Nimmer, P. M., O'Connor, J. M., Oleksijew, A., Petros, A. M., Reed, J. C., Shen, W., Tahir, S. K., Thompson, C. B., Tomaselli, K. J., Wang, B., Wendt, M. D., Zhang, H., Fesik, S. W., and Rosenberg, S. H. (2005) *Nature* **435**, 677-681
11. Lee, E. F., Sadowsky, J. D., Smith, B. J., Czabotar, P. E., Peterson-Kaufman, K. J., Colman, P. M., Gellman, S. H., and Fairlie, W. D. (2009) *Angew Chem Int Ed Engl* **48**, 4318-4322
12. Soman, N. R., Baldwin, S. L., Hu, G., Marsh, J. N., Lanza, G. M., Heuser, J. E., Arbeit, J. M., Wickline, S. A., and Schlesinger, P. H. (2009) *J Clin Invest* **119**, 2830-2842
13. Pan, H., Ivashyna, O., Sinha, B., Lanza, G. M., Ratner, L., Schlesinger, P. H., and Wickline, S. A. (2011) *Biomaterials* **32**, 231-238
14. Danial, N. N., Walensky, L. D., Zhang, C. Y., Choi, C. S., Fisher, J. K., Molina, A. J., Datta, S. R., Pitter, K. L., Bird, G. H., Wikstrom, J. D., Deeney, J. T., Robertson, K., Morash, J., Kulkarni, A., Neschen, S., Kim, S., Greenberg, M. E., Corkey, B. E., Shirihai, O. S., Shulman, G. I., Lowell, B. B., and Korsmeyer, S. J. (2008) *Nat Med* **14**, 144-153
15. Lucken-Ardjomande, S., Montessuit, S., and Martinou, J. C. (2008) *Cell Death Differ* **15**, 484-493
16. Montero, J., Morales, A., Llacuna, L., Lluis, J. M., Terrones, O., Basanez, G., Antonsson, B., Prieto, J., Garcia-Ruiz, C., Colell, A., and Fernandez-Checa, J. C. (2008) *Cancer Res* **68**, 5246-5256

APPENDIX I

Apoptosis' Next Top Model

I.1 | Reconfiguration

BAX & BAK undergo significant structural remodeling to become competent for pore formation. Frustratingly, elucidations of the membrane-active BAX/BAK structures have proven resistant to standard techniques like NMR and x-ray crystallography. Thus the precise conformational alterations have largely been obscure but a few recent studies have more clearly delineated the temporal process of this reconfiguration (1-5). BAX's putative pore-forming domain, the α5-6 hairpin, is protected from solution by the encompassing amphipathic helices (6) (Fig. 1.3); deletion of this hairpin abrogates the poration functionality of BAX (7,8). Topological labeling of activated BAX has indicated that α5-6 and α9 helices are buried in mitochondrial membranes (9). A few other lines of experimentation provided support for the α5-6 insertion hypothesis: electrophysiological investigation of BCL-2 channel formation (10) and interrogation of detergent-induced unfolding of BAX and BCL-X_L (6,11,12). Generation of pore competent BAX thus entails exposure of α5-6 by global destabilization of the protein's tertiary fold. These evidences provided for adoption of the umbrella model (13) from the study of bacterial colicins, which posits that membrane permeabilization is effected by transmembrane insertion of a hydrophobic hairpin while the remaining helices lie at the bilayer/solution interface. Unlike the membrane-active forms of colicins, which emerge spontaneously upon membrane interaction, evocation of a corresponding BAX/BAK conformation is a tightly-regulated process.

The first BAX conformational change discovered was its detergent-induced unfolding and consequent homodimerization and heterodimerization with BCL-X_L (14); this unfolding also everts BAX α1/BH4 to render a buried epitope (residues 12-24) available for 6A7 antibody

binding (15). Deletion of the predicted C-terminal membrane anchor (α9) was then demonstrated to abrogate mitochondrial translocation (16,17). Intriguingly,α9 deletion also promotes α1 eversion as indicated by 6A7 antibody binding (18,19). Under non-stressed conditions, thiol-reactive crosslinkers intramolecularly tether the BAK N-terminus to α6; this crosslink is lost after cell death initiation (20). Upon apoptotic stimulus, α1 of mitochondrially-translocated BAX becomes protease-sensitive and deletion of the first 19 amino acids promotes BAX membrane insertion (17). Immunostaining of fixed & permeabilized cells has indicated that, *in vivo*, eversion of α1 is downstream of death signal initiation as BAK and mitochondrially-targeted BAX^{S184V} (α9 point mutant) did not expose the α1 antibody epitope until after a cell stressor is applied (18,21). This suggests that exposures of the two helices are separable events. Conversely, more recent reports indicate that BAK and mitochondrial BAX obligately expose their α1 or demonstrate that α1/α9 dislocation is concomitant. (5,19,22).

A number of instigators of BAX α1/BH4 eversion have been identified. BH3-only BAX activators tBID & PUMA and a BIM BH3 peptide all interact with and dislocate the N-terminal BAX helix (4,23,24). The activating interaction of tumor suppressor p53 with BAK was mapped to α1 of the pore-former (25). Transient BAX interaction with vesicle bilayers also triggers reversible dislodging of α1 (26). Gavathiotis *et al*. and Kim *et al*. have produced evidence that dislocation of α1 allosterically induces exposure of α9 (3,5). In aggregate, these findings reveal that the N & C-terminal helices reinforce the globular, monomeric fold of BAX (5,6,27).

Extrication of the BAX autoinhibitory α1/BH4 & α9 helices appears to be the initial stage of generating a membrane-permeabilizing conformation (Fig. I.1). After α1/BH4 dislocation and α9 mobilization, the BH3 helix (α2) of BAX/BAK everts and its previously buried, hydrophobic face becomes available for antibody binding (2,3). These newly liberated BAX/BAK BH3s helices, no longer packed against the protein core (Fig. 1.3), are then available for propagating the autoactivation cascade (3,28,29), homodimerization (2,30), or incarceration by antiapoptotics (31-33).

Fig. I.1

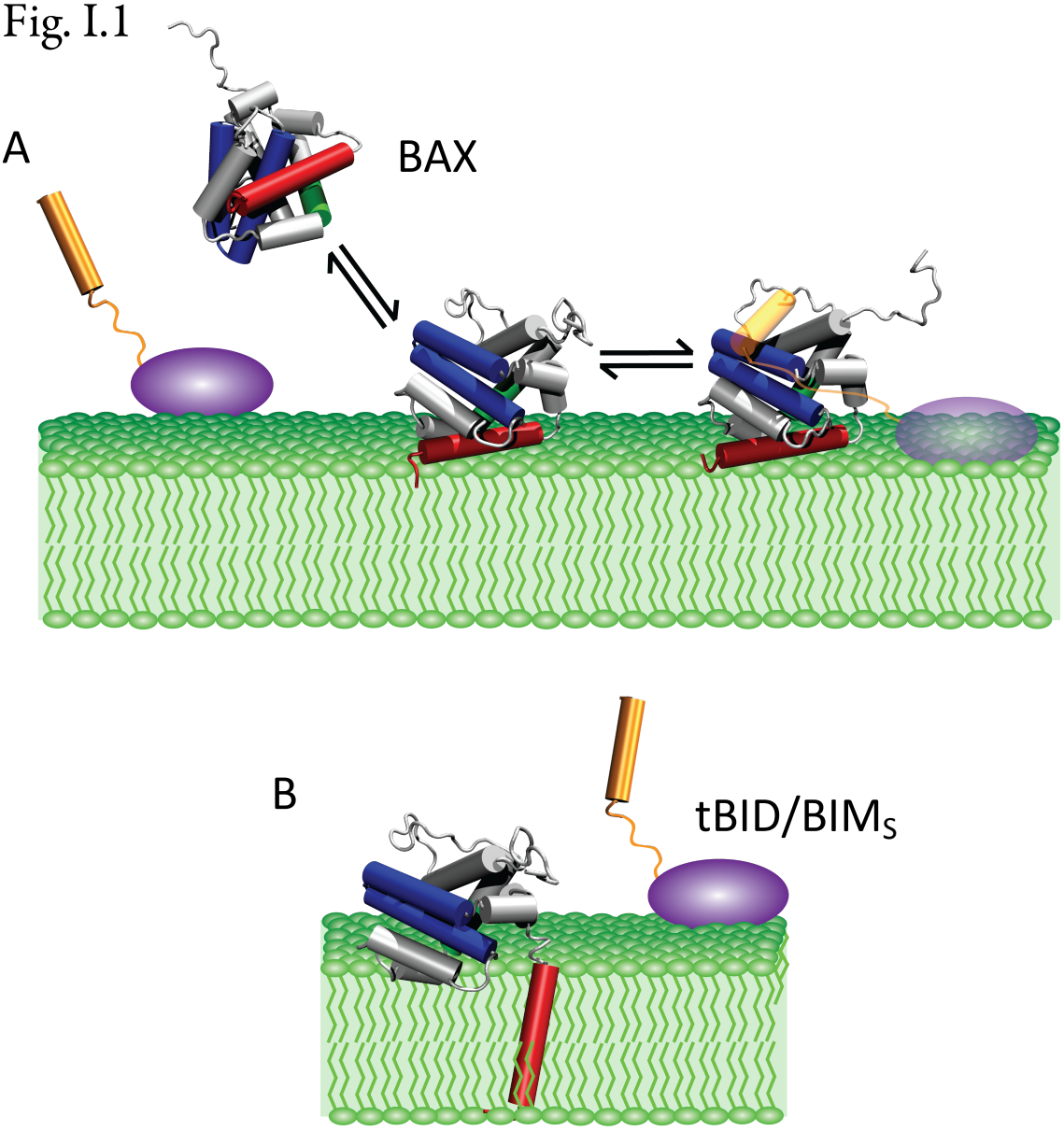

Fig. I.1 | **BAX translocation.** *A*, Soluble, monomeric BAX equilibrates between aqueous and membrane-adsorbed states. *B*, Interaction with a bilayer can induce eversion of BAX α1 & 9 to allow membrane anchoring. Presence of a BH3-only activator (tBID/BIM_S) can accelerate α9 mobilization and anchoring by interacting with and dislocating α1 (*A*). BAX PDBs adapted: 1F16, 2K7W

Generation of the culminating, pore competent BAX/BAK conformation entails dissolution of the conserved hydrophobic core (encoded by BH1 & 2) which reinforces close packing of the α5-6 hairpin (Fig. I.2). This final step, which would permit membrane insertion of the pore-forming hairpin, is alluded to by a few evidential lines. Tellingly, mutation to alanine of an invariant tryptophan in BH1 of BCL-X_L significantly destabilizes the tertiary fold and accelerates vesicle leakage induced by the protein (34). $BAX^{\Delta C}$ & $BAK^{\Delta C}$, deleted of their α9 membrane anchors (but retaining both invariant BH2 tryptophans), are dispersed as cytosolic monomers when expressed in cells (2,5). Further truncation of $BAX^{\Delta C}$, to remove α8 (and the more C-terminal BH2 tryptophan), induces cytosolic aggregation of the protein (35); intriguingly, this BAX truncation also fosters detergent-free interaction with BIM. A pair of crosslinking studies concluded that formation of the second activated BAX/BAK interface is consequential of BH3 helix ingress to the BH3 groove (see two paragraphs down) (1,36).

To summarize, we propose that the conformational rearrangement of BAX/BAK into their active states encompasses four steps: 1) eversions of α1 & 9, 2) eviction of the BH3 helix (α2), 3) disruption of the tryptophan staple restraining α5-6, and 4) spontaneous insertion of the hairpin.

Fig. I.2

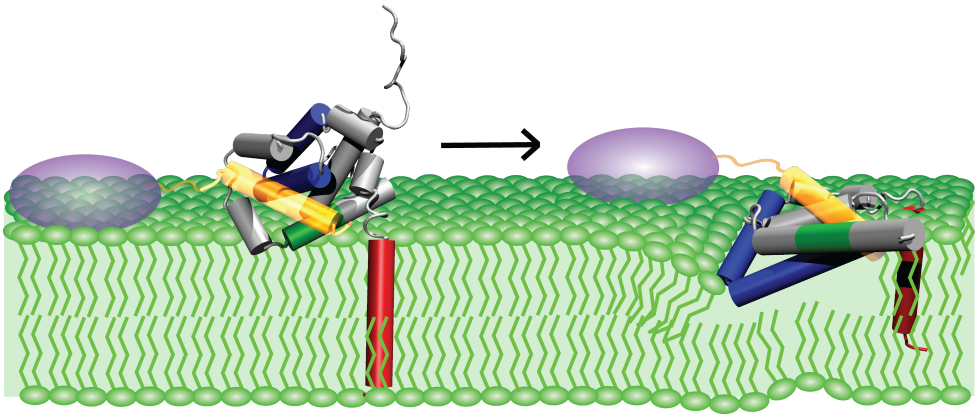

Fig. I.2 | **BAX integration.** BAX assumes its in-membrane monomeric state after disruption of the hydrophobic core that coordinates tight packing of the α5-6 hairpin. This collapse can occur spontaneously or is enhanced by BH3 helix (from tBID, BIM_S, or integrated BAX) intercalation into the BAX BH3 groove. BAX acceptance of donor BH3 helix is homology modeled on BCL-$X_L^{\Delta C}$/BIM BH3 complex (PDB: 1PQ1). For visual clarity, BAX α1 is deleted from integrated BAX.

I.2 | Oligomerization

These previous stages describe only alterations of the monomeric species but mitochondrial permeabilization requires BAX/BAK oligomerization. The structural basis of this higher-order assembly is slowly coming unveiled. Early mutational studies revealed the necessity for intact BH1 & BH3 domains in dimerization (30,37,38). The canonical BH3 groove—encompassing α2-5—was defined by a deletion/chimæra study as the minimal BAX unit competent for multimerization (39). This finding was followed up by Dewson *et al*. who employed disulfide trapping of introduced cysteines to uncover that activated BAK homodimerizes via symmetric domain swapping (BH3 helix:BH3 groove interactions) (2). Recombinant $BAK^{\Delta C}$ has its poration activity severely ablated by substitution with valine of an invariant BH1 glycine (40) and mutation to glutamic acid of the homologous BH1 glycine in BAX permits only dimer formation (5). Electron paramagnetic resonance spectroscopy of spin-labeled BAX & BAK demonstrates that, as homodimers, their BH3 helices form an interface and lie antiparallel (40,41). Membrane-bound BAX and activator tBID also can remain engaged, apparently via BAX BH3 groove:tBID BH3 helix interaction, as adduced by FRET assays (42). Taken together, the evidence has become clear that activated BAX & BAK retain their canonical BH3 grooves to function as acceptor sites of donor BH3 helices (Fig. I.3).

Fig. I.3

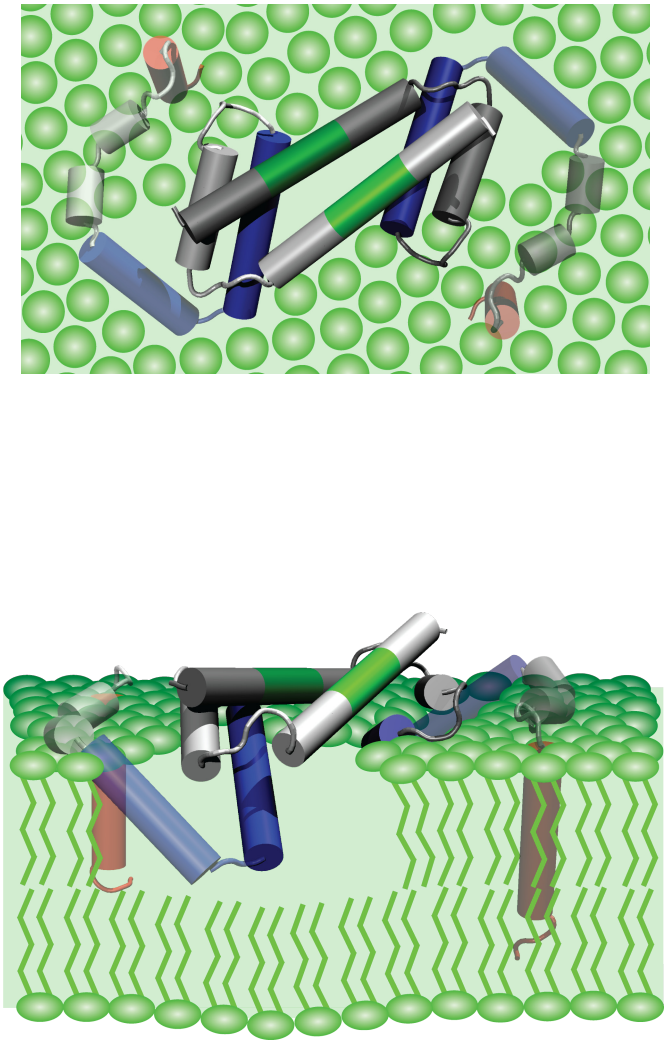

Fig. I.3 | **BAX dimerization.** Overhead and side views of BAX reciprocal domain swap via BH3 helix:BH3 groove interactions. BAX α1 is deleted for visual clarity.

Reciprocal exchange of BH3 helices provides only a means for BAX/BAK dimerization; a second binding surface is required for oligomer accretion. Little evidence pertains to this obscurity, unfortunately. One publication indentifies an α6:α6 interface by which BAK symmetric dimers can further assemble (1). Another study mapped BAX interfaces via introduced crosslinks; these were performed in Triton X-100, (a detergent whose fidelity as a membrane mimetic is questionable) but the data are at least partly reconcilable with BH3 helix:BH3 groove & α6:α6 interfaces (36). Distance constraints determined by EPR are also somewhat, though not entirely, consistent with the α6:α6 hypothesis (40) (Fig. I.4).

One potential missing puzzle piece is whether BAX/BAK α1 contributes to an oligomer interface. Microsomal glycosylation mapping suggests that a peptide embodying BAX α1 assumes a transmembrane orientation while NMR of detergent-treated BAX indicated that α1 is excluded from micelles. Reconciling this apparent disparity, ATR spectroscopy has revealed that a BAX α1 peptide is shifted to a membrane parallel orientation at the headgroup/solvent interface by cardiolipin (43,44). One study implies a role for BAX α1 in oligomerization, having concluded that BAX deleted of the helix functions as a BH3-only protein and requires full-length BAX to foment mitochondrial permeabilization (45).

I.3 | Pore Formation

The preceding amasses evidence pertaining to the proteinaceous structure of oligomeric BAX/BAK but fails to describe the nature of the membrane pore itself. The best characterized biological pores are β-barrels, like porins. Structures of a number of these proteins have been solved to high resolution by x-ray crystallography and NMR. Pores induced by α-helical peptides and proteins are considerably more labile and less acquiescent to interrogation,

prompting introduction of multiple models of pore formation, predominantly the barrel-stave and toroidal (lipidic) schemes. The barrel-stave model describes bilayer pores whose edges are composed of transmembrane α-helices that shield the lipid acyl chains from an aqueous milieu; alamethicin is a prominent barrel-stave pore-forming peptide.

Most membrane-disrupting peptides, however, are better described by the toroidal model, in which peptides and lipid head groups cooperate to line pore edges resulting in continuity (and lipid exchange) between bilayer leaflets. A growing body of data, produced by our lab and others, strongly support a toroidal, proteolipidic pore as the means by which BAX/BAK effects membrane permeabilization (Fig. I.4).

Fig. I.4

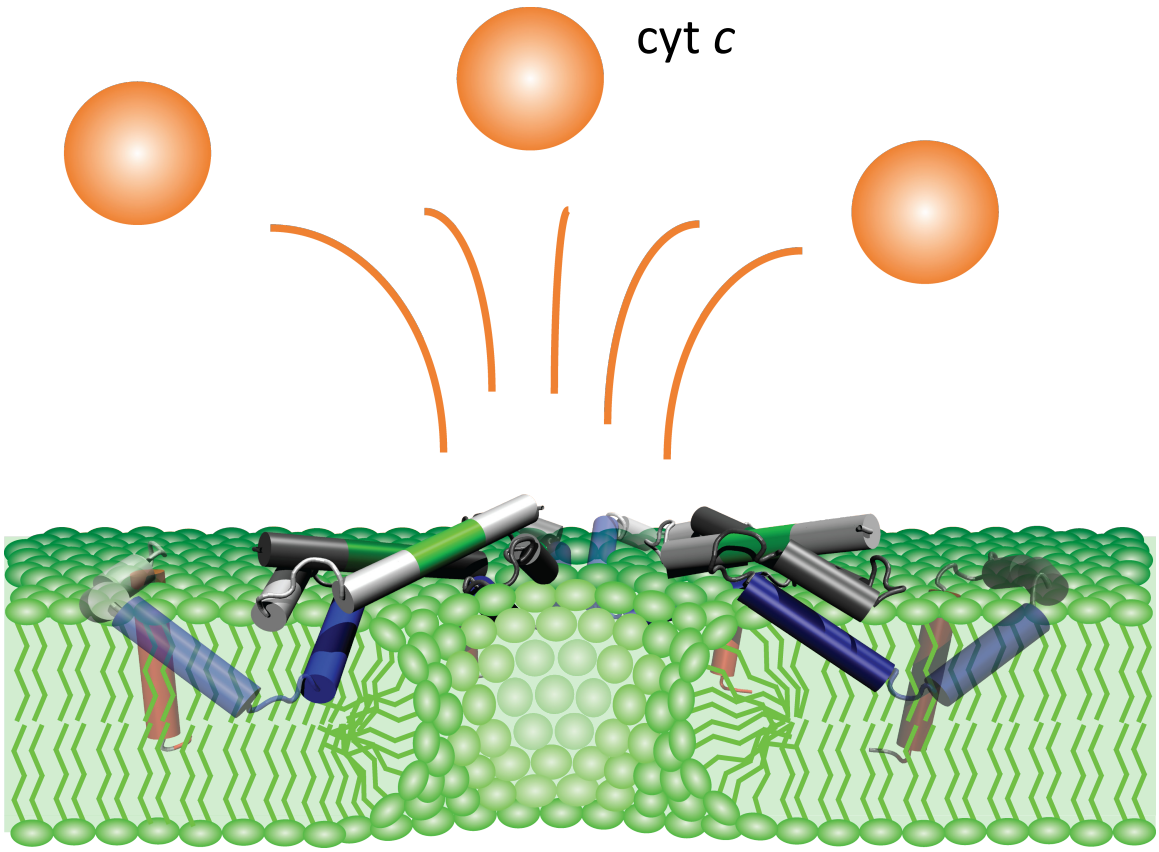

Fig. I.4 | **BAX oligomerization.** BAX accumulates, locally induces negative Gaussian curvature, and cooperates with lipids to organize toroidal pores through which cytochrome *c* can escape. BAX α1 is deleted for visual clarity.

First suggesting the lipid dependence and toroidal nature of BAX pores was the observation that BAX destabilizes bilayers and produces arbitrary, rather than stepwise, variations in membrane permeability (46). Corroborating this report were demonstrations of BAX poration dependence on intrinsic lipid curvature and BAX induction of lipid transfer between leaflets (47-50). More recently, x-ray diffraction was employed to glean details of membrane structures induced by BAX α5 peptides (51); presence of the peptide in oriented membranes bent the discrete leaflets into contiguous monolayers in pore rims. Our work, using confocal microscopy and small-angle x-ray scattering, confirms and extends these findings that BAX evinces proteolipidic, toroidal pores (Appendices III & V).

A key underlying and largely unexamined premise of BCL2 protein family study remains the umbrella model (13) of unfolding and subsequent pore formation. Specifically, that BAX/BAK unfold and orient their pore-forming α5-6 hairpins in a transmembrane, barrel-stave fashion (52). This rearrangement almost certainly would dissolve the BAX/BAK BH3 grooves, thus it is difficult to reconcile in-membrane dimerization via BH3 helix:BH3 groove interactions with the adopted umbrella model. Further weakening the case for the umbrella, barrel-stave model is the BAX/BAK α5-6 hairpins are, in fact, too short to span mitochondrial membranes (53). Therefore, we propose eschewing the umbrella scheme and instead adapting a competing hypothesis of colicin pore formation—the penknife model (54). This model posits that colicin A arranges its α-hairpin roughly parallel to the membrane-water interface to instigate pore formation. In actuality, a wide array of evidence has been marshaled in support of both models pertaining to colicin poration, suggesting that the two arrangements exist in

equilibrium (55,56). This insight may be apposite to BAX/BAK function but given our present knowledge is speculative at best.

Our proposed quasi-penknife model integrates a host of information regarding BAX/BAK structural rearrangement and assembly and their perturbations of bilayer architecture. It is further supported by evidence relating to α-hairpin orientation across the three BCL2 subclasses. For instance, solid-state NMR of BCL-$X_L^{\Delta C}$ treated with detergent and reconstituted into oriented bilayers demonstrated that the protein's α5-6 helices can tilt relative to membrane normal (12). The corresponding hairpin of BH3-only tBID has been shown to only shallowly tilt into the bilayer by EPR and solid-state NMR (57,58). Oriented circular dichroism has revealed that peptides derived from BAX α5 also assume a tilted, non-bilayer-spanning orientation (51,59). Most pertinently, Oh *et al*. determined via EPR that the α5-6 hairpin of spin-labeled, oligomeric $BAK^{\Delta C}$ is partly exposed to the hydrophobic bilayer interior but α6 is immersed less than 1 nm, strongly implying a shallow tilt rather than transmembrane arrangement of the hairpin (40).

I.4 | References

1. Dewson, G., Kratina, T., Czabotar, P., Day, C. L., Adams, J. M., and Kluck, R. M. (2009) *Mol Cell* **36**, 696-703
2. Dewson, G., Kratina, T., Sim, H. W., Puthalakath, H., Adams, J. M., Colman, P. M., and Kluck, R. M. (2008) *Mol Cell* **30**, 369-380
3. Gavathiotis, E., Reyna, D. E., Davis, M. L., Bird, G. H., and Walensky, L. D. (2010) *Mol Cell* **40**, 481-492
4. Gavathiotis, E., Suzuki, M., Davis, M. L., Pitter, K., Bird, G. H., Katz, S. G., Tu, H. C., Kim, H., Cheng, E. H., Tjandra, N., and Walensky, L. D. (2008) *Nature* **455**, 1076-1081
5. Kim, H., Tu, H. C., Ren, D., Takeuchi, O., Jeffers, J. R., Zambetti, G. P., Hsieh, J. J., and Cheng, E. H. (2009) *Mol Cell* **36**, 487-499
6. Suzuki, M., Youle, R. J., and Tjandra, N. (2000) *Cell* **103**, 645-654
7. Heimlich, G., McKinnon, A. D., Bernardo, K., Brdiczka, D., Reed, J. C., Kain, R., Kronke, M., and Jurgensmeier, J. M. (2004) *Biochem J* **378**, 247-255
8. Oh, K. J., Barbuto, S., Pitter, K., Morash, J., Walensky, L. D., and Korsmeyer, S. J. (2006) *J Biol Chem* **281**, 36999-37008
9. Annis, M. G., Soucie, E. L., Dlugosz, P. J., Cruz-Aguado, J. A., Penn, L. Z., Leber, B., and Andrews, D. W. (2005) *Embo J* **24**, 2096-2103
10. Schendel, S. L., Xie, Z., Montal, M. O., Matsuyama, S., Montal, M., and Reed, J. C. (1997) *Proc Natl Acad Sci U S A* **94**, 5113-5118
11. Losonczi, J. A., Olejniczak, E. T., Betz, S. F., Harlan, J. E., Mack, J., and Fesik, S. W. (2000) *Biochemistry* **39**, 11024-11033
12. Franzin, C. M., Choi, J., Zhai, D., Reed, J. C., and Marassi, F. M. (2004) *Magn Reson Chem* **42**, 172-179
13. Parker, M. W., Pattus, F., Tucker, A. D., and Tsernoglou, D. (1989) *Nature* **337**, 93-96
14. Hsu, Y. T., and Youle, R. J. (1997) *J Biol Chem* **272**, 13829-13834
15. Peyerl, F. W., Dai, S., Murphy, G. A., Crawford, F., White, J., Marrack, P., and Kappler, J. W. (2007) *Cell Death Differ* **14**, 447-452
16. Wolter, K. G., Hsu, Y. T., Smith, C. L., Nechushtan, A., Xi, X. G., and Youle, R. J. (1997) *J Cell Biol* **139**, 1281-1292
17. Goping, I. S., Gross, A., Lavoie, J. N., Nguyen, M., Jemmerson, R., Roth, K., Korsmeyer, S. J., and Shore, G. C. (1998) *J Cell Biol* **143**, 207-215
18. Nechushtan, A., Smith, C. L., Hsu, Y. T., and Youle, R. J. (1999) *Embo J* **18**, 2330-2341
19. Brock, S. E., Li, C., and Wattenberg, B. W. (2010) *Apoptosis* **15**, 14-27
20. Cheng, E. H., Sheiko, T. V., Fisher, J. K., Craigen, W. J., and Korsmeyer, S. J. (2003) *Science* **301**, 513-517

21. Griffiths, G. J., Dubrez, L., Morgan, C. P., Jones, N. A., Whitehouse, J., Corfe, B. M., Dive, C., and Hickman, J. A. (1999) *J Cell Biol* **144**, 903-914
22. Wang, Q., Sun, S. Y., Khuri, F., Curran, W. J., and Deng, X. (2010) *PLoS One* **5**, e13393
23. Desagher, S., Osen-Sand, A., Nichols, A., Eskes, R., Montessuit, S., Lauper, S., Maundrell, K., Antonsson, B., and Martinou, J. C. (1999) *J Cell Biol* **144**, 891-901
24. Cartron, P. F., Gallenne, T., Bougras, G., Gautier, F., Manero, F., Vusio, P., Meflah, K., Vallette, F. M., and Juin, P. (2004) *Mol Cell* **16**, 807-818
25. Pietsch, E. C., Perchiniak, E., Canutescu, A. A., Wang, G., Dunbrack, R. L., and Murphy, M. E. (2008) *J Biol Chem* **283**, 21294-21304
26. Yethon, J. A., Epand, R. F., Leber, B., Epand, R. M., and Andrews, D. W. (2003) *J Biol Chem* **278**, 48935-48941
27. Lalier, L., Cartron, P. F., Juin, P., Nedelkina, S., Manon, S., Bechinger, B., and Vallette, F. M. (2007) *Apoptosis* **12**, 887-896
28. Ruffolo, S. C., and Shore, G. C. (2003) *J Biol Chem* **278**, 25039-25045
29. Tan, C., Dlugosz, P. J., Peng, J., Zhang, Z., Lapolla, S. M., Plafker, S. M., Andrews, D. W., and Lin, J. (2006) *J Biol Chem* **281**, 14764-14775
30. Wang, K., Gross, A., Waksman, G., and Korsmeyer, S. J. (1998) *Mol Cell Biol* **18**, 6083-6089
31. Ku, B., Liang, C., Jung, J. U., and Oh, B. H. (2010) *Cell Res*
32. Sattler, M., Liang, H., Nettesheim, D., Meadows, R. P., Harlan, J. E., Eberstadt, M., Yoon, H. S., Shuker, S. B., Chang, B. S., Minn, A. J., Thompson, C. B., and Fesik, S. W. (1997) *Science* **275**, 983-986
33. Czabotar, P. E., Lee, E. F., Thompson, G. V., Wardak, A. Z., Fairlie, W. D., and Colman, P. M. (2011) *J Biol Chem* **286**, 7123-7131
34. Feng, Y., Zhang, L., Hu, T., Shen, X., Ding, J., Chen, K., Jiang, H., and Liu, D. (2009) *Archives of Biochemistry and Biophysics* **484**, 46-54
35. Liu, X., Dai, S., Zhu, Y., Marrack, P., and Kappler, J. W. (2003) *Immunity* **19**, 341-352
36. Zhang, Z., Zhu, W., Lapolla, S. M., Miao, Y., Shao, Y., Falcone, M., Boreham, D., McFarlane, N., Ding, J., Johnson, A. E., Zhang, X. C., Andrews, D. W., and Lin, J. (2010) *J Biol Chem* **285**, 17614-17627
37. Meijerink, J. P., Mensink, E. J., Wang, K., Sedlak, T. W., Sloetjes, A. W., de Witte, T., Waksman, G., and Korsmeyer, S. J. (1998) *Blood* **91**, 2991-2997
38. Wang, K., Yin, X. M., Chao, D. T., Milliman, C. L., and Korsmeyer, S. J. (1996) *Genes Dev* **10**, 2859-2869
39. George, N. M., Evans, J. J., and Luo, X. (2007) *Genes Dev* **21**, 1937-1948
40. Oh, K. J., Singh, P., Lee, K., Foss, K., Lee, S., Park, M., Aluvila, S., Kim, R. S., Symersky, J., and Walters, D. E. (2010) *J Biol Chem* **285**, 28924-28937
41. Bleicken, S., Classen, M., Padmavathi, P. V., Ishikawa, T., Zeth, K., Steinhoff, H. J., and Bordignon, E. (2010) *J Biol Chem* **285**, 6636-6647

42. Lovell, J. F., Billen, L. P., Bindner, S., Shamas-Din, A., Fradin, C., Leber, B., and Andrews, D. W. (2008) *Cell* **135**, 1074-1084
43. Garcia-Saez, A. J., Mingarro, I., Perez-Paya, E., and Salgado, J. (2004) *Biochemistry* **43**, 10930-10943
44. Sani, M. A., Dufourc, E. J., and Grobner, G. (2009) *Biochim Biophys Acta* **1788**, 623-631
45. Cartron, P. F., Oliver, L., Juin, P., Meflah, K., and Vallette, F. M. (2004) *J Biol Chem* **279**, 11503-11512
46. Basanez, G., Nechushtan, A., Drozhinin, O., Chanturiya, A., Choe, E., Tutt, S., Wood, K. A., Hsu, Y., Zimmerberg, J., and Youle, R. J. (1999) *Proc Natl Acad Sci U S A* **96**, 5492-5497
47. Basanez, G., Sharpe, J. C., Galanis, J., Brandt, T. B., Hardwick, J. M., and Zimmerberg, J. (2002) *J Biol Chem* **277**, 49360-49365
48. Epand, R. F., Martinou, J. C., Montessuit, S., and Epand, R. M. (2003) *Biochemistry* **42**, 14576-14582
49. Garcia-Saez, A. J., Coraiola, M., Serra, M. D., Mingarro, I., Muller, P., and Salgado, J. (2006) *Febs J* **273**, 971-981
50. Terrones, O., Antonsson, B., Yamaguchi, H., Wang, H. G., Liu, J., Lee, R. M., Herrmann, A., and Basanez, G. (2004) *J Biol Chem* **279**, 30081-30091
51. Qian, S., Wang, W., Yang, L., and Huang, H. W. (2008) *Proc Natl Acad Sci U S A* **105**, 17379-17383
52. Martinez-Caballero, S., Dejean, L. M., Kinnally, M. S., Oh, K. J., Mannella, C. A., and Kinnally, K. W. (2009) *J Biol Chem* **284**, 12235-12245
53. Garcia-Saez, A. J., Fuertes, G., Suckale, J., and Salgado, J. (2010) *Adv Exp Med Biol* **677**, 91-105
54. Duche, D., Parker, M. W., Gonzalez-Manas, J. M., Pattus, F., and Baty, D. (1994) *J Biol Chem* **269**, 6332-6339
55. Kienker, P. K., Qiu, X., Slatin, S. L., Finkelstein, A., and Jakes, K. S. (1997) *J Membr Biol* **157**, 27-37
56. Prieto, L., and Lazaridis, T. (2011) *Proteins* **79**, 126-141
57. Gong, X. M., Choi, J., Franzin, C. M., Zhai, D., Reed, J. C., and Marassi, F. M. (2004) *J Biol Chem* **279**, 28954-28960
58. Oh, K. J., Barbuto, S., Meyer, N., Kim, R. S., Collier, R. J., and Korsmeyer, S. J. (2005) *J Biol Chem* **280**, 753-767
59. Garcia-Saez, A. J., Coraiola, M., Dalla Serra, M., Mingarro, I., Menestrina, G., and Salgado, J. (2005) *Biophys J* **88**, 3976-3990

APPENDIX II

Detergent-Activated BAX Protein is a Monomer

(The content of this chapter has been adapted from Ivashyna, O., García-Sáez, A. J., Ries, J., Christenson, E. T., Schwille, P., Schlesinger, P. H. (2009) *J Biol Chem* 284, 23935-23946)

II.1 | Summary

BAX is a pro-apoptotic member of the BCL-2 protein family. At the onset of apoptosis, monomeric, cytoplasmic BAX is activated and translocates to the outer mitochondrial membrane, where it forms an oligomeric pore. The chemical mechanism of BAX activation is controversial, and several *in vitro* and *in vivo* methods of its activation are known. One of the most commonly used *in vitro* methods is activation with detergents, such as *n*-octyl glucoside. During BAX activation with *n*-octyl glucoside, it has been shown that BAX forms high molecular weight complexes that are larger than the combined molecular weight of BAX monomer and one detergent micelle. These large complexes have been ascribed to the oligomerization of BAX prior to its membrane insertion and pore formation. This is in contrast to the *in vivo* studies that suggest that active BAX inserts into the outer mitochondrial membrane as a monomer and then undergoes oligomerization. Here, to simultaneously determine the molecular weight and the number of BAX proteins per BAX-detergent micelle during detergent activation, we have used an approach that combines two single-molecule sensitivity techniques—fluorescence correlation spectroscopy and fluorescence-intensity distribution analysis. We have tested a range of detergents as follows: *n*-octyl glucoside, dodecyl maltoside, Triton X-100, Tween 20, CHAPS, and cholic acid. With these detergents we observe that BAX is a monomer before, during, and after interaction with micelles. We conclude that detergent activation of BAX is not congruent with oligomerization and that in physiologic buffer conditions BAX can assume two stable monomeric conformations, one inactive and one active.

II.2 | Introduction

BAX is a pro-apoptotic member of the BCL-2 protein family. In a simplified apoptosis model, monomeric inactive BAX is localized in the cytoplasm of healthy nondying cells (1). During apoptosis BAX is activated and translocates to the outer mitochondrial membrane (2) where it inserts as a monomer (3), undergoes oligomerization (4), and forms a pore through which cytochrome *c* and other apoptotic factors are released into the cytoplasm. Once in the cytoplasm, these apoptotic factors induce the activation of the effector caspases that execute the cell death process. This mechanism, which is generally correct, requires that soluble BAX becomes integrated into the mitochondrial membrane where it forms a functional oligomeric pore capable of cytochrome *c* release. However, the molecular mechanism of BAX activation remains controversial (5, 6).

It has been understood for some time, but frequently ignored, that activity of the BCL-2 family proteins is exhibited in cells when these proteins are associated with the hydrophobic environment of membranes. Therefore, it has always seemed that attention to the effect of hydrophobic environments on the BCL-2 family proteins would be rewarding. It has been shown that BAX can be directly activated by treatment with nonionic detergents such as *n*-octyl glucoside, dodecyl maltoside, and Triton X-100 (1, 7). During activation by nonionic detergents, to gain the ability to form pores in a bilayer membrane, BAX needs to undergo a major conformational transition from a globular protein with two pore-forming α-helices 5 and 6 hidden in the protein core (8) to a conformation in which these two helices are exposed and inserted into a lipid membrane (3, 5, 9). The nature of this active conformation of BAX is

important for the understanding of the death decision in cells. Most proposals suggest that in a cell this activated form of BAX protein is initiated and maintained by the interactions with other proteins, such as tBID, or by BAX itself as a homo-oligomer (7, 10).

Nonionic detergents have been commonly used to activate BAX for *in vitro* studies because they are reliably effective and simple to employ. However, little is known about the detailed molecular mechanism of BAX activation by these detergents and its comparability with *in vivo* activation of BAX. What is known is that concentrations of detergent above their critical micelle concentration (CMC) are necessary for BAX activation. This suggests that, to be activated, BAX needs to interact with detergent micelles instead of monomeric detergent molecules. For example, in the case of BAX activation by *n*-octyl glucoside, it has been shown that *n*-octyl glucoside concentration should be 1% (w/v) (7), which is well above the CMC for this detergent (0.6% w/v) (11). In addition, it has also been shown that above their individual CMC concentrations most BAX-activating detergents produce a change in BAX conformation that can be detected by a conformation-sensitive 6A7 antibody against BAX (1, 12, 13). In cellular experiments this feature of BAX reactivity to 6A7 antibody is commonly associated with the onset of apoptosis (14, 15). However, CHAPS does not generate the antibody-detected conformational change or the activation of BAX. The small micelle size of this detergent (10 kDa) suggests that perhaps BAX cannot adopt an activated state with this detergent. However, cholic acid with even smaller micelle size (4 kDa) can partially activate BAX (1).

Many important detergent properties are associated with micelles. The formation of detergent micelles in solution is concentration-dependent beginning at the CMC. The CMC value for a detergent has practical importance because in most cases only monomers of detergent can be removed by dialysis, and therefore, it is easier to remove detergent monomers for a detergent with high CMC value than for a detergent with low CMC (11). For BAX this same consideration applies to its activation with *n*-octyl glucoside (CMC ~23 mM) as compared with its activation with Triton X-100 (CMC ~0.25 mM). The ease of dialysis is why, in most cases, OG is used to activate BAX *in vitro*.

It has been shown by analytical gel filtration that, when incubated with *n*-octyl glucoside, BAX creates complexes with molecular weight larger than the combined size of a BAX monomer (21 kDa) and an *n*-octyl glucoside micelle (~26 kDa) (7, 11). It has also been shown that in defined liposomes BAX pore formation requires oligomerization (16). These data combined with the knowledge that oligomerization is important for the biological function of BAX led to a hypothesis that BAX oligomerizes during its detergent activation prior to membrane insertion (7). However, it has been shown that *in vivo* activated BAX inserts into the outer mitochondrial membrane as a monomer (3), and to create a pore, BAX undergoes oligomerization in this membrane (4). This discrepancy between the oligomeric state of active BAX prior to its insertion into a lipid membrane *in vivo* (monomer) and *in vitro* (possibly hexamer or octamer) led us to study the oligomerization state of BAX in detergent micelles. The important issue is whether BAX activation requires protein oligomerization or whether active BAX conformation can be generated from a single protein monomer. To solve

this issue we used two single-molecule sensitivity techniques: fluorescence correlation spectroscopy (FCS) (17) and fluorescence-intensity distribution analysis (FIDA) (18). Combined use of FCS and FIDA allows simultaneous determination of the apparent molecular weight and the number of fluorescently labeled BAX monomers per protein-detergent micelle. Our results are consistent with previously established results in which BAX forms high molecular weight protein-detergent micelles with *n*-octyl glucoside (4) and show that BAX is present as a monomer in these complexes. In addition, we determined the apparent molecular weight and the number of BAX proteins bound per protein-detergent micelles formed by BAX and micelles of five additional detergents (dodecyl maltoside, Triton X-100, Tween 20, cholic acid, and CHAPS). Our data show that BAX is a monomer before, during, and after interaction with the micelles of all tested detergents.

II.3 | Results

Detergent-activated Fluorescently Labeled BAXΔC Can Release Cytochrome c *from Isolated Mitochondria*

For the FCS and FIDA experiments, we prepared recombinant, fluorescently labeled human BAXΔC containing a fluorophore at a single cysteine residue (Fig. II.1*A* & *B*). Human BAXΔC contains two indigenous cysteines (Cys-62 and Cys-126), which we considered inappropriate for fluorophore conjugation due to structural and functional reasons (8). Previously full-length BAX with G40C, C62A, and C126A mutations has been reported to be functional *in vivo* (3). Therefore, we removed cysteines, Cys-62 and Cys-126, by mutation to alanine and added an additional cysteine residue in place of glycine 40 creating BAXΔC(G40C) (Fig. II.1*A*). BAXΔC(G40C) labeled with Bodipy FL maleimide fluorophore became fluor-BAXΔC.

To check the biological activity of the fluor-BAXΔC protein, we studied its ability to release cytochrome *c* using mitochondria isolated from HeLa cells (Fig. II.1*C*). Our results show that fluor-BAXΔC activated with 2% (w/v) *n*-octyl glucoside releases cytochrome *c* from isolated mitochondria similar to BAXΔC but with slightly lower efficiency. For both proteins significant cytochrome *c* release required detergent activation, suggesting that the detergent activation of fluor-BAXΔC was comparable with the detergent activation of the BAXΔC (7, 12, 26). In each cytochrome *c* release experiment the final concentration of *n*-octyl glucoside was 0.005% (w/v) or lower, which is well below the CMC for this detergent (0.6% w/v) (11),

so that detergent micelles played no role in the release of cytochrome *c* or the maintenance of the active BAXΔC conformation during the assay.

Fig. II.1

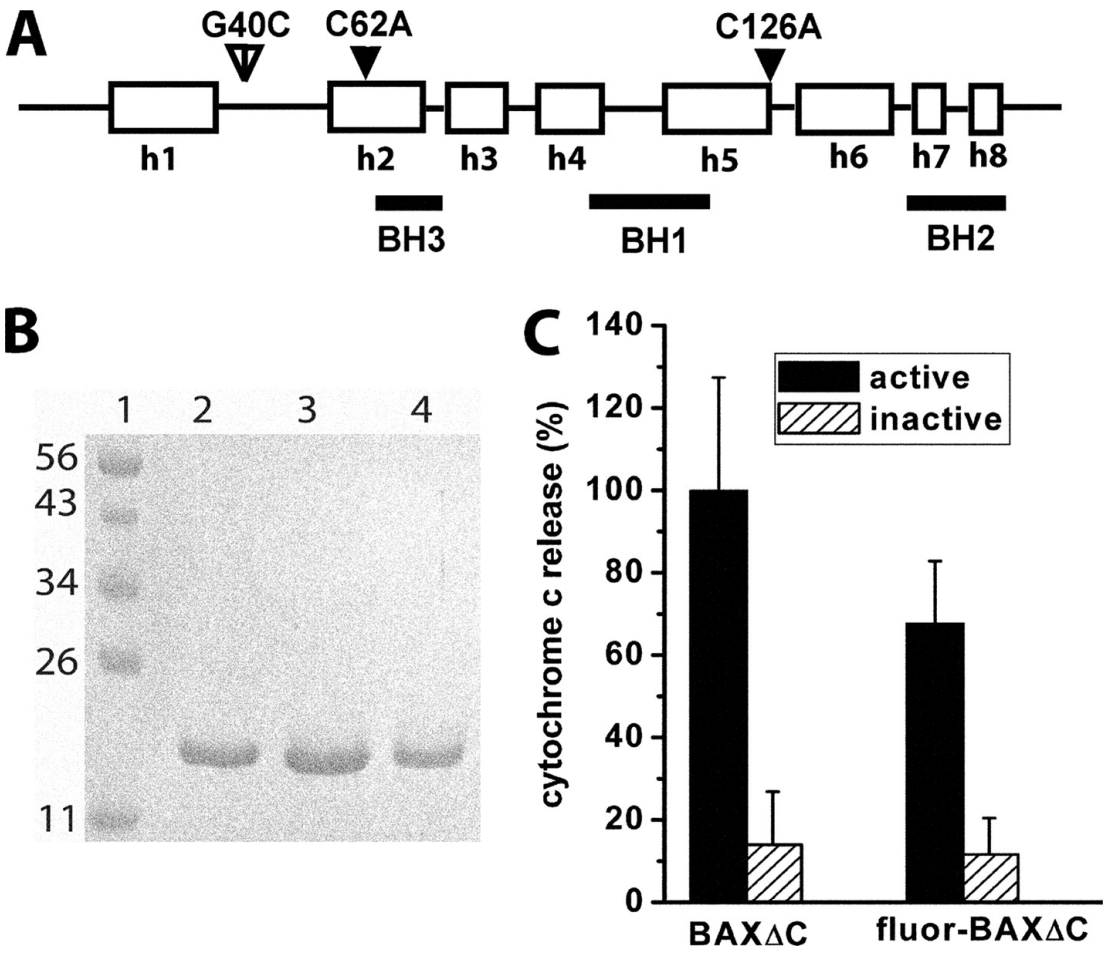

Fig. II.1 | *A,* schematic structure of human BAXΔC(G40C). Introduced mutations and their relative position with respect to the helices and BCL-2 homology domains are indicated with *arrows. B,* SDS-PAGE of purified recombinant proteins; protein standards with molecular weight indicated (*lane 1*), human BAXΔC(G40C) (*lane 2*), human BAXΔC (*lane 3*), and human fluor-BAXΔC (*lane 4*). *C,* cytochrome *c* release from mitochondria isolated from HeLa cells. Mitochondria isolated from HeLa cells were incubated for 20 min at 37 °C with 100 nM of the indicated recombinant protein. Where indicated, protein was activated by incubation with 2% (w/v) *n*-octyl glucoside for 1 h at 4°C after which the protein/detergent mixture was diluted to obtain a final detergent concentration of 0.5% (w/v) and the 100 nM protein concentration used in the assays. Cytochrome *c* content of each fraction was normalized for the basal release of cytochrome *c* in mitochondria samples with only detergent added and in mitochondria samples without detergent or protein added. *Error bars* were calculated based on three independent experiments.

Surface Plasmon Resonance Studies of Membrane Binding and Integration by BAXΔC and Fluor-BAXΔC

Direct analysis of the membrane binding and integration by detergent-activated fluor-BAXΔC was compared with that of BAXΔC using surface plasmon resonance (SPR) as described previously (22) (Fig. II.2). SPR has been applied to the study of membrane binding and integration of a number of pore-forming proteins and peptides (27, 28), including BAX (22). Using this technique it is not necessary to label or chemically modify the protein under study. Therefore, we could use this method to determine the effect of the mutations and the added fluorophore on fluor-BAXΔC membrane binding and integration by comparison with the same properties of BAXΔC.

These SPR experiments were done using cardiolipin-containing liposomes (DOPC:DOPA:cardiolipin 70:20:10 mol %) immobilized on the SPR-chip surface, and the proteins of interest were injected over this surface. Both BAXΔC and fluor-BAXΔC required *n*-octyl glucoside activation to generate significant interaction with liposome membranes (Fig. II.2, *A* and *B*).

To determine the concentration dependence of BAX integration into the liposome membranes, we sequentially injected increasing concentrations of BAX over the same liposome-covered surface and determined the amount of BAX integrated into the lipid membrane based on sensorgram response after 300 s of washing. Our results show that, when activated with *n*-octyl glucoside, fluor-BAXΔC and BAXΔC have comparable integration into the liposome membrane (Fig. II.2*C*). This similarity in membrane integration suggests that the slight

decrease in cytochrome *c* release by fluor-BAXΔC (Fig. II.1*C*) is not the result of reduced membrane retention of the labeled protein but possibly a result of reduced stability of the in-membrane open pore conformation. However, despite a possible reduction in the stability of fluor-BAXΔC pores, the cytochrome *c* release experiments (Fig. II.1*C*) together with the SPR binding data (Fig. II.2) suggest that both BAXΔC and fluor-BAXΔC, when activated with *n*-octyl glucoside, follow a similar mechanism of membrane interaction and pore formation.

Fig. II.2

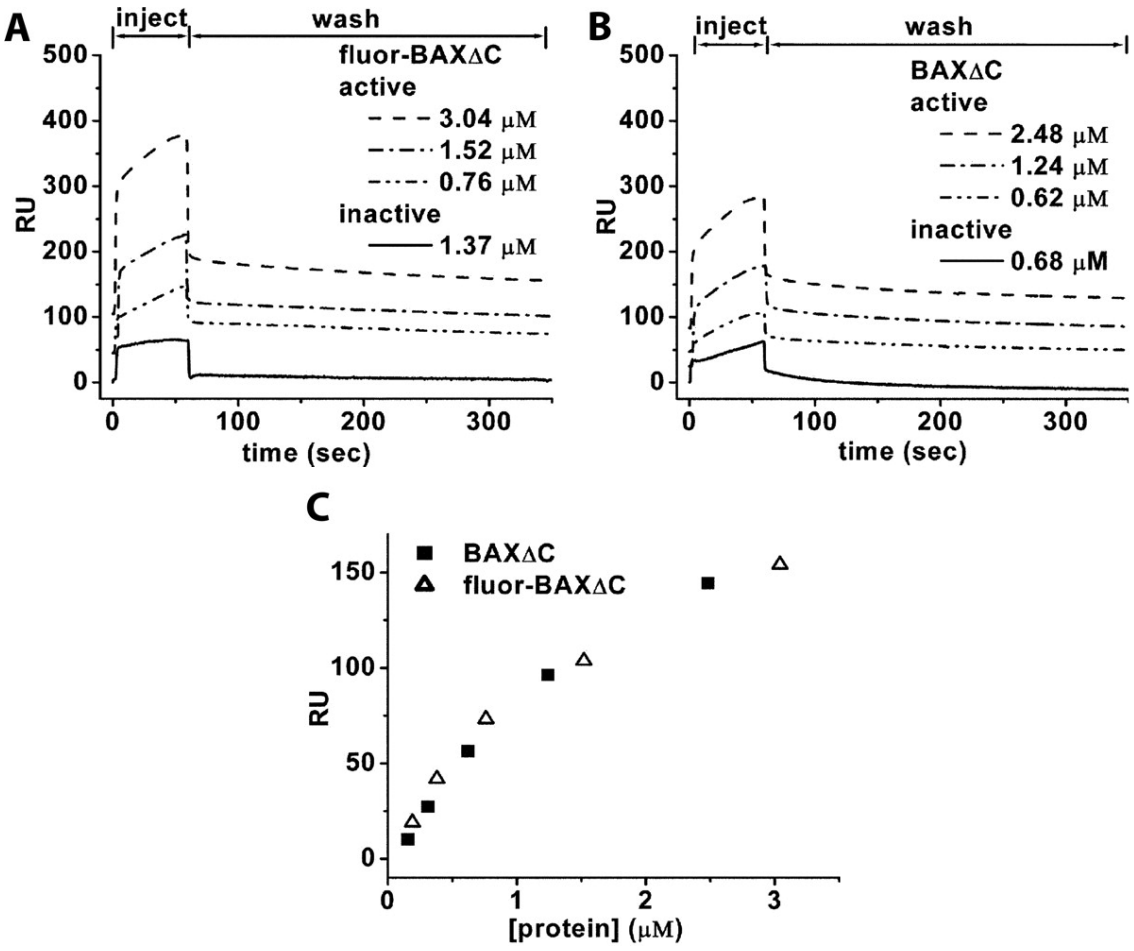

Fig. II.2 | **Surface plasmon resonance data of fluor-BAXΔC and BAXΔC binding to cardiolipin-containing liposomes (200 nm in diameter; DOPC:DOPA:CL 70:20:10 mol %).** Increasing concentrations of protein activated with 2% (w/v) *n*-octyl glucoside was flowed over immobilized liposomes. Protein accumulation on the surface of the liposomes is shown with response units (*RU*) (28). *A,* data for fluor-BAXΔC binding. *B,* data for BAXΔC binding. *C,* results of concentration dependence analysis of protein integration into liposomes for BAXΔC (*squares*) and fluor-BAXΔC (*triangles*).

Analytical Gel Filtration of BAXΔC(G40C) with n-Octyl Glucoside or CHAPS Present

To show that fluor-BAXΔC interacts with detergent micelles of *n*-octyl glucoside and CHAPS comparably with BAXΔC, we performed analytical gel filtration following the procedure of Antonsson *et al.* (7). We carried out our analytical gel filtration studies using BAXΔC(G40C) incubated with either 2% (w/v) *n*-octyl glucoside or CHAPS (Fig. II.3). The obtained results show that in the absence of detergents BAXΔC(G40C) eluted as a monomer with a molecular mass of slightly less than 25 kDa (Fig. II.3*A*), whereas in the presence of 2% (w/v) *n*-octyl glucoside, protein eluted at a molecular mass slightly below 440 kDa (Fig. II.3*C*). In contrast, when BAXΔC(G40C) was incubated with and eluted in the presence of 2% (w/v) CHAPS in the column, protein eluted mostly (73%) as a monomer in a broad peak (Fig. II.3*B*). These results are consistent with previously reported analytical gel filtration of BAXΔC (7) and show that mutant BAXΔC(G40C) interacts with micelles of *n*-octyl glucoside and CHAPS similarly as BAXΔC.

Fig. II.3

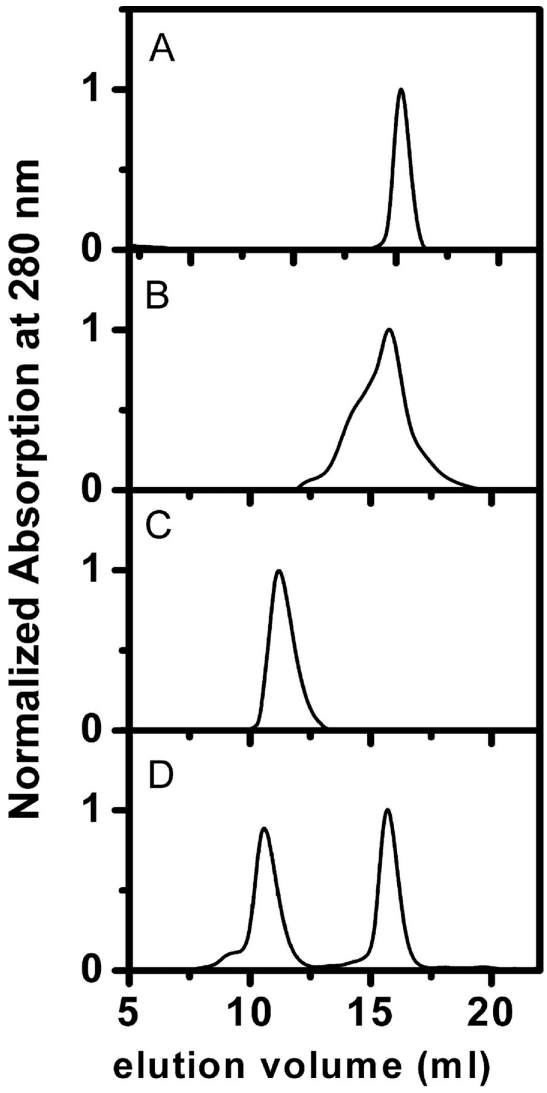

Fig. II.3 | **Analytical gel filtration of BAXΔC(G40C) incubated with indicated detergents.** BAXΔC(G40C) was incubated with 2% (w/v) of indicated detergent for 1 h at 4°C. BAXΔC(G40C) incubated with detergent was passed through a Superdex-200 column equilibrated with 10 mM HEPES/KOH, pH 7.0, 300 mM KCl buffer containing 2% (w/v) of the same detergent in which BAX was incubated. The Superdex-200 column was calibrated with two protein standards. *A,* BAXΔC(G40C) without detergents. *B,* BAXΔC(G40C) + 2% (w/v) CHAPS. *C,* BAXΔC(G40C) + 2% (w/v) *n*-octyl glucoside. *D,* standards (chymotrypsinogen, 25 kDa, and ferritin, 438.7 kDa).

Activation of BAX with Nonionic Detergents

Compared with the amount of protein required for the analytical gel filtration studies, the amount of fluor-BAXΔC required for the FCS and FIDA analyses is at least 100 times lower. Therefore, we decided to extend the range of the detergents used in our study. We chose *n*-octyl glucoside, CHAPS, Triton X-100, dodecyl maltoside, and Tween 20 because these detergents have specific and known effects on BAXΔC activity (7, 26). We also chose cholic acid because of its similarity in structure to CHAPS, because it is a physiologic detergent and because it can activate BAX (1). In all cases the 2% (w/v) concentration of the detergent was well above the CMC (11).

Before proceeding to the FCS and FIDA studies, we first tested the ability of all chosen detergents to activate BAXΔC using an assay of carboxyfluorescein release from liposomes (Fig. II.4*A*) (22). For these experiments we used recombinant human BAXΔC purified from E. coli cells without detergent. This BAXΔC protein was monomeric (23 ± 4 kDa as determined by dynamic light scattering) and had very low (<10%) carboxyfluorescein release activity. Upon 1 h of incubation at 4°C with selected nonionic detergents (*n*-octyl glucoside, dodecyl maltoside, Triton X-100, and Tween 20), BAXΔC released carboxyfluorescein from liposomes (Fig. II.4*A*), indicating that protein became activated. Incubation with cholic acid, an ionic detergent, also resulted in activation of BAXΔC. However, upon a similar 1-h incubation at 4°C with CHAPS (detergent known for its inability to activate BAX) no significant carboxyfluorescein release was observed.

Similar carboxyfluorescein release results were obtained for BAXΔC(G40C) incubated with all six detergents (Fig. II.4*B*). Comparison of the maximum carboxyfluorescein release values for both proteins after 90 min presents two instructive observations (Fig. II.4*C*). First, upon incubation with all detergents BAXΔC has almost a 20% higher carboxyfluorescein releasing activity than its mutant, BAXΔC(G40C). Second, for both proteins incubation with Triton X-100 resulted in the most activated form of BAX followed by *n*-octyl glucoside, dodecyl maltoside, cholic acid, and Tween 20, whereas CHAPS failed to activate either of the two proteins.

Fig. II.4

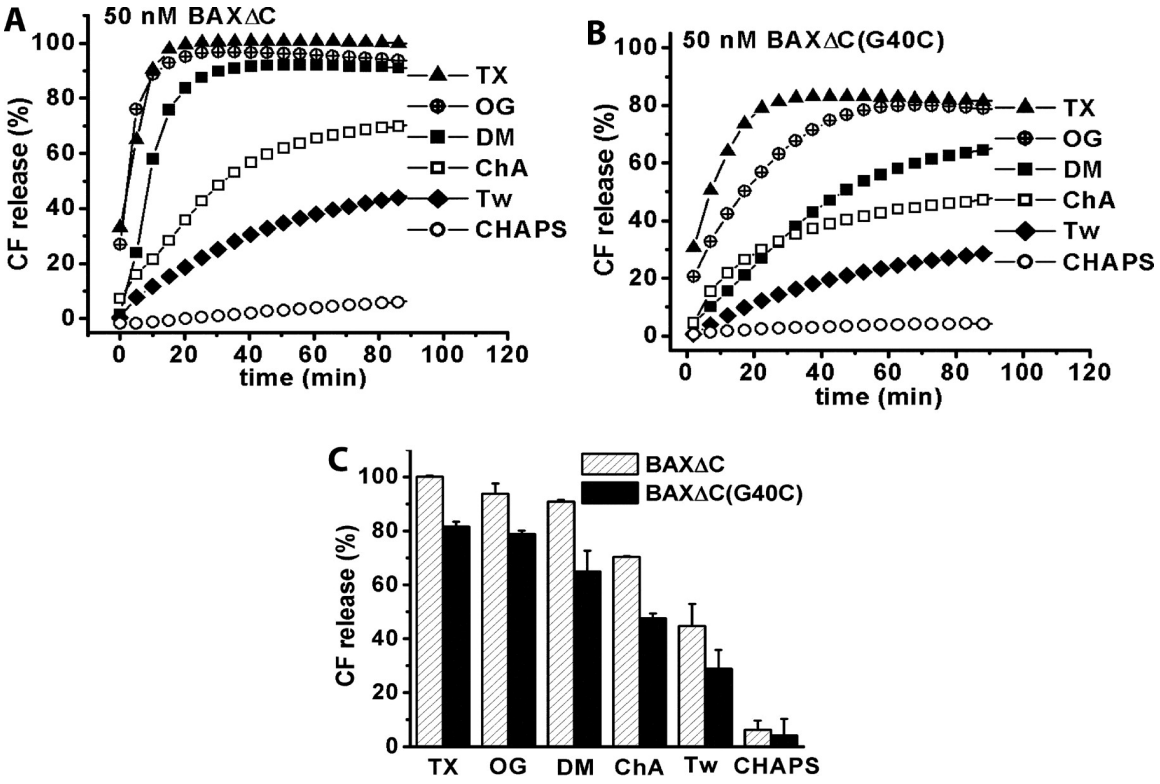

Fig. II.4 | **Release of CF from liposomes by the detergent-activated BAXΔC and BAXΔC(G40C).** *A,* monomeric inactive BAXΔC was incubated for 1 h at 4°C with 2% (w/v) *n*-octyl glucoside (*OG*), 0.6% (w/v) dodecyl maltoside (*DM*), 0.076% (w/v) Triton X-100 (*TX*), 0.038% (w/v) Tween 20 (*Tw*), 2% (w/v) CHAPS, or 2% (w/v) cholic acid (*ChA*). During this incubation the concentration of each detergent was above the CMC, whereas protein concentration was 70 µM. Before addition to liposomes protein was diluted to 50 nM. Total lipid mass in each assay was 17.5 µg. Liposomes composition was DOPC:DOPA 70:30 mol %. Final detergent concentration in the release assays was below the CMC for each detergent. Releases were normalized to carboxyfluorescein release by 20% Triton X-100 and corrected for basal carboxyfluorescein release by each detergent. Each release curve represents an average of at least three independent experiments. *B,* release of carboxyfluorescein from liposomes by detergent-activated BAXΔC(G40C). Protein was treated the same way as BAXΔC in *A. C,* single point comparison of the carboxyfluorescein release values at 90 min for BAXΔC and BAXΔC(G40C) activated with indicated detergents. Representative *error bars* are shown for each release curve.

CD Spectroscopy on BAXΔC in Detergent Micelles

Circular dichroism measurements were performed to determine whether any significant secondary structure changes occur in BAXΔC during interaction with detergent micelles. BAXΔC without detergent produced CD spectra with strong α-helical pattern (Fig. II.5). In the presence of micelles of Triton X-100, Tween 20, or cholic acid, no significant changes in the BAXΔC spectra were observed. However, in the presence of micelles of *n*-octyl glucoside or dodecyl maltoside, a slight increase in the α-helical content of BAXΔC CD spectra was observed. The CD spectra of BAXΔC in the presence of CHAPS were not collected because of high CD signal from CHAPS (because of presence of amide bond in CHAPS structure).

Fig. II.5

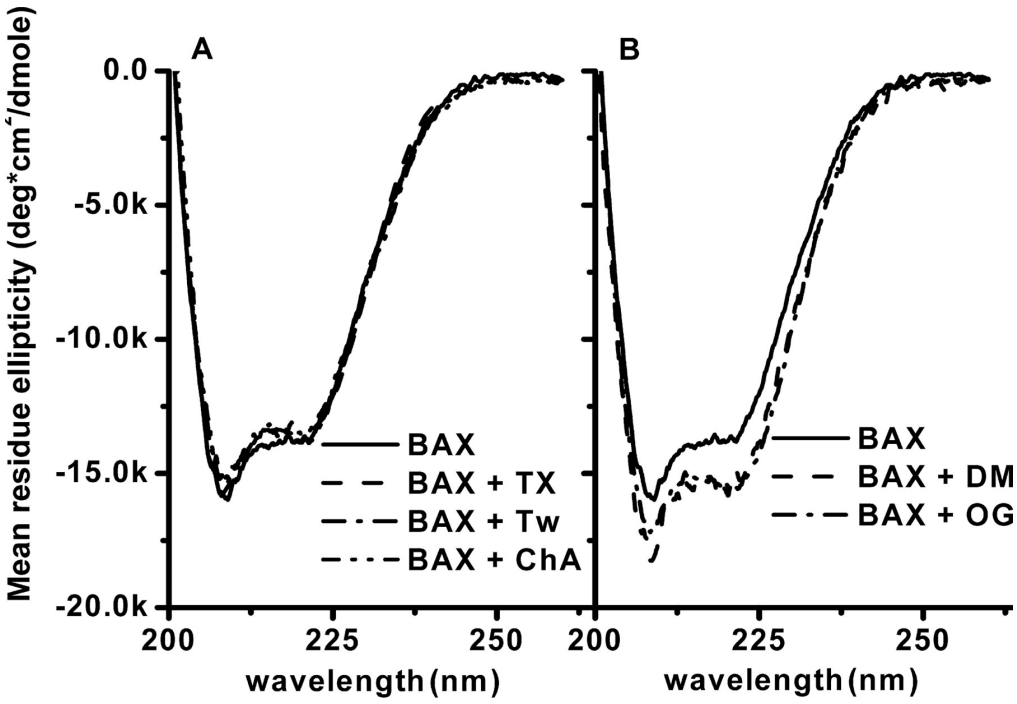

Fig. II.5 | **CD spectroscopy of BAXΔC in the presence of detergent micelles in 10 mM HEPES, pH 7.0, 100 mM KCl.** *A,* comparison of the CD spectra for BAXΔC alone and in the presence of either 0.08% Triton X-100 (*TX*), 0.04% Tween 20 (*Tw*), or 2% cholic acid (*ChA*). *B,* comparison of the CD spectra for BAXΔC alone and in the presence of either 2% *n*-octyl glucoside (*OG*) or 0.6% dodecyl maltoside (*DM*).

FCS Detection Volume Is Not Affected by the Presence of Detergents

The maintenance of consistent detection volume is critical for accurate comparison of FCS characteristics of different particles. Size and shape of the FCS detection volume depend on a number of parameters, one of which is the refractive index of solution (29, 30). The latter can be affected by the presence of detergents leading to the distortion of the FCS detection volume.

Commonly AlexaFluor 488 dye is used for calibration of the FCS detection volume (30, 31). During this calibration procedure the diffusion time (τ_D) of the dye molecules and the structure parameter of the FCS detection volume (ω) were obtained by fitting the measured autocorrelation curve using Equation 1. Using such analysis for AlexaFluor 488 diffusing freely in solution in the absence of detergent, we get the following values: τ_D 22.7 ± 0.9 μs, ω = 5.5 ± 0.8. To determine whether the presence of detergent has an effect on our FCS measurements, we determined τ_D and ω values for AlexaFluor 488 in solution containing increasing concentrations of *n*-octyl glucoside detergent (Fig. II.6). The results of these experiments show that over the range of 0–5% (w/v) of *n*-octyl glucoside, the diffusion time of the dye and the structure parameter of the detection volume do not change indicating that the FCS detection volume is not affected by the detergent presence. Similar experiments were done with the rest of the detergents, and they yielded analogous results (data not shown).

Fig. II.6

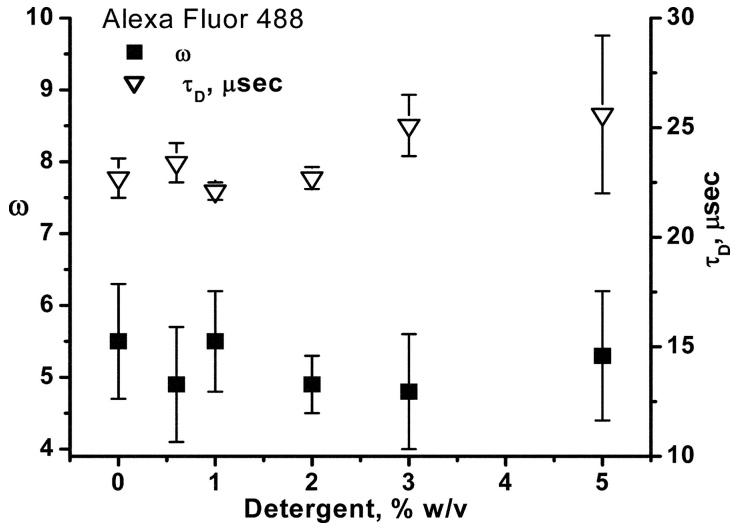

Fig. II.6 | **Effect of detergent on the shape and size of the FCS detection volume.** Measurement of the diffusion time (τ_D) of AlexaFluor 488 and the structure parameter of the detection volume (ω) at various detergent concentrations. *n*-Octyl glucoside was used as a detergent of choice, whereas buffer composition was 10 mM HEPES, pH 7.2, 100 mM KCl. *Error bars* were calculated based on nine 10-s measurements. For some data points *error bars* are smaller than the symbol.

FCS Characterization of Fluor-BAXΔC in Detergent Micelles

We used fluorescence correlation spectroscopy to confirm the detergent-dependent change in the apparent molecular weight of BAXΔC protein as seen by analytical gel filtration. The diffusion characteristics of fluor-BAXΔC were studied in the absence and in the presence of 2% (w/v) of selected detergents (Fig. II.7 and Table II.1). The FCS diffusion times were obtained by fitting the autocorrelation curves (Fig. II.7) and are shown in Table II.1. Fluor-BAXΔC incubated with 2% (w/v) of either *n*-octyl glucoside, dodecyl maltoside, Triton X-100, or Tween 20 had a significant increase in diffusion time, τ_D, compared with the diffusion time of fluor-BAXΔC monomer in the absence of detergent. In contrast, the diffusion time of fluor-BAXΔC in the presence of 2% (w/v) CHAPS or cholic acid did not increase significantly (Table II.1).

Fig. II.7

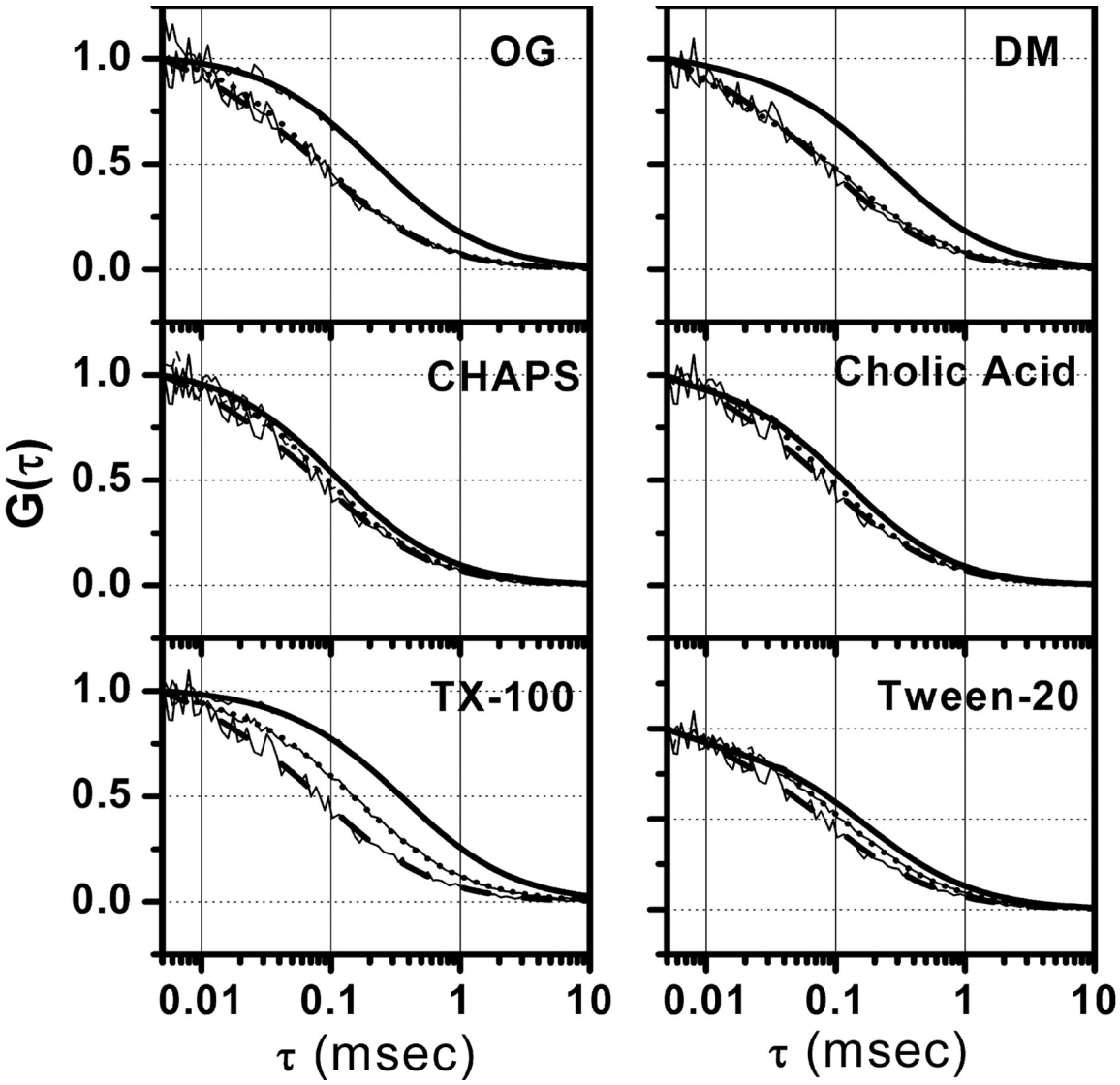

Fig. II.7 | **Normalized FCS autocorrelation curves of fluor-BAXΔC incubated with various detergents, as indicated (*OG*, *n*-octyl glucoside; *DM*, dodecyl maltoside; *TX-100*, Triton X-100).** For each autocorrelation experiment, protein was incubated in 10 mM HEPES/KOH, pH 7.2, 100 mM KCl, with 2% (w/v) of the indicated detergent at 4 °C for 1 h. In each *graph* the normalized autocorrelation curve for fluor-BAXΔC in the absence of detergent (*dashed line*), normalized autocorrelation curve for fluor-BAXΔC incubated with 2% (w/v) of the indicated detergent (*solid line*), and normalized autocorrelation curve for fluor-BAXΔC after detergent was diluted to the concentration below its CMC (*dotted line*). Raw data for each autocorrelation curve are shown with *thin jagged line*. See Table II.1 for the numerical results of the analysis of these autocorrelation curves.

Table II.1 | **Results of the FCS studies with fluor-BAXΔC-detergent micelles**

The molecular weight of the fluor-BAXΔC-detergent micelles was calculated using Equation 6.

Fluor-BAXΔC	[Detergent] 2% (w/v)		After Detergent Dilution		
+	τ_D	Mol. mass	[Detergent] (w/v)	τ_D	Mol. Mass
	μs	*kDa*	*%*	*μs*	*kDa*
No detergent	91±4		0	91±4	
n-Octyl Glucoside	223±5	280±12	0.003	100±5	25±1
Triton X-100	366±8	1236±223	0.003	158±4	99±2
Dodecyl Maltoside	262±21	453±31	0.003	90±4	18±1
CHAPS	115±4	38±1	0.004	87±3	17±1
Cholic acid	124±5	48±1	0.003	86±2	17±1
Tween-20	161±12	105±2	0.003	112±3	35±1

Using Equation 6 and the diffusion time of the fluorescent particles, we calculated the apparent molecular weight of the BAXΔC-detergent micelle complexes for each detergent (Table II.1). The apparent molecular weight of fluor-BAXΔC in the presence of *n*-octyl glucoside and CHAPS calculated from the FCS data are the same as the molecular weight obtained by analytical gel filtration of BAX in the presence of these detergents (Fig. II.3). The large molecular weight complexes of BAX generated in the presence of *n*-octyl glucoside, dodecyl maltoside, and Triton X-100 detergents were significantly larger than the sum of BAX and micelle of the respective detergents.

To determine the size of fluor-BAXΔC after interaction with detergent micelles, we removed micelles by diluting detergent concentration below CMC. In most cases this resulted in dissociation of the protein-detergent micelles as well as of the detergent micelles in solution. Each measurement of fluor-BAXΔC size after detergent dilution was done at least 1 h after dilution to allow dissociation of the detergent micelles bound to the protein. In all cases the diffusion time of fluor-BAXΔC decreased significantly upon detergent dilution (Table II.1 and Fig. II.7). For all detergents, except Triton X-100, the diffusion time decreased close to that of fluor-BAXΔC monomer. These observations indicate that upon detergent dilution the molecular weight of the protein-detergent micelle complexes is reduced, and for most of the detergents this molecular weight is reduced to that of a fluor-BAXΔC monomer. In addition, it should be mentioned that *n*-octyl glucoside-treated fluor-BAXΔC used in the FCS dilution experiments was used with similar dilution as in the cytochrome *c* release experiments (Fig. II.1*C*).

Fluorescence Intensity Distribution Analysis of Fluor-BAXΔC in Detergent Micelles

Analysis of the distribution of the photon counts in the FCS data sets was used to determine the number of fluor-BAXΔC molecules per protein-detergent micelle formed with micelles of all tested detergents. This analysis used the FIDA algorithm developed by Kask *et al.* (18). Using FIDA we determined fluorescence brightness of BAX molecules before, during, and after interaction with detergent micelles. Comparison of these fluorescence brightness values shows that BAX is a monomer in all cases (Table II.2). However, in case of dodecyl maltoside and Triton X-100, the calculated values of fluorescence brightness per protein-detergent micelle were 90% higher than the fluorescence brightness of the fluor-BAXΔC monomer. It is possible that BAX is dimerized in micelles of these detergents. Interestingly, in the presence of cholic acid or Tween 20 protein fluorescence brightness decreased by 36 and 15%, respectively, whereas in the presence of the rest of the detergents protein fluorescence brightness increased or stayed the same as in the absence of detergents. Therefore, because protein fluorescence brightness was clearly affected by the detergent we studied this effect directly.

Table II.2 | **Analysis of the fluorescence-intensity distribution of the fluor-BAXΔC protein detergent-micelle complexes**

Protein (at the concentration indicated in the table) was preincubated with detergent for 1 h at 4°C. Upon incubation with detergent, the protein was diluted below 0.5 µM into a solution containing the identical detergent concentration as during activation. The measurements were done immediately upon this dilution. Mean and standard deviations of the brightness values were calculated based on nine measurements at 50 s each.

Fluor-BAXΔC +	[Detergent] 2% (w/v)		After Detergent Dilution	
	Fluorescence Brightness **25 µM** BAX	Fluorescence Brightness **3 µM** BAX	[Detergent] (w/v)	Fluorescence Brightness
	kHz	*kHz*	*%*	*kHz*
No detergent			0	5.5±0.1
n-Octyl Glucoside	7.4±0.2	7.2±0.3	0.003	4.7±0.2
Triton X-100	10.5±0.1	10.4±0.1	0.003	7.1±0.1
Dodecyl Maltoside	8.5±0.1	10±0.1	0.003	5.0±0.1
CHAPS	5.9±0.1	5.8±0.1	0.004	5.6±0.1
Cholic acid	3.49±0.06		0.003	4.71±0.09
Tween-20	4.70±0.24		0.003	5.41±0.06

For three detergents where micelle size was significantly increased by the addition of BAX (*n*-octyl glucoside, dodecyl maltoside, and Triton X-100), we varied the degree of protein to detergent ratio while holding either detergent or protein concentration constant. First, we varied the concentration of the fluor-BAXΔC from 25 to 3 μM while keeping detergent concentration constant at 2% (w/v). We reasoned that, if fluor-BAXΔC forms oligomers in micelles, the decrease in protein concentration while keeping detergent concentration constant would lead to a change, *e.g.* reduction, of the oligomeric state of protein in detergent micelles. Such change in the oligomeric state of protein with increasing detergent concentration has been previously demonstrated for some transmembrane peptides in detergent micelles (32). In this case there was no significant change in the fluorescence brightness of the fluor-BAXΔC-detergent micelles (Table II.2).

Second, we measured the effect of increasing detergent concentration on the fluorescence brightness of fluor-BAXΔC at constant protein concentration. If protein fluorescence brightness increases because of the presence of detergent, then the total fluorescence intensity of the sample containing constant protein concentration will increase with increasing detergent concentration. As shown in Fig. II.8*A* (*empty circles*), for constant protein concentration in the presence of increasing *n*-octyl glucoside concentrations total fluorescence intensity increases. Furthermore, fluorescence brightness per particle of protein-detergent micelles determined by single-component fitting of resulting FCS autocorrelation curves also increased (Fig. II.8*A, filled squares*). The ratio of the total fluorescence intensity to the fluorescence brightness per particle (also known as cpp) represents the average number of

particles in the FCS observation volume. As expected, this number stayed constant for all *n*-octyl glucoside concentrations clearly showing that increase in *n*-octyl glucoside concentration leads to increase in protein fluorescence brightness. For *n*-octyl glucoside the FCS and FIDA yield similar protein fluorescence brightness values (Table II.2 and Fig. II.8). Such an agreement between FCS and FIDA results further shows that fluor-BAXΔC is present as a monomer in *n*-octyl glucoside micelles.

Analogous detergent titration experiments were performed for the rest of the detergents giving the same result that protein fluorescence brightness of the fluor-BAXΔC is changing with increasing concentrations of detergent (Fig. II.8*C*). In addition, in the *n*-octyl glucoside titration experiment gradual increase in the protein diffusion time was observed together with increase in protein fluorescence brightness. This observation suggests that with increasing *n*-octyl glucoside concentration protein-detergent micelles grow in size (Fig. II.8*B*).

For all tested detergents after micelle removal by dilution, the fluorescence brightness of the fluor-BAXΔC returned to that of a protein monomer. However, upon removal of Triton X-100 protein fluorescence brightness decreased but was still 29% higher than that for the protein monomer in the absence of the detergent. This result suggests incomplete dissociation of the Triton X-100 molecules from BAX and is in accordance with the FCS diffusion time, which shows that upon Triton X-100 dilution below CMC, the apparent molecular weight of the fluor-BAXΔC was higher than that of a protein monomer.

Fig. II.8

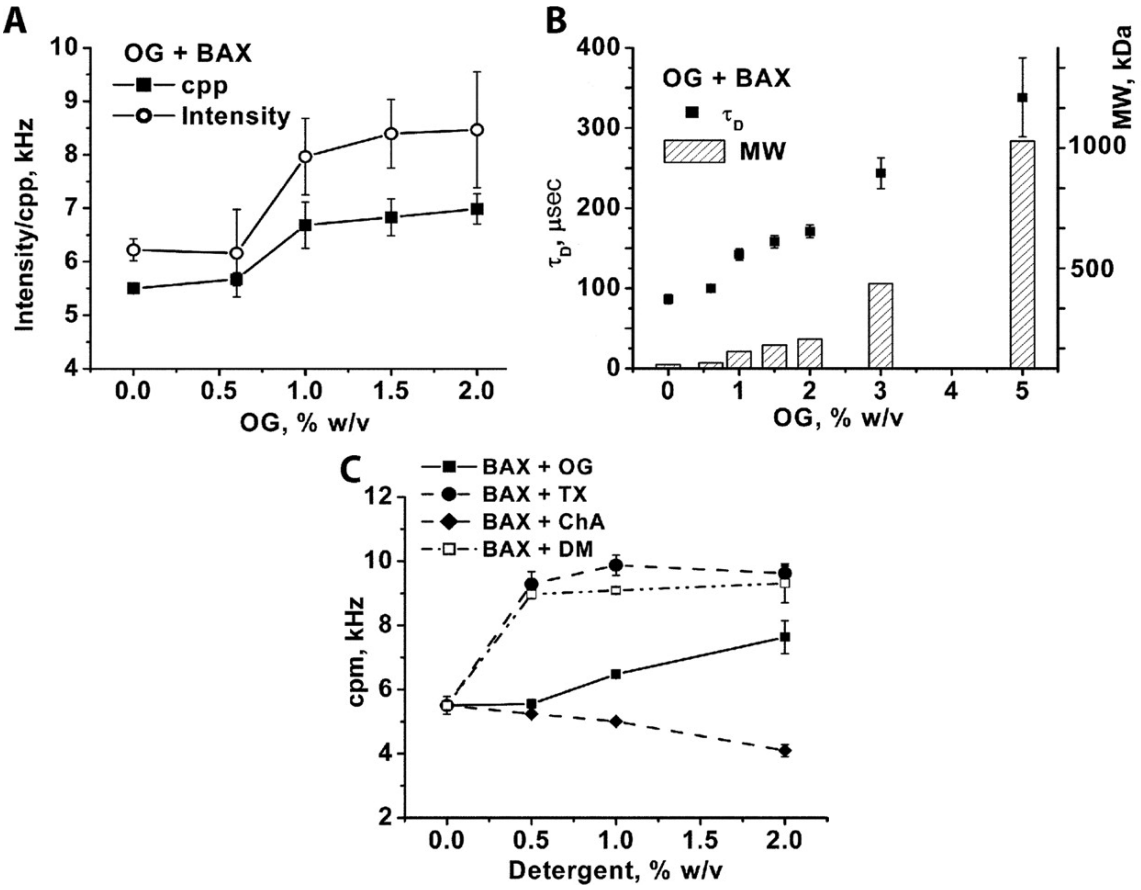

Fig. II.8 | **Enhancement of the fluor-BAXΔC fluorescence intensity upon interaction with detergents.** *A,* constant concentration (3 µM) of fluor-BAXΔC was incubated with increasing concentrations of *n*-octyl glucoside (*OG*) for 1 h at 4°C. The fluorescence intensity of the protein samples incubated with detergent was measured using ConFocor 3 (Zeiss, Germany). For each measurement the protein incubated with detergent was diluted to a final concentration of 24 nM in EB buffer containing the same detergent concentration as in the protein sample. All measurements were done at 22°C. cpp values were determined using the single-component fit of the FCS autocorrelation curves. *B,* increase in the apparent molecular weight (*MW*) of BAXΔC upon interaction with micelles of *n*-octyl glucoside. Molecular weight values were calculated using Equation 6. *C,* change in the cpp value of fluor-BAXΔC with increasing detergent concentration. Samples were prepared, and measurements were done similar to the Fig. II.6*A*. Detergent abbreviations are similar to Fig. II.5.

FCCS Analysis of BAXΔC in Detergent Micelles

To show the absence of BAX oligomerization in detergent micelles, FCCS analysis was used. FCCS is a variation of the FCS that allows determination of the degree of interaction between two fluorescent molecules or macromolecular assemblies. In these experiments we used two types of fluorescently labeled BAX as follows: fluor-BAXΔC and Bodipy 630/650 maleimide-BAXΔC. The degree of interaction between these two proteins in detergent micelles is proportional to the cross-correlation value that is determined by FCCS analysis. The results of these FCCS experiments show low cross-correlation values between two fluorescent forms of BAXΔC compared with the theoretically predicted cross-correlation value of BAXΔC dimer. These FCCS results suggest the absence of interaction between the two fluorescent variants of BAXΔC in detergent micelles of all tested detergents (Fig. II.9).

Fig. II.9

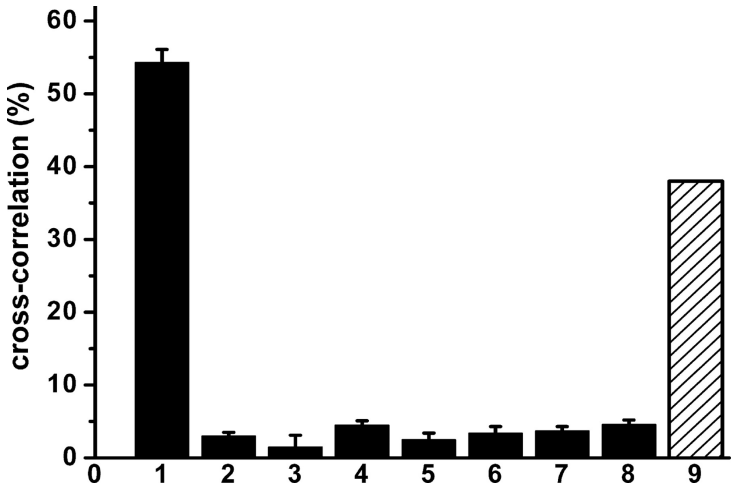

Fig. II.9 | **Results of the FCCS experiments with fluor-BAXΔC (50% labeled) and Bodipy 630/650 maleimide-BAXΔC (80% labeled) in the presence of the indicated detergents.** *Lane 1,* cross-correlation standard (double-stranded RNA with AlexaFluor 488, Cy5 labels); *lane 2,* no detergent present; *lane 3,* +2% *n*-octyl glucoside; *lane* 4, +2% Triton X-100; *lane 5,* + 2% CHAPS; *lane 6,* + 2% cholic acid; *lane 7,* + 2% Tween 20; *lane 8,* + 2% dodecyl maltoside; *lane 9,* maximum expected cross-correlation value for a formation of protein dimer from a mix of 50 and 80% labeled protein. Experiments were done in 10 mM HEPES, pH 7.2, 100 mM KCl buffer at 22 °C. All detergent concentrations are given in % of w/v.

II.4 | Discussion

Fluorescently Labeled BAXΔC Is Active

To apply FCS to the study of BAX, we generated a soluble form of the protein. We employed the BAXΔC in these solution studies of the protein activity and oligomerization because we found that it remained in solution and could be activated by detergent throughout all the manipulations that were used in these studies. To label this protein with a fluorophore, we substituted endogenous cysteines with alanine (C62A and C126A) and converted glycine 40 in an unstructured region of BAX to a cysteine. The position of these changes in the BAXΔC protein are shown not to interfere with the function of the full-length BAX *in vivo* (3), and the resulting protein was well expressed by bacteria. The added cysteine was exposed in the engineered protein and formed disulfide cross-linked BAXΔC(G40C) dimers at high concentrations (data not shown). After substitution with the fluorescent probe, the disulfide formation did not occur. Therefore, further characterization of the activity of the engineered protein was performed on the fluor-BAXΔC.

To assess the functional capability of fluor-BAXΔC, we tested its ability to promote cytochrome *c* release from isolated mitochondria as compared with that of BAXΔC. Because our engineered BAXΔC was based upon the human protein, we used mitochondria isolated from HeLa cells to study cytochrome *c* release (33). In these experiments we observed that fluor-BAXΔC releases 71 ± 15% of the mitochondrial cytochrome *c* when activated with *n*-octyl glucoside, whereas BAXΔC releases 100 ± 30% (Fig. II.1). Based on this result we conclude that mutation and fluorophore labeling of BAXΔC alter pore forming activity of this

protein but only in a minor way. In addition, to these experiments, we also studied the ability of various detergents to activate BAXΔC and its mutant in liposomes (Fig. II.4). Again we saw a reduction in pore activation by the mutant protein. However, it is clear that the reduction is consistent across the range of tested detergents (Fig. II.4*C*). Finally, we compared the integration of BAXΔC and its mutant into lipid membranes using SPR. We have recently developed methods to quantitatively study binding and integration of BAX to membranes using SPR (22). In those studies protein integration into lipid membranes was critical for pore formation and only occurred after protein incubation with *n*-octyl glucoside. In the SPR comparison mutant of BAXΔC, BAXΔC(G40C) was fully functional and integrated into lipid membranes as well as BAXΔC (Fig. II.2). Taken together these studies indicate that BAXΔC(G40C) is fully functional, but its specific activity for pore formation is slightly lessened by the introduced mutations, possibly due to lower oligomerization rate or changed pore topology.

Fluor-BAXΔC Forms High Molecular Weight Protein-Detergent Micelles with Most Activating Detergents

BAXΔC has been shown to form high molecular weight complexes with *n*-octyl glucoside but not with CHAPS (7). To show that our mutated BAX, BAXΔC(G40C), can form high molecular weight complexes with *n*-octyl glucoside and not with CHAPS, we performed analytical gel filtration studies similar to those in Ref. 7. The results of these analytical gel filtration experiments show that in the presence of 2% (w/v) of *n*-octyl glucoside, BAXΔC(G40C) elutes at a molecular mass slightly below 440 kDa, whereas in the presence of

2% (w/v) CHAPS this protein elutes mostly as a monomer (73%). These results are similar to the previously published results for BAXΔC (7) indicating that mutations introduced into BAXΔC do not interfere with formation of high molecular weight complexes of this protein with *n*-octyl glucoside.

Next we proceeded to measure the molecular weight of fluor-BAXΔC in the presence of *n*-octyl glucoside and CHAPS using FCS. In the FCS experiments we measured the diffusion time, τ_D, of fluor-BAXΔC molecules in the presence of 2% (w/v) of these detergents. Then by using Equation 6, we calculated the molecular weight of the fluor-BAXΔC protein-detergent micelle complexes (Table II.1). The molecular weights of BAXΔC protein-detergent micelle complexes determined by FCS and analytical gel filtration were fairly similar, further demonstrating that mutagenesis and fluorescent labeling of BAXΔC do not affect the interactions of this protein with *n*-octyl glucoside and CHAPS. This result also shows that FCS can be used to determine the apparent molecular weight BAXΔC with other detergents. Therefore, we extended the range of detergents used in our study to dodecyl maltoside, Triton X-10, Tween 20, and cholic acid. As a result of these FCS studies, we determined that fluor-BAXΔC forms high molecular weight complexes in the presence of activating nonionic detergents (*n*-octyl glucoside, dodecyl maltoside, Triton X-100, and Tween 20). However, in the presence of cholic acid, activating ionic detergent, fluor-BAXΔC does not form high molecular weight complexes. Fluor-BAXΔC also did not form high molecular weight complexes with CHAPS, a zwitterionic detergent known for its inability to activate BAXΔC.

In addition, all of the tested activating detergents did not induce significant secondary structure changes in the BAXΔC protein (Fig. II.5).

For the studies of BAXΔC pore formation in lipid membranes, it is desirable that detergent is removed after BAXΔC activation because detergent at concentrations above the CMC can alter the integrity of lipid membranes. Therefore, it is important to know the molecular weight of BAXΔC after interaction with detergent micelles. To determine the latter, excess detergent was removed from fluor-BAXΔC by dilution below the CMC. After removal of detergent micelles, the molecular weight of fluor-BAXΔC decreased to that of the fluor-BAXΔC monomer for most of the detergents (Table II.1). The results for fluor-BAXΔC treated with Triton X-100 were an exception. Upon Triton X-100 dilution the molecular weight of fluor-BAXΔC was five times larger than that of fluor-BAXΔC monomer. There are two possible explanations for this result. The first explanation is based on incomplete dissociation of Triton X-100 molecules bound to fluor-BAXΔC upon detergent dilution, and the second explanation is possible formation of fluor-BAXΔC homo-oligomers. To differentiate between these two explanations and to determine the stoichiometry of fluor-BAXΔC before, during, and after interactions with detergent micelles we performed FIDA.

BAXΔC Is Present as a Monomer in Protein-Detergent Micelles

To further investigate the stoichiometry of the fluor-BAXΔC-detergent micelles, we performed FIDA on the FCS data (Table II.2). The fluorescence brightness of the individual protein-detergent micelles varied ~90% as a function of the detergent used, but all of them contained one BAX protein molecule. The reason for such variation of the fluorescence

brightness of the protein monomer in various detergents was because of the enhancement or quenching of the Bodipy FL fluorophore brightness upon transfer into the hydrophobic environment of a detergent micelle. Similar effects of the fluorophore brightness enhancement were reported previously for the fluorescently labeled diphtheria toxin T-domain interacting with detergent micelles (34). In our case there appears to be an enhancement of the fluorescence brightness of fluor-BAXΔC in the presence of *n*-octyl glucoside, dodecyl maltoside, and Triton X-100 detergents, and a decrease in protein fluorescence brightness in the presence of cholic acid and Tween 20. Studies of detergent titration into constant protein concentration show that this effect is because of the enhancement of the fluorophore brightness and not because of protein oligomerization (Fig. II.8). In addition, detergent dilution studies show that upon detergent dilution, which leads to the dissolution of the fluor-BAXΔC-detergent micelles, the fluorophore brightness of the protein returns to that of the protein monomer prior to the interaction with detergent micelles (Table II.2).

The FIDA results mean clearly that before, during, and after interaction with detergent micelles the fluor-BAXΔC protein is a monomer. This observation suggests that BAXΔC interaction with micelles is fundamentally different from the interaction that it establishes in bilayer membranes. In a bilayer membrane BAXΔC assumes conformation, which allows assembly of homo-oligomers resulting in pore formation. In contrast, in a detergent micelle BAXΔC assumes conformation that in the case of nonionic detergents leads to a dramatic enlargement of the resulting protein-detergent micelle without necessary protein homo-oligomerization (Table II.1 and Fig. II.3). Because this increase in size can no longer be

attributed to additional BAX molecules per micelle, it must be due to the incorporation of additional detergent.

To study the interaction of the fluor-BAXΔC with detergent micelles, we used detergents at 2% (w/v) concentration, which is well above the CMC for all tested detergents. If expressed in molar units, this detergent concentration will be on the order of millimolars for all tested detergents (*n*-octyl glucoside, 68 mM; Triton X-100, 32 mM; CHAPS, 33 mM; dodecyl maltoside, 40 mM). In contrast, in all of the experiments the concentration of fluor-BAXΔC during incubation with detergent was 20–30 μM. Solution containing 20–30 μM protein and >30 mM detergent has an excess of detergent micelles over the number of protein molecules. Fleming (32) has shown that an excess of detergent micelles moves the protein to a more dissociated state. Fleming (32) also shows that for a glycophorin A transmembrane α-helix, 40% of dimers of this α -helix are detected for a 40 times lower mole ratio of protein to detergent than was used in our experiments. This demonstrates that if fluor-BAXΔC is forming oligomers in detergent micelles, then we would not have been prevented from detecting them. The above outlined argument together with the FCCS results (Fig. II.9) led us to the conclusion that fluor-BAXΔC is present as a monomer in detergent micelles.

The outcome of this conclusion is that during and after detergent activation BAXΔC is a monomer. Therefore, this protein has two stable monomeric conformations in physiological buffer conditions, one inactive and one active. Second, this implies that the detergent-activated species of BAX is a monomeric protein, and the large molecular weight in the presence of the micelles of nonionic detergents is a result of the detergent component of the complex.

Consequences for the Physiological Activation of BAX

These studies suggest that detergent activation of BAX is not merely a mimicry of the physiologic BAX activation. The characteristics of the detergent activation indicate two intriguing characteristics that may concern *in vivo* activation of BAX. First, because BAX remains active after we effectively remove the detergent substrate upon which it has activated, there must be two stable conformations of monomeric solution BAX, one active and the other inactive. Because this activation requires a large template and is distinct from the oligomer-competent conformation, which BAX assumes in membranes, we can consider the possibility that BAX is activated as a soluble protein and then integrates into the membrane. Second, the existence of a soluble active form of BAX suggests that this process can be reversed, which is a potential therapeutic approach.

II.5 | Conclusion

In this work we studied in detail the process of BAXΔC activation by nonionic detergents. Based on the results of our study we conclude that BAXΔC is a monomer before, during, and after interaction with detergent micelles. In this study we used fluorescently labeled analogue of BAXΔC in combination with two single-molecule sensitivity techniques (FCS and FIDA). Because the determination of the oligomeric state of proteins in detergent micelles is important for structural and functional studies of integral membrane proteins (35, 36), we are hopeful that the method presented here can be used for other proteins.

II.6 | Experimental Procedures

All chemicals used in this paper were from Sigma, unless otherwise stated. All lipids were obtained from Avanti Polar Lipids. Fluorescent dyes for protein labeling were purchased from Molecular Probes.

Protein Constructs, Protein Purification, and Protein Labeling

The cDNA for human BAX with 19-amino acid truncation on the C terminus (BAXΔC) was fused to the C-terminal intein/chitin-binding domain of the pTYB1 vector (New England Biolabs) (8). Three mutations (G40C, C62A, and C126A) were introduced into each of the DNA plasmids using a QuikChange mutagenesis kit (Stratagene), and the presence of mutations was confirmed by sequencing. The resulting construct and purified protein were dubbed as BAXΔC(G40C). All proteins (human BAXΔC and human BAXΔC(G40C)) were purified from BL21(DE3) Escherichia coli cells without detergent. Briefly, bacterial cultures were grown at 37°C in Terrific Broth (19) to an A_{600} of 1.5–2.0, and then the cultures were induced with 0.1 mM isopropyl 1-thio-β-d-galactopyranoside (Research Products International. Corp., Mt. Prospect, IL), and the temperature was dropped to 25 °C. After 12–15 h, bacteria were collected via centrifugation; the resulting pellet was resuspended in lysis buffer (phosphate-buffered saline, pH 7.2, 1 mM EDTA, 0.25 mM phenylmethylsulfonyl fluoride), and cells were broken by four passages through a Microfluidizer (Microfluidics) at 1000 bar. Lysate was clarified by centrifugation, and the supernatant containing BAX was incubated with chitin affinity resin (New England Biolabs) overnight at 4°C on a rocker. Resin was subjected to a high salt wash and then equilibrated in

cleavage buffer (10 mM HEPES/NaOH, pH 8.0, 100 mM NaCl, 50 mM dithiothreitol) and incubated for 48 h at 4°C. The purity of the proteins were assessed by SDS-PAGE. BAXΔC(G40C) was labeled with Bodipy FL c_5-maleimide (Molecular Probes) according to the manufacturer's protocol. Labeled protein was separated from the free dye using a Sephadex G-25 column. The degree of protein labeling was determined using a NanoDrop spectrophotometer (Thermo Scientific) by measuring absorbance at 280 nm (for protein concentration) and 504 nm (for Bodipy FL concentration). Resulting protein was ~ 80% labeled and was stored in EB buffer (10 mM HEPES/KOH, pH 7.2, 100 mM KCl) at 4°C.

Incubation of BAX with Detergent Micelles

Prior to FCS studies and cytochrome *c* and carboxyfluorescein release experiments, fluorescently labeled BAXΔC(G40C) or BAXΔC (20–30 μM) was incubated with 2% (w/v) of the indicated detergent in EB buffer for 1 h at 4 °C. For FCS studies of the fluor-BAXΔC in detergent micelles, after incubation with detergent, protein was diluted to a concentration below 0.5 μM in a solution containing the same detergent concentration as the activated protein. This dilution was done to ensure that the fluorescent signal emitted by the protein sample is within the dynamic range of the detector in the ConFocor 3 (Zeiss, Germany). To remove detergent micelles for the cytochrome *c* release and for the FCS studies of post-micelle-activated fluor-BAXΔC, the BAX/detergent mixture was diluted below the CMC of each particular detergent. The disappearance of micelles occurred at different rates (<1 min for OG and longer but <60 min for Triton X-100) but was allowed to finish before further studies on the sample (cytochrome *c* release or FCS) proceeded.

Cytochrome c Release Assay

Mitochondria from HeLa cells were isolated using a previously published procedure (20). Isolated mitochondria were resuspended in 10 mM HEPES/KOH, pH 7.4, 100 mM KCl, 1 mM EGTA, 200 mM sucrose. For the cytochrome *c* release assay isolated mitochondria were incubated with 100 nM of protein that was detergent-activated but micelle-diluted as described above or inactive protein at 37°C for 20 min. After the incubation with BAX protein or detergent control solutions, mitochondria were spun down at 10,000 × *g* for 10 min at 4°C and then pellet and supernatant fractions were collected and stored at −20°C. For the cytochrome *c* release assay we used 0.5 μg of mitochondria in a 30 μl volume. Protein concentration in the preparation of isolated mitochondria was determined by protein assay (Bio-Rad). Cytochrome *c* content in the pellet and supernatant fractions was determined using TiterZyme EAI human cytochrome *c* enzyme immunometric assay kit (Assay Designs) in combination with Synergy HT plate reader (Bio-Tek Instruments, Inc.).

Surface Plasmon Resonance Studies of BAX Binding to Liposomes

These studies were done using Biacore X instrument (GE Healthcare) at an ambient temperature of 25°C. Liposomes with lipid composition of DOPC:DOPA:bovine heart cardiolipin (70:20:10 mol %) were prepared using the reverse-phase evaporation method (21) following the procedure described in detail in Ref. 22. The buffer was EB unless otherwise noted. The rest of the experimental conditions, experimental protocol, and data analysis were the same as described previously (22).

Analytical Gel Filtration

Analytical gel filtration experiments were performed on a Superdex 200 HR 10/30 column (GE Healthcare) equilibrated with 20 mM HEPES/KOH, pH 7.5, 300 mM KCl, 0.2 mM dithiothreitol. In the corresponding samples, 2% (w/v) of the indicated detergent was included in the equilibration buffer. Prior to loading the sample on the column, 2.5 nmol of BAXΔC(G40C) were incubated in 2% (w/v) of the corresponding detergent for 1 h at 4°C. Then samples were loaded into the column and run at 0.5 ml/min. BAXΔC(G40C) elution was detected by light absorption at 280 nm.

Carboxyfluorescein Release Assay

Liposomes containing 50 mM carboxyfluorescein (CF) were prepared following the procedure described previously (22). Incubation with detergent protein was diluted into wells in a black bottom 96-well plate (NUNC, Denmark) using EB buffer. Liposomes (200 nm in diameter, DOPC:DOPA, 70:30 mol %) were added to the wells last. Immediately upon addition of liposomes, measurement of CF fluorescence was done using a Synergy HT plate reader (Bio-Tek Instruments, Inc.). CF releases for all protein samples containing detergent were corrected for the base-line CF release in the presence of detergents without protein. Data were analyzed in Origin 6.1 (OriginLab Corp.).

Circular Dichroism Spectroscopy

Samples for CD spectroscopy were prepared at 5 μM protein concentration in 10 mM potassium phosphate buffer, pH 7.0. Detergents (*n*-octyl glucoside (2% w/v), dodecyl maltoside (0.6% w/v), Triton X-100 (0.08%), Tween 20 (0.04% w/v), cholic acid (2% w/v))

were added to protein samples 1 h prior to measurements and stored at 4°C. Samples were measured at 20°C on Jasco J-715 spectropolarimeter using a 1-mm path length cell. Data were collected every 0.1 nm at 50 nm/min scan speed from 260 to 200 nm, and results were averaged from five scans. Because of high CD signal from Triton X-100 at 200 nm for samples containing this detergent, data were collected from 240 to 205 nm. Spectra for all protein samples containing detergent were corrected for the base line of detergents in the absence of protein.

FCS, FCCS, and FIDA Analyses, Instrumentation, and Measurements

LSM 510 ConFocor 3 system coupled with a Zeiss Axiovert 200 M inverted microscope (Zeiss, Germany) was used for FCS and FIDA experiments. A water immersion C-Apochromat ×40 objective (Zeiss, Germany) focused the excitation light to a diffraction-limited spot. The pinhole size was set to 70 μm for 488 nm excitation laser light. The excitation light of a 25-milliwatt 488 nm argon laser was set at 1% of the acousto-optical tunable transmission. Laser power in the sample was 7 microwatts. In front of the detector LP 530-nm filter was used. For the FCS and FIDA analyses, each sample was measured at least nine times for 50 s. The detection volume was previously calibrated with free Bodipy FL maleimide in solution (diffusion time 22.6 ± 0.5 μs, structure parameter 5.0 ± 0.4).

FCS Analysis

FCS measurements provide three characteristic parameters for interpretation as follows: τ_D, diffusion time of a fluorescent particle (*i.e.* the average time a particle spends in the detection volume); *N*, number of fluorescent particles in the detection volume, and the

counts/particle (cpp) or the average fluorescent intensity per particle. These parameters are extracted by performing a fit of FCS auto-correlation data to one component diffusion model as shown in Equation 1, which takes into account photophysical dynamics of fluorophores,

$$G(\tau) = \frac{1}{N} \cdot \left(1 + \frac{T \exp(-\tau/\tau_T)}{1-T}\right) \cdot \left(1 + \frac{\tau}{\tau_D}\right)^{-1} \cdot \frac{1}{\sqrt{1 + \tau/\omega^2\tau_D}} \quad \text{(Eq. 1)}$$

In this equation $G(\tau)$ is the auto-correlation function; τ is the lag time; T is the fraction of molecules in the triplet state; τ_T triplet decay time; ω is the structure parameter (aspect ratio) of the Gaussian detection volume. Fitting of the FCS auto-correlation curves was done using Equation 1 with software written in MATLAB (Mathworks) using a weighted nonlinear least squares fitting algorithm.

Calculation of Protein-Detergent Micelle Molecular Weight Based on FCS Diffusion Time

For a particle in solution the diffusion time is inversely proportional to the diffusion coefficient as shown in Equation 2,

$$\tau_D = \frac{\omega^2}{4D} \quad \text{(Eq. 2)}$$

In general, protein molecules diffusing in solution are assumed to approximate a spherical shape permitting the Einstein-Stokes relationship to be used in evaluating the diffusion constant as shown in Equation 3,

$$D = \frac{k_B T}{6\pi\eta R} \quad \text{(Eq. 3)}$$

where, k_B is the Boltzmann constant; T is temperature in degrees Kelvin; η is viscosity of solution in which particle is diffusing, and R is the radius of the spherical particle. The radius of

diffusing particle depends on the molecular weight of the particle ($R \propto (MW)$). Under these conditions a relationship can be established between the FCS diffusion time of a particle and its molecular weight as shown in Equations 4 and 5.

$$\tau_D = \frac{\omega^2}{4} \cdot \frac{6\pi\eta}{k_B T} \cdot R \qquad \text{(Eq. 4)}$$

$$\tau_D \propto \frac{\omega^2}{4} \cdot \frac{6\pi\eta}{k_B T} \cdot (MW)^{1/3} \qquad \text{(Eq. 5)}$$

In the case of BAXΔC, we know diffusion time of a BAXΔC monomer, $\tau_{D,\text{monomer}}$, and its molecular weight, MW_{monomer} = 19 kDa. We also know the diffusion time of BAXΔC protein-detergent micelle, $\tau_{D,\text{oligomer}}$. Using Equation 5 we can determine the apparent molecular weight of the BAXΔC protein-detergent micelle as shown in Equation 6.

$$MW_{\text{oligomer}} = MW_{\text{monomer}} \left(\frac{\tau_{\text{D,oligomer}}}{\tau_{\text{D,monomer}}} \right)^3 \qquad \text{(Eq. 6)}$$

FCCS Analysis

FCCS employing BAX labeled with dyes having nonoverlapping fluorescence spectra and a two-channel collection of data was used to determine the presence or absence of BAX homo-oligomers in detergent micelles (23, 24). Using Bodipy FL maleimide-BAXΔC and Bodipy 630/650 maleimide-BAXΔC, we studied cross-correlation in micelle-associated protein. The cross-correlation value, a ratio of the number of the fluorescent complexes containing both proteins of interest to the number of the fluorescent species of one of the proteins, was used to estimate the micelles with more than one BAX molecule. As a positive control and as a calibration sample, the 21-bp-long double-stranded RNA labeled with AlexaFluor 488 and Cy5 on each 3′-end was used (25).

Fluorescence Intensity Distribution Analysis

Analysis of the fluorescence brightness of a particle can provide an additional measure of the number of fluorescent proteins associated with a detergent micelle. The particle fluorescence brightness determined by FIDA is extracted by fitting the distribution of the number of photon counts and is similar to the cpp value determined by FCS for a monodisperse fluorophore solution. Determination of the particle brightness of the BAX-detergent micelle and comparison with particle brightness of monomeric BAX molecules estimate the number of BAX molecules in detergent micelles. FIDA was performed according to Kask *et al.* (18). The raw data of photon arrival times was binned to 20 μs, and photon counting histograms were constructed. Parameters describing the detection volume were determined in a solution of fluor-BAXΔC in the absence of detergent. As indicated, histograms were fitted to model functions for one or two components, as described in Kask *et al.* (18) subtracting a background of 310 Hz for the buffer solution.

II.7 | References

1. Hsu, Y. T., and Youle, R. J. (1998) *J. Biol. Chem.* 273, 10777–10783
2. Wolter, K. G., Hsu, Y. T., Smith, C. L., Nechushtan, A., Xi, X. G., and Youle, R. J. (1997) *J. Cell Biol.* 139, 1281–1292
3. Annis, M. G., Soucie, E. L., Dlugosz, P. J., Cruz-Aguado, J. A., Penn, L. Z., Leber, B., and Andrews, D. W. (2005) *EMBO J.* 24, 2096–2103
4. Antonsson, B., Montessuit, S., Sanchez, B., and Martinou, J. C. (2001) *J. Biol. Chem.* 276, 11615–11623
5. Lalier, L., Cartron, P. F., Juin, P., Nedelkina, S., Manon, S., Bechinger, B., and Vallette, F. M. (2007) *Apoptosis* 12, 887–896
6. Youle, R. J., and Strasser, A. (2008) *Nat. Rev. Mol. Cell Biol.* 9, 47–59
7. Antonsson, B., Montessuit, S., Lauper, S., Eskes, R., and Martinou, J. C. (2000) *Biochem. J.* 345, 271–278
8. Suzuki, M., Youle, R. J., and Tjandra, N. (2000) *Cell* 103, 645–654
9. García-Sáez, A. J., Mingarro, I., Pérez-Payá, E., and Salgado, J. (2004) *Biochemistry* 43, 10930–10943
10. Lovell, J. F., Billen, L. P., Bindner, S., Shamas-Din, A., Fradin, C., Leber, B., and Andrews, D. W. (2008) *Cell* 135, 1074–1084
11. le Maire, M., Champeil, P., and Moller, J. V. (2000) *Biochim. Biophys. Acta* 1508, 86–111
12. Yethon, J. A., Epand, R. F., Leber, B., Epand, R. M., and Andrews, D. W. (2003) *J. Biol. Chem.* 278, 48935–48941
13. Hsu, Y. T., and Youle, R. J. (1997) *J. Biol. Chem.* 272, 13829–13834
14. Dewson, G., Snowden, R. T., Almond, J. B., Dyer, M. J., and Cohen, G. M. (2003) *Oncogene* 22, 2643–2654
15. Hou, Q., and Hsu, Y. T. (2005) *Am. J. Physiol. Heart Circ. Physiol.* 289, H477–H487
16. Saito, M., Korsmeyer, S. J., and Schlesinger, P. H. (2000) *Nat. Cell Biol.* 2, 553–555
17. Haustein, E., and Schwille, P. (2004) *Curr. Opin. Struct. Biol.* 14, 531–540
18. Kask, P., Palo, K., Ullmann, D., and Gall, K. (1999) *Proc. Natl. Acad. Sci. U.S.A.* 96, 13756–13761
19. Tartof, K. D., and Hobbs, C. A. (1987) *Focus* 9, 12
20. Frezza, C., Cipolat, S., and Scorrano, L. (2007) *Nat. Protoc.* 2, 287–295
21. Szoka, F., Jr., and Papahadjopoulos, D. (1978) *Proc. Natl. Acad. Sci. U.S.A.* 75, 4194–4198
22. Christenson, E., Merlin, S., Saito, M., and Schlesinger, P. (2008) *J. Mol. Biol.* 381, 1168–1183
23. Rika, J., and Binkert, T. (1989) *Phys. Rev. A* 39, 2646–2652
24. Schwille, P., Meyer-Almes, F. J., and Rigler, R. (1997) *Biophys. J.* 72, 1878–1886

25. Ohrt, T., Merkle, D., Birkenfeld, K., Echeverri, C. J., and Schwille, P. (2006) *Nucleic Acids Res.* 34, 1369–1380
26. Kuwana, T., Mackey, M. R., Perkins, G., Ellisman, M. H., Latterich, M., Schneiter, R., Green, D. R., and Newmeyer, D. D. (2002) *Cell* 111, 331–342
27. Bavdek, A., Gekara, N. O., Priselac, D., Gutiérrez Aguirre, I., Darji, A., Chakraborty, T., Macek, P., Lakey, J. H., Weiss, S., and Anderluh, G. (2007) *Biochemistry* 46, 4425–4437
28. Anderluh, G., Macek, P., and Lakey, J. H. (2003) *Toxicon* 42, 225–228
29. Enderlein, J., Gregor, I., Patra, D., and Fitter, J. (2004) *Curr. Pharm. Biotechnol.* 5, 155–161
30. Meacci, G., Ries, J., Fischer-Friedrich, E., Kahya, N., Schwille, P., and Kruse, K. (2006) *Phys. Biol.* 3, 255–263
31. Saffarian, S., Li, Y., Elson, E. L., and Pike, L. J. (2007) *Biophys. J.* 93, 1021–1031
32. Fleming, K. G. (2002) *J. Mol. Biol.* 323, 563–571
33. Jürgensmeier, J. M., Xie, Z., Deveraux, Q., Ellerby, L., Bredesen, D., and Reed, J. C. (1998) *Proc. Natl. Acad. Sci. U.S.A.* 95, 4997–5002
34. Rodnin, M. V., Posokhov, Y. O., Contino-Pe´pin, C., Brettmann, J., Kyrychenko, A., Palchevskyy, S. S., Pucci, B., and Ladokhin, A. S. (2008) *Biophys. J.* 94, 4348–4357
35. Bamber, L., Harding, M., Butler, P. J., and Kunji, E. R. (2006) *Proc. Natl. Acad. Sci. U.S.A.* 103, 16224–16229
36. MacKenzie, K. R., and Fleming, K. G. (2008) *Curr. Opin. Struct. Biol.* 18, 412–419

APPENDIX III

Evidence for a Giant BAX Pore

(The contents of this chapter were adapted from Ivashyna, O., García-Sáez, A. J., Christenson, E. T., Schwille, P., Schlesinger, P. H. (2011) (*in preparation*))

III.1 | Summary

BAX is a proapoptotic member of the BCL2 protein family that induces permeabilization of the outer mitochondrial membrane, likely via oligomeric pores. *In vitro* reconstitution experiments strongly support BAX oligomerization and membrane poration which correlates with genetic and biochemical evidence. The size and composition of BAX pores remains controversial, however, largely due to the absence of high-resolution structural information on membrane-affiliated BAX. To interrogate BAX pore formation and its long-term effects on artificial lipid membranes we developed a system consisting of giant unilamellar vesicles (GUVs) and recombinant fluorescently-labeled BAX and unlabeled BH3-only activator cBID which we studied using confocal microscopy. Our data show that BAX can bind and permeabilize lipid bilayers of GUVs and prolonged exposure of GUVs to BAX leads to dramatic morphological changes in and disintegration of GUV structure. In addition, we found that in the large format of GUVs BAX forms giant pores which we have termed mega-pores. The line tension in the rim of a BAX mega-pore was calculated to be 3.7±1.7 fN while the size distribution of these pores was 5-20 μm and lifetime ranged from 8 min. to many hours. The presence of BAX mega-pores supports the proposal that BAX can form pores of varying diameters, not only on the nanoscopic scale but also the microscopic, and suggests there is no upper limit on the number of BAX monomers that can participate in a BAX pore.

III.2 | Introduction

BCL-2 associated protein X (BAX), a member of the B-cell lymphoma-2 (BCL2) protein family, is directly involved in controlling integrity of the outer mitochondrial membrane (OMM) (1). In a cell, the function of BAX is to permeabilize the OMM, possibly via formation of oligomeric pores, through which mitochondrial intermembrane proteins can escape into the cytoplasm and activate the cascade of caspases which dismantle the cell. However, such BAX pores have not been directly observed *in vivo* but only via cell-free reconstitution schemes. *In vitro* BAX pores were observed in systems consisting of purified BAX and artificial lipid membranes – in most cases represented by the unilamellar lipid vesicles of 0.1-0.2 μm in diameter (2-4). Such small liposomes can only be imaged by electron microscopy where samples have to be dried and fixed prior to imaging, which conceivably can introduce artifacts (5). Therefore, we developed an *in vitro* system consisting of fluorescence-labeled (fl-) BAX, BH3-only direct activator cut BID (cBID), antiapoptotic BCL-X_L, and giant unilamellar vesicles (GUVs) – with diameters ranging from 10-100 μm – which can be non-invasively studied in physiological buffer conditions over relatively long periods of time.

We began our studies by establishing the ability of fl-BAX to form pores in unilamellar vesicles of 0.2 μm in diameter, after which we transitioned to confocal imaging studies of fl-BAX binding and permeabilization of GUVs. To ensure that fluorescence-labeling of BAX did not interfere with its ability to permeabilize lipid membranes, we produced two forms of fl-BAX, labeled with structurally distinct fluorophores. The relevance of our experimental regime

is evinced by employing cBID to enhance the permeabilization activity of BAX and BCL-X_L to suppress BAX poration.

Confocal microscopy experiments allowed observation of intriguing BAX effects on the morphology and stability of GUVs, the most striking being formation of gigantic BAX pores which we have dubbed BAX mega-pores. To characterize these pores with respect to other known types of giant pores in GUVs we measured the line tension in the rims and the lifetimes of these mega-pores. Our evidence reveals that BAX mega-pores are the most stable giant pores yet observed. While BAX mega-pores should not exist in a cellular environment, their interrogation provides insight into the assembly of mitochondrial, nanoscale pores.

III.3 | Results

Fluorescently-labeled BAX is functional

For our imaging experiments human full-length BAX—with a single cysteine residue engineered at position 4 (S4→C) and the two endogenous cysteines, C62 and C126, mutated to serine and alanine respectively—was produced in *E. coli* without use of detergent as described in Methods section. This protein was labeled with Alexa Fluor 488 dye (BAX-G) or with Atto 655 dye (BAX-R). The two dyes were used to ensure that fluorescence labeling does not interfere with the liposome permeabilization activity of BAX. The liposome permeabilization activity of both fluorescently labeled proteins was checked using assay of carboxyfluorescein release from liposomes (6,7). In this assay cBID was used to activate the liposome permeabilization by BAX. However, without the addition of cBID, BAX produced a slow release of carboxyfluorescein from liposomes, suggesting an intrinsic permeabilization activity of BAX in our preparation (8) (Fig III.1). Interestingly, addition of BCL-X_L, an inhibitor of BAX pore formation, inhibited only the cBID induced permeabilization of liposomes by BAX but not the permeabilization of liposomes induced by BAX alone, (Fig. III.1B). However, the intrinsic permeabilization activity of BAX was inhibited by BCL-X_L, when both proteins were added simultaneously to liposomes in the absence of cBID.

Further verification of fl-BAX functionality was done using GUVs prepared from DOPC:bovine heart cardiolipin mixture of 80:20 mol% (Fig. III.1C). In these experiments BAX-R (25 nM), BAX-G (25 nM), cBID (4 nM), and free Alexa 546 dye (1 μM) were added to GUVs and time series of images were taken to follow the GUV permeabilization. As a result

BAX bound and permeabilized GUVs (Fig III.1C). BAX binding to the GUVs can be seen from the time-dependent increase in the fluorescence in the GUV membranes, while permeabilization of GUVs can be seen from the filling of GUV lumen with free dye and with BAX (Fig. III.1C).

We also tested the effect of BCL-X_L on BAX binding and permeabilization of GUVs (Fig. III.1D-E). In these experiments, as expected BCL-X_L prevented pore formation by BAX without inhibiting the ability of BAX to bind GUV membranes (Fig. III.1D). However, when liposomes were initially preincubated with BCL-X_L and cBID for one hour and then BAX added, no BAX binding to GUVs was observed, suggesting that BCL-X_L, when present in a lipid membrane, inhibits BAX binding to the membrane (9) (Fig. III.1E). Taken together, these results show that both fluorescence-labeled BAX proteins can bind lipid membranes and form pores in liposomes and thus recapitulate native BAX function.

Fig. III.1

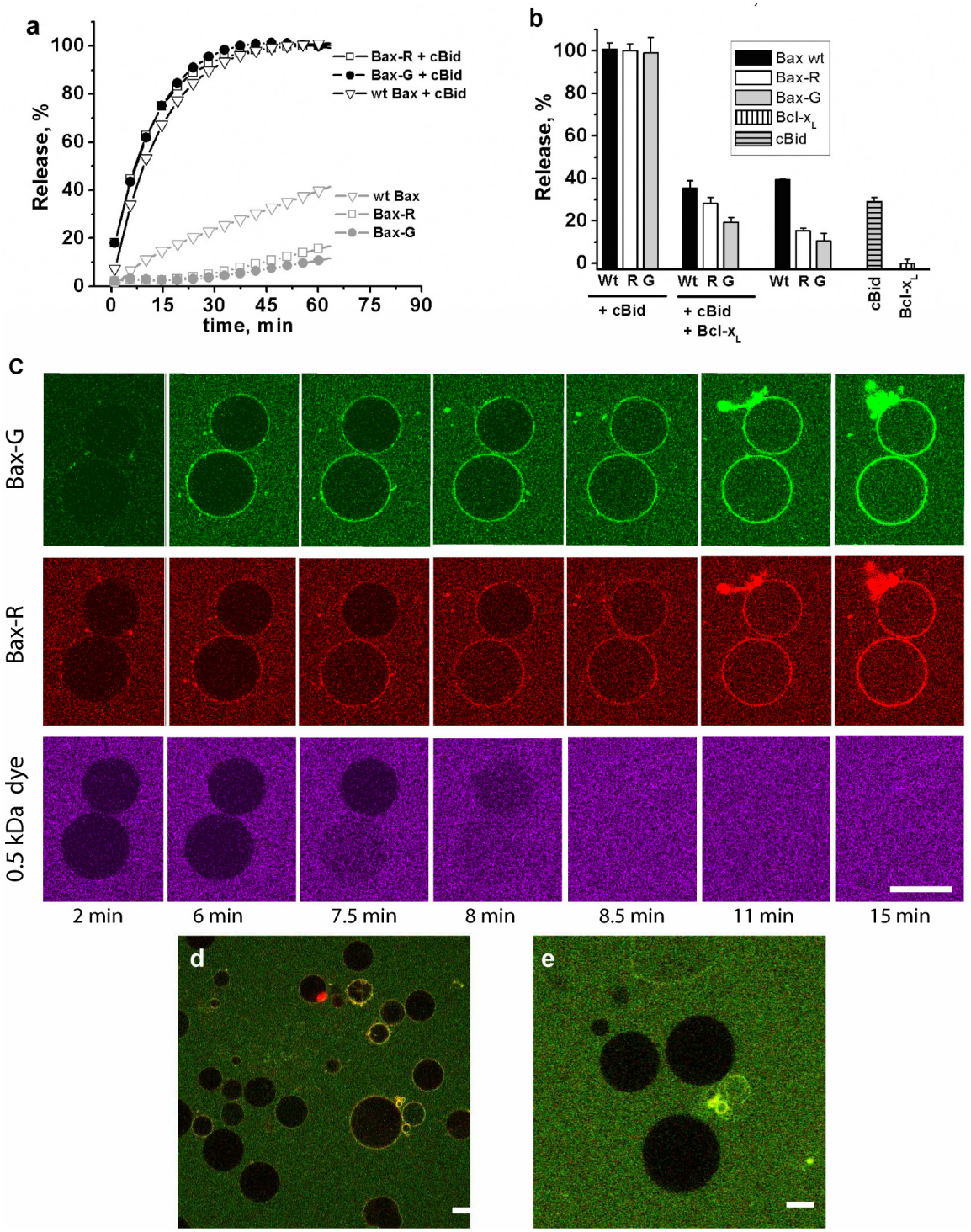
a
Release, %
time, min
Bax-R + cBid
Bax-G + cBid
wt Bax + cBid
wt Bax
Bax-R
Bax-G
b
Release, %
Bax wt
Bax-R
Bax-G
Bcl-x_L
cBid
Wt R G
+ cBid
+ cBid
+ Bcl-x_L
cBid
Bcl-x_L
c
Bax-G
Bax-R
0.5 kDa dye
2 min
6 min
7.5 min
8 min
8.5 min
11 min
15 min
d
e

Fig. III.1 | **Assays of liposomes permeabilization by BAX.** *A*, Kinetics of carboxyfluorescein release from liposomes. Each release curve is normalized and represents an average of three independent measurements. Protein concentrations used: 100 nM wild-type (wt) BAX, 100 nM BAX-R, 100 nM BAX-G, 10 nM cBID, 100 nM BCL-X_L. Total lipid concentration was 16 µM, while lipid composition was DOPC:cardiolipin 80:20 mol%. *B*, End point measurement of the % release one hour after addition of indicated proteins to liposomes filled with carboxyfluorescein. *C*, Confocal microscopy images of GUV permeabilization by BAX-R (25 nM) and BAX-G (25 nM) activated with cBID (4 nM). Alexa 546 was used as a small soluble 0.5 kDa dye to follow the GUV permeabilization (1 µM). Time stamps indicate time after protein addition to GUVs. *D*, Confocal microscopy images with overlayed spectral channels from BAX-R and BAX-G of BAX binding to GUVs in the presence of BCL-X_L (50 nM) and cBID (4 nM). BAX-R and BAX-G total concentration is 50 nM. *E*, BAX does not bind GUVs preincubated for one hour with 50 nM BCL-X_L and 4 nM cBID. In all images scale bar is 20 µm.

Morphological changes in GUVs upon BAX binding

The ability of BAX to from pores in GUVs has been reported previously but not with a fluorescence-labeled protein or with the intent to characterize the evolution of membrane morphology upon prolonged interaction with BAX protein (10,11). Here, we used confocal microscopy to establish the effect of the fl-BAX on GUVs. We determined that incubation with 50 nM BAX and 4 nM cBID allowed us to simultaneously observe the accumulation of fl-BAX in and permeabilization of the GUV membrane (Fig. III.1C) and that the GUVs were stable for 7 to 8 hours after protein addition. However, after 24 hours this preparation became a mass of collapsed GUV remnants, reflecting the gross distortions by BAX of bilayer architecture (Fig. III.2F). After one hour of incubation with this BAX concentration, 100% of GUVs were permeabilized and had homogeneous distribution of labeled BAX on the bilayer membrane. At the same time, in these experiments, we noted variable fluorescence intensity in various GUV membranes, representing a diversity of BAX concentration in these membranes (Fig. III.S1A). We hypothesize that this heterogeneity of BAX binding to GUVs stems from variation in cardiolipin content of the GUVs which is known to affect the BAX, BAK, and cBID binding (2,5,12) (See Supplement Discussion). After 3-4 hours of incubation with BAX and cBID the heterogeneity of BAX binding to GUVs was no longer visible suggesting BAX saturation in the lipid membrane of GUVs (Fig. III.2A). Prolonged incubation of GUVs with these concentrations of BAX and cBID led to major morphology changes in the GUVs. The vesicles change shape from spherical to potato- and tubule-like forms reflecting BAX-induced changes in the elastic coupling to lipid bilayer forces in membranes (Fig. III.2A-D).

Additionally, we observed formation of gigantic BAX mega-pores and other large visible BAX aggregates in GUV membranes (Fig. III.2B, 3, 4). During incubation with BAX occasional GUVs ruptured into smaller liposomes (Fig. III.2E-F) and by 24 hours of incubation with BAX almost no GUVs were left in the observation chamber. These proceedings clearly defined the time period when these GUVs could be studied by confocal microscopy. BAX binding to GUVs and consequent deformation and rupture of GUVs is dependent upon BAX concentrations demonstrating that mass action and thermodynamics governs these processes.

Fig. III.2

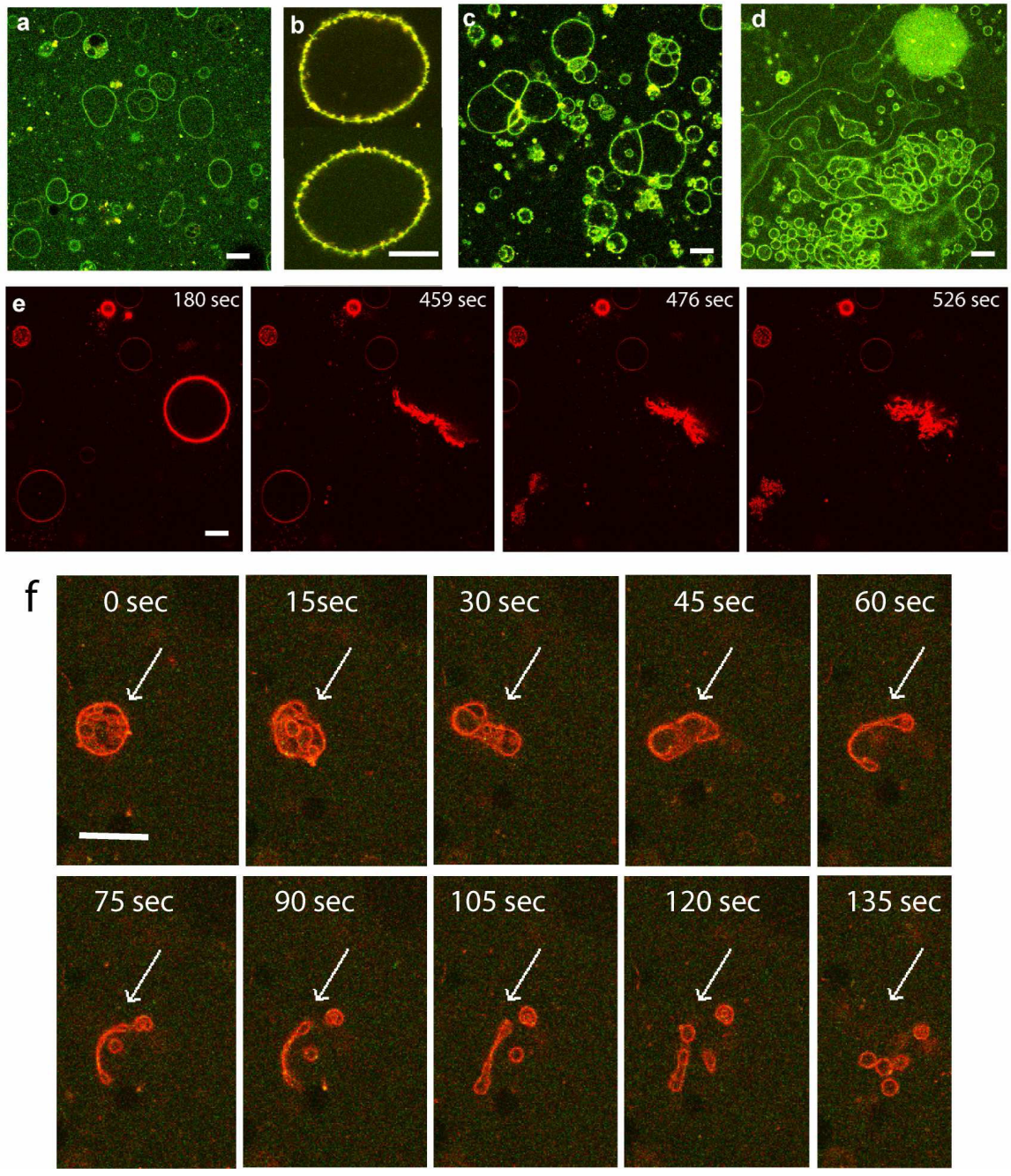
a
b
c
d
e
180 sec
459 sec
476 sec
526 sec
f
0 sec
15sec
30 sec
45 sec
60 sec
75 sec
90 sec
105 sec
120 sec
135 sec

Fig. III.2 | **BAX binding to GUVs: confocal microscopy images.** *A*, Distortion of spherical GUVs by BAX. *B*, Aggregates of BAX in GUV membranes. *C*, Agglomeration of GUVs after four hours of incubation with BAX. *D*, Formation of tubule-like lipid membrane structures after 7-8 hours of incubation with BAX. *E*, Rupture and collapse of GUVs upon BAX addition. Time steps represent the time after BAX addition. *F*, Transformation of GUV shape upon BAX binding (4 nM cBID and 50 nM combined concentration of BAX-R and BAX-G). In all images scale bar is 20 μm.

BAX forms long lived mega-pores in GUVs

While using confocal microscopy to study BAX-R and BAX-G binding to GUVs in the presence of cBID, we were intrigued by the formation of giant BAX pores which we named BAX mega-pores (Fig. III.3, 4). These pores ranged from 5-20 μm in diameter (Fig. III.4D), appeared within 10 minutes of BAX addition to GUVs, and were extremely stable, with lifetimes of 8 minutes up to many hours. Interestingly, all observed BAX mega-pores had increased BAX concentration in the rim of the pore, which can be seen from increased fluorescence signal from the membrane portion creating the pore edge. In addition, these mega-pores did not expand or lead to GUV collapse (13). Although the mega-pores usually closed over the observation period of 1-2 hours, the presence of a simple obstacle in the pore closure path, *e.g.* another liposome, was observed to arrest the closure process (Fig. III.3C). For comparison, an impedimentary lipid vesicle present in the closure path of a giant pore opened by the stimulation with visible light was cut into two vesicles when the pore closed (14). This observation shows that BAX reduces the line tension in the pore rim, thus resulting in the arrest of the pore closure by an impedimentary vesicle. The line tension is the energy per unit length of the membrane contour at the pore edge, and it arises due to the exposure to water of the hydrophobic lipid tails in the rim of the pore. In GUVs where a BAX mega-pore did close, fl-BAX concentrated at the rim of the pore dispersed over the GUV surface producing a homogeneous BAX fluorescence signal (Fig. III.3B, 4A). Additionally, GUVs which have gone through the process of the mega-pore formation and closure did not have another mega-pore open and appeared to be stable for hours afterwards.

Fig. III.3

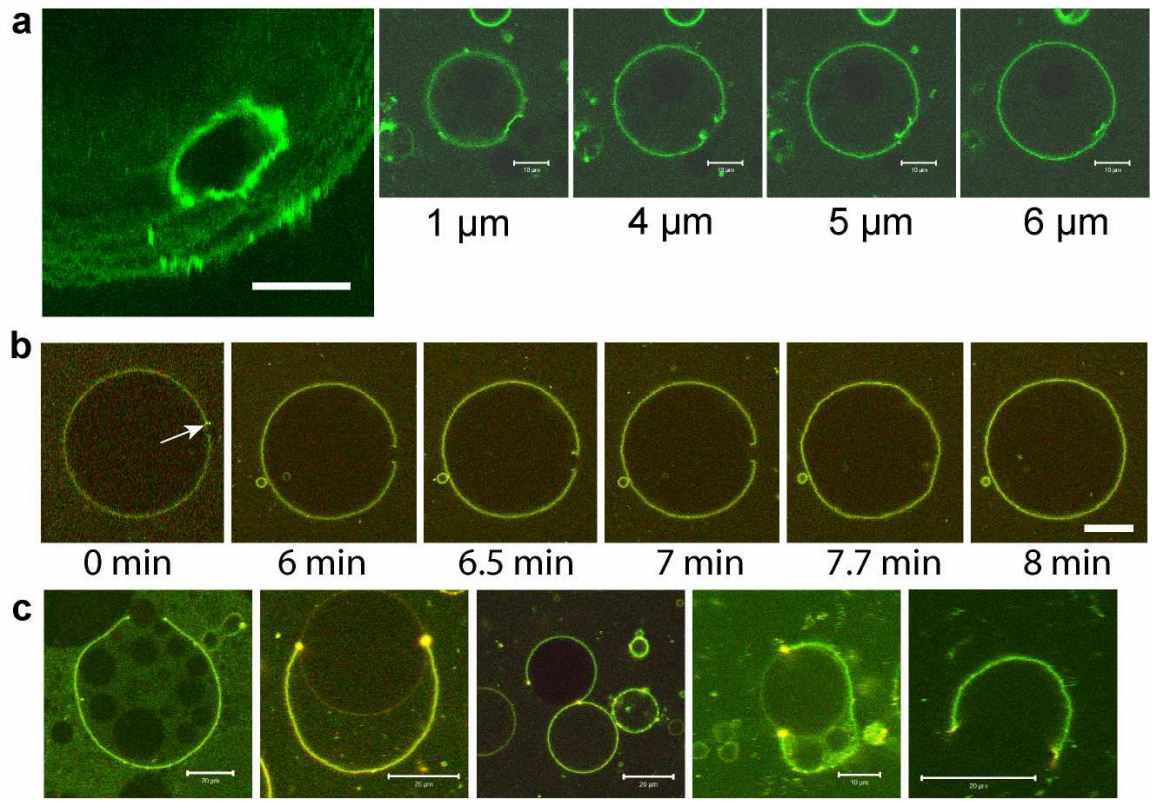

Fig. III.3 | **BAX mega-pore visualization.** *A*, 3D reconstruction of the BAX mega-pore shown together with confocal images used to produce this reconstruction. Values in µm indicate distance from the bottom of a GUV resting on the coverslip surface. *B*, Confocal images of the time series of opening, persistence, and closure of the BAX megapore. Arrow in the first image indicates the position at which the BAX mega-pore opened. Time stamps represent time since the opening of the pore. *C*, Confocal images of other examples of BAX mega-pores.

Size distribution of BAX mega-pores

To determine whether a correlation exists between the sizes of BAX mega-pores and GUVs, we performed the Pearson's correlation test. In this test we compared the distribution of BAX mega-pore diameters with diameters of encompassing GUVs (Fig. III.4C-D); only weak correlation was found between these two sets of values (with the Pearson correlation coefficient of 0.25). The maximum value for the Pearson correlation coefficient is 1 which corresponds to a direct positive correlation between two sets of values, i.e. increase in the value of one data set leads to linear increase in the values of the other data set. The relatively small correlation between the diameter of a mega-pore and its cognate GUV diameter weakly suggests that the larger the GUV the larger mega-pore it can accommodate. However, a GUV with a certain diameter can have mega-pores of various diameters which are most likely distributed around a certain mean value. For example, a GUV 22 μm in diameter can support a mega-pore of 15±5 μm (n=3) (Fig. III.4D). The latter observation suggests that there is effectively no limit on the number of BAX monomers participating in the formation of a BAX mega-pore and reveals a continuum of BAX mega-pore sizes.

Line tension in the rim of a BAX mega-pore

Kinetics and thermodynamics of giant pores in GUVs can be explained by theoretical models (14,15) where the energy E_r of a pore of radius r is described as

$$E_r = 2\pi r\Gamma - \pi r^2\sigma \qquad \text{(Eqn. 1)}$$

where Γ is the line tension while σ is the surface tension. Interplay between line and surface tension allows opening, persistence, and closure of giant pores in GUVs. Following the model

of Brochard-Wyart F. *et al*. (16) the life of a pore in a GUV can be described in four steps: (i) pore opens due to an increase of the membrane surface tension (σ) which can be induced by application of an electrical field (17,18), insertion of molecules with non-zero spontaneous curvature such as detergents (14), or insertion of BAX α5-derived peptides (19); (ii) while the surface tension term in Equation 1 is larger than the line tension term the pore expands to some critical radius (r_c); (iii) while the surface tension and line tension terms in the equation 1 are equal (i.e. pore energy $E_r = 0$) the pore exists in an unstable equilibrium state; (iv) when the line tension begins to increase the pore initiates closure. Using this theoretical framework the line tension in the rim of the pore during the pore closure stage can be calculated using

$$k = -\frac{2\Gamma}{3\pi\eta} \qquad \text{(Eqn. 2)}$$

where k is the slope of the $R^2 \ln(r)$ versus time and η is the solution viscosity (1.035×10^{-3} Pa·s for 30 mM sucrose solution), R is the radius of a GUV containing a pore of radius r. Examples of the evolution of BAX mega-pore radii (r) are shown in Figure III.4B-C. From these data we estimate the line tension in the rim of the BAX mega-pore to be 3.7±1.7 fN (n=3) which is four orders of magnitude lower than the line tension of a pore opened by intense illumination of a DOPC vesicle (Γ = 20.7±3.5 pN) (14) and two orders of magnitude lower than the line tension of a detergent stabilized giant pore (0.2 pN).

The ability of the BAX to reduce the line tension of artificial lipid membranes has been reported previously but without a direct measurement of the line tension (20). Here, we quantify BAX reduction of bilayer line tension and find the protein to be drastically more effective in eliciting membrane poration than other previously studied effectors. It is

hypothesized that cone-shaped detergents reduce the line tension in giant lipid pores based on their propensity to partition to the high curvature regions in the edge a pore (14,21). Therefore, the ability of BAX to reduce line tension lower than that of detergents indicates that BAX is a remarkable protein evolutionarily crafted to stabilize edges of lipid membranes.

Interestingly, the line tension generated by full-length BAX is three orders of magnitude lower than the line tension generated by the pore-forming BAX α5 peptide in a supported lipid bilayer ($\Gamma = 3.8 \pm 0.4$ pN) (19). This disparity indicates that the full length protein is able to stabilize the pore edge more efficiently than a single α-helix of BAX, suggesting that the non-pore forming helices of BAX also contribute to edge stabilization. Previously the non-pore forming helices were attributed two major roles in the function of BAX: first, to shield the pore-forming helices of BAX (α5-6) from interaction with lipid membranes in the inactive conformation of BAX (22); and second, to facilitate the communication between BAX and other proteins involved in the apoptosis decision via BH3 domain interaction. Our findings ascribe a third role for these non-pore forming helices of BAX: stabilizing the edges of BAX mega-pores and thus likely stabilizing the edges of kindred nanoscopic BAX pores. A substantial fraction of this improved edge stabilization of the full-length protein vs. thα5 peptide is probably an effe ct of BAX homo-oligomerization which locally concentrates the α5s (23-25).

Fig. III.4

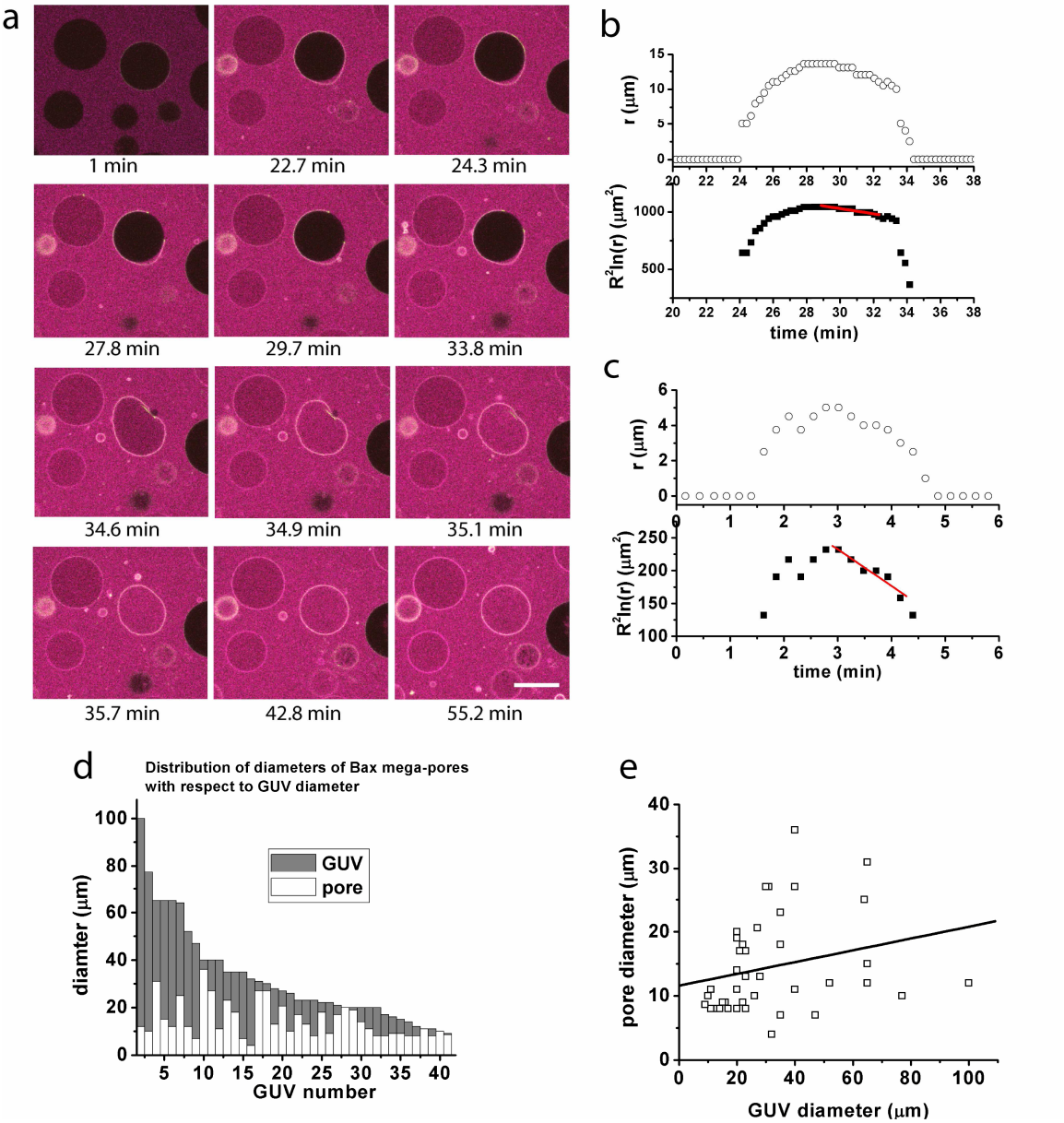
a
1 min
22.7 min
24.3 min
27.8 min
29.7 min
33.8 min
34.6 min
34.9 min
35.1 min
35.7 min
42.8 min
55.2 min
b
r (μm)
R²ln(r) (μm²)
time (min)
c
r (μm)
R²ln(r) (μm²)
time (min)
d
Distribution of diameters of Bax mega-pores with respect to GUV diameter
GUV
pore
diamter (μm)
GUV number
e
pore diameter (μm)
GUV diameter (μm)

Fig. III.4 | **Analysis of line tension and distribution of BAX mega-pore diameters.** *A*, These confocal images represent an overlay of three channels: red (BAX-R), green (BAX-G), and pink (free dye Alexa 546). Time stamps indicate time after protein addition to GUVs. The GUV positioned in the center of each frame has a daughter liposome inside. The outer GUV develops a BAX mega-pore; the inner liposome is then ejected thorough the BAX mega-pore and the mega-pore then closes. Scale bar is 40 μm**.** *B*, The $R^2\ln(r)$ versus time plot for the GUV shown in panel A. *C*, The $R^2\ln(r)$ versus time plot for the GUV shown in Fig. 3B. *D*, Bar plot of GUV diameters (gray bars) and corresponding diameters of BAX mega-pores (white bars). Number of GUVs used for this plot is 44. *E*, Result of Pearson correlation test for the correlation between GUV and corresponding BAX mega-pore diameters. Pearson correlation test value is 0.25 (maximum possible value is 1).

The lifetime of BAX mega-pore

The lifetime of lipid pores in DOPC vesicles immersed in water solution is estimated to be 10-200 ms which can be extended by increasing the viscosity of solution (15). Therefore, 66% glycerol solution, having 30 times higher solution viscosity than water, is commonly used to measure the lifetimes of giant lipid pores (14,26,27). The reported lifetimes of giant pores in 66% glycerol ranges from seconds for lipid pores opened by a physical method to minutes for lipid pores stabilized with detergent (14) while the lifetime of BAX mega-pores ranges from 8 min to many hours when measured in 30 mM sucrose solution (which has viscosity very close to that of water). Hence, if the lifetimes of all three types of giant pores are compared in the same solution, the BAX mega-pore will have the longest lifetime, as explained by the extremely low line tension measured in the rim of this pore.

III.4 | Discussion

The size and oligomeric state of a BAX pore is somewhat controversial in the field of apoptosis. In fact, the BAX pore has not been observed *in vivo* by electron microscopy in mitochondria of cells undergoing apoptosis, where BAX appears to aggregate at the fission sites on the surface of the OMM (28). Nonetheless, *in vitro* studies using electrophysiological and pore-sizing techniques have shown that BAX forms pores of 2-5 nm in diameter (7,10,11,29,30) while electron and atomic force microscopies revealed the formation of 100-200 nm disruptions in liposomes and supported lipid bilayers incubated with BAX (5,23,31). In light of this controversy about the size and composition of BAX pores, our observations of 5-20 μm diameter BAX mega-pores in GUVs support the hypothesis that BAX is able to form pores of various sizes (32).

In addition to extremely large diameters, BAX mega-pores also exhibited uncommonly long life times ranging from 10 min to hours. Based on the lifetime and size, these BAX mega-pores are very similar to the giant pores formed in GUVs by detergents or by the physical disruption of GUVs (14-16,18,26,27,33). The latter two types of giant pores can be differentiated on the basis of the magnitude of the force responsible for closing a pore – the line tension (14,21). The line tension is highest in giant pores opened by physical disruption (10-20 pN) (14,33) and is two orders of magnitude lower in the giant pores stabilized by detergents (0.2 pN) (14). Therefore, to characterize the BAX mega-pores with respect to the other two known types of giant pores we used an established microscopy technique to measure the line tension in the rim of the BAX mega-pore; this quantity was ascertained to be two orders of

magnitude lower than the line tension in the rim of a detergent stabilized giant pore (16). Furthermore, integrating this line tension measurement with other knowledge of BAX interaction with lipid membranes, we introduce a model of the formation, persistence, and closure of BAX mega-pores.

Fig. III.5

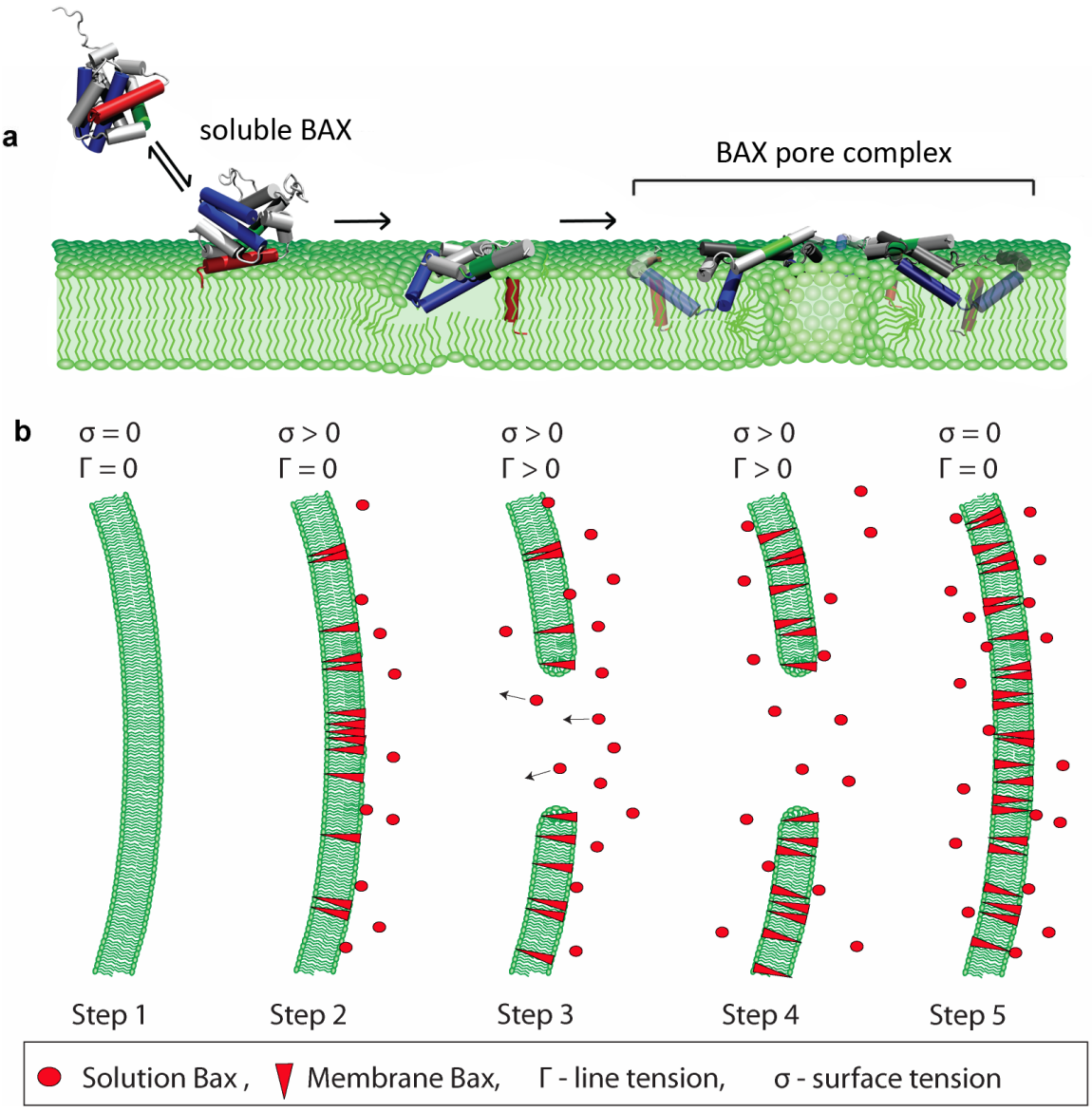

Fig. III.5 | **Model of BAX interaction with lipid membranes.** *A*, Schematic of BAX binding, integration and oligomerization in a lipid membrane. *B*, Proposed mechanism of BAX mega-pore opening and closure.

Model of BAX mega-pore formation, persistence, and closure

We propose the following mechanism for BAX mega-pore assembly based on GUVs shown in Figures III.3 and III.4. In this mechanism BAX inserts into a lipid membrane from the outside of a GUV and transforms from a globular soluble protein (22) to a membrane-integrated protein with an extended structure shallowly inserted into the membrane (3,34) (Fig. III.5A). BAX insertion produces a dramatic area increase in the outer membrane leaflet while the area of the inner leaflet remains unperturbed (Fig. III.5B). The localized area differential between the two membrane leaflets induces curvature frustration and increase in the surface tension of the membrane (35,36) ($\Delta\sigma>0$). When surface tension increases to a critical value the membrane structure ruptures and the mega-pore is formed. Once the pore is formed its line tension provides a force for reclosure of the mega-pore which counteracts the surface energy such that the GUV continues to persist and does not collapse (See also Eqn. 1). However, now through the open mega-pore soluble BAX is able to diffuse into the lumen of the GUV and insert into the inner leaflet of the GUV membrane. This results in an area increase of the inner leaflet leading to an increase in surface tension in this leaflet. Meanwhile, membrane BAX has accumulated in the rim of the pore, reducing line tension and decreasing the rate of pore closure as surface energies of the inner and outer leaflets equilibrate (Fig. III.5B). Consequently the BAX mega-pore closes very slowly over tens of minutes even though the surface energy of the two leaflets is equalizing. After pore closure, membrane-integral BAX monomers, dimers, or small oligomers diffuse away from the position where the membrane

resealed such that within seconds after pore closure no heterogeneities are observed on the GUV surface (Fig. III.3B, 4A).

BAX mega-pore: connection to physiology

It is clear that the BAX mega-pore structures we observed in GUVs cannot occur *in vivo* simply due to their size (5-20 μm) versus the size of mitochondria (0.2-1 μm). Furthermore BAX mega-pores scaled for the smaller size of mitochondria would need to be scaled for the reported localization of BAX to fission sites (28). Also, the simple lipid composition of our synthetic GUVs (DOPC:cardiolipin, 80:20 mol %) provides only a basic mimic of the complex, heterogeneous distribution of lipids and proteins of mitochondrial outer membranes. Therefore, on the mitochondrial surface BAX has a relatively limited membrane area to form protein-membrane complexes, while on the surface of GUV membrane the area available to BAX is many times greater and can generate the mega-pores that we observed. Nevertheless, mechanistic insights gleaned from microscale BAX mega-pores are applicable to nanoscale, mitochondrial BAX pores.

III.5 | Conclusion

The existence of microscopic BAX mega-pores further supports the hypothesis that BAX can form a variety of pore sizes in artificial lipid membranes and that the BAX pore is a lipidic pore stabilized by the presence of the BAX protein in the pore rim (20,30). Accumulation of BAX in the pore rim not only reduces the line tension to extremely low values but also leads to the dramatic increase of the pore lifetime. Furthermore, existence of BAX mega-pores implies that theoretically an unlimited number of BAX monomers can participate in the formation of a BAX mega-pore, i.e. the larger the diameter of a mega-pore, the bigger the number of BAX monomers participating in the formation of this mega-pore.

BAX is not the first protein which is reported to form giant pores in GUVs. For example, protein talin and other FERM domain-containing proteins have been shown to stabilize the edges of giant pores in GUVs but only in conditions of zero salt concentration (37,38). At physiological salt concentrations these proteins do not promote the formation of giant pores. Furthermore, the physiological relevance of pore stabilization by talin and other FERM domain-containing proteins is not clear—the *in vivo* function of these proteins is to connect actin filaments to the cell membrane. In contrast to these proteins, BAX forms giant pores in physiologic buffer conditions and is a bona fide pore-forming protein whose activity is directly linked to its cellular function, thus making the discovery of the ability of BAX to form mega-pores more significant.

III.6 | Experimental Procedures

Protein preparation and labeling.

Human cDNA for BAX, BID and BCL-X_L were subcloned into pTYB1 vector (New England Biolabs). For production of the fluorescently-labeled BAX two endogenous cysteines of BAX were substituted (C62S, C126A) and additional cysteine was engineered, S4C. All proteins were expressed in BL21(DE3) *E. coli*, and purified as an intein/chitin-binding domain fusion protein without use of detergents similar to Ivashyna *et al.* (6). Purified proteins were estimated to be >95% pure by Coomassie staining SDS-PAGE gels and stored at 4°C. BID was cut with recombinant caspase-8 to produce cBID. Mutant BAX with single cysteine was labeled according to the manufacturer's protocol with Alexa Fluor 488 maleimide (Invitrogen) and Atto 655 maleimide (AttoTech).

Protein functionality check

Functionality comparison of the fluorescently-labeled BAX to the wild-type BAX was performed using liposome-carboxyfluorescein leakage assays and fluorescence was measured by 96-well plate format (Tecan) (6). All release assays were done in triplicate using 10 mM HEPES, pH 7.2, 100 mM KCl buffer, at room temperature. Protein concentrations used: BAX (100 nM), BAX-R (100 nM), BAX-G (100 nM), cBID (10 nM), BCL-X_L (100 nM). Total lipid concentration in each release assay was 16 μM; liposomes were prepared from 1,2-dioleoyl-sn-glycero-3-phosphocholine (DOPC):bovine heart cardiolipin (80:20 mol%; Avanti Polar Lipids) using a reverse phase method and containing 50 mM carboxyfluorescein (Invitrogen).

Preparation of giant unilamellar vesicles

GUVs were prepared by the electroformation method (39) from a lipid mixture containing 80 mol% DOPC and 20 mol% bovine heart cardiolipin. For the confocal microscopy observation 50 μl of solution containing GUVs was transferred into a Lab-Tek observation chamber (Fisher Scientific) containing 450 μl of 10 mM HEPES, pH 7.2, 100 mM KCl and a mixture of BAX, cBID and BCL-X_L.

Confocal Microscopy

Assays were performed at 22°C on a laser-scanning confocal microscope Meta 510 system (Carl Zeiss) using 40× NA 1.2 UV-Vis-IR C Apochromat water-immersion objective. For excitation the 488 nm line of an Argon-ion laser (25 μW) and the 633 nm line of the HeNe laser (15 μW) were used. Collection and processing of images was done using Zeiss software provided with the microscope (AIM, version 4.2).

Line tension measurement

Calculations were performed using the theoretical framework developed by Brochard-Wyart F. *et al.* (16). For this time lapse confocal microscopy images of GUVs which developed mega-pores were analyzed to derive a time-dependent relationship between the radius of a GUV (R) and the radius of a BAX mega-pore (r). Then a scatter plot of $R^2 \ln(r)$ versus time was plotted in Origin 6.0 and fitted to a line. The slope of a fitted line was used to calculate the line tension of a mega-pore using Equation 2.

III.7 | Supplement

Heterogeneity of BAX binding to GUVs

In all confocal microscopy experiments the lipid composition of GUVs was DOPC:bovine heart cardiolipin (80:20 mol%). Assuming homogeneous distribution of lipids among GUVs during electroformation we expected homogeneous BAX binding to GUVs, i.e. similar fluorescence brightness of bound BAX on the GUV surface for all GUVs in an observation chamber. However, we observed wide variation in the amount of BAX binding to GUVs electroformed from the same lipid mixture, which can be seen in the different fluorescence intensity of GUV membranes (Fig. III.S1A). We hypothesize that this heterogeneity of BAX binding to GUVs is based on the heterogeneity of lipid distribution among GUVs during the electroformation. In particular, we hypothesize that the heterogeneity comes from unequal distribution of cardiolipin among the GUVs. Cardiolipin is known for its ability to promote non-lamellar lipid bilayer formation (i.e. lipid bilayers with high curvature) and in our GUV preparations with 80:20 mol% of DOPC:cardiolipin we observe formation of both unilamellar and multilamellar vesicles (Fig. III.5B), with the multilamellar vesicles showing high curvature regions. We hypothesize that these multilamellar vesicles contain higher concentration of cardiolipin than the rest of the vesicles from the same GUV preparation. However, we do not have a direct way to measure the cardiolipin concentration in these vesicles.

Fig. III.S1

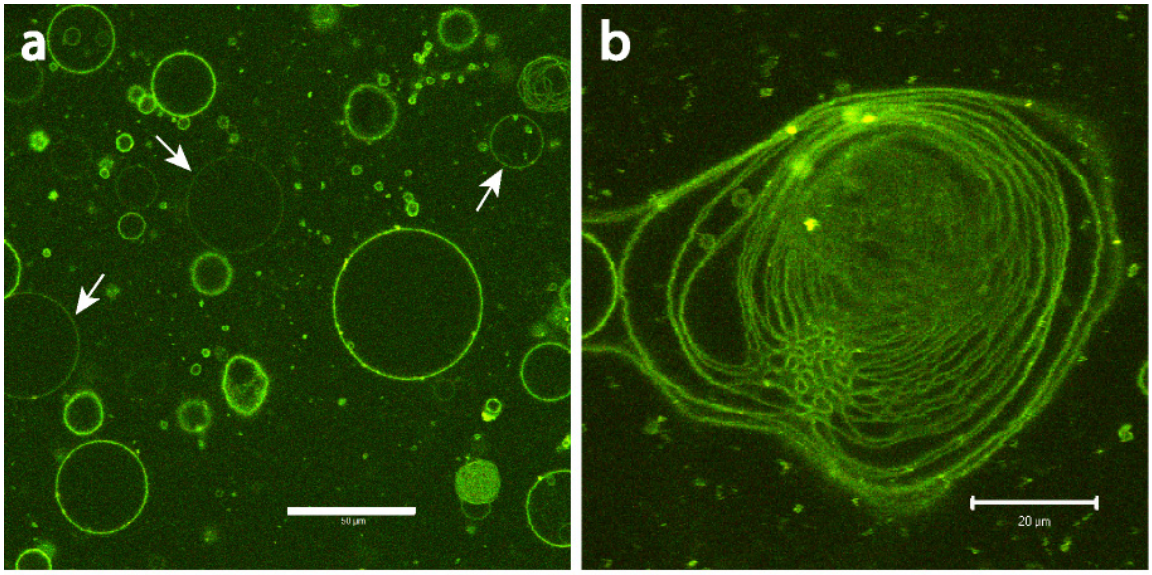

Fig. III.S1 | **Heterogeneity of BAX binding to GUVs.** GUVs were prepared by electroformation from DOPC:bovine heart cardiolipin (80:20 mol%) and added to the solution containing BAX-R (50 nM), BAX-G (50 nM) and cBID (10 nM). The confocal image was taken approximately 30 minutes after mixing. The confocal image is an overlay of red and green channels corresponding respectively to BAX-R and BAX-G. *A*, Confocal image of the field view of multiple GUVs with the fluorescently labeled BAX bound. Scale bar is 50 µm. *B*, Confocal image of a giant multilamellar vesicle containing high concentration of the bovine heart cardiolipin which resulted in the production of high curvature in the portions of this vesicle. Images A and B were taken in the same chamber, indicating that these vesicles were from the same preparation and were exposed to the same concentration of the cBID and fluorescent BAX. Scale bar is 20 µm.

III.8 | References

1. Wei, M. C., Zong, W. X., Cheng, E. H., Lindsten, T., Panoutsakopoulou, V., Ross, A. J., Roth, K. A., MacGregor, G. R., Thompson, C. B., and Korsmeyer, S. J. (2001) *Science* **292**, 727-730
2. Kuwana, T., Mackey, M. R., Perkins, G., Ellisman, M. H., Latterich, M., Schneiter, R., Green, D. R., and Newmeyer, D. D. (2002) *Cell* **111**, 331-342
3. Oh, K. J., Barbuto, S., Meyer, N., Kim, R. S., Collier, R. J., and Korsmeyer, S. J. (2005) *J Biol Chem* **280**, 753-767
4. Terrones, O., Antonsson, B., Yamaguchi, H., Wang, H. G., Liu, J., Lee, R. M., Herrmann, A., and Basanez, G. (2004) *J Biol Chem* **279**, 30081-30091
5. Schafer, B., Quispe, J., Choudhary, V., Chipuk, J. E., Ajero, T. G., Du, H., Schneiter, R., and Kuwana, T. (2009) *Mol Biol Cell* **20**, 2276-2285
6. Ivashyna, O., Garcia-Saez, A. J., Ries, J., Christenson, E. T., Schwille, P., and Schlesinger, P. H. (2009) *J Biol Chem* **284**, 23935-23946
7. Saito, M., Korsmeyer, S. J., and Schlesinger, P. H. (2000) *Nat Cell Biol* **2**, 553-555
8. Tan, C., Dlugosz, P. J., Peng, J., Zhang, Z., Lapolla, S. M., Plafker, S. M., Andrews, D. W., and Lin, J. (2006) *J Biol Chem* **281**, 14764-14775
9. Billen, L. P., Kokoski, C. L., Lovell, J. F., Leber, B., and Andrews, D. W. (2008) *PLoS Biol* **6**, e147
10. Schlesinger, P. H., and Saito, M. (2006) *Cell Death Differ* **13**, 1403-1408
11. Dejean, L. M., Martinez-Caballero, S., Manon, S., and Kinnally, K. W. (2006) *Biochim Biophys Acta* **1762**, 191-201
12. Landeta, O., Landajuela, A., Gil, D., Taneva, S., Diprimo, C., Sot, B., Valle, M., Frolov, V., and Basanez, G. (2011) *J Biol Chem*
13. Bar-Ziv, R., Moses, E., and Nelson, P. (1998) *Biophys J* **75**, 294-320
14. Karatekin, E., Sandre, O., Guitouni, H., Borghi, N., Puech, P. H., and Brochard-Wyart, F. (2003) *Biophys J* **84**, 1734-1749
15. Sandre, O., Moreaux, L., and Brochard-Wyart, F. (1999) *Proc Natl Acad Sci U S A* **96**, 10591-10596
16. Brochard-Wyart, F., de Gennes, P. G., and Sandre, O. (2000) *Physica A: Statistical Mechanics and its Applications* **278**, 32-51
17. Needham, D., and Hochmuth, R. M. (1989) *Biophys J* **55**, 1001-1009
18. Riske, K. A., and Dimova, R. (2005) *Biophys J* **88**, 1143-1155
19. Garcia-Saez, A. J., Chiantia, S., Salgado, J., and Schwille, P. (2007) *Biophys J* **93**, 103-112
20. Basanez, G., Nechushtan, A., Drozhinin, O., Chanturiya, A., Choe, E., Tutt, S., Wood, K. A., Hsu, Y., Zimmerberg, J., and Youle, R. J. (1999) *Proc Natl Acad Sci U S A* **96**, 5492-5497
21. May, S. (2000) *European Physical Journal E* **3**, 37-44
22. Suzuki, M., Youle, R. J., and Tjandra, N. (2000) *Cell* **103**, 645-654

23. Bleicken, S., Classen, M., Padmavathi, P. V., Ishikawa, T., Zeth, K., Steinhoff, H. J., and Bordignon, E. (2010) *J Biol Chem* **285**, 6636-6647
24. Dewson, G., Kratina, T., Sim, H. W., Puthalakath, H., Adams, J. M., Colman, P. M., and Kluck, R. M. (2008) *Mol Cell* **30**, 369-380
25. Oh, K. J., Singh, P., Lee, K., Foss, K., Lee, S., Park, M., Aluvila, S., Kim, R. S., Symersky, J., and Walters, D. E. (2010) *J Biol Chem* **285**, 28924-28937
26. Rodriguez, N., Cribier, S., and Pincet, F. (2006) *Phys Rev E Stat Nonlin Soft Matter Phys* **74**, 061902
27. Brochard-Wyart, F., de Gennes, P., and Sandre, O. (2000) *Physica A* **278**, 32-51
28. Karbowski, M., Lee, Y. J., Gaume, B., Jeong, S. Y., Frank, S., Nechushtan, A., Santel, A., Fuller, M., Smith, C. L., and Youle, R. J. (2002) *J Cell Biol* **159**, 931-938
29. Schlesinger, P. H., Gross, A., Yin, X. M., Yamamoto, K., Saito, M., Waksman, G., and Korsmeyer, S. J. (1997) *Proc Natl Acad Sci U S A* **94**, 11357-11362
30. Qian, S., Wang, W., Yang, L., and Huang, H. W. (2008) *PNAS* **105**, 17379-17383
31. Epand, R. F., Martinou, J. C., Montessuit, S., Epand, R. M., and Yip, C. M. (2002) *Biochem Biophys Res Commun* **298**, 744-749
32. Martinez-Caballero, S., Dejean, L. M., Kinnally, M. S., Oh, K. J., Mannella, C. A., and Kinnally, K. W. (2009) *J Biol Chem* **284**, 12235-12245
33. Zhelev, D. V., and Needham, D. (1993) *Biochim Biophys Acta* **1147**, 89-104
34. Annis, M. G., Soucie, E. L., Dlugosz, P. J., Cruz-Aguado, J. A., Penn, L. Z., Leber, B., and Andrews, D. W. (2005) *EMBO J* **24**, 2096-2103
35. Zemel, A., Ben-Shaul, A., and May, S. (2008) *J Phys Chem B* **112**, 6988-6996
36. Lee, A. G. (2003) *Biochim Biophys Acta* **1612**, 1-40
37. Saitoh, A., Takiguchi, K., Tanaka, Y., and Hotani, H. (1998) *Proc Natl Acad Sci U S A* **95**, 1026-1031
38. Takeda, S., Saitoh, A., Furuta, M., Satomi, N., Ishino, A., Nishida, G., Sudo, H., Hotani, H., and Takiguchi, K. (2006) *J Mol Biol* **362**, 403-413
39. Angelova, M. I., and Dimitrov, S. D. (1986) *Faraday Discuss. Chem. Soc.* **81**, 303-311

APPENDIX IV

FCCS Study of BAX Self-Assembly and Modulation by BCL-X_L & cBID

(The content of this chapter has been adapted from Ivashyna, O., García-Sáez, A. J., Christenson, E. T., Schwille, P., Schlesinger, P. H. (2011) (*in preparation*))

IV.1 | Summary

It is widely accepted that during apoptosis, permeabilization of the outer mitochondrial membrane by the pore-forming members of the BCL2 protein family is a critical point after which the cell cannot be resuscitated. However, without direct evidence of how they interact in bilayers the molecular mechanism of the mitochondrial permeabilization remains controversial. Here we have reconstituted the pore formation by protein BAX in giant vesicles and show that in this environment BAX can form a heterogeneous distribution of coexisting pore sizes ranging from 1 nm to 20 μm in diameter. Evidence is provided by directly examining oligomerization and mobility change of BAX molecules in GUVs by fluorescence cross-correlation spectroscopy and by studying the large complexes by confocal microscopy. We show that in the presence of BCL-X_L, an inhibitor of BAX pore formation, membrane bound BAX was primarily monomeric. We also show that, in the large length scale format of a GUV, BAX form structures that reveal its affinity for highly curved membranes, and that it dramatically reduces line tension while stabilizing its lipidic pores. Finally, our results demonstrate that BAX forms pores by increasing membrane surface energy and changing curvature of lipid membranes, thus manifesting an ability to sculpt lipid bilayers.

IV.2 | Introduction

BAX is a pro-apoptotic member of the BCL2 protein family and its paramount function is to permeabilize the OMM during apoptosis (1,2). Upon apoptotic stimulation BAX translocates to the OMM where it changes conformation, inserts as a monomer, and then undergoes in-membrane homo-oligomerization to form a pore. Once the BAX pore is formed, cytochrome *c* and other mitochondria-resident proteins escape into the cytoplasm where they activate the cascade of caspases that dismantle the cell. To date the structure of the inactive, cytoplasm-resident, form of BAX is known (3); however, the structure of the active, membrane-integrated, form of BAX remains unsolved. The absence of a membrane structure for this protein has lead to a vigorous debate about: the nature of the BAX pore (lipidic versus barrel-stave) (4-6), the number of BAX monomers participating in the pore formation (7-10), the possible molecular interactions formed among them in a pore (11,12), and the progression and variety of pores formed by BAX (i.e. dimer, tetramer and higher order polymers (4,5,13,14). To address these questions we used two-focus two-color scanning FCCS (15-17) to non-intrusively measure the mobility and self-association of the fluorescently-labeled BAX in a hydrated lipid membrane of GUVs for 5-7 hours after BAX insertion into the lipid membrane (See Chapter 5 for the confocal microscopy analysis of the fluorescent BAX binding to GUV). In these FCCS experiments the microscope output was multiplexed for simultaneous determination of the membrane diffusion coefficients and concentrations of BAX-R, BAX-G and BAX-RG complexes and the analysis of the BAX pore activation. Using the membrane diffusion coefficients for the monomeric BAX-R and BAX-G proteins and for the BAX-RG complexes

we estimated the hydrodynamic radius of these complexes in lipid membranes which is close to the reported in the literature values. Furthermore, using the values for the membrane diffusion coefficient we were able to clearly differentiate between two monomeric species of BAX in lipid membranes – membrane associated and membrane integrated BAX. In support of this analysis we used cBID to activate BAX and BCL-X_L to regulate the membrane integration and self-association of BAX.

IV.3 | Results

BAX is monomeric in solution and oligomerizes only in lipid membranes

It was recently shown by a FRET study that BAX does not oligomerize prior to membrane binding (14). To confirm this finding, we compared the cross-correlation of BAX-R & BAX-G in the presence or absence of GUVs. Using FCCS we observe a similar result that BAX-R and BAX-G in the presence of cBID are monomeric and do not oligomerize in solution (Fig. IV.1A). In solution, the diffusion coefficient for BAX-G is 114±6 μm^2/sec (mean±s.e., n=3) and for BAX-R it is 134±12 μm^2/sec (mean±s.e., n=3) which is similar to that of monomeric tBID and BCL-X_L (17). Having established the membrane-binding functionality of BAX (Fig. IV.1A), FCCS measurements were done on a population of GUVs (10 min measurement time per GUV) (Fig. IV.C). We observe oligomerization of BAX-R and BAX-G only in the environment of a lipid membrane as shown by the increased cross correlation in Fig. IV.1C (blue line).

Fig. IV.1

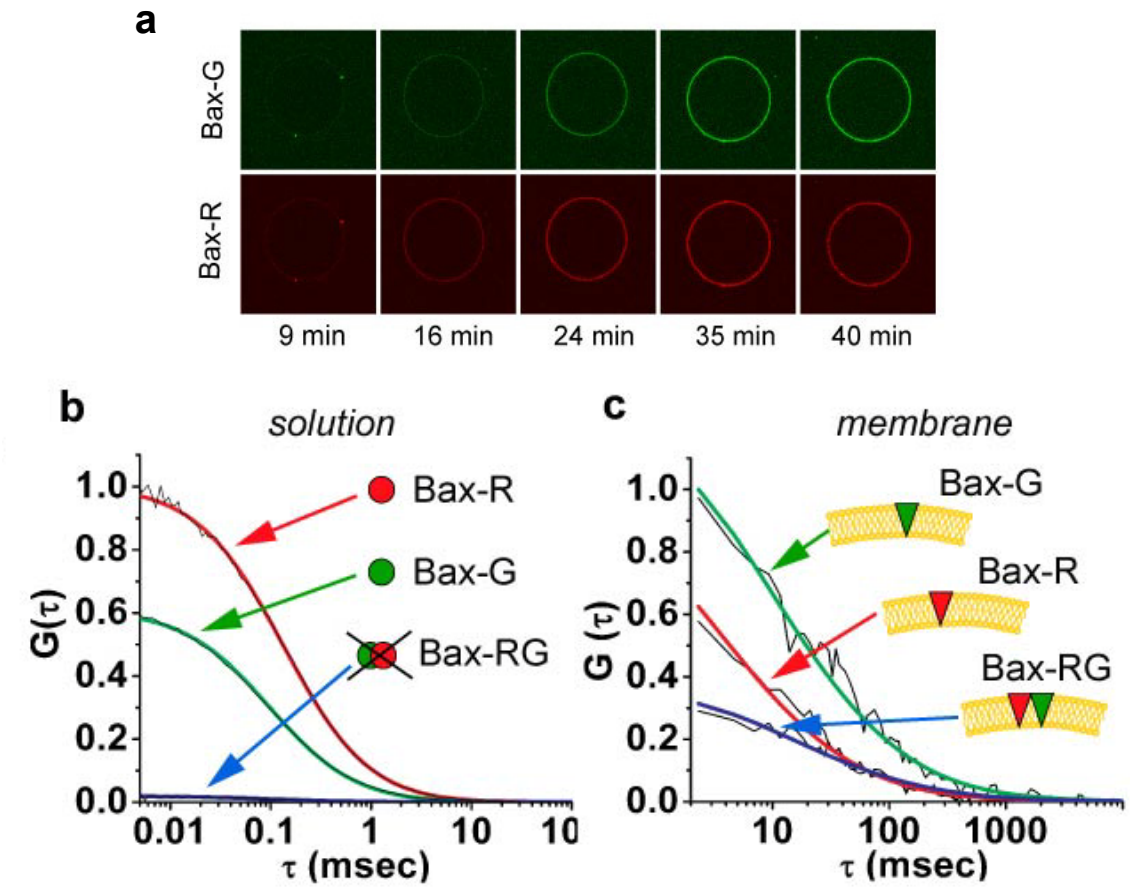

Fig. IV.1 | **FCCS on BAX in solution and a lipid membrane.** *A*, Confocal microscopy images of BAX-GUV binding. BAX-R (25 nM), BAX-G (25 nM) and cBID (4 nM) were added to GUVs upon which collection of the time-series of images was initiated. Time stamps represent the time after protein addition to GUVs. *B*, Normalized auto-correlation curves and cross-correlation curve (blue) for BAX-R and BAX-G in solution in the presence of cBID. *C*, Normalized auto-correlation curves and cross-correlation curve (blue) for BAX-R and BAX-G in a GUV membrane in the presence of cBID.

In a lipid membrane BAX forms a population of varying in size oligomers

Two-color two-focus scanning FCCS allows simultaneous measurement of the fluorescent protein concentration, diffusion coefficient and self-association in a lipid membrane (15-18). To study BAX self-association in a lipid membrane we used BAX-R and BAX-G proteins (50 nM total concentration) activated with 4 nM cBID (as was determined by the confocal microscopy experiments described in Appendix III).

The FCCS analysis of membrane BAX produced a clear result that BAX protein complexes increased in size with time as can be seen from the decrease in the average mobility of these BAX-RG containing complexes (Fig. IV.2D, blue squares). At the same time the number of membrane BAX particles (which include monomers and oligomers) was increasing, so it was clear that for the >6 hours of these experiments BAX was continuing to accumulate in the membrane. Each time point on the Figure IV.2C and IV.2D represents an independent GUV measurement such that amount of BAX in the membrane and the average diffusion coefficient of the BAX particles is not uniform and reflects the variation in the vesicle lipid composition (See Appendix III for discussion).

The average diffusion coefficient of BAX-RG complexes in GUV membranes incubated for five hours with 50 nM of the fluorescent BAX and 4 nM cBID is 2.0±0.4 μm^2/sec (mean±s.d., n=21) which is slower than the membrane diffusion coefficient of monomeric tBID and BCL-$X_L^{\Delta C}$ measured by the same technique (5 μm^2/sec) (17) suggesting formation of a bulky, slowly-diffusing BAX-RG complex in a lipid membrane (Table IV.1). Since the diffusion coefficient of a particle in a lipid membrane depends on the in-membrane

hydrodynamic diameter of the particle, we can use the value for the diffusion coefficient of BAX-RG complexes to determine their approximate in-membrane hydrodynamic diameter using a modified Saffman-Delbruck formula (19) but for this the membrane diffusion coefficient of a BAX monomer must be determined.

Fig. IV.2

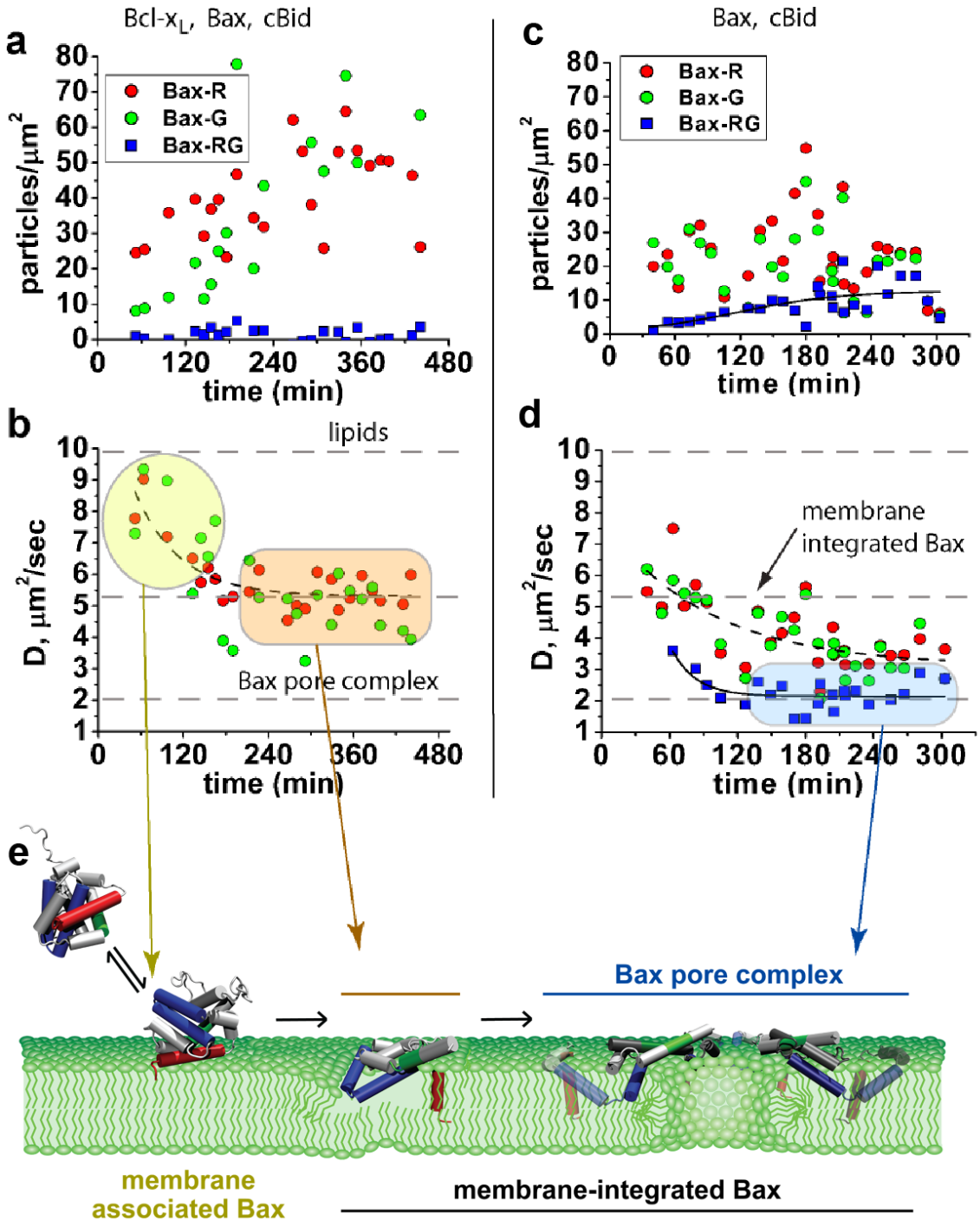

Fig. IV.2 | **Two-color two-focus scanning FCCS experiments on BAX.** *A & B*, FCCS of BAX-R/BAX-G cross-correlation (50 nM total BAX concentration) in the presence of 50 nM BCL-X_L and 4 nM cBID. C *& D*, FCCS of BAX-R/BAX-G cross-correlation (50 nM total BAX concentration) in the presence of 4 nM cBID (BCL-X_L absent). *E*, Schematic of various diffusion species of BAX in a lipid membrane.

BCL-X_L prevents the self-assembly of BAX in lipid membranes

To determine the membrane diffusion coefficient of a BAX monomer, BAX self-assembly and pore formation in a lipid membrane should be inhibited. This was accomplished by using full length human BCL-X_L protein which is an anti-apoptotic member of the BCL2 family that inhibits BAX pore formation (20). When GUVs were preincubated with BCL-X_L (50 nM) and cBID (4 nM) for one hour and then BAX (50 nM) was added, no binding of BAX to GUV membranes was observed (Fig. III.1E, Appendix III) which does not allow for the FCCS measurements. However, this observation reflects the ability of BCL-X_L to sequester cBID in an inactive complex which is unable to activate and promote membrane integration of BAX (14,17,20). Simultaneous addition to GUVs of BAX, cBID and BCL-X_L at these same concentrations resulted in sufficient membrane binding of BAX for the FCCS measurements but did not result in GUV permeabilization (Fig. III.1D, Appendix III). Comparison of the fluorescence intensity of BAX-R accumulation in the GUV membranes in the presence and absence of BCL-X_L shows that in the presence of BCL-X_L the amount of BAX binding to the GUV membranes is lower than in the absence of BCL-X_L (Fig. IV.3).

Based on the results of the FCCS experiments shown in Figure IV.2A&B in the presence of BCL-X_L the membrane concentration of BAX increased over 7 hours and its diffusion coefficient decreased from 8.3±1.0 μm^2/sec (mean±s.d, n=6) to 5.2±0.7 μm^2/sec (mean±s.d., n=26). The latter diffusion coefficient value is typical of a transmembrane alpha-helical peptide (21) and it is also similar to the in-membrane diffusion coefficient of monomeric membrane integrated tBID or C-terminal truncated BCL-X_L described by the

Saffman-Delbruck model of membrane protein diffusion (Table IV.1) (17,22). In addition, we observed no cross-correlation between BAX-R and BAX-G at this concentration of BCL-X_L (Fig. IV.2B). Based on these data we conclude that the diffusion coefficient of membrane integrated BAX monomers is 5.2±0.7 μm^2/sec.

Furthermore, we propose that the gradual decrease in the membrane diffusion coefficient of BAX in the presence of inhibiting concentrations of BCL-X_L represents the transition of BAX from being a monomeric membrane-associated protein sliding on the membrane surface with fast diffusion to becoming a monomeric membrane-integrated protein with appropriately slower diffusion (Fig. IV.2E). However, we do not discount the possibility that the monomeric integrated BAX forms heterodimers with BCL-X_L in lipid membranes (20). In the Saffman-Delbruck theory scaling of the diffusion coefficient with the in-membrane diameter of the protein is logarithmic implying that integrated monomeric BAX would have membrane diffusion coefficient similar to that of a BAX/ BCL-X_L heterodimer.

Fig. IV.3

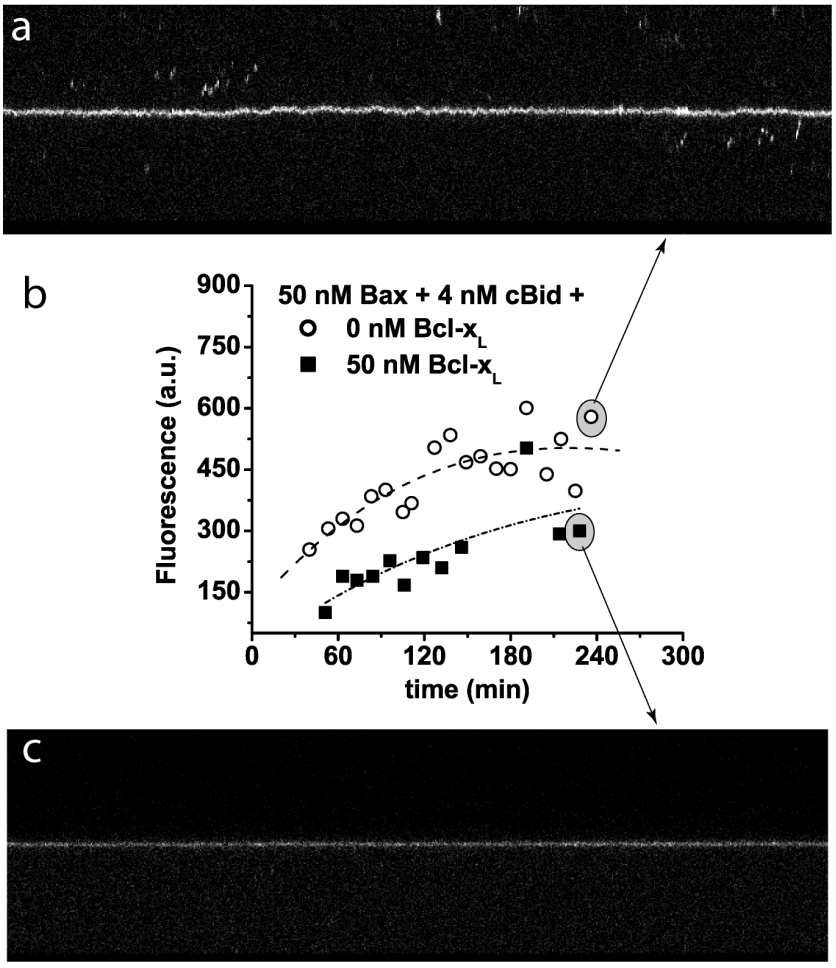

Fig. IV.3 | **Comparison of BAX-R binding to GUV membranes in the presence and absence of BCL-X_L.** *A*, Map of fluorescence intensity changes in a line scan through the GUV membrane (vertical direction) with time (horizontal direction). This membrane trace comes from a GUV exposed only to BAX-R protein and cBID. *B*, Change in cumulative fluorescence intensity in membranes of GUVs exposed to BAX-R and cBID in the absence and presence of BCL-X_L. The trace for the last point in each measurement is shown in *A* and *C*. *C*, Map of fluorescence intensity changes in a GUV exposed to BAX-R, cBID, and BCL-X_L. In these experiments following protein and lipid concentrations were used: 25 nM BAX-R, 25 nM BAX-G, 50 nM BCL-X_L, 4 nM cBID, and 5 μM total lipid.

Table IV.1 | **Comparison of BAX diffusion coefficients with lipid diffusion coefficients.**

Type of molecule	**Diffusion coefficient, $\mu m^2/sec$**	**in-membrane diameter, nm**
in solution:		-
monomeric inactive BAX	114±5	
monomeric tBID (17)	143±9	
monomeric BCL-$X_L^{\Delta C}$ (17)	78±10	
in a lipid membrane:		
lipids	10.0±0.5	1
monomeric membrane associated BAX	8.3±1.0	-
monomeric membrane integrated BAX	5.2±0.7	≈1
monomeric tBID (17)	5.0±0.3	-
monomeric BCL-$X_L^{\Delta C}$ (17)	4.8±0.7	-
BAX pore complex (at 50 nM total BAX concentration)	2.0±0.4	53±12

Calculation of the BAX pore complex diameter

Traditionally the Saffman-Delbruck equation is used to calculate the hydrodynamic radius of a membrane inclusion from its diffusion coefficient (21-25) (See Eqn. 1 in the Experimentals section). It has also been shown that Saffman-Delbruck equation faithfully describes diffusion of membrane inclusions traversing both leaflets of a lipid membrane in the case of small proteins, however, in the case of larger membrane inclusions (for example, such as lipid rafts) this theory underestimates the diameter of membrane inclusions. As a consequence of this, a modified version of a Saffman-Delbruck equation has been developed by Petrov and Schwille for the description of the diffusion of large membrane inclusions (19) (See Eqn. 2 in the Experimental Procedures section).

In the case of the diffusion of BAX in lipid membranes the diffusion coefficient of a BAX monomer (5.2±0.7 μm^2/sec) is consistent with the Saffman-Delbruck theory, however, the diffusion coefficient of BAX-RG protein complex is two times slower than the diffusion of a BAX monomer and thus according Petrov and Schwille the in-membrane hydrodynamic diameter of this complex should be calculated according to the modified Saffman-Delbruck formula. As a result the diameter of the BAX-RG protein complex diffusing with diffusion coefficient of 2.0±0.4 μm^2/sec is 53±12 nm. This value is one order of magnitude larger than the size of a BAX pore measured by the dextran blocking of a pore and by the electrophysiology methods (13,26). However, this value is consistent with the electron microscopy imaging of a BAX pore in liposomes and AFM measurement of the pore in supported lipid bilayers (4,27) where it has been shown that the diameter of a BAX pore can be 100-200 nm.

It is worth noting here that the calculated hydrodynamic radius of a BAX-RG complex does not necessarily represent the size of a pore formed by this complex. In spite of the obvious connection between the calculated diameter of a BAX-RG complex and the electron microscopy and AFM experiments, it is still possible that the size of the pore is smaller than 53 nm and the rest of the size of the pore is occupied by the lipids trapped in the concerted motion of a lipidic pore.

Titration of BAX in lipid membranes: mass action law

We next asked a question whether by increasing the amount of BAX in a lipid membrane we can control for the size and the concentration of BAX-RG complexes. For this purpose the various amounts of total soluble BAX-R and BAX-G proteins were added to the constant concentration of GUVs and the FCCS measurements were done on these GUV populations. In each case BAX binding to GUVs was activated by the addition of 4 nM cBID. As a result of these experiments we find that with the increasing concentration of total BAX added to the system the higher concentration of BAX particles is found in a lipid membrane (Fig IV.4, grey bars). It is important to note that these BAX particles include monomers and oligomers of BAX. Additionally, with increasing concentration of BAX particles in a lipid membrane the greater number of the BAX-RG complexes was observed (Fig. IV.4, black bars). Analysis of the diffusion coefficients for the BAX-RG complexes formed at different total concentrations of BAX also showed an increase in the average size of these complexes (Table IV.2). Such correlation between the size and concentration of BAX-RG complexes with the

total concentration of BAX in a system shows that BAX pore formation follows the mass action law.

Fig. IV.4

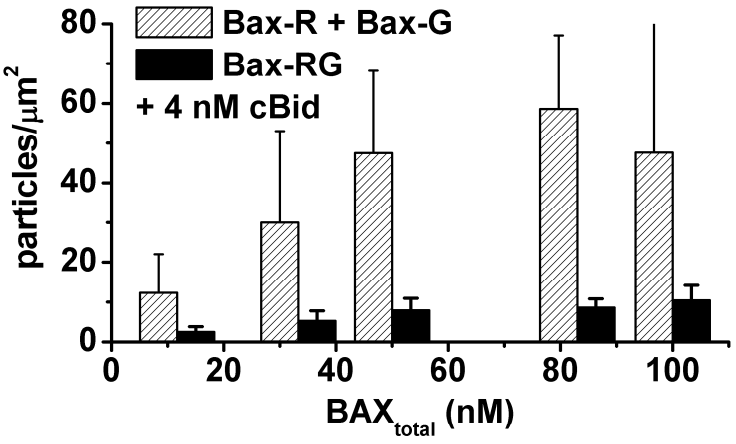

Fig. IV.4 | **Titration of BAX.** BAX-R and BAX-G were added to GUVs (5μM total lipid concentration) in the presence of cBID and FCCS measurement were done on a population of no less than 10 GUVs upon 1-2 hours after protein addition to GUVs.

Table IV.2 | **FCCS results of the titration of BAX.** Experimental conditions were the same as described in the legend to Fig. IV.4. The hydrodynamic diameter was calculated using modified Saffman-Delbruck formula (19).

Total BAX concentration, nM	BAX-RG complexes, particles/μm^2	measured diffusion coefficient, μm^2/sec	calculated in-membrane hydrodynamic diameter, nm
50	7.9	2.0±0.4	53.2
83	8.8	1.5±0.4	102.2
100	9.6	1.4±0.3	120

Moderating the activity of BAX with cBID

To study the effects of increasing concentrations of cBID onto the distribution of BAX particles in a lipid membrane we varied cBID concentrations in our FCCS experiments while keeping BAX and total lipid concentration constant. As a result we observed correlation between the increase of cBID concentration and the resulting concentration of BAX particles in the lipid membrane (Fig. IV.5). However, the concentration of BAX-RG complexes did not follow this correlation pattern. The concentration of BAX-RG complexes in a lipid membrane remained constant (within the margin of error) for all cBID concentrations (Fig. IV.5, blue bars). This observation indicates that cBID must be affecting only the kinetics of BAX integration into the lipid membranes without a significant effect on the resulting concentration of the BAX oligomers.

Fig. IV.5

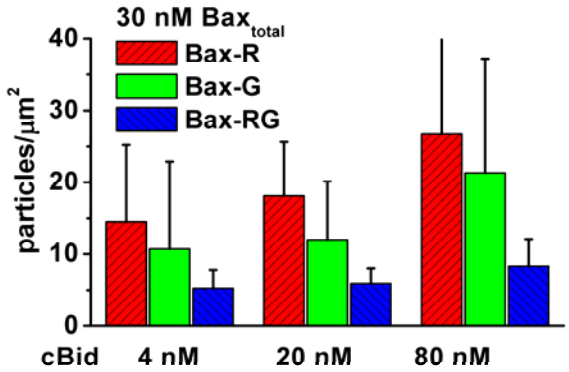

Fig. IV.5 | **Effects of cBID titration on the distribution of the membrane forms of BAX.** Results were obtained using two-color two-focus scanning FCCS analysis.

Interactions among BAX, cBID, and BCL-X_L: rheostat model

In Fig. IV.2 we have shown that BCL-X_L inhibits oligomerization of BAX in a lipid membrane. However, we were intrigued to know whether the inhibitory effect of BCL-X_L on BAX can be rescued by the addition of excess cBID. According to the rheostat model proposed by Korsmeyer *et al.* the apoptosis decision in cells depends on the relative concentrations of pro- and anti-apoptotic proteins (28). Therefore, in our minimal *in vitro* system we expect to observe an increase in the oligomerization of BAX in a lipid membrane containing BCL-X_L when cBID concentration is increased due to the competition for cBID between BAX and BCL-X_L (29).

Simultaneous addition to GUVs of 50 nM BAX and BCL-X_L at 1:1 protein to protein ratio with 4 nM cBID resulted in complete inhibition of BAX oligomerization as can be seen from the absence of BAX-RG complex formation, while in the absence of BCL-X_L the same concentrations of BAX and cBID resulted in the formation of 16% of BAX-RG complexes (normalized to the total concentration of BAX particles in the membrane) (Fig. IV.6). This observation is consistent with the rheostat model where cBID can interact with both BAX and BCL-X_L while having higher affinity for the interaction with BCL-X_L (14,17,29) and thus when BCL-X_L is present majority of the cBID molecules is sequestered in the interaction with BCL-X_L (assuming 1:1 stoichiometry of protein binding) leaving few cBID molecules for the interaction with BAX. However, when excess of cBID is added—equimolar BAX, BCL-X_L and cBID in the system—then there is sufficient cBID for the interaction with both BAX and BCL-X_L, and as a result we observe rescue of the BAX-RG complex formation (Fig. IV.6).

Therefore, using a minimal *in vitro* system we were able to show that the outcome of the interaction among BAX, cBID, and BCL-X_L can be described by the rationale of the rheostat model.

Fig. IV.6

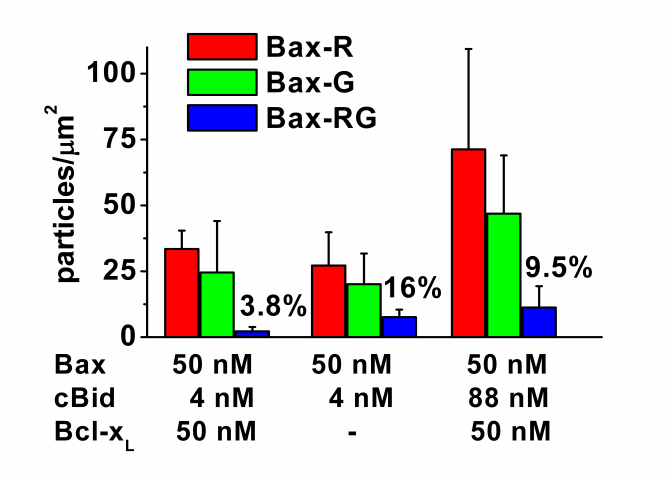

Fig. IV.6 | **BAX, cBID, and BCL-X_L: rheostat model.** Results were obtained using two-color two-focus scanning FCCS analysis.

IV.4 | Discussion

For use with two-color two-focus FCCS we produced two forms of the fluorescently labeled full length BAX protein, BAX-R and BAX-G. These fluorescently-labeled BAX proteins have been shown to have the pore formation activity similar to that of the recombinant wild type BAX (See Appendix III for details). Furthermore, we show that these two fluorescent forms of BAX are monomeric in solution and oligomerize only in lipid membranes (Fig. IV.1).

BAX binding to lipid membranes: associated versus integrated BAX

Using two-color two-focus scanning FCCS we show that prior to oligomerization in a lipid membrane monomeric BAX associates with the lipid membrane, and then becomes membrane integrated. The transition between the membrane associated and integrated forms of BAX most likely occurs via a conformational change, which is aided by cBID protein already present in the membrane. We differentiate between these two monomeric forms of BAX based on their diffusion coefficient: membrane-associated monomeric BAX, due to incomplete insertion into a lipid bilayer, has faster diffusion coefficient (8 μm^2/sec) than the monomeric membrane-integrated BAX (5 μm^2/sec). It is important to note, that this transition from associated to integrated BAX could only be observed by scanning FCCS in the presence of BCL-X_L protein in GUV membranes. BCL-X_L slows down membrane binding of BAX, and thus allowed us to observe this transition process. BCL-X_L has been proposed to inhibit the pore formation by BAX in three ways: by directly binding monomeric integrated BAX, by binding cBID protein and thus eliminating it as an activator of BAX, and by preventing BAX

binding to a lipid membrane (20,30). However, the mechanism of the last inhibition pathway is not clear. Therefore, BCL-X_L inhibition of BAX binding, oligomerization, and pore formation in lipid membranes, which were observed in our experiments, agree with literature.

In the absence of BCL-X_L in the membrane, the association and integration of BAX is rapid, and cannot be resolved by the scanning FCCS. In this case we observe the decrease in the average diffusion coefficient of BAX from 5 μm^2/sec to 2μm^2/sec, which likely represents the transition from monomeric integrated BAX to a proteo-lipidic complex containing multiple BAX monomers. Furthermore, the time frame of the BAX transition from the associated to integrated protein in the presence of BCL-X_L is longer than the time frame of the transition from the monomeric membrane integrated protein to the proteo-lipid complex in the absence of BCL-X_L (Fig. IV.2B&D), thus supporting our proposal that BCL-X_L slows down the process of BAX integration in a lipid membrane. Our observation of the transition from membrane integrated to membrane associated forms of BAX can be further supported by the SPR studies (31) and by the studies of the conformation of BAX loosely associated with the lipid membrane of LUVs (32).

Self-assembly of BAX in lipid membranes

It has been shown that in order to form a pore in artificial lipid membranes, BAX must undergo self-assembly in the lipid membrane environment (4,10,13,14,33) while *in vivo,* during apoptosis, BAX has also been shown to form large aggregates (10,34,35). Therefore, our observation of the BAX-RG complex formation was expected. However, what was unexpected, is the progressive decrease in the diffusion coefficient of BAX upon membrane integration.

According to the Saffman-Delbruck formula, diffusion of a membrane protein is primarily affected by the in-membrane hydrodynamic diameter of the protein. Therefore, dimerization and even tetramerization of a protein in a lipid bilayer would not result in a significant change in the diffusion coefficient of the resulting complex, compared to that of a monomer (36,37). Therefore, our observation of the significant decrease in the diffusion coefficient of BAX-RG complex compared to that of a BAX monomer, indicates that BAX is not simply oligomerizing, but most likely is forming lipidic pores (4,6,38). These lipidic pores involve lipids which contribute to the size of the in-membrane hydrodynamic diameter of a complex (See Fig. IV.2E for a proposed model of a BAX lipidic pore). Therefore, our estimation of the diameter of these slowly diffusing BAX-RG proteo-lipidic complexes most likely over-estimates the size of pores formed by these complexes in a lipid bilayer. However, we do not have direct experimental evidence for the presence of pores in these complexes. The reason for our assumption, that these BAX-RG proteo-lipidic complexes contain a pore, is based on the transmission electron microsocopy and AFM measurement of the BAX pore diameters, which show that BAX is capable of forming pores with the diameter of 100-200 nm. Calculated in-membrane diameter of a BAX-RG complex falls into this range.

Rheostat model: connection to physiology

The finding that pro- and anti-apoptotic proteins of the BCL2 family can heterodimerize, and that their relative concentrations to each other affects the decision whether a cell should undergo apoptosis, lead to the proposal of the rheostat model by Korsmeyer *et al.* (28). The results obtained using our model system of BAX pore formation in GUVs support

this hypothesis (Fig. IV.6). These results show that, when equimolar concentrations of BAX and BCL-X_L are present in a lipid membrane together with low concentration of cBID, there is no oligomerization and pore formation by BAX. However, when cBID is added, such that there is approximately one cBID molecule for each BAX and BCL-X_L molecule, then oligomerization and pore formation by BAX is rescued. Similarly, in the presence of low cBID concentration and the complete absence of BCL-X_L, BAX is able to oligomerize and form pores.

The results of scanning FCCS shown that BAX, cBID and BCL-X_L obey the law of mass action (Fig. IV.4, IV.5, IV.6). These results show that increase in the concentration of soluble protein leads to the concentration increase of the membrane bound protein, with a certain saturation limit. Results of the titration experiments with BAX-R and BAX-G show that not only the total concentration of membrane bound BAX monomers increases, but also that the distribution of BAX-RG proteo-lipidic complexes changes, resulting in the larger mean diameter of complexes (Table IV.2).

IV.5 | Conclusions

The work presented in this appendix represents the first example of the application of two-color two-focus scanning FCCS to study oligomerization and pore formation by BAX in lipid membranes of GUVs. The results of this study provide an insight into the mechanism of BAX pore formation in lipid membranes and the regulation of this mechanism by the pro-apoptotic BH3-only protein cBID and anti-apoptotic protein BCL-X_L. These results show that BAX binds lipid membranes containing cBID as a monomer, by first associating with the lipid membrane, likely via electrostatic interaction, and then undergoing conformational transition to become a membrane integrated protein, likely due to the interaction with cBID. Once in

lipid membrane, integrated BAX monomers initiate self-association which leads to the formation of pores. Formation of pores reduces the concentration of monomeric BAX monomers in the lipid membrane, thus allowing for the integration of additional BAX proteins. This continual insertion of BAX monomers into the lipid membrane leads to increase in the average BAX pore size resulting in the heterogeneous distribution of BAX pores. Increase in the number of BAX pores in the lipid membrane leads to the disruption of elastic forces of the lipid membrane, thus leading to the deformation and destruction of GUVs.

IV.6 | Experimental Procedures

Protein purifications and labelings were performed as described in Chapter 4 & Apendix III.

Sample preparation for the FCCS experiments

For the FCCS experiments GUVs were prepared from a lipid mixture of DOPC:bovine heart cardiolipin (80:20 mol%) using the electroformation method described in Appendix III. After the preparation 50 µl of GUVs were transferred to an observation well containing 450 µl of 1xEB buffer (10 mM Hepes, pH 7.2, 100 mM KCl) and a mixture of proteins (BAX, cBID, BCL-X_L) depending on the experiment. For all experiments observation chambers (8 well LabTak, Nunc) were treated for at least one hour with a solution containing 4 mg/ml BSA. BSA treatment was done with the purpose to prevent protein adsorption to the plastic walls of the observations chamber. All FCCS measurements were performed at room temperature (22 °C) in a dark room.

Fluorescence cross-correlation spectroscopy

FCCS measurements were performed on a laser-scanning microscope Meta 510 system (Carl Zeiss) using 40× NA 1.2 UV-Vis-IR C Apochromat water-immersion objective. For excitation the 488 nm line of an Argon-ion laser (25 µW) and the 633 nm line of the HeNe laser (15 µW) were used, while detection was done using a home-built detection unit at the fiber output channel. A dichroic mirror and band-pass filters (D555, HQ520/40 and HQ700/75; AHF Analyze Technik) were used behind a collimating achromat to split the emission for the dual-color detection and to reject residual laser and background light. We then

used achromats (LINOS Photonics) to image the internal pinhole onto the apertures of the fibers connected to the avalanche photodiodes (APD, PerkinElmer). The photon arrival times were recorded in the photon mode of the hardware correlator Flex 02-01D (http://correlator.com).

For scanning FCCS, the detection volume was repeatedly scanned perpendicularly through the equator of a GUV. We controlled its movement directly with the Zeiss LSM operation software. We used the frame mode with *Nx2* pixels to scan the two parallel lines. We measured their distance *d* by repeatedly scanning over a film of dried fluorophores and measuring the distance between the bleached traces in a high-resolution LSM image.

Data analysis was performed with software written in MATLAB (MathWorks). For scanning FCCS, we binned the photon stream in bins of 2 μs and arranged it as a matrix such that every row corresponded to one line scan. Corrected for movements of the membrane was done by calculating the position of the maximum of a running average over several hundred line scans and shifting it to the same column. We fitted an average over all rows with a Gaussian and we added only the elements of each row between -2.5σ and 2.5σ to construct the intensity trace. We computed the auto- and cross-correlation curves of the resulting intensity traces with a multiple tau correlation algorithm and fitted them with a nonlinear least-squares fitting algorithm. In all FCCS data processing, we excluded from further analysis irregular curves resulting from major instabilities identified by distortions of the curves and a systematic change in the intensity trace. For details of data fitting see Supplementary information.

Calculation of the diameter for the BAX pore complex

According to the Saffman-Delbruck theory of the diffusion of particles in lipid membranes translational diffusion coefficient (D) of the particle depends on the radius (R) of the particle in the following way

$$D = \frac{k_B T}{4\pi\mu_{mem} h}\left(\ln\frac{\mu_{mem} h}{\mu_{sol} R} - \gamma\right) \qquad \text{(Eqn.1)}$$

where μ_{mem} is membrane viscosity, μ_{sol} is solution viscosity, h is membrane thickness, T temperature, k_B is Boltzmann constant, and γ is Euler's constant (0.5772) (22). Schematic representation of a diffusing particle in a lipid membrane is shown in Figure IV.7.

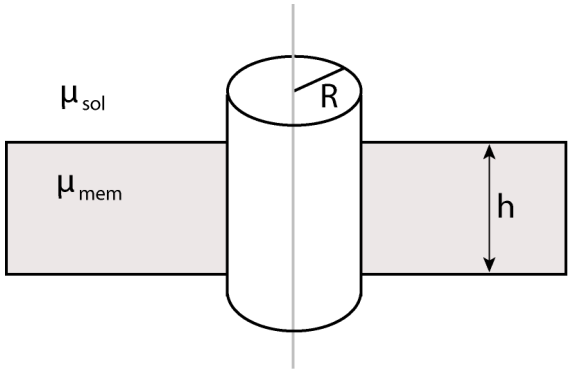

Fig. IV.7 | Schematic representation of the hydrodynamic model of a particle diffusing in a lipid membrane described by the Saffman-Delbruck equation (Eqn. 1).

As was mentioned previously that Saffman-Delbruck formula describes well diffusion of small proteins in a lipid membrane but fails to describe the membrane diffusion of larger complexes such as lipid rafts (19). Since BAX-RG proteo-lipidic complexes have diffusion coefficient two times smaller that the diffusion coefficient of a BAX monomer we used modified Saffman-Delbruck formula (17) to determine the in-membrane hydrodynamic radius

of these complexes. In our analysis we made assumptions that membrane viscosity is 0.7 cP (15), membrane thickness is 5 nm. The expression for the modified Saffman-Delbruck formula is following

$$D(\varepsilon) = \frac{k_B T}{4\pi\mu_{mem} h} \frac{\left(\ln\left(\frac{2}{\varepsilon}\right) - \gamma + \frac{4\varepsilon}{\pi} - \left(\frac{\varepsilon^2}{2}\right)\ln\left(\frac{2}{\varepsilon}\right)\right)}{\left(1 - \left(\frac{\varepsilon^3}{\pi}\right)\ln\left(\frac{2}{\varepsilon}\right) + c_1\varepsilon^{b_1} \Big/ (1 + c_2\varepsilon^{b_2})\right)} \qquad \text{(Eqn. 2)}$$

where, ε is the reduced radius, $\varepsilon = 2R\mu_{sol}/\mu_{mem}$, while c_1, c_2, b_1, and b_2 are constant ($c_1 = 0.73761$, $c_2 = 0.52119$, $b_1 = 2.74819$, $b_2 = 0.61465$).

To calculate the error for this value we used the fact that membrane viscosity is not very well defined and according to Ramadurai *et al.* (15) it varies for a lipid membrane composed of DOPC/DOPG mixture from 0.6 cP to 0.8 cP. Using this uncertainty in the actual value for the membrane viscosity together with the fact that lipid composition used in our work has similar viscosity as the one used in Ramadurai *et al.* based on the measurements of translational lipid diffusion we estimated that standard error for the diameter of the BAX pore complex is 12 nm. Therefore, we estimate that the diameter of the BAX pore complex in a lipid membrane is 53±12 nm.

IV.7 | References

1. Chipuk, J. E., Moldoveanu, T., Llambi, F., Parsons, M. J., and Green, D. R. (2008) *Mol Cell* **37**, 299-310
2. Youle, R. J., and Strasser, A. (2008) *Nat Rev Mol Cell Biol* **9**, 47-59
3. Suzuki, M., Youle, R. J., and Tjandra, N. (2000) *Cell* **103**, 645-654
4. Schafer, B., Quispe, J., Choudhary, V., Chipuk, J. E., Ajero, T. G., Du, H., Schneiter, R., and Kuwana, T. (2009) *Mol Biol Cell* **20**, 2276-2285
5. Martinez-Caballero, S., Dejean, L. M., Kinnally, M. S., Oh, K. J., Mannella, C. A., and Kinnally, K. W. (2009) *J Biol Chem* **284**, 12235-12245
6. Qian, S., Wang, W., Yang, L., and Huang, H. W. (2008) *Proc Natl Acad Sci U S A* **105**, 17379-17383
7. Hsu, Y. T., and Youle, R. J. (1998) *J Biol Chem* **273**, 10777-10783
8. Ivashyna, O., Garcia-Saez, A. J., Ries, J., Christenson, E. T., Schwille, P., and Schlesinger, P. H. (2009) *J Biol Chem* **284**, 23935-23946
9. Antonsson, B., Montessuit, S., Lauper, S., Eskes, R., and Martinou, J. C. (2000) *Biochem J* **345 Pt 2**, 271-278
10. Antonsson, B., Montessuit, S., Sanchez, B., and Martinou, J. C. (2001) *J Biol Chem* **276**, 11615-11623
11. Bleicken, S., Classen, M., Padmavathi, P. V., Ishikawa, T., Zeth, K., Steinhoff, H. J., and Bordignon, E. (2009) *J Biol Chem*
12. Dewson, G., and Kluck, R. M. (2009) *J Cell Sci* **122**, 2801-2808
13. Saito, M., Korsmeyer, S. J., and Schlesinger, P. H. (2000) *Nat Cell Biol* **2**, 553-555
14. Lovell, J. F., Billen, L. P., Bindner, S., Shamas-Din, A., Fradin, C., Leber, B., and Andrews, D. W. (2008) *Cell* **135**, 1074-1084
15. Ries, J., Chiantia, S., and Schwille, P. (2009) *Biophys J* **96**, 1999-2008
16. Ries, J., and Schwille, P. (2006) *Biophys J* **91**, 1915-1924
17. Garcia-Saez, A. J., Ries, J., Orzaez, M., Perez-Paya, E., and Schwille, P. (2009) *Nat Struct Mol Biol* **16**, 1178-1185
18. Yu, S. R., Burkhardt, M., Nowak, M., Ries, J., Petrasek, Z., Scholpp, S., Schwille, P., and Brand, M. (2009) *Nature* **461**, 533-536
19. Petrov, E. P., and Schwille, P. (2008) *Biophys J* **94**, L41-43
20. Billen, L. P., Kokoski, C. L., Lovell, J. F., Leber, B., and Andrews, D. W. (2008) *PLoS Biol* **6**, e147
21. Ramadurai, S., Holt, A., Krasnikov, V., van den Bogaart, G., Killian, J. A., and Poolman, B. (2009) *J Am Chem Soc* **131**, 12650-12656
22. Saffman, P. G., and Delbruck, M. (1975) *Proc Natl Acad Sci U S A* **72**, 3111-3113
23. Peters, R., and Cherry, R. J. (1982) *Proc Natl Acad Sci U S A* **79**, 4317-4321
24. Guigas, G., and Weiss, M. (2006) *Biophys J* **91**, 2393-2398

25. Gambin, Y., Lopez-Esparza, R., Reffay, M., Sierecki, E., Gov, N. S., Genest, M., Hodges, R. S., and Urbach, W. (2006) *Proc Natl Acad Sci U S A* **103**, 2098-2102
26. Schlesinger, P. H., Gross, A., Yin, X. M., Yamamoto, K., Saito, M., Waksman, G., and Korsmeyer, S. J. (1997) *Proc Natl Acad Sci U S A* **94**, 11357-11362
27. Epand, R. F., Martinou, J. C., Montessuit, S., Epand, R. M., and Yip, C. M. (2002) *Biochem Biophys Res Commun* **298**, 744-749
28. Korsmeyer, S. J., Shutter, J. R., Veis, D. J., Merry, D. E., and Oltvai, Z. N. (1993) *Semin Cancer Biol* **4**, 327-332
29. Nickells, R. W. (2010) *Exp Eye Res* **91**, 2-8
30. Cheng, E. H., Levine, B., Boise, L. H., Thompson, C. B., and Hardwick, J. M. (1996) *Nature* **379**, 554-556
31. Christenson, E., Merlin, S., Saito, M., and Schlesinger, P. (2008) *J Mol Biol* **381**, 1168-1183
32. Yethon, J. A., Epand, R. F., Leber, B., Epand, R. M., and Andrews, D. W. (2003) *J Biol Chem* **278**, 48935-48941
33. Kuwana, T., Mackey, M. R., Perkins, G., Ellisman, M. H., Latterich, M., Schneiter, R., Green, D. R., and Newmeyer, D. D. (2002) *Cell* **111**, 331-342
34. Karbowski, M., Lee, Y. J., Gaume, B., Jeong, S. Y., Frank, S., Nechushtan, A., Santel, A., Fuller, M., Smith, C. L., and Youle, R. J. (2002) *J Cell Biol* **159**, 931-938
35. Kim, H., Rafiuddin-Shah, M., Tu, H. C., Jeffers, J. R., Zambetti, G. P., Hsieh, J. J., and Cheng, E. H. (2006) *Nat Cell Biol* **8**, 1348-1358
36. Garcia-Saez, A. J., and Schwille, P. (2008) *Methods* **46**, 116-122
37. Haustein, E., and Schwille, P. (2007) *Annu Rev Biophys Biomol Struct* **36**, 151-169
38. Terrones, O., Antonsson, B., Yamaguchi, H., Wang, H. G., Liu, J., Lee, R. M., Herrmann, A., and Basanez, G. (2004) *J Biol Chem* **279**, 30081-30091

APPENDIX V

BAX & BCL-X_L Can Induce Opposing Gaussian Membrane Curvatures to Regulate Apoptosis

(The content of this chapter has been adapted from Lai, G. H., Ivashyna, O., Sanders, L. K., Christenson, E. T., Mishra, A., Schmidt, N. W., Santangelo, C. D., Schlesinger, P. H., Wong, G. C. L. (2011) (*in preparation*))

V.1 | Summary

The morphologic expression of programmed cell death, apoptosis, has a clear genetic basis on the B cell lymphoma-2 (BCL2) family of proteins. Critical interactions among BCL2 protein members occur in the outer mitochondrial (OM) membrane where they control mitochondrial function and permeability to initiate the mortality decision via cytochrome *c* release (1,2). While BCL2 regulation of apoptosis has been demonstrated, difficulties elucidating intra-membrane binding partners, and tracking protein structure after membrane insertion, oligomerization, and direct binding have made a consistent, molecular picture elusive (3-5). Here we report a parallel mode of BCL2 action, mediated by induced membrane curvature, with recombinant BAX (pore forming), BID (activator) and BCL-X_L (inhibitor). Using synchrotron x-ray scattering, we found activated BAX induces strong negative Gaussian membrane curvature topologically necessary for pore formation and other membrane destabilizing mechanisms. Fluorescence microscopy demonstrated this behavior correlates with vesicle permeation and is cognate to that of antimicrobial peptides and cell-penetrating peptides (6,7). Furthermore, x-ray evidence suggests BCL-X_L generates a complementary membrane curvature that cancels out the pore-enabling curvature induced by BAX. Consistent with a membrane-mediated mechanism, curvature generated by BCL-X_L similarly suppresses negative Gaussian curvature induced by pore-forming peptides unrelated to BCL2 proteins, and in pure lipid systems without proteins. These observations are supported by a model based on linear membrane elasticity.

V.2 | Introduction

To characterize membrane poration and its regulation, recombinant full-length human BAX, caspase-8-cleaved BID (cBID), and BCL-X_L were studied in cell-free assays. BAX, BID, and BCL-X_L have remarkably similar secondary structures given their drastically different functions (3,8). The multidomain executioner proteins BAX and BAK present obligate but alternate gateways to mitochondrial outer membrane permeabilization (MOMP). BAX is available as a stable soluble full-length protein as found in the cytosol of healthy cells. BID, widely used to activate BAX, has a single BCL2 homology (BH) domain and belongs to the large BH3-only pro-apoptotic subfamily. BCL-X_L has all four BH domains and is an inhibitor of apoptosis prominent in oncogenic transformation (1-5).

Unilamellar vesicles, both large (≈200 nm LUVs) and giant (≈10 μm GUVs), were prepared at different lipid compositions mimicking mitochondrial membranes, primarily with unsaturated (dioleoyl-) lipids (to avoid liquid-gel transition) like dioleoylphosphatidyl choline (DOPC), and lipids with nonzero intrinsic (spontaneous) curvature c_0, such as unsaturated ethanolamine (PE) and cardiolipin (CL). CL is concentrated mainly at highly curved contact sites (25 w% or ≈16 mol%) that connect the outer (≈3 mol%) to the inner mitochondrial membrane (≈10 mol%) (9,10). With a ternary lipid system comprising anionic CL, zwitterionic DOPE and DOPC, we can independently adjust membrane charge density and intrinsic curvature through typical ranges of physiological compositions to study the effects of BAX, cBID, and BCL-X_L. Vesicles were incubated with ternary mixtures of BAX (pore former), BCL-X_L (inhibitor/antagonist), and cBID (activator/agonist) at defined

stoichiometries (BAX/lipid molar ratios at 1/500-1/600) under physiological relevant conditions (pH 7.0, 100 mM KCl).

V.3 | Results & Discussion

Tracking efflux from dye-loaded GUVs with confocal microscopy allowed macroscopic characterization of pore formation, and results were consistent with cell-based experiments. With a lipid composition of 70/20/10 mol% PE/PC/CL, we observed complete dye efflux from all GUVs with cBID-activated BAX (≈0.35 μM, cBID/BAX ≈1:1) in several tens of minutes (Fig. V.1A-C), whereas addition of equimolar BCL-X_L significantly suppressed BAX-induced dye leakage, as expected, with most GUVs full of dye hours after introduction (data not shown).

Fig. V.1

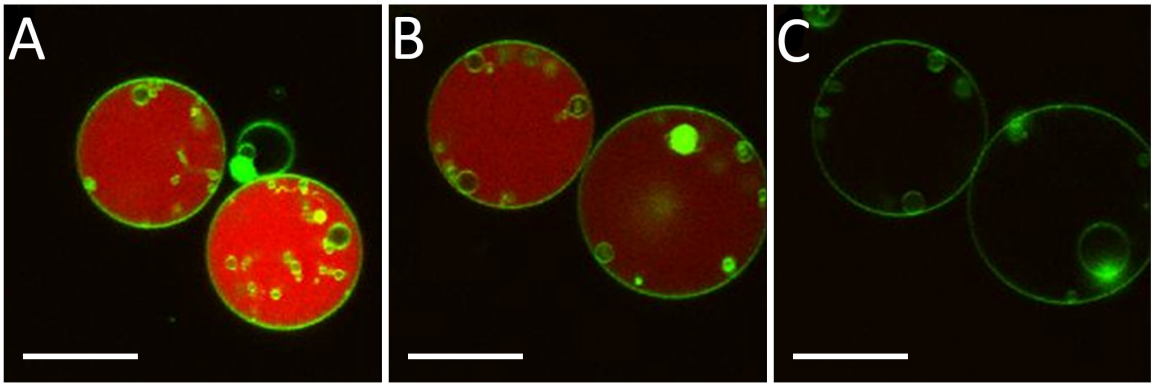

Fig. V.1 | **Verifying permeabilization activity of activated BAX in GUVs.** *A-C*, Confocal microscopy of 70:20:10 PE:PC:CL GUVs (+1% DiO, green) filled with 4 µM Alexa-Fluor 633 C_5-maleimide dye (1.3 kDa, red). Scale bar is 20 µm. Panels *B* and *C* track dye leakage of same vesicles after introducing 0.35 µM cBID-activated FL BAX (15 and 30 minutes later, respectively). Movie of GUV evolution in supplement.

High-resolution synchrotron small angle x-ray scattering (SAXS) revealed nanoscopic details of the protein-membrane interactions. Before exposure to BAX, SAXS data measured from LUVs at 75/20/5 mol% PE/PC/CL showed a broad feature consistent with the form factor of single lipid bilayers and typical of LUVs (Fig. V.2A, bottom trace). Incubating LUVs at 37°C with full-length (FL) BAX at 1/500 protein/lipid (P/L) molar ratio (≈25 μM protein to ≈12.5 mM lipids), activated with cBID (1:1 or ⅕:1) cBID/BAX molar ratio with similar result, latter not shown), gave rise to a drastically different diffraction signature. SAXS data displayed many sharp correlation peaks (Fig. V.2A, red trace) with q-value ratios √2, √3, √4, √6, √8, √9, and so on, that indexed precisely (Fig. V.2B) to a Pn3m (Q^{224}) 'double-diamond' lattice, an inverse bicontinuous cubic phase where two non-intersecting water channels are separated by a lipid bilayer (11) (Fig. V.2C). The centre of the bilayer traces out a minimum surface with negative Gaussian curvature K (also known as saddle-splay curvature). Like a saddle, the surface curves upwards (principal curvature c_1) in one direction and downwards (c_2) in the orthogonal direction, so that the Gaussian curvature $K \equiv c_1 c_2 < 0$. Negative Gaussian membrane curvature is broadly enabling: saddle-shaped (anticlastic) surfaces line the hole of a torus, the base of a bleb, and the neck of a bud, but are absent on spheres (which lack holes). Consistent with this physical picture, extensive mitochondrial fragmentation occurs almost simultaneously with MOMP in a caspase-independent fashion (12), and significant crosstalk has been reported between machineries of apoptosis and mitochondrial dynamics: BAX and BAK can promote mitochondrial fusion and fission (13-15); conversely, Drp1 from the mitochondrial fission

machinery is recently shown to stimulate BAX oligomerization and resultant MOMP in a manner sensitive to the spontaneous membrane curvature (16).

Slope fitting of measured peak *q*-values (Fig. V.2B) gave a lattice constant d_{Pn3m} of 15.58±0.03 nm. A weak Im3m (Q^{229}) cubic phase was sometimes also observed (Fig. V.2C), with a lattice constant that related to the Pn3m phase by the Bonnet ratio (1.279), indicating equivalent Gaussian curvature in the two coexisting cubic phases (11). Accounting for membrane thickness (2.5 nm), effective lipidic pore diameter in the Pn3m phase is ≈11.6 nm, which is sufficiently large for cytochrome *c* efflux. The apoptotic pore is known to be highly variable in size, and our result is comparable to those derived from vesicle leakage studies with BAX proteins (1-4 nm (8)) and truncated BAX peptides (11.6 nm (17), ≈4.6 nm (18)), from patch clamp conductance studies (1-6 nm (19)) and from cryo-electron microscopy of BAX-permeabilized liposomes that revealed BCL-X_L-inhibitable openings of varying sizes (25-100 nm (20)).

In vivo, BAX must be activated to cause apoptosis (1-5,21). Experimentally, we have triggered BAX activation to a pore-forming state with the active form of BID (cBID), or with nonprotein factors like non-ionic detergent and pH cycling (8,22,23). In addition, we have used both FL BAX and $BAX^{\Delta C}$ (transmembrane domain removed) activated by these protocols (see methods) to study their capacity to generate pore-forming geometries with bilayer membranes. With 85/7/8 PE/PC/CL LUVs, all the different activation methods induced drastically stronger cubic phases than native untreated FL BAX (Fig. V.2F) or $BAX^{\Delta C}$ (data not shown). Strikingly, different activation routes resulted in porous cubic structures with slightly different

amounts of negative Gaussian curvature, but activation by cBID consistently generated the strongest correlation peaks as well as the most negative Gaussian curvature (Fig. V.2F-G).

When BCL-X_L was introduced with cBID-activated FL BAX (½:1:1 molar ratio), all correlation peaks corresponding to negative Gaussian membrane curvature generation weakened and systematically shifted to lower q-values (Fig. V.2A, blue trace), with an indexed d_{Pn3m} of 21.59±0.04 nm. Weaker peak intensities indicate reduced occurrence of the cubic phase. The increased lattice constant reflects decreased saddle-splay curvature within the cubic phase, because the average Gaussian curvature is inversely proportional to the square of the cubic lattice constant (11) (Fig. V.2B). At BCL-X_L to BAX molar ratios 1:1 and greater, all correlation peaks were fully quenched (Fig. V.2A, top two traces), signaling the absence of saddle-splay curvature characteristic of porated spongy phases.

The physiologic functions of BAX (pore formation), cBID (BAX-activator) and BCL-X_L (inhibitor of pore formation) in OM membranes are entirely consistent with the structural tendency each protein introduces when incorporated into liposomes composed of OM membrane-like lipids. BCL-X_L's antagonistic action against BAX's pore forming activity and ensuing inhibition of cytochrome *c* release can be correlated with its suppression of negative Gaussian curvature generation, a crucial ingredient for pore formation. Supporting this interpretation, we consistently found BCL-X_L reduced correlation peak intensities (less pores) and increased the cubic lattice constant (lower curvature) before complete shutdown of BAX.

We find BAX activity is strongly influenced by the composition of mitochondrial lipids, which have distinct spontaneous curvatures: neutral ($c_0 \approx 0$) for PC, negative ($c_0 < 0$) for

PE(24), and tunable for CL depending on the bound cation (25) ($c_0 \approx 0$ with monovalent salt, $J_s < 0$ with divalent cations like Ca^{2+} and Mg^{2+}). To modify effective membrane c_0, we varied PE content. PE headgroups are small compared to their tails (wedge-shaped) and tend to bend the lipid monolayer towards the water region and away from the hydrocarbon chain region (negative intrinsic curvature) (24). By increasing PE content to 85/12/3 PE/PC/CL, FL BAX was enough to induce cubic correlation peaks (Fig. V.2D, bottom red trace) without help from activator cBID. Conversely, increasing CL from 3 mol% (Fig. V.2D) to 8 mol% (Fig. V.2F), keeping PE at 85 mol%, gave significantly weaker cubic correlation peaks for FL BAX alone. This decrease is more pronounced in the absence of cBID, whose targeting of mitochondria (26) and activation of BAX (20) are widely cited as CL dependent. We next examined membrane structures induced by BAX, activated using all three different methods, for a broad range of lipid compositions relevant to mitochondrial membranes (Fig. V.2H for phase diagram of ternary PE/PC/CL liposomes with activated BAX at P/L=1/500). Occurrence of porous phases correlates with high PE and low mitochondrial-like CL levels. No porous cubic phases were observed when CL content approached and exceeded levels found in the inner mitochondrial (IM) membrane (10-16 mol%) (9,10), the integrity of which remains undisturbed following BID/BAX-induced cytochrome *c* release (27,28).

Fig. V.2

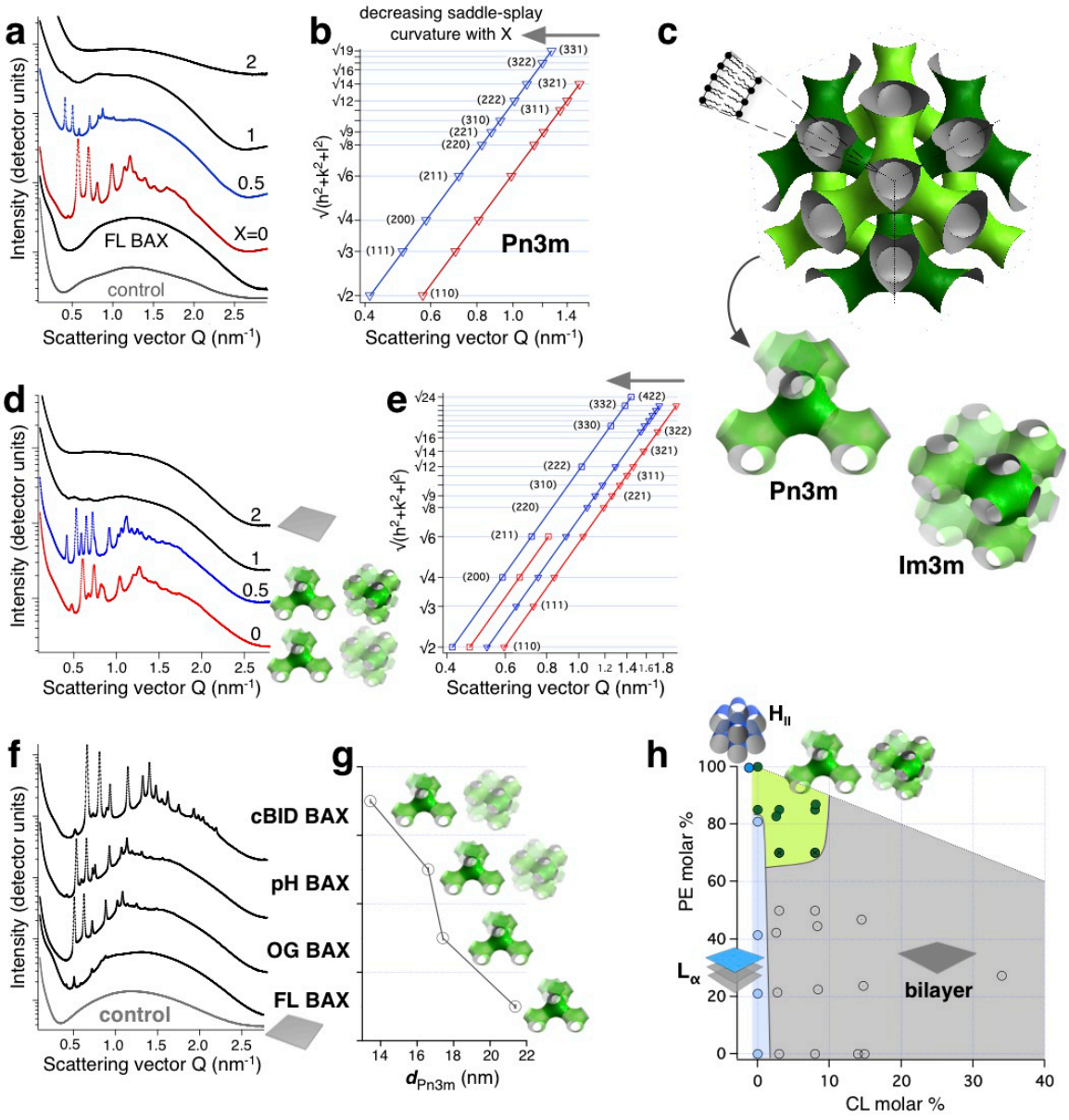
a
Intensity (detector units)
2
1
0.5
X=0
FL BAX
control
Scattering vector Q (nm^{-1})
b
decreasing saddle-splay
curvature with X
Pn3m
Scattering vector Q (nm^{-1})
c
Pn3m
Im3m
d
Intensity (detector units)
2
1
0.5
0
Scattering vector Q (nm^{-1})
e
Scattering vector Q (nm^{-1})
f
Intensity (detector units)
cBID BAX
pH BAX
OG BAX
FL BAX
control
Scattering vector Q (nm^{-1})
g
d_{Pn3m} (nm)
h
H_{II}
PE molar %
L_α
bilayer
CL molar %

Fig. V.2 | **cBID activates BAX to induce saddle-splay curvature, while BCL-X_L suppresses curvature generation.** *A*, Experimental SAXS data on 75/20/5 PE/PC/CL LUVs, offset vertically for comparison. While FL BAX alone was insufficient, 1:1-activation with cBID (red) precipitated a dominant cubic Pn3m phase. Annotations denote BCL-X_L/BAX molar ratio (X), showing clear suppression of BAX-induced cubic diffraction peaks at high X. *B*, Pn3m peak indexing for X=0 (red) and ½ (blue) gave lattice constants d=15.58±0.03 nm, 21.59±0.04 nm respectively. Peak q-values relate Miller indices (h, k, l) to d by $q=2\pi\sqrt{(h^2+k^2+l^2)}/d$, so a left shift on log-log plot denotes an increase in d, with a commensurate decrease in saddle-splay curvature because $\langle K \rangle \approx 2\pi\chi/d^2A_0$, with Euler characteristic χ and unit cell surface area A_0 (11). *C*, Top schematic show double-diamond topology of inverse bicontinuous cubic Pn3m phase, bottom show representative repeating units of cubic Pn3m and Im3m. *D*, FL BAX alone induced cubic phases in 85/12/3 PE/PC/CL. Annotations denote X. *E*, Peak positions in *D* indexed for X=0 (red) and X=½ (blue). Triangle and square markers denote Pn3m and Im3m peak q-values respectively. At X=0, d_{Pn3m}=14.98±0.03 nm, d_{Im3m}=19.1±0.1 nm. At X=½, d_{Pn3m}=16.87±0.03 nm, d_{Im3m}=21.34±0.03 nm. *F*, Different methods of activating BAX gave rise to the same class of curvature with 85/7/8 PE/PC/CL LUVs, with d_{Pn3m} comparison in *G*. *H*, Composite protein-membrane phase diagram for BAX (P/L=1/500) activated with all 3 methods in ternary PC/PE/CL LUVs show propensity for porous states at high PE and low CL.

Although BAX and BCL-X_L are structurally similar, they remodel membranes in drastically different ways. BCL-X_L did not induce sharp correlation peaks for a broad range of lipid compositions, suggesting its curvature generation ability is weaker than BAX's. Considering PE's strong role in BAX-induced porous phases, we examined the action of BCL-X_L on pure hydrated PE lipids, which possess sufficient negative c_0 to self-assemble into an inverted hexagonal (H_{II}) lipidic phase (peak q-positions at $1:\sqrt{3}:\sqrt{4}:\sqrt{7}$ ratios, Fig. V.3A). The H_{II} PE phase has negative curvature only along one direction (11) (and zero curvature orthogonally, so that $H \equiv c_1+c_2<0$, but $K \equiv c_1c_2=0$). SAXS data showed that BCL-X_L was able to grow porous cubic phases that have negative curvature along one principal direction and positive curvature along the other ($c_1c_2<0$). This suggests that BCL-X_L has restructured the negative mean curvature target membrane to produce new positive curvature. Isotropic generation of positive curvature leads to positive Gaussian curvature. Since both BAX and BCL-X_L can act on the OM membrane, we need to understand how positive Gaussian curvature induced by BCL-X_L interacts with negative Gaussian curvature induced by BAX (Fig. V.3B for possible picture).

We developed a theoretical model for mixtures of two membrane-bound proteins, one inducing negative GC (BAX-like), the other positive GC (BCL-X_L-like). Each protein is taken to induce local principal curvatures in the membrane, ξ_1 and ξ_2, which works against the membrane deformations given by the Helfrich free energy, $F_{\text{Helfrich}}=(B/8)\int dA(c_1+c_2)^2$, with the integral over the membrane area, and bending rigidity B. The energy of a single protein is $E_{\text{Protein}}=(\Delta E/2)[(c_1-\xi_1)^2+(c_2-\xi_2)^2]$, where $\Delta E(\xi_1^2+\xi_2^2)/2$ is the energy cost of binding a protein to

a flat membrane, and the induced principal curvatures depend on the protein type (see supplementary for calculation details). Analogous to classical nucleation theory, the free energy scales as $E=-\sigma\pi r^2+\tau 2\pi r$ for a pore of radius r and pore rim line tensionτ on a membrane with effective surface tension σ. This model exhibits an energy barrier $E_{barrier}=\pi\tau^2/\sigma$ at a radius $r_0=\tau/\sigma$. When this energy is comparable to thermal energy, pore formation becomes favourable. We find that BAX-like $K<0$-inducing proteins universally suppress the free energy barrier, while BCL-X_L-like proteins inducing positive Gaussian curvature ($K>0$) enhance it. Mixtures of proteins inducing competing curvatures can control pore formation via the free energy barrier (Fig. V.3C). Setting $\xi_1\approx0.5$ nm^{-1}, commensurate with the curvature on the inside of a pore, and $\Delta E(\xi_1^2+\xi_2^2)/2\approx 4k_BT$, we find $\xi_2=-0.05$ nm^{-1} induces an average Gaussian curvature of -0.022 nm^{-2}, consistent with a Schwartz' D (Pn3m) surface of lattice size 17 nm (11). We use $\xi_1=\xi_2=0.375$ nm^{-1} for $K>0$-inducing proteins. Even at very modest area fractions, a $K>0$-inducing protein will inhibit pore formation by raising the energy barrier drastically (Fig. V.3C). The precise values used for constants do not change the generic behaviour observed in the model, and computed d_{Pn3m} grows with increasing BCL-X_L/BAX ratio (Fig. V.3D) in good agreement with our measured lattice constants.

Fig. V.3

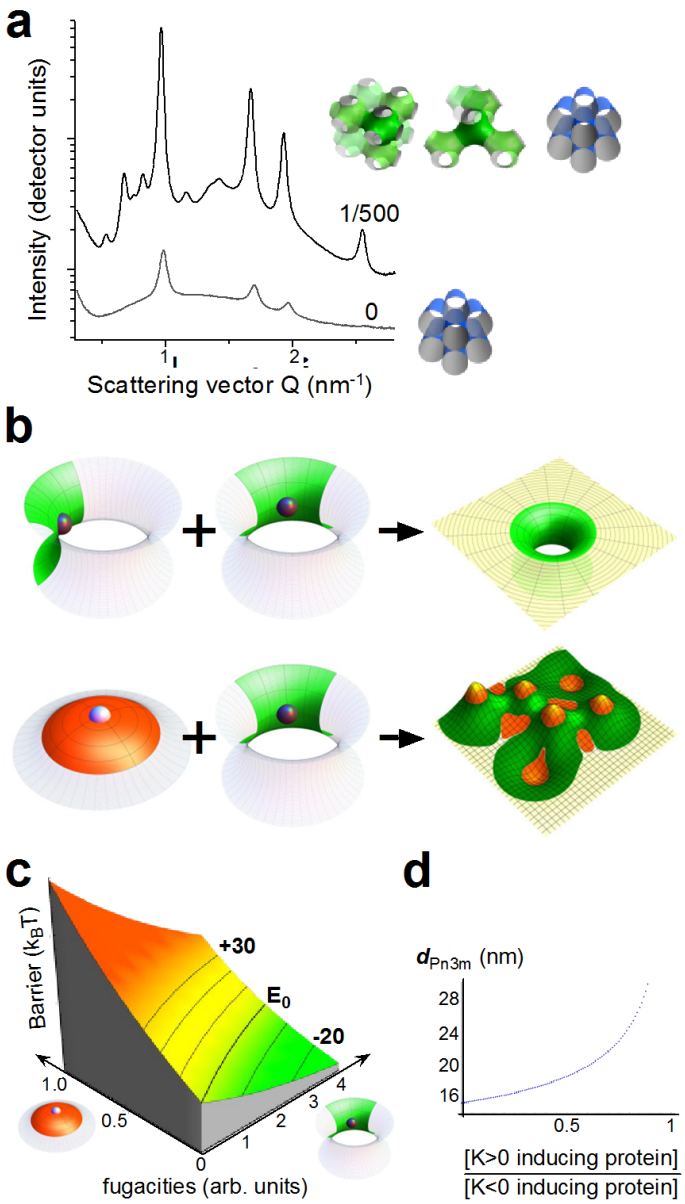
a
Intensity (detector units)
1/500
0
Scattering vector Q (nm-1)
b
c
Barrier (kBT)
+30
E0
-20
1.0
0.5
0
1
2
3
4
fugacities (arb. units)
d
dPn3m (nm)
28
24
20
16
0.5
1
[K>0 inducing protein]
[K<0 inducing protein]

Fig. V.3 | **BCL-X_L introduces positive curvature to curb BAX-induced pore formation.** *A*, Annotations denote BCL-X_L/lipid molar ratios (X/L). Hydrated PE self-assembles into a H_{II} phase (negative mean curvature, dark blue) with d_H=7.5 nm and principal curvatures c_1<0 and c_2=0, but addition of BCL-X_L grew cubic phases (d_{Pn3m}=13.2 nm, d_{Im3m}=16.9 nm) with c_1<0 and c_2>0, indication that positive curvature was introduced into the system. *B*, Schematic portray possible end-states when curved membrane patches interact. Saddle-splay patches (*K*<0, green) induced by proteins can come together to stabilize a pore, while introducing patches of isotropic positive curvature (*K*>0, orange) separate saddle defects to frustrate pore formation and leave an "egg-carton" surface (29). *C*, Barrier height of pore opening in mixtures of positive (orange) and negative (green) Gaussian curvature-generating proteins in theoretical model. Bare line tension τ0=10-11 J/m, bare surface tension σ0=10-3 N/m. Barrier without proteins E0=π τ02/σ0, with contours spaced 10 kBT apart. *D*, Pn3m lattice constants grow with increasing molar ratio of K>0-generating proteins to K<0-generating proteins in theoretical model, and the range of lattice constants are in rough agreement with experimental data on BAX and BCL-X_L.

Taken together, these observations propose the possibility that BCL2 family proteins, in addition to direct protein-protein binding, may also interact with one another via a membrane-curvature mediated mechanism. To test our hypothesis, we examined whether BCL-X_L could be used to turn off pore-formers other than BAX. Cell-penetrating peptides (CPPs) and antimicrobial peptides (AMPs) are obvious targets that can generate pores through negative Gaussian curvature (6,7). Mitochondrial membranes also resemble bacterial membranes (presence of CL, rich in PE and low cholesterol) (30). We incubated 80/20 PE/PS (phosphor-L-serine) LUVs with varying BCL-X_L levels while the cell-penetrating peptide TAT is kept at a peptide/lipid (P/L) molar ratio of 1:40. TAT induced correlation peaks characteristic of coexisting lamellar L_α (peak *q*-positions at 1:2:3 ratio), Pn3m cubic, and inverted hexagonal H_{II} lipid phases (6) (Fig. V.4A, bottom trace). Upon raising BCL-X_L/lipid molar ratios (X/L), BCL-X_L first quenched diffraction peaks of the H_{II} phase at X/L=1/500, before completely suppressing the TAT-generated Pn3m peaks at X/L=1/100. Synthetic cell-penetrating peptides, polyarginine-(polyethylene-glycol) or $R_4(PEG)_XR_4$, were also tested with BCL-X_L. $R_4(PEG)_5R_4$ restructured 80/20 PE/PS LUVs to give diffraction peaks similar to TAT's, and BCL-X_L was again able to suppress all correlation peaks (Fig. V.4B) in a manner analogous to its antagonistic effect on BAX. Strikingly, BCL-X_L can even quench negative Gaussian membrane curvature in a pure lipid system. High monovalent salt (300 mM KCl) was used to restructure 80/20 PE/PS LUVs into porous cubic phases (Pn3m and Im3m) with a coexisting hexagonal H_{II} phase (Fig. V.4C). Incubation with BCL-X_L suppressed the low-*q* cubic diffraction peaks, while higher BCL-X_L levels grew the lamellar L_α phase at the expense of

the H_{II} phase (Fig. V.4C, top trace), consistent with BCL-X_L's generation of positive curvature. In line with a membrane-mediated mechanism, BCL-X_L was able to suppress negative Gaussian membrane curvature generation across a broad range of systems, ranging from pore forming peptides drastically different from BAX in charge, hydrophobicity and molecular weight, to a pure lipid system lacking protein-protein interactions.

Fig. V.4

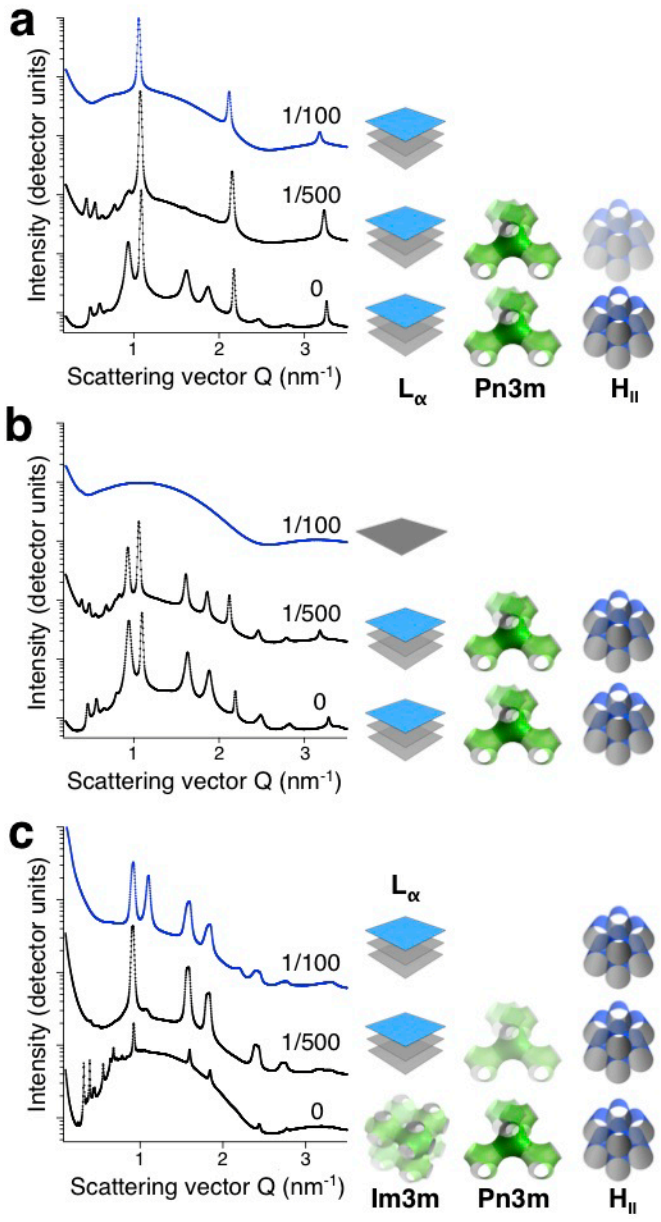

Fig. V.4 | **BCL-X_L inhibits pore formers unrelated to the BCL2 family.** *A*, TAT in 80/20 PE/PS liposomes generated Pn3m (diffraction peaks at low *q*) and H_{II} phases suppressible by high BCL-X_L/lipid levels (X/L, annotated), leaving only the lamellar L_α phase. *B*, $R_4(PEG)_5R_4$ in 80/20 PE/PS induces Pn3m and H_{II} phases, both suppressed at high X/L. *C*, 300 mM KCl can induce 80/20 PE/PS liposomes into cubic and hexagonal phases, but increasing X/L blocked any growth of cubic peaks.

V.4 | Conclusion

The formulation of BCL2 regulation has largely been based on BH3 domain interactions. Specific protein-protein contacts produce allosteric and displacement changes that modulate protein activity to control apoptosis (2-5). Our findings here demonstrate that in addition to BH3-mediated interactions between family members, a parallel mechanism mediated by BCL2 induced mitochondrial membrane curvature plays an important role. It is possible that under different biological conditions, specific protein-protein interactions can appear dominant or secondary (5,21,31,32). This model comports well with a recent finding that reduced BH3 interactions between BAX and BCL-X_L do not suppress inhibition of apoptosis (33), and suggests a new general class of strategies for engineering apoptosis.

V.5 | Experimental Procedures

Protein/peptide preparation

Recombinant human BCL-X_L, cBID, and BAX (both FL and truncated (ΔC19)), were produced as intein constructs, expressed in BL21 (DE3) *E. coli*, isolated and purified without exposure to detergent (22,23). All proteins were found homogeneous (denaturing gel electrophoresis) and monomeric (fluorescence correlation spectroscopy) at physiological salt conditions. Octyl glucoside-activated BAX (OG BAX) was obtained by incubating $BAX^{\Delta C}$ with 1% (w/v) OG for 1 h at 4°C, and dialyzing for 4 h at room temperature against pH 7.0 buffer (10 mM Hepes, 100 mM KCl). pH-activated (pH BAX) was prepared by dialyzing against pH 5.0 buffer (10 mM NaOAc, 100 mM KCl), then back against pH 7.0 buffer just before sample preparation. Activation by cBID involved mixing FL BAX or $BAX^{\Delta C}$ with cBID

at 1:1 or 5:1 stoichiometry. Cell penetrating peptide TAT 47-57 (trans-activator of transcription protein transduction domain from HIV-1) was purchased (Anaspec) and $R_4(PEG)_XR_4$ peptides were prepared using automated solid-state synthesis (Protein Sciences Facility, University of Illinois).

GUV preparation for confocal microscopy

1,2-Dioleoyl-*sn*-Glycero-3-Phosphocholine (DOPC), 1,2-Dioleoyl-*sn*-Glycero-3-Phosphoethanolamine (DOPE), 1,2-Dioleoyl-*sn*-Glycero-3-Phospho-L-Serine (DOPS, sodium salt), bovine liver L-α-phosphatidylinositol (PI, sodium salt), bovine heart cardiolipin (CL, sodium salt) were purchased from Avanti Polar Lipids. Giant unilamellar vesicles (GUVs) labelled with DiO (Invitrogen) were prepared using electroformation. Lipid solutions in chloroform were desiccated on indium tin oxide (ITO) coated glass slides and swelled in 100 mM sucrose solution containing Alexa Fluor 546 C_5-maleimide or succinimidyl ester dye (≈1 kDa, non-reactive after Tris pretreatment) under 10 Hz sinusoidal AC electric field. After GUV detachment with 4 Hz square AC, suspension was diluted 100× into 100 mM glucose, 100 mM KCl medium and imaged in a 200μl chamber with a Leica TCS SP2 laser scanning confocal microscope (63×, 1.4 N.A.).

LUV preparation for x-ray measurements

Lipid solutions in chloroform were dried under N_2 and desiccated overnight under vacuum, then rehydrated in pH 7.0 buffer to 20 mg/ml at 37°C overnight before sonication to clarity and extrusion through 0.2μm Nucleopore (Whatman) filters to yield large unilamellar vesicles (LUVs). BCL2 proteins were mixed with LUVs at specific molar stoichiometries

(BAX:lipid = 1:500 or 1:600) while cell-penetrating peptides were introduced at peptide-to-lipid molar ratios (P:L) just below the isoelectric point (P:L=1:40). Samples were incubated at 37°C overnight and sealed in quartz capillaries.

Synchrotron x-ray scattering

Small angle x-ray scattering (SAXS) data were collected on BL4-2 (9-11 keV) at Stanford Synchrotron Radiation Laboratory (Palo Alto, CA), BL7.3.3 (10 keV) at Advanced Light Source (Berkeley, CA), and BESSRC-CAT (BL12-IDC) and BioCAT (12 keV) at the Advanced Photon Source (Argonne, IL). Scattered intensity was collected with MAR-Research (Hamburg, Germany) CCD detector (79 μm pixel) and integrated using NIKA (http://usaxs.xor.aps.anl.gov/staff/ilavsky/nika.html) on Igor Pro (Wavemetrics) and FIT2D (http://www.esrf.eu/computing/scientific/FIT2D/).

V.6 | References

1. Danial, N. N., and Korsmeyer, S. J. (2004) *Cell* **116**, 205--219
2. Tait, S. W. G., and Green, D. R. (2010) *Nat. Rev. Mol. Cell Biol.* **11**, 621--632
3. Youle, R. J., and Strasser, A. (2008) *Nat. Rev. Mol. Cell Biol.* **9**, 47--59
4. Chipuk, J. E., Moldoveanu, T., Llambi, F., Parsons, M. J., and Green, D. R. (2010) *Mol. Cell* **37**, 299--310
5. Letai, A. G. (2008) *Nat. Rev. Cancer* **8**, 121--132
6. Mishra, A., Gordon, V. D., Yang, L., Coridan, R., and Wong, G. C. L. (2008) *Angew. Chem. Int. Ed.* **47**, 2986--2989
7. Schmidt, N., Mishra, A., Lai, G. H., Davis, M., Sanders, L., Tran, D., Garcia, A., Tai, K., McCray, P., Ouellette, A., Selsted, M., and Wong, G. C. L. (2011) *J. Am. Chem. Soc.* **accepted**
8. Schlesinger, P. H., and Saito, M. (2006) *Cell Death Differ.* **13**, 1403--1408
9. Ardail, D., Privat, J. P., Egret-Charlier, M., Levrat, C., Lerme, F., and Louisot, P. (1990) *J. Biol. Chem.* **265**, 18797--18802
10. de Kroon, A. I., Dolis, D., Mayer, A., Lill, R., and de Kruijff, B. (1997) *Biochim. Biophys. Acta* **1325**, 108--116
11. Shearman, G. C., Ces, O., Templer, R. H., and Seddon, J. M. (2006) *J. Phys.: Condens. Matter* **18**, S1105--S1124
12. Frank, S., Gaume, B., Bergmann-Leitner, E. S., Leitner, W. W., Robert, E. G., Catez, F., Smith, C. L., and Youle, R. J. (2001) *Dev. Cell* **1**, 515--525
13. Autret, A., and Martin, S. J. (2009) *Mol Cell* **36**, 355-363
14. Youle, R., and Karbowski, M. (2005) *Nat Rev Mol Cell Biol* **6**, 657--663
15. Hoppins, S., Edlich, F., Cleland, M. M., Banerjee, S., McCaffery, J. M., Youle, R. J., and Nunnari, J. (2011) *Mol Cell* **41**, 150-160
16. Montessuit, S., Somasekharan, S. P., Terrones, O., Lucken-Ardjomande, S., Herzig, S., Schwarzenbacher, R., Manstein, D. J., Bossy-Wetzel, E., Basañez, G., Meda, P., and Martinou, J.-C. (2010) *Cell* **142**, 889--901
17. García-Sáez, A. J., Coraiola, M., Serra, M. D., Mingarro, I., Müller, P., and Salgado, J. (2006) *FEBS J.* **273**, 971--981
18. Fuertes, G., García-Sáez, A. J., Esteban-Martín, S., Giménez, D., Sánchez-Muñoz, O. L., Schwille, P., and Salgado, J. (2010) *Biophys J* **99**, 2917--2925
19. Martinez-Caballero, S., Dejean, L. M., Kinnally, M. S., Oh, K. J., Mannella, C. A., and Kinnally, K. W. (2009) *J. Biol. Chem.* **284**, 12235--12245
20. Schafer, B., Quispe, J., Choudhary, V., Chipuk, J. E., Ajero, T. G., Du, H., Schneiter, R., and Kuwana, T. (2009) *Mol. Biol. Cell* **20**, 2276--2285
21. Lovell, J. F., Billen, L. P., Bindner, S., Shamas-Din, A., Fradin, C., Leber, B., and Andrews, D. W. (2008) *Cell* **135**, 1074--1084

22. Christenson, E., Merlin, S., Saito, M., and Schlesinger, P. (2008) *J. Mol. Biol.* **381**, 1168--1183
23. Ivashyna, O., García-Sáez, A. J., Ries, J., Christenson, E. T., Schwille, P., and Schlesinger, P. H. (2009) *J. Biol. Chem.* **284**, 23935--23946
24. Zimmerberg, J., and Kozlov, M. M. (2006) *Nat. Rev. Mol. Cell Biol.* **7**, 9--19
25. Som, A., Yang, L., Wong, G. C. L., and Tew, G. N. (2009) *J. Am. Chem. Soc.* **131**, 15102--15103
26. Lutter, M., Fang, M., Luo, X., Nishijima, M., Xie, X., and Wang, X. (2000) *Nat. Cell Biol.* **2**, 754-761
27. Kluck, R. M., Esposti, M. D., Perkins, G., Renken, C., Kuwana, T., Bossy-Wetzel, E., Goldberg, M., Allen, T., Barber, M. J., Green, D. R., and Newmeyer, D. D. (1999) *J. Cell Biol.* **147**, 809--822
28. von Ahsen, O., Renken, C., Perkins, G., Kluck, R. M., Bossy-Wetzel, E., and Newmeyer, D. D. (2000) *J. Cell Biol.* **150**, 1027--1036
29. Dommersnes, P. G., and Fournier, J. B. (2002) *Biophys. J.* **83**, 2898-2905
30. van Meer, G., Voelker, D. R., and Feigenson, G. W. (2008) *Nat. Rev. Mol. Cell Biol.* **9**, 112--124
31. Willis, S. N., Fletcher, J. I., Kaufmann, T., van Delft, M. F., Chen, L., Czabotar, P. E., Ierino, H., Lee, E. F., Fairlie, W. D., Bouillet, P., Strasser, A., Kluck, R. M., Adams, J. M., and Huang, D. C. S. (2007) *Science* **315**, 856--859
32. Kim, H., Tu, H.-C., Ren, D., Takeuchi, O., Jeffers, J. R., Zambetti, G. P., Hsieh, J. J.-D., and Cheng, E. H.-Y. (2009) *Mol. Cell* **36**, 487--499
33. Fletcher, J. I., Meusburger, S., Hawkins, C. J., Riglar, D. T., Lee, E. F., Fairlie, W. D., Huang, D. C. S., and Adams, J. M. (2008) *Proc. Natl. Acad. Sci. U.S.A.* **105**, 18081--18087